

# Study of stability, reactivity and longevity of clay barriers used in the sealing process under extreme conditions of pH

Vanessa dos Santos Guimarães

Programa Doutoral em Geociências

Especialidade em Recursos Geológicos e Geomateriais

Departamento de Geociências, Ambiente e Ordenamento do Território da  
Universidade do Porto, Departamento de Geociências da Universidade de  
Aveiro

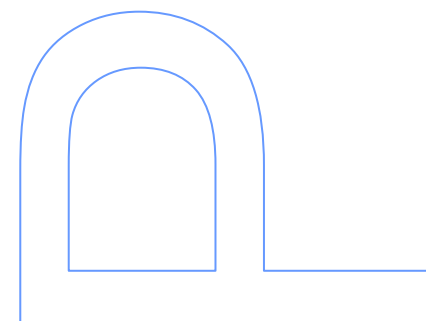
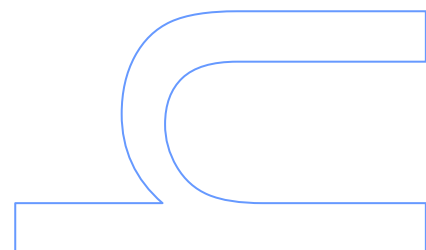
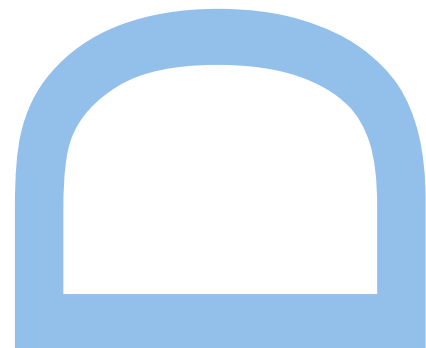
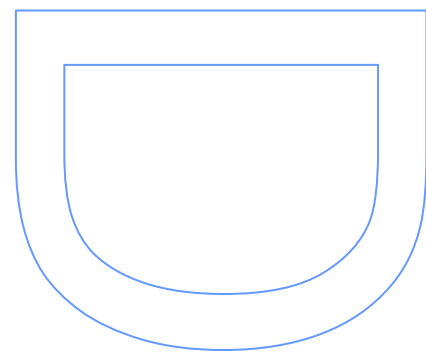
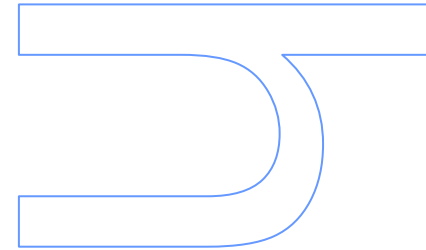
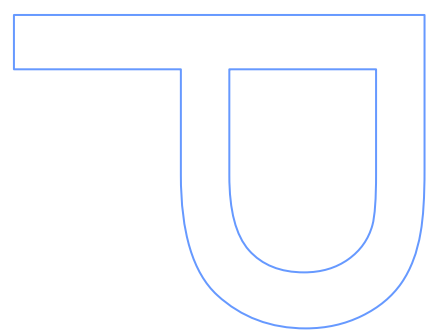
2016

## Orientador

Iuliu Bobos Radu, Professor Associado com Agregação, Faculdade de  
Ciências da Universidade do Porto

## Coorientador

Fernando Tavares Rocha, Professor Catedrático, Departamento de  
Geociências, Universidade de Aveiro



## Acknowledgment

First, I would like to thank to Portuguese Foundation for Science and Technology (FCT) from Lisbon (Portugal) for the PhD scholarship (Ref. SFRH/BD/79969/2011) which financed this work by FEDER through the funds of the Competitiveness Factors Operational Programme (COMPETE) and with national funds. This work was not possible without the financial support came from the FCT Lisbon.

During the 4 years the PhD project was accompanied by the supervisor (PhD Director), Prof. Dr. Iuliu Bobos and I'm indebted to him for the patient guidance, all support and encouragement provided throughout my time as her student.

Also my gratitude goes to Prof. Dr. Fernando Rocha (Co-supervisor) for his laboratorial and scientific support given during this period.

I'm deeply indebted to Professor Enrique Castellon from the University of Malaga for his greatly and generous help given for X-ray photoelectron spectroscopy measurements carried out in his lab and for very useful lessons received during my staying in Malaga about XPS.

I'm also deeply grateful to Dr. Manuel Algarra for his help with chemical measurements made by inductively coupled plasma mass spectrometry where thousands of analyses were carried out. Without his help, never this work would be finished. Thank you Manolo!

During my work in the Faculty of Sciences of Porto, I thank to Mestre Cândida Garcia for her laboratorial help during my sorption experiments, to Eng. Fernanda Guimarães for electron microprobe analysis and to Maria Irene Lopes for her help with samples preparation.

Firstly, I spent half year in University of Aveiro when I started the PhD Program in Geoscience. My acknowledgments go to Denise Terroso and Cristina Sequeira for their help and assistance.

I am grateful to Prof. Dr. António Fernando Silva and Prof. Dr. Manuel Azenha for their availability and support in all the experiments carried out in Chemistry Department.

During the PhD project I had a great privilege to visit and to stay one month in Paul Scherer Institute, ETH –Zurich, where I benefitted to discuss my results and my PhD project with Dr. Bart Bayens and Dr. Maria Marques. It was great challenge for me to have a very

constructive dialog about what mean sorption experiments on clay minerals. Many thanks to Marie for her courtesy and help.

I thank to Professor Fernando Noronha, the former Director of PhD Course in Geoscience which finally believed in my capacity to finish the PhD project.

I would also like to extend my deepest gratitude to my family, especially to my Mother and Sister, who gave me all the strength to overcome this difficult challenge. I thank to Pedro for his guidance, patience and support. Definitely, behind a great women there is a great man!

Last but not least I thank to Rui Rocha, Juan Martinez, Cristiana Ferreira and all my friends for their great support during this long period.

## Abstract

Clay minerals are the main materials used to limit seepage from tailings impoundments and to cover solid waste disposal landfills, low and intermediate level waste (LILW) and high level waste (HLW). The increase of temperature and pressure due to waste package, or the extreme pH conditions and chemical composition of the contaminated solutions may affect the clays performance, causing significant changes on smectite structure and in the mechanism of adsorption and contaminant retention on clay surface. This is the reason why this study selected heterogeneous smectite samples, resulted from hydrothermal alteration processes, to test their behavior in solutions with metals and actinides. A multibarrier principle with natural and engineering barriers ensures a redundant safety system if a failure in any of the protection barriers occurs.

Heterogeneous smectite samples collected from the Portuguese bentonite rocks (Porto Santo Island, Madeira Arquipelago and Benavila area, Ossa Morena Zone, Portugal) were tested for their reactivity and sorption properties using  $\text{Sr}^{2+}$  and  $\text{UO}_2^{2+}$ . The heterogeneity of smectite samples (BA1, PS2 and PS3) was tested by X-ray diffraction (XRD) and Infrared spectroscopy (FTIR) after the  $\text{K}^+$ ,  $\text{Na}^+$  and  $\text{Ca}^{2+}$  saturation. Also the samples were saturated with  $\text{Li}^+$  and heated at  $300^\circ\text{C}$  (Greene-Kelly test). The layer charge and charge distribution were evaluated by means of XRD analysis after Li- and K-smectite being submitted to glycerol (GLY) and ethylene glycol (EG) solvation. The reactivity of smectite samples was also tested after smectite treatment in acid and alkaline solutions.

Several experimental conditions were taken into account in this work to evaluate the adsorption and desorption of  $\text{Sr}^{2+}$  onto smectite, such as: contact time, pH,  $\text{Sr}^{2+}$  concentrations and ionic strength. The adsorption and desorption of  $\text{Sr}^{2+}$  onto smectite with high charge deficit was carried out in extreme pH conditions and different  $\text{Sr}^{2+}$  concentrations. The kinetic data were achieved using a continuously stirred flow-through reactor (CSTR) enhanced an intensive pre-washing and a good pre-conditioning of smectite, providing an appropriate control of the chemical conditions imposed during our experiments. Breakthrough studies were carried out to evaluate the effect of pH (4 and 8) and  $\text{Sr}^{2+}$  concentration (7.00 mg/L, 27.00 mg/L and 34.00 mg/L) during adsorption and desorption processes. Several models were used to describe the kinetic behavior of  $\text{Sr}^{2+}$  adsorption onto smectite. Additionally, batch experiments were performed, at different pH (4 and 8) and ionic strength ( $I=10^{-2}$  and  $I=10^{-3}$ ) conditions, to obtain the sorption data under equilibrium

and isothermal conditions. The results showed that the gradient of concentration acted as an increasing driving force since the amount of  $\text{Sr}^{2+}$  adsorbed increased as increasing of  $\text{Sr}^{2+}$  concentration during the flow-through experiments. The largest adsorption value was obtained at pH 8.0 ( $[\text{KNO}_3]=10^{-3}$  M) with  $q_m=41.49$  mg  $\text{Sr}^{2+}/\text{g}$  from the Langmuir isotherm. The amount of  $\text{Sr}^{2+}$  desorbed at pH 4 was only half of the amount desorbed at pH 8, revealing that the retention of  $\text{Sr}^{2+}$  onto smectite was enhanced at pH 4.

The degree of interaction between  $\text{UO}_2^{2+}$  and heterogeneous dioctahedral smectite, characterized by different charge distribution and distinct proportions of tetrahedral and octahedral substitutions, was investigated in order to predict the possible changes on sorption mechanism caused by structural modification of smectite during alteration. The heterogeneous smectite structure used in sorption experiments represents in fact the first alteration stage of smectite exposed to circulation of hydrothermal fluids or as backfilling materials in nuclear waste disposal. The adsorption experiments were carried out to evaluate the role of pH and ionic strength on the  $\text{UO}_2^{2+}$  sorption mechanism. The pH variation influences of the  $\text{UO}_2^{2+}$  aqueous speciation defining the species involved during the sorption mechanism. Also, it may play an important role in the surface sites distribution, controlling the adsorption capacity and the binding strength of surface complexes.

The  $\text{UO}_2^{2+}$  retardation onto heterogeneous smectite samples was studied through the adsorption and desorption experiments using a continuous stirred tank reactor and different pH and ionic strengths conditions (pH 4,  $I=1 \times 10^{-4}$ ; pH=6,  $I=2 \times 10^{-1}$ ). Three different smectite samples characterized by heterogeneous structures, with distinct proportions of tetrahedral and octahedral substitutions, were used. The kinetics of sorption process was interpreted by means of reaction-controlled models (pseudo-first order and pseudo-second order) and diffusion-controlled models (intra-particle diffusion and liquid-film diffusion). The results obtained are in agreement with the previous studies that revealed that multiple surface species are involved on the interaction between  $\text{UO}_2^{2+}$  and smectite, resulted from ion exchange on planar sites at acid pH and surface coordination reactions in the edge sites from near neutral pH at high ionic strengths. The results revealed that the kinetics of sorption process was highly influenced by the structural properties of heterogeneous smectite and the surface complexation mechanism involved. Lower reversibility of the  $\text{UO}_2^{2+}$  previously adsorbed and a stronger complexation was observed at pH 6. The XPS results revealed two binding energies obtained at pH 4,  $380.8 \pm 0.3$  eV and  $382.4 \pm 0.3$  eV, before and after desorption processes. The proportion of the higher binding energy component decreased after desorption process, suggesting that the  $\text{UO}_2^{2+}$  adsorbed in this conditions was

previously desorbed. The results obtained at pH 6 show two different binding energies for smectite samples,  $380.3 \pm 0.3$  eV and  $381.8 \pm 0.3$  eV, whose proportions remained unchanged before and after desorption process, indicating the higher retention of  $\text{UO}_2^{2+}$  on smectite.

The influence of pH, layer charge and crystal thickness distribution was evaluated in the adsorption of  $\text{UO}_2^{2+}$  on different heterogeneous smectite samples, through batch experiments using different pH and ionic strength conditions, pH 4 ( $I=0.02\text{M}$ ) and pH 6 ( $I=0.2\text{M}$ ). The adsorption process was simulated through the development of cation exchange and surface complexation models based on diffuse double layer (DDL). The surface complexation and cation exchange reactions were used on PHREEQC-code to describe the  $\text{UO}_2^{2+}$  sorption on smectite. The amount of  $\text{UO}_2^{2+}$  adsorbed on smectite samples decreased significantly at pH 6 and higher ionic strength, where the sorption mechanism was restricted to the edge sites of smectite. The  $\equiv\text{AlOUO}_2^+$  and  $\equiv\text{SiOUO}_2^+$  were the major surface species involved. The results obtained were compared with the XPS results. Two different binding energy components at  $380.8 \pm 0.3$  and  $382.2 \pm 0.3$  eV assigned to hydrate  $\text{UO}_2^{2+}$  adsorbed by cation exchange and by inner-sphere complexation on the external sites at pH 4 were identified by X-photoelectron spectroscopy after the  $\text{U}4f_{7/2}$  peak deconvolution. Two new binding energy components at  $380.3 \pm 0.3$  and  $381.8 \pm 0.3$  eV assigned to  $\equiv\text{AlOUO}_2^+$  and  $\equiv\text{SiOUO}_2^+$  surface species were observed at pH 6. Both results obtained from the model developed and from the XPS analysis were in agreement.

**Keywords:** heterogeneous smectite, charge distribution, reactivity, layer charge, infrared spectroscopy, X-ray diffraction, structural changes, Strontium; Uranyl, batch and flow-through experiments; breakthrough curves; sorption vs. desorption; kinetic models.



## Resumo

Os minerais argilosos são os principais materiais utilizados para a modelação e selagem de escombreliras e bacias de resíduos radioativos, incluindo resíduos de baixo e médio nível e resíduos de alto nível.

O aumento de temperatura e de pressão, devido ao empacotamento de resíduos radioativos, bem como as condições extremas de pH e a composição química das soluções contaminadas, podem afetar o desempenho e eficácia das argilas, desencadeando alterações estruturais significativas e alterações no mecanismo de adsorção e retenção de contaminantes na superfície da argila. Neste sentido, foram selecionadas para este estudo um conjunto de amostras de esmectite Portuguesa, caracterizadas por estruturas heterogéneas, diferentes cargas estruturais e distribuição de carga heterogénea, com o objetivo de testar o seu comportamento enquanto adsorvente de metais e actinídeos, perante condições distintas de pH e força iónica.

As amostras de esmectite selecionadas foram recolhidas a partir de rochas bentónicas Portuguesas (Ilha de Porto Santo no arquipélago da Madeira e Benavila, Zona de Ossa Morena, Portugal) e submetidas a processos de tratamento e sedimentação, no sentido de recolher a fração pura de argila  $<2\mu\text{m}$ . As amostras de esmectite foram posteriormente submetidas a experiências com o intuito de estudar a sua reatividade nos processos de adsorção de  $\text{Sr}^{2+}$  e  $\text{UO}_2^{2+}$  em condições extremas de pH e força iónica. A heterogeneidade das amostras de esmectite (BA1, PS2 e PS3) foi testada por difração de raios-X (DRX) e espectroscopia de infravermelho (FTIR) após a saturação das amostras de esmectite com  $\text{K}^+$ ,  $\text{Na}^+$  e  $\text{Ca}^{2+}$ . O teste de Greene-Kelly foi também utilizado no estudo da distribuição de carga das amostras esmectíticas, no qual se procedeu à saturação prévia com  $\text{Li}^+$  e posterior solvatação com Glicerol.

No estudo dos processos de adsorção de  $\text{Sr}^{2+}$  na esmectite foram tidas em conta diferentes variáveis, tais como: tempo de contato, pH, concentração de  $\text{Sr}^{2+}$  e força iónica. Os processos de adsorção e desadsorção de  $\text{Sr}^{2+}$  ocorreram a pH 4 e a pH 8, utilizando diferentes concentrações de  $\text{Sr}^{2+}$  (7.00 mg/L, 27.00 mg/L and 34.00 mg/L). O estudo cinético do processo de adsorção teve como base a utilização de um reator de fluxo contínuo com agitação permanente (CSTR), o qual permitiu uma pré-lavagem intensiva e um adequado pré-condicionamento da esmectite, proporcionando assim um controlo adequado das condições químicas impostas. As experiências de fluxo contínuo foram desenvolvidas com

o intuito de avaliar a influência das diferentes condições experimentais impostas nos processos de adsorção e desadsorção. A interpretação dos dados cinéticos foi efetuada através da utilização de diferentes modelos cinéticos. Com o objetivo de estudar o processo de adsorção de  $\text{Sr}^{2+}$  em condições de equilíbrio, utilizando diferentes condições de pH (4 e 8) e força iónica ( $I=10^{-2}$  e  $I=10^{-3}$ ), realizaram-se ensaios em batch que permitiram determinar a quantidade de  $\text{Sr}^{2+}$  adsorvida para diferentes concentrações de  $\text{Sr}^{2+}$  utilizadas em solução. A interpretação destes resultados foi efetuada através da utilização de diferentes modelos isotérmicos (Langmuir and Freundlich).

O grau de interação entre o  $\text{UO}_2^{2+}$  e diferentes amostras de esmectite dioctaédrica, caracterizadas por estruturas heterogéneas que evidenciam diferentes graus de substituições tetraédricas e octaédricas e distribuição de carga heterogéneas, foi investigada com o intuito de compreender quais as consequências da utilização destes materiais nos mecanismos de sorção, tendo em conta que a heterogeneidade da estrutura da esmectite pode ser afetada por processos hidrotermais que ocorrem frequentemente em repositórios. As experiências de sorção podem também ser fortemente influenciadas pela variação de pH e força iónica do meio. Ambos os fatores exercem uma influência significativa quer sobre as espécies de urânio presentes em solução, quer pelas reações que ocorrem na superfície do mineral argiloso e que podem definir o tipo de mecanismo de adsorção mais favorável.

A capacidade de retenção de  $\text{UO}_2^{2+}$  nas diferentes amostras de esmectite foi investigada através de experiências de adsorção e desadsorção que ocorreram a pH 4 ( $I=10^{-4}$ ) e 6 ( $I=2 \times 10^{-1}$ ). Os dados cinéticos foram interpretados através de diferentes modelos cinéticos, incluído os modelos de pseudo-primeira ordem, pseudo-segunda ordem, difusão intra-partícula e modelo de difusão em filme. Os resultados obtidos estão de acordo com estudos prévios que indicaram que o mecanismo de adsorção por troca iónica é dominante em condições acídicas, enquanto que a pH neutro o processo de adsorção dominante ocorre entre o  $\text{UO}_2^{2+}$  e a superfície externa da esmectite ("sitios externos"). Os resultados revelaram que a cinética de ambos os processos de adsorção e desadsorção é influenciada quer pelo grau de heterogeneidade da esmectite, quer pelas condições de pH utilizadas. A pH 6 foi observada maior capacidade de retenção de  $\text{UO}_2^{2+}$ , o que resulta provavelmente de um mecanismo de adsorção de esfera interna na superfície externa da esmectite. Os resultados de XPS obtidos a pH 4 revelam dois componentes com energias de ligação distintas, a  $380.8 \pm 0.3$  eV e  $382.4 \pm 0.3$  eV, antes e após o processo de desadsorção, respetivamente. A proporção do pico correspondente à maior energia de

ligação diminuiu após o processo de desadsorção, o que sugere que parte do  $\text{UO}_2^{2+}$  adsorvido nestas condições foi desadsorvido. Os resultados obtidos a pH 6 revelam 2 novos picos caracterizados por energias de ligação diferentes, 380.3 eV e 381.8 eV, cujas proporções permaneceram inalteradas após o processo de desadsorção, justificando a elevada capacidade de retenção de  $\text{UO}_2^{2+}$  observada nestas condições.

A influência do pH, carga de camada e distribuição da espessura do cristal foi avaliada na adsorção de  $\text{UO}_2^{2+}$  em diferentes amostras de esmectite, caracterizadas por estruturas heterogêneas, através de experiências utilizando diferentes condições de pH e força iónica (pH 4,  $I = 0.02 \text{ M}$ ; pH 6,  $I = 0.2$ ). O processo de adsorção foi simulado através do desenvolvimento de modelos de troca iónica e de complexação na superfície com base na teoria da dupla camada difusa (DDL). As reações que descrevem os processos de troca iónica e de complexação na superfície foram utilizadas no código geoquímico do programa PHREEQC. A quantidade de  $\text{UO}_2^{2+}$  adsorvido em amostras de esmectite diminuiu significativamente a pH 6 e maior força iónica ( $I=0.2$ ), onde as espécies  $\equiv\text{AlOUO}_2^+$  e  $\equiv\text{SiOUO}_2^+$  foram identificadas como as principais envolvidas neste processo. Os resultados obtidos através do modelo desenvolvido foram comparados com os resultados de XPS: A pH 4 foram identificados dois picos a  $380.8 \pm 0.3$  e  $382.2 \pm 0.3$  eV, que foram atribuídos à adsorção de uranilo através de troca iónica e por complexação na superfície externa da esmectite, respetivamente. Dois novos componentes energéticos foram identificados a pH 6, a  $380.3 \pm 0.3$  e  $381.8 \pm 0.3$  eV, atribuídos às espécies  $\equiv\text{AlOUO}_2^+$  e  $\equiv\text{SiOUO}_2^+$ , respetivamente. Os resultados obtidos quer pelo modelo desenvolvido, quer pelas análises de XPS efetuadas, apresentaram consonância.

**Palavras-chave:** smectite heterogênea, distribuição de carga, reatividade, carga de camada, espectroscopia de absorção no infravermelho, difração de raios-X, alterações estruturais, Estrôncio, urânio, experiências de fluxo contínuo; adsorção vs. Desadsorção, modelos cinéticos.



# Contents

Acknowledgment .....	III
Abstract .....	V
Resumo .....	IX
Contents .....	XIII
List of Figures .....	XIX
List of Tables .....	XXIII
List of Acronyms .....	XXV
1. Introduction.....	1
1.1. Framework and Objectives .....	7
1.2. Thesis Structure .....	9
1.3. References .....	10
2. Mineralogy and geology of bentonite rocks in Portugal .....	15
2.1. Clay Minerals: A brief introduction. ....	15
2.1.1. Smectite: The main clay mineral of bentonite rocks.....	19
2.1.1.1. Formation, physico-chemical properties and applications.....	19
2.1.1.2. Total negative charge of smectite: Permanent and variable charge .....	23
2.1.2. Interstratified clay minerals.....	26
2.1.2.1. I-S mixed-layer clay minerals.....	28
2.1.2.2. X-ray diffraction spectroscopy in the identification of mixed-layer clay minerals .....	28
2.2. Geology of bentonite rocks from Portugal.....	30
2.2.1. Bentonite .....	30
2.2.2. Bentonite rocks from Porto Santo Island, Madeira Archipelago .....	30
2.2.2.1. Geology.....	30
2.2.2.2. Bentonite deposits from Porto Santo Island .....	31
2.2.3. Bentonite rocks from Avis.....	32
2.2.4. References .....	34



4.4. Structural characterization and reactivity study of smectite from bentonite rocks of Portugal	68
4.4.1. Introduction	69
4.4.2. Materials and Methods	70
4.4.2.1. Materials	70
4.4.2.2. Experimental Procedures	70
4.4.2.3. Methods and analytical techniques	71
4.4.3. Results and Discussion	73
4.4.3.1. Physical properties and crystal chemistry of smectite samples	73
4.4.3.2. X-ray diffraction	74
4.4.3.2.1. Interpretation	82
4.4.3.3. Infrared spectroscopy	84
4.4.3.3.1. Characterization of vibrational planes of smectite samples	84
4.4.3.4. Conclusion	90
4.4.4. References	91
4.5. Influence of pH, concentration and ionic strength during batch and flow-through continuous stirred reactor experiments of Sr <sup>2+</sup> -adsorption onto montmorillonite	96
4.5.1. Introduction	96
4.5.2. Experimental	98
4.5.2.1. Materials and Techniques	98
4.5.2.2. Kinetics Experiments	98
4.5.2.2.1. Modeling of mass balance	99
4.5.2.2.2. Kinetics models	100
4.5.3. Results and Discussions	104
4.5.3.1. Surface properties and mineralogy of selected material	104
4.5.3.2. Continuous stirred flow-through experiments	104
4.5.3.3. Sorption kinetics	108
4.5.3.4. Sorption isotherm analysis	113
4.5.4. Conclusion	117
4.5.5. References	118

4.6. Kinetics of uranyl ions sorption on heterogeneous smectite structure at pH 4 and 6 using a continuous stirred flow-through reactor .....	121
4.6.1. Introduction .....	122
4.6.2. Materials and Methods .....	124
4.6.2.1. Materials .....	124
4.6.2.1.1. Methods and analytical techniques .....	125
4.6.3. Kinetics of sorption processes .....	127
4.6.3.1. Modelling of mass balance .....	127
4.6.3.2. Kinetic models .....	129
4.6.4. Results and Discussion .....	130
4.6.4.1. Influence of heterogeneous layers and layer charge location distributions .....	130
4.6.4.2. Uranyl aqueous speciation .....	131
4.6.4.3. Continuous stirred flow-through experiments .....	132
4.6.4.3.1. Adsorption experiments .....	134
4.6.4.3.2. Desorption experiments .....	136
4.6.4.4. Kinetics of Sorption-Desorption .....	138
4.6.4.5. X-ray photoelectron spectroscopy .....	144
4.6.5. Conclusion .....	147
4.6.6. References .....	149
4.7. Influence of pH, layer charge location and crystal thickness distribution of U(VI) sorption onto heterogeneous dioctahedral smectite .....	153
4.7.1. Introduction .....	153
4.7.2. Materials and methods .....	156
4.7.2.1. Clay minerals selection and preparation .....	156
4.7.2.2. Methods and analytical techniques .....	157
4.7.3. Experimental .....	160
4.7.3.1. Batch Experiments .....	160
4.7.3.1.1. Isothermal models .....	160
4.7.4. Diffuse double layer surface complexation and cation exchange modelling .....	162

4.7.5. Results and Discussion .....	166
4.7.5.1. Crystal thickness distribution .....	166
4.7.5.2. Effect of layer charge location and heterogeneous layers distribution .....	166
4.7.5.3. $UO_2^{2+}$ aqueous speciation .....	168
4.7.5.4. Modelling the sorption isotherms .....	169
4.7.5.5. Surface complexation and cation exchange modelling .....	173
4.7.5.6. X-ray photoelectron spectroscopy .....	175
4.7.6. Conclusion .....	180
4.7.7. References .....	181
5. Conclusions .....	187



# List of Figures

Fig.1 - Schematic representation of both configurations 1:1 layer and 2:1 layer that form clay minerals structures .....	16
Fig.2 - Montmorillonite structure: a) Ca-montmorillonite and b) Na-montmorillonite .....	22
Fig.3 - Mixed layers formed at different stages of rock cycle: S-smectite, I-illite, K-kaolinite, V-vermiculite and G-glaucinite (Środoń, 1999) .....	27
Fig.4 - Transition process from smectite to illite via interstratified I-S layers .....	29
Fig.5 – Geological map of the N-E Porto Santo Island (after Schmidt and Schmincke et al., 2002) .....	32
Fig.6 - Geological map of Benavila region: the location of Bentonite rocks is delimited by the square contour (Piçarra et al., 2009).....	33
Fig.7 - Different sources of contamination of hydrological systems caused by mining activities.....	48
Fig.8 - Cover system adopted for sealing proposes in Urgeiriça mine.....	54
Fig.9 - Six main types of adsorption isotherms according to the IUPAC classification .....	59
Fig.10 - XRD patterns of samples BA1. a) air-dried and ethylene glycol solvation; b) Li-saturation (Greene-Kelly test); c) K-saturation and heat at 300 °C; d) Mg-saturation and glycerol solvation .....	75
Fig.11 - XRD patterns of sample PS2. a) air-dried and ethylene glycol solvation; b) Li-saturation (Greene-Kelly test); c) K-saturation and heat at 300 °C; d) Mg-saturation and glycerol solvation .....	76
Fig.12 - XRD patterns of sample PS3. a) air-dried and ethylene glycol solvation; b) Li-saturation (Green-Kelly test); c) K-saturation and heat at 300 °C; d) Mg-saturation and glycerol solvation .....	77
Fig.13 - XRD patterns of sample BA1 treated at acid (pH = 2) and alkaline (pH=11) conditions .....	79
Fig.14 - XRD patterns of Ca-saturated smectite sample (BA1) treated at acid (pH = 2) and alkaline (pH=11) conditions.....	79
Fig.15 - XRD patterns of Ca <sup>2+</sup> and Na <sup>+</sup> -saturated smectite samples (BA1, PS2 and PS3) in air-dried conditions and after ethylene glycol solvation .....	81
Fig.16 - Idealization of smectite structure samples used in sorption experiments: a) BA1: beidellite and low-charge montmorillonite interstratified structure; b) PS2: beidellite,	

illite and low-charge montmorillonite randomly interstratified structure; c) PS3: illite and low-charge montmorillonite randomly interstratified structure.....	83
Fig.17 - Infrared spectra of Li-, K- and Na-smectite (BA1, PS2 and PS3) after heating at 300°C during 6 hours. The black lines correspond to the IR spectra of air dried smectite .....	86
Fig.18 - Infrared spectra of Li-smectite (BA1, PS2 and PS3) after 30 min., 3h and 6 h of heating at 300°C. Comparing with pyrophyllite IR spectra. The black lines correspond to the IR spectra of air dried smectite.....	88
Fig.19 - Infrared spectra of Li-smectite (BA1, PS2 and PS3) after heating at 300°C during 6 h before and after glycerol solvation .....	89
Fig.20 - Break-through curves corresponding to adsorption processes at different $\text{Sr}^{2+}$ concentrations and different pH .....	106
Fig.21 - Distribution Coefficients and ratio $q_{ads}/q_{input}$ (%), during the adsorption process .....	107
Fig.22 - Kinetic modeling of the sorption of $\text{Sr}^{2+}$ onto montmorillonite. Pseudo-first order model for adsorption process at pH 4 and pH8, at different $\text{Sr}^{2+}$ concentrations ....	109
Fig.23 - Kinetic modelling of the sorption of $\text{Sr}^{2+}$ onto montmorillonite. Pseudo-second order model for adsorption process at pH 4 and pH8, at different $\text{Sr}^{2+}$ concentrations ....	111
Fig.24 - Kinetic modelling of the sorption of $\text{Sr}^{2+}$ onto montmorillonite. Intra-particle model for adsorption process at pH 4 and pH8, at different $\text{Sr}^{2+}$ concentrations.....	111
Fig.25 - Kinetic modelling of the sorption of $\text{Sr}^{2+}$ onto montmorillonite. Film diffusion model for adsorption process at pH 4 and pH8, at different $\text{Sr}^{2+}$ concentrations.....	112
Fig.26 - Behavior of experimental isotherm data for sorption of $\text{Sr}^{2+}$ . .....	114
Fig.27 - Langmuir isotherms for $\text{Sr}^{2+}$ adsorption onto montmorillonite under different experimental conditions. ....	115
Fig.28 - Freundlich isotherms for $\text{Sr}^{2+}$ adsorption onto montmorillonite under different experimental conditions. ....	116
Fig.29 - Idealization of smectite structures: a) BA1 structure that results from interstratification between beidellite and low charge montmorillonite; b) PS2 interstratified structure that consists on Beidellite, Illite and low charge montmorillonite; c) PS3 structure composed by illite and low charge montmorillonite interstratified	131
Fig.30 - Distribution of uranyl aqueous species: a) from pH 3 to pH 6, using $1.00 \times 10^{-4} \text{M}$ ( $\text{UO}_2^{2+}$ ) and $2.00 \times 10^{-2} \text{M}$ (NaCl) and b) from pH 5 to pH 9, using $1.00 \times 10^{-4} \text{M}$ ( $\text{UO}_2^{2+}$ ) and $2.00 \times 10^{-1} \text{M}$ (NaCl), considering the atmospheric $\text{CO}_2$ effect ( $P=39 \text{ Pa}$ ).....	132

Fig.31 - Breakthrough curves corresponding to the flow-through reactor experiments occurred at pH 4 ( $[U(VI)]=1.0 \times 10^{-4}M$ ). The blank curve corresponds to the theoretical BTC for an inert specie. The pore volume corresponds to the number of reactor volumes that have passed through the reactor .....	133
Fig.32 - Breakthrough curves corresponding to the flow-through reactor experiments occurred at pH 6 ( $[U(VI)]=1.00 \times 10^{-4}M$ ). The blank curve corresponds to the theoretical BTC for an inert specie. The pore volume corresponds to the number of reactor volumes that have passed through the reactor .....	134
Fig.33 - Comparison between experimental desorption curves (pH6 – high I) and predicted desorption curves calculated assuming the total reversibility of the uranyl previously adsorbed and identical rates for de adsorption and desorption processes .....	138
Fig.34 - Kinetics of adsorption and desorption processes of sample BA1 at pH 4 and 6: fit to PFO and PSO models .....	140
Fig.35 - Kinetics of adsorption and desorption processes of sample PS2 at pH 4 and 6: fit to PFO and PSO models .....	140
Fig.36 - Kinetics of adsorption and desorption processes of sample PS3 at pH 4 and 6: fit to PFO and PSO models .....	141
Fig.37 - Kinetics of adsorption at pH 4 and pH 6: fit to intra-particle diffusion model .....	141
Fig.38 - $U4f_{7/2}$ XPS spectra of the U(VI)-smectite samples (BA1, PS2 and PS3), obtained from the flow-through reactor experiments at pH 4 (low I) and pH 6 (High I). Curve fit showing a contribution of two components for $UO_2^{2+}$ ions .....	146
Fig.39 - Comparison of uranium adsorption data on BA1, PS2 and PS3 and the surface complexation model (FITEQL). $[UO_2^{2+}]=1.00 \times 10^{-4}M$ , S:L=3.60, $P_{CO_2}=10^{-3.5}$ Pa, 25°C, I=0.2M .....	165
Fig.40 - Idealization of smectite structure: a) BA1 structure that results from interstratification between beidellite and low charge montmorillonite; b) PS2 interstratified structure that consists on beidellite, illite and low charge montmorillonite; c) PS3 structure composed by illite and low charge montmorillonite interstratified .....	167
Fig.41 - Distribution of uranyl aqueous species: a) from pH 3 to pH 6, using $6.00 \times 10^{-4}M$ ( $UO_2^{2+}$ ) and $1.00 \times 10^{-2}M$ (NaCl) and b) from pH 5 to pH 9, using $1.00 \times 10^{-4}M$ ( $UO_2^{2+}$ ) and $2.00 \times 10^{-1}M$ (NaCl), considering the atmospheric $CO_2$ effect ( $P=39$ Pa).....	168
Fig.42 - Adsorption isotherms describing the $UO_2^{2+}$ adsorption onto different smectites at pH 4 (I=0.02M) and pH 6 (I=0.2M) .....	171

Fig.43 - Sorption of  $UO_2^{2+}$  on smectite at pH4 (I=0.02M) and pH 6 (I=0.2M) as function  $UO_2^{2+}$  equilibrium concentration and its model simulation ..... 176

Fig.44 -  $U4f_{7/2}$  XPS spectra of the U(VI)-smectite samples (BA1, PS2 and PS3), obtained at pH 4 (I=0.02M) and pH 6 (I=0.2M), and fitting curves showing a contribution of two components for  $UO_2^{2+}$  ions ..... 179

# List of Tables

Table 1. Classification of phyllosilicates with emphasis on clay minerals. ....	18
Table 2. Physicochemical parameters of 1:1 and 2:1 clay minerals .....	20
Table 3. Charge distribution on smectite clays for an ideal structure and when isomorphous substitutions occur. Determination of layer charge (general case). ....	23
Table 4. Physicochemical properties of clay minerals .....	42
Table 5. Chemical composition, crystal chemistry, cation exchange capacity and BET of smectite samples .....	73
Table 6. Vibration planes of smectite in the region 1100 - 400 cm <sup>-1</sup> .....	85
Table 7. Amounts of Sr <sup>2+</sup> adsorbed/desorbed and total amounts of Sr <sup>2+</sup> retained by montmorillonite. ....	105
Table 8. Kinetic models parameters for Sr <sup>2+</sup> adsorption onto montmorillonite at pH 8. ...	110
Table 9. Kinetic models parameters for Sr <sup>2+</sup> adsorption onto montmorillonite at pH 4 ....	112
Table 10. Isothermic models parameters for Sr <sup>2+</sup> adsorption onto Montmorillonite .....	114
Table 11. Physicochemical properties of clay minerals .....	124
Table 12. Amounts of UO <sub>2</sub> <sup>2+</sup> adsorbed and desorbed from smectite samples and respective retention capacities.....	133
Table 13. Kinetic parameters obtained from the fit to the flow-through sorption data using different kinetic models .....	139
Table 14. Kinetic parameters obtained from the fit to the flow-through desorption data using the pseudo-first order model .....	142
Table 15. The element composition in atomic concentration (%) and the Si/U and Al/U atomic ratios of the studied samples after UO <sub>2</sub> <sup>2+</sup> sorption in flow-through conditions.....	147
Table 16. Binding energies and relative proportions of the two components fitted to U4f Spectra, obtained from U(VI)-smectite samples .....	147
Table 17. Crystal chemistry and physico-chemical properties of clay minerals.....	156
Table 18. Model parameters used to simulate the UO <sub>2</sub> <sup>2+</sup> adsorption on smectite .....	163
Table 19. Isotherm parameters obtained from Langmuir, Freundlich and SIPS models fit to sorption data.....	172
Table 20. Proportions of UO <sub>2</sub> <sup>2+</sup> adsorbed (%) by cation exchange and by surface complexation on the edge sites.....	174
Table 21. The element composition in atomic concentration (%) and the Si/U and Al/U atomic ratios of the studied samples after UO <sub>2</sub> <sup>2+</sup> sorption in batch experiments .....	175

Table 22. Binding energies and relative proportions of the two components fitted to U4f  
spectra, obtained from U(VI)-smectite samples ..... 177

## List of Acronyms

AAS: Atomic absorption spectroscopy

AMD: Acid mine drainage

ASTM: American Society for Testing and Materials

ATSDR: Agency for Toxic Substances and Disease Registry

BET: Brunauer-Emmett-Teller

CCLs: Compacted clay liners

CEC: Cation exchange capacity

Di: Dioctahedral

EDM: Empresa de Desenvolvimento Mineiro

EPA: Environmental Protection Agency

EG: Ethylene Glycol

FTIR: Fourier transformation infrared

GCLs: Geosynthetic clay liners

GLY: Glycerol

Huc: Half of unit cell

IAEA: International Atomic Energy Agency

I-S: Illite-Smectite

LNEG: Laboratório Nacional de Energia e Geologia

LC: Layer charge

NEA: Nuclear Energy Agency

NRC: Nuclear Regulatory Commission

pH: Potential hydrogen

PZNPC: Point of zero net proton charge

SC/CE: Surface complexation/cation exchange

SCM: Surface complexation model

SEM: Scanning electron microscopy

SSA: Specific surface area

Tr: Trioctahedral

Uc: Unit cell

X: Charge per unit formula

XPS: X-ray photoelectron spectroscopy

XRD: X-ray diffraction

# 1. Introduction

The clay liners are the main materials used to limit seepage from tailings impoundments and to cover solid waste disposal landfills. They consist of compacted clay liners (CCLs) and geosynthetic clay liners (GCLs) whose physic and mechanic properties are distinct (Yilmaz et al., 2008). The GCLs reveal some advantages, when compared to CCLs, including the quicker and easier construction, the lower permeability and the higher capacity to resist to desiccation and freeze/thaw cycles (Li et al., 2009; Well, 1997). However, the GCLs are not recommended due to their small thickness that may trigger a large hydraulic gradient across the liner (Haug and Pauls, 2001).

The GCLs were first developed in the 1980s and consist of thin layers of bentonite (3-6%/m<sup>2</sup>) sandwiched between geotextiles, or bonded onto a geomembrane, including widths of 4 to 5 m and a thickness of 7 to 10 mm in their hydrated state (Nicholson, 2014). The first application of GCLs in a solid waste containment occurred in 1986 near Chicago, USA (Kogel et al., 2006). Nevertheless, specific standards for GCL quality control were not developed and the results of the inconsistent quality control programs applied varied greatly and were not conclusive (Athanasopoulos, 2007). The improvement of GCL properties in the subsequent years led to widespread recognition from community. During this period, several organizations were integrated into the development of standardized procedures and more formal quality control programs (Athanasopoulos, 2007; Harpur, 1992; Koerner, 1997). In 1993, the American Society for Testing and Materials (ASTM), in collaboration with the Geosynthetic Research institute (GRI), promoted the development of 14 consensus standards for GCLs, which were later used industry-wide and worldwide (Harpur, 1992; Koerner, 1997). About 40 near surface disposal facilities for low- and intermediate-level radioactive waste have been in operation since 1980 and the International Atomic Energy Agency (IAEA) was expecting that other 30 will be active in the next 15 year (IAEA, 2012).

Bentonite is a smectite-rich clay of volcanic origin and is the main component of the barrier system (Norris et al., 2014). Smectite clay-minerals are known to exhibit important physicochemical properties such as low hydraulic conductivity, swelling capacity, ion exchange capacity and high surface area (Bergaya and Lagaly, 2013). Gee et al. (1990) have investigated the permeability level that ensures the clay liner integrity, suggesting that 1 m of compacted clay including a permeability in the order of  $10^{-6}$  -  $10^{-9}$  cm/s reveals a proper containment that reduces the level of contamination leaving the impoundments. The

United States Nuclear Regulatory Commission (NRC) required the isolation of low-level waste for 500 years. Specifically, in the case of uranium and thorium mining and milling tailings a period of 1000 years were defined according to the 40 CFR192 rules (NRC, 2007). However, several researchers have concluded that the long-term integrity and performance of the barrier systems is difficult to predict and may be affected by several external and/or internal factors (Cho et al., 1999).

The radioactive waste may be classified according to the NRC (2002) as high-level or low-level waste. High-level waste is a by-product of nuclear reactors activity in the production of electricity, whereas low-level waste is mostly associated with reactor operations, industrial and medical applications (Gieré and Stille, 2004; NRC, 2002). In most cases, it is not intended to recover the low-level waste and it is mainly transported to specific waste disposal sites with appropriate containers or stored on-site until the decay process is concluded and it can be handled as ordinary waste. In the first case, the waste containers are usually isolated by a material such as clay minerals (bentonite) that act as a barrier system (buffer and/or backfill) (NRC, 2002; Pusch and Yong, 2006).

The milling tailings produced during uranium or thorium exploitation activities is characterized as an individual type of waste (Campbell, 2009; NRC, 2002). In this case, the most important challenge is to avoid the dissolution of radioactive particles, deposited in the milling tailings, from rain water, and the efficient treatment of surface water and groundwater already contaminated (Lottermoser, 2010; NEA, 2014). Therefore, several proposals of remediation techniques have been applied in the last years. The “pump and treat” strategy involves the continuously pumping of contaminated groundwater to the treatment system and further deposition in the aquifer (Kuo, 2014). This is particularly efficient for mobile contaminants, which weakly interacts with soil. Another possibility consists in soil washing process that pretends to remove particles with elevated concentrations of contaminant, preventing their percolation and possible water contamination (Wise, 1994). These both conventional techniques may provide an efficient remediation but are expensive and slow (Campbell, 2009). Other conventional technique used for effluent treatment is based on metal precipitation by means of increasing the water alkalinity. However, the results are not satisfactory when the elements remain soluble at pH higher than 7 (Lange et al., 2010). In the last years, the bioremediation processes and the use of engineered waste containment barriers have provided the most satisfactory results (National Research Council et al., 2007). The geosynthetic clay liners (GCLs) is the major containment structures currently used for remediation of tailing ponds (Bouazza and Bowders, 2009; The Organizing Committee of the

14th International Conference on Tailings and Mine Waste, 2010). They are being successfully used for the environment control and safe closure of mining activities. More recently, some research works have also demonstrate their efficiency into retain heavy metals from the mining leachates (Lange et al., 2010). It could be an effective solution to solve the problems related to the current water treatment process, which although have provided good results, releases large quantities of radioactive sludge from effluent treatments (Lottermoser, 2010).

The increase of temperature and pressure due to waste package, or the extreme pH conditions and chemical composition of the contaminated solutions may affect the clay liners performance, causing significant changes in the mechanism of adsorption and contaminant retention on clay surface (National Research Council et al., 2007; Metcalfe et al., 1999).

Consistently, the main external factors identified as affecting their viability were the physical, climatic, geological and environmental factors. Shear tests performed by Shan and Daniel (1991) on three early types of GCLs have confirmed that bentonite based clay liners cannot sustain appreciable tension or shearing forces. Collins (1993) and Rowe (1998) have concluded that the increase of temperature may undergo unfavourable increases in the hydraulic conductivity leading to pollutant infiltration and compromising the clay-liner long-term performance. The geological factors, namely the soil properties and terrain morphology, were also considered important taking into account the risk of infiltration of wastewater and subsequent groundwater contamination, and the risk of flooding in low lands (Popov et al., 2012; Qian et al., 2002). Additionally, the presence of faults may also contribute to stability problems and should be avoided (Qian et al., 2002).

The environmental factors, such as pH, ionic strength and redox conditions of water sources, as well as the physicochemical conditions imposed on the barrier systems, may contribute to chemical incompatibility increasing the hydraulic conductivity of clay barriers (National Research Council et al., 2007; Rahman, 2000; Tournassat et al., 2015). Several researchers have been concluding that the ionic strength in solution increases, as decreasing of pH, leading to more competition between positive ions for the available clay sorption sites and consequent decrease of their retention capacity (Bradl, 2002b; Farrah and Pickering, 1979; Liu et al., 2016). Extremely low and high pH conditions in solutions have also revealed a greater influence in the dissolution of silica and/or aluminium from clay structure, which contributes to form relatively large pores that increases the hydraulic conductivity and reduces the sealing capacity of clay barrier systems (Carroll and Starkey, 1971; Tournassat et al., 2015). Therefore, the detailed investigation of these specific

perturbations in the interaction radionuclide-clay surface, as well as, the adsorption study under flow-through conditions, are both mandatory for a better control of the treatment processes involving engineered barriers or dedicated to remove radionuclides from the dynamic natural systems (surface water and groundwater) (Norris et al., 2014).

Radionuclides existing on earth result from primordial or cosmogenic sources. Primordial radionuclides, such as uranium ( $^{238}\text{U}$ ) or thorium ( $^{232}\text{Th}$ ), formed before and during the creation of earth, are sources of natural radioactivity (Atwood, 2013; Poschl and Nollet, 2006). The 1930s was a decade of world dramatic economic and political changes. During this period, several investigators concluded that the energy produced by nuclear fission could be useful in the development of atomic weapons and nuclear industries in medicine and energy (Krivit et al., 2011; Shultis and Faw, 2007). Later, in 1942, pioneering successfully experiments conducted in the University of Chicago's Stagg Field stadium, involving controlled reactions of nuclear fission, were the first step in the development of nuclear weapons and nuclear industries (Poschl and Nollet, 2006). From this point, the exploitation of radionuclides has increased exponentially, mainly for  $^{238}\text{U}$ , which is the most abundant isotope available on earth that may produce energy from nuclear fission (Hall, 2000; Walther, 2013). Several European countries have been involved in the exploitation of  $^{238}\text{U}$ . In Portugal, important deposits of uranium, related with the late tectonic and metallogenic phenomena that have affected the post-tectonic granite, have been explored between 1950 and 1991, producing about 4200 tons of uranium oxide ( $\text{U}_3\text{O}_8$ ) that was delivered to the British and US nuclear industries (LNEG, 1998). These operations led to extremely long-lived waste that is costly and highly problematic to deal with (Lottermoser, 2007; Merkel and Hasche-Berger, 2008).

Nowadays, the incessant demand for non-renewable energy resources is exceeding their natural production and Nuclear energy is the only energy source that may suppress the world's growing energy needs (Ghosh and Prelas, 2009; Merkel and Schipek, 2011). However, the treatment systems of long-lived nuclear waste produced during radionuclides exploitation are not yet controlled and requires a large capital investment (Azcue, 2012). The release of natural radionuclides in the environment depends primarily on the mining and milling activities, particularly from uranium ores, the nuclear fission products resulted from nuclear weapon tests, the nuclear accidents and the storage of nuclear wastes (Atwood, 2013; Azcue, 2012). Radionuclides may be transported from the mining wastes to the surface water and groundwater causing serious environment impacts and health problems on the communities exposed to high levels of radiation (Lal, 2006). Uranium mining

operation was considered the major contributor in the radiation dose to the global public, once it is the most widespread radionuclide contaminant present in ground water and soil. Therefore, the control and remediation of these contaminated sites is still one of the most important challenges facing by the environmental radionuclide science (Merkel and Schipek, 2011).

Unstable isotopes of strontium (Sr) are also widely used for several industrial and medical applications (Ochs et al., 2015).  $^{90}\text{Sr}$  is currently found in spent fuel rods in nuclear reactors, as a radioactive tracer in medical studies and in agricultural studies (Choppin et al., 2013; Le Gall et al., 2015).  $^{89}\text{Sr}$  was considered an effective systemic radiopharmaceutical for the palliation of bony cancer and  $^{85}\text{Sr}$  is widely used in the production of radiologic imaging of bones (Bahk et al., 2013; Bärenholdt et al., 2009; Guerra et al., 2016). The exposure to high concentration of radioactive strontium may cause severe damage in the human health, such as anaemia and oxygen shortages, and serious risk of cancer resulted by genetic mutations on cells (Agency for Toxic Substances and Disease Registry, 2004; Höllriegl and München, 2011). Consequently, it is of great importance the careful storage of its waste (low-level waste), followed by an efficient treatment, in order to avoid their mobility into the ground and a possible contamination of aquifer resources (Bley et al., 2012; Hamby, 1996).

The influence of pH and ionic strength conditions in the adsorption and retention capacity of strontium and uranium on smectite have been studied in detail by several researchers in order to control and predict the long-term integrity and performance of clay liners. Missana and García-Gutiérrez (2007) have investigated the  $\text{Sr}^{2+}$  adsorption onto FEBEX bentonite and concluded that  $\text{Sr}^{2+}$  adsorption is highly dependent on ionic strength and practically independent on pH. At  $\text{pH} > 8$ , the increase of  $\text{Sr}^{2+}$  adsorbed was more pronounced due to the additional uptake on the external sites of clay surface. It was more significant at higher ionic strengths. In this case, the adsorption process was also characterized by the total saturation of sorption sites as increasing of  $\text{Sr}^{2+}$  concentrations. Galamboš et al. (2009) have also studied the adsorption of  $\text{Sr}^{2+}$  on bentonite samples and have found that as increasing of  $\text{Sr}^{2+}$  concentrations in the solution in equilibrium with bentonite, a decrease of pH is observed, most probably due to the exchange of protons for  $\text{Sr}^{2+}$  on the OH groups.

Contrary to the mechanism of  $\text{Sr}^{2+}$  adsorption, the adsorption of  $\text{UO}_2^{2+}$  on smectite is highly dependent on pH and ionic strength (Chisholm-Brause et al., 2004; Korichi and Bensmaili, 2009; Sylwester et al., 2000). Previous research studies have confirmed that at

low pH and low ionic strength, the  $\text{UO}_2^{2+}$  sorption mechanism is controlled by ion-exchange in the interlayer space, whereas at near neutral pH and high ionic strength the sorption mechanism occurs mainly on the edge sites of smectite, following a decrease in the amount of  $\text{UO}_2^{2+}$  adsorbed (Hennig et al., 2002; Marques Fernandes et al., 2012; Sylwester et al., 2000). The investigators also concluded that the adsorption on the external sites of smectite is characterized by stronger surface complexes (inner-sphere complexes) formed between  $\text{UO}_2^{2+}$  and smectite surface.

The kinetic of radionuclides adsorption on smectite have also been studied in the last years (Bachmaf and Merkel, 2011; Galamboš et al., 2013; Missana et al., 2004). Nevertheless, relatively low information is known about the retention capacity of smectite and the kinetics of desorption process. Moreover, most of kinetics studies have carried out using batch reactors, whose method involves a high dependency of the sorbent sorption behavior on the solid concentration (particle concentration effect) and the permanent accumulation of solutes that increases the risk of precipitation of secondary phases (Brantley et al., 2007; Grolimund, 1998). Regarding to desorption experiments, additionally drawbacks were also identified, such as, the re-suspension of the solid particles that remain compacted at the bottom of the tube. These disadvantages may, however, be overcome by the continuous stirred tank reactors, which allow to identify the factors responsible for apparent deviations in sorption parameters measured under distinct environmental conditions (Brantley et al., 2007; Fernández-Calviño et al., 2010; Grolimund, 1998; Helfferich, 2004) and are characterized by the continuously removal of solution from the system, avoiding reverse reactions and enhancing the study of desorption kinetics phenomena (Grolimund, 1998; Sparks, 1999). Therefore, the use of continuous stirred tank reactors must be considered as a promising method and a better alternative to study the kinetics of sorption processes.

Although the result of various research has been reported in regard to the radionuclides adsorption behavior on montmorillonite (low charge smectite), the effect of the heterogeneous structures of different smectite samples on radionuclides adsorption has generally been neglected and must be subject of study, once it also have substantial influence in the sorption capacity of clay minerals (Dazas et al., 2015; Laird, 2006). Previous research studies have concluded that the swelling capacity of smectite depends on the balance between repulsive forces between 2:1 layers and attractive forces between interlayer cations and the negatively charged 2:1 layers of smectite (Ferrage et al., 2007; Laird, 1996, 1999; Van Olphen, 1965). Therefore the amount of negative charge and charge

location control smectite colloidal behavior and crystalline swelling and influence smectite sorption capacity (Dazas et al., 2015). Consistently, an increase in layer charge increases attractive forces between the hydrated interlayer cation and the 2:1 layers, decreases the interlayer thickness of smectite, reducing their capacity to adsorb by ion-exchange (Laird, 2006). Moreover, the increase of negative charge in the tetrahedral sheet due to hydrothermal alterations tends to form beidellite-like layers and consequently interstratified structures containing low-charge and high-charge layers, as well as, mixed layer structures composed by illite and smectite interstratified that also may influence the sorption behaviour (Ferrage et al., 2007; Sato et al., 1996).

The adsorption/desorption of radionuclides on heterogeneous smectite, as well as, the development of efficient models (SC/CE) in order to predict the behavior of radionuclides adsorption on heterogeneous smectite, may be subject of intense investigation, taking into account the permanent changes (temperature and pressure) occurring in the waste repositories or in the landfill liner systems, which may change the physico-chemical properties of smectite.

## 1.1. Framework and Objectives

The good performance assessments of clay liners have demonstrated their capacity to prevent the risk of radionuclide migration in the environment and avoid adverse effects to the overall ecosystem (Bouazza and Bowders, 2009; Lange et al., 2010). However, previous studies have also suggested their instability, when submitted to extreme environmental conditions, which are dependent on changes in the physicochemical properties of clay minerals and/or the contaminant speciation (National Research Council et al., 2007; Mackey and von Maubeuge, 2004). From a general point of view, this work pretends to evaluate the reactivity of Portuguese smectite as a potential radionuclide adsorbent under extreme environment conditions. The main objectives are contextualized with the research problem and are described as follows.

Most of clay liners include bentonite in their structures, which is mainly composed by smectite (Toll et al., 2008). After long periods of remediation, the increase of temperature and pressure, due to waste package, triggers isomorphic substitutions on smectite structure causing an increase of negative charge in the tetrahedral sheet that contributes to their structural heterogeneity (Laird, 2006; Lee et al., 2010). Therefore, <2 $\mu$ m fractions of three

different smectite samples, characterized by distinct net layer charge and heterogeneous charge distribution, will be used in our sorption experiments in order to understand how the structural changes will influence the adsorption mechanism. It is also pretended to determinate their physicochemical properties and perform a detailed characterization of the respective structures by means of X-ray diffraction and Infrared Spectroscopies.

One of the major consequences resulted from mining activities is associated with the contaminated effluents resulted from acid mine drainage (AMD) (Anawar, 2015). The major causes of this problem are the oxidation process of iron pyrite ( $\text{FeS}_2$ ) and other sulphidic minerals when dissolved in water (Johnson and Hallberg, 2005) and the use of sulphuric acid in the leaching of uranium from the host rock (Merkel and Arab, 2014). The contaminated acid mine waters are usually submitted to the lime neutralization process involving large quantities of calcium sulphate. This excess of  $\text{Ca}^{2+}$  in solution may affect significantly the following treatment procedure, especially using clay minerals as adsorbents, where the exchange of  $\text{Ca}^{2+}$  for  $\text{Na}^+$  will readily occur and drastically change their properties. The use clay mineral in the treatment of radioactive sludge is relatively recent and must be the subject of intense research. Therefore, different smectite samples, with distinct proportions of  $\text{Na}^+$  and  $\text{Ca}^{2+}$  in the interlayer, will be used in our experiments in order to predict the main changes in the sorption and retention properties of smectite, occurring after ion exchange process.

The interaction between clay surface and radionuclide is influenced by a large number of factors including: pH, ionic strength, partial pressure of  $\text{CO}_2$ , amount and structural properties of the adsorbent and contaminant concentration (Pan et al., 2011; Yu et al., 2015; Zhao et al., 2008). The variation of pH and ionic strength will be investigated in our sorption experiments in order to understand how the adsorption mechanism and the adsorbent retention capacity are affected. In this way it will also be possible to predict the consequences of the chemical incompatibility in the clay liners performance. As described before, the chemical incapability is defined by the type and properties of the liquid and the adsorbent, and the physical conditions imposed on the clay barrier.

Two different radionuclides will be considered in this study, strontium ( $^{87}\text{Sr}$ ) and uranium ( $^{238}\text{U}$ ). The influence of their respective concentrations in the adsorption process will also be evaluated.

The mechanism of adsorption of radionuclides on smectite as well as the reversibility of this process are of particular interest in the natural sorbents research field (Chisholm-Brause et al., 2004). The stability of their interaction over time may lead to a considerable

enhancement in the control of radionuclide migration. In this way, the reversibility of the adsorption process and retention capacity of smectite will be studied through flow-through experiments using a continuous stirred flow-through reactor, where the amount of  $\text{UO}_2^{2+}$  or  $\text{Sr}^{2+}$  adsorbed/desorbed will be followed to determinate the stability and retention capacity of smectite under different experimental conditions. These experiments are also particularly important if we consider the use of clay minerals as potential agents in the remediation of contaminated surface water and groundwater, where the adsorbent efficiency in flow-through conditions should be evaluated.

Surface complexation models (SCMs) have been widely used to describe metal ion adsorption on natural adsorbents (Ding et al., 2014; Korichi and Bensmaili, 2009; Rihs et al., 2014). In order to predict the adsorption process of  $\text{UO}_2^{2+}$  on different smectite samples, surface complexation models will be developed on PHREEQC. The sorption data obtained from batch experiments will be compared to the modelled sorption data.

The spectroscopic evidence of the interaction between uranyl and smectite will be investigated by means of X-ray photoelectron spectroscopy analysis (XPS). It is intended to identify and quantify the surface complexation species formed at different pH conditions and ionic strengths, before and after desorption processes. Their proportions will be compared with the proportions obtained by the surface species predicted by the SCM in order to evaluate the viability of the model developed.

## 1.2. Thesis Structure

This thesis was projected according to the article-based format, where a set of research papers published or submitted to publish in international peer reviewed journals are presented. Specifically, we outline the structure of this thesis as follows:

*Chapter I - Introduction.* This chapter introduces a relevant information regarding to the research area and defines the context for the research problems. The main objectives proposed to this project are established in this chapter in order to present the experiments that will be developed to better understand the research problems and improve the knowledge in this topics.

### *Chapter II - Mineralogy and geology of bentonite rocks in Portugal*

This chapter presents information about the structure of clay minerals and their physicochemical properties. The geology of bentonite rocks from Portugal is also discussed.

*Chapter III - Experimental methods and analytical techniques.* It is divided in two parts: The first part is dedicated to the materials selected for sorption experiments and the respective procedure adopted to collect the lower clay fractions, whereas the 2<sup>nd</sup> part describes the methods and analytical techniques used in the present research work.

*Chapter IV - This chapter entitled as “Clay liners reactivity and behavior during metal and actinide sorption experiments at variable pH, ionic strength and concentrations”* is divided in three main parts:

1. The situation point about uranium contaminated sites in Portugal and important cases of study.
2. The interaction between radionuclides and smectite: Sr<sup>2+</sup> and UO<sub>2</sub><sup>2+</sup> cases.
3. The results, respective discussions and conclusions will be provided in this part. It comprises four chapters that corresponds to four scientific papers:
  - Part 1. Reactivity study and characterization of Portuguese heterogeneous smectite;
  - Part 2. Influence of pH, concentration and ionic strength during batch and flow-through continuous stirred reactor experiments of Sr<sup>2+</sup>-adsorption onto montmorillonite;
  - Part 3. Kinetics of uranyl ions sorption on heterogeneous smectite structure at pH 4 and 6 using a continuous stirred flow-through reactor;
  - Part 4. Surface complexation modelling of U(VI) sorption onto heterogeneous dioctahedral smectite: influence of pH, layer charge and crystal thickness distribution.

*Chapter V – Conclusions.*

## **1.3. References**

Agency for Toxic Substances and Disease Registry (ATSDR), 2004. Public health statement: Strontium. Agency for Toxic Substances and Disease Registry.

- Anawar, H.M., 2015. Sustainable rehabilitation of mining waste and acid mine drainage using geochemistry, mine type, mineralogy, texture, ore extraction and climate knowledge. *Journal of Environmental Management* 158, 111-121.
- Athanassopoulos, C., 2007. Beyond MQC: The evolution of quality in a mature GCL industry WasteMINZ Conference, New Zealand.
- Atwood, D.A., 2013. *Radionuclides in the Environment*. Wiley, Oxford Balonov MI.
- Azcue, J.M., 2012. *Environmental Impacts of Mining Activities: Emphasis on Mitigation and Remedial Measures*. Springer Berlin Heidelberg.
- Bahk, Y.W., Lee, M., Wagner, H.N.J., 2013. *Combined Scintigraphic and Radiographic Diagnosis of Bone and Joint Diseases*. Springer Berlin Heidelberg.
- Bärenholdt, O., Kolthoff, N., Nielsen, S.P., 2009. Effect of long-term treatment with strontium ranelate on bone strontium content. *Bone* 45, 200-206.
- Bley, D., Droppo, J.G., Eremenko, V.A., 2012. *Risk Methodologies for Technological Legacies*. Springer Netherlands.
- Bouazza, A., Bowders, J.J., 2009. *Geosynthetic Clay Liners for Waste Containment Facilities*. Taylor & Francis.
- Brantley, S., Kubicki, J., White, A., 2007. *Kinetics of Water-Rock Interaction*. Springer.
- Campbell, K.M., 2009. *Radionuclides in surface and ground water: Handbook of Water Purity and Quality*. Elsevier, Amestardam.
- Carroll, D., Starkey, H.C., 1971. Reactivity of clay minerals with acids and alkalies. *Clays and Clay Minerals* 19, 321-333.
- Chisholm-Brause, C.J., Berg, J.M., Little, K.M., Matzner, R.A., Morris, D.E., 2004. Uranyl sorption by smectites: spectroscopic assessment of thermodynamic modeling. *Journal of Colloid and Interface Science* 277, 366-382.
- Cho, W.J., Lee, J.O., Chun, K.S., 1999. The temperature effects on hydraulic conductivity of compacted bentonite. *Applied Clay Science* 14, 47-58.
- Choppin, G., Liljenzin, J.-O., Rydberg, J., Ekberg, C., 2013. Chapter 18 - Uses of Radioactive Tracers, *Radiochemistry and Nuclear Chemistry (Fourth Edition)*. Academic Press, Oxford, pp. 545-593.
- Collins, H.J., 1993. Impact of temperature inside the landfill on the behaviour of barrier system Proceedings of 4th International Landfill Symposium. CISA, Cagliari, pp. 417-432.
- Dazas, B., Lanson, B., Delville, A., Robert, J.-L., Komarneni, S., Michot, L.J., Ferrage, E., 2015. Influence of Tetrahedral Layer Charge on the Organization of Interlayer Water and Ions in Synthetic Na-Saturated Smectites. *The Journal of Physical Chemistry C* 119, 4158-4172.
- Ding, M., Kelkar, S., Meijer, A., 2014. Surface complexation modeling of americium sorption onto volcanic tuff. *Journal of Environmental Radioactivity* 136, 181-187.
- Fernández-Calviño, D., Pérez-Novo, C., Bermúdez-Couso, A., López-Periago, E., Arias-Estévez, M., 2010. Batch and stirred flow reactor experiments on Zn sorption in acid soils: Cu competition. *Geoderma* 159, 417-424.
- Ferrage, E., Lanson, B., Sakharov, B.A., Geoffroy, N., Jacquot, E., Drits, V.A., 2007. Investigation of dioctahedral smectite hydration properties by modeling of X-ray diffraction profiles: Influence of layer charge and charge location. *American Mineralogist* 92, 1731-1743.
- Galamboš, M., Krajňák, A., Roskopfová, O., Viglašová, E., Adamcová, R., Rajec, P., 2013. Adsorption equilibrium and kinetic studies of strontium on Mg-bentonite, Fe-bentonite and illite/smectite. *Journal of Radioanalytical and Nuclear Chemistry* 298, 1031-1040.
- Galamboš, M., Kufčáková, J., Roskopfová, O.g., Rajec, P., 2009. Adsorption of cesium and strontium on natrified bentonites. *Journal of Radioanalytical and Nuclear Chemistry* 283, 803-813.

- Gee, G.W., Peterson, S.R., Opitz, B.E., 1990. Optimization of linings for prevention of radium dispersion from tailings, *The Behaviour of Radium*. IAEA Technical Report Series 310, Vienna, pp. 163-194.
- Ghosh, T., Prelas, M., 2009. *Energy Resources and Systems: Volume 1: Fundamentals and Non-Renewable Resources*. Springer Netherlands.
- Gieré, R., Stille, P., 2004. *Energy, Waste and the Environment: A Geochemical Perspective*. Geological Society.
- Grolimund, D., 1998. *Mobile colloidal particles in subsurface systems*, Swiss Federal Institute of Technology Zürich.
- Hall, N., 2000. *The New Chemistry*. Cambridge University Press.
- Hamby, D.M., 1996. Site remediation techniques supporting environmental restoration activities—a review. *Science of The Total Environment* 191, 203-224.
- Harpur, W.A., Wilson-Fahmy, R.F., and Koerner, R.M., 1992. Evaluation of the Contact between Geosynthetic Clay Liners and Geomembranes in Terms of Transmissivity, *Proceedings of the 7th GRI Seminar, Geosynthetic Liner Systems: Innovations, Concerns and Designs*. Geosynthetic Research Institute, Drexel University, Philadelphia, pp. 138-149.
- Haug, M.D., Pauls, G., 2001. *A Review of Non-Traditional Dry Covers: MEND 2.21.3b*, Dept. of Civil Engineering. University of Saskatchewan Canada.
- Helferich, F.G., 2004. *Kinetics of Multistep Reactions*. Elsevier Science.
- Hennig, C., Reich, T., Dahn, R., Scheidegger, A.M., 2002. Structure of uranium sorption complexes at montmorillonite edge sites. *Radiochim Acta* 90, 653-657.
- Höllriegel, V., München, H.Z., 2011. Strontium in the Environment and Possible Human Health Effects A2 - Nriagu, J.O, *Encyclopedia of Environmental Health*. Elsevier, Burlington, pp. 268-275.
- Johnson, D.B., Hallberg, K.B., 2005. Acid mine drainage remediation options: a review. *Science of The Total Environment* 338, 3-14.
- Koerner, R.M., 1997. Perspectives on Geosynthetic Clay Liners: Testing and Acceptance Criteria for Geosynthetic Clay Liners, ASTM STP 1308, American Society for Testing and Materials, Philadelphia, pp. 3-22.
- Kogel, J.E., Society for Mining, M., Exploration, 2006. *Industrial Minerals & Rocks: Commodities, Markets, and Uses*. Society for Mining, Metallurgy, and Exploration.
- Korichi, S., Bensmaili, A., 2009. Sorption of uranium (VI) on homoionic sodium smectite experimental study and surface complexation modeling. *J. Hazard. Mater.* 169, 780-793.
- Krivit, S.B., Lehr, J.H., Kingery, T.B., 2011. *Nuclear Energy Encyclopedia: Science, Technology, and Applications*. Wiley.
- Kuo, J., 2014. *Practical Design Calculations for Groundwater and Soil Remediation*, Second Edition. CRC Press.
- Laird, D.A., 1996. Model for crystalline swelling of 2:1 phyllosilicates. *Clays and Clay Minerals* 44, 553-559.
- Laird, D.A., 2006. Influence of layer charge on swelling of smectites. *Applied Clay Science* 34, 74-87.
- Lange, K., Rowe, R.K., Jamieson, H., 2010. The potential role of geosynthetic clay liners in mine water treatment systems. *Geotextiles and Geomembranes* 28, 199-205.
- Le Gall, M., Evrard, O., Thil, F., Foucher, A., Salvador-Blanes, S., Cerdan, O., Ayrault, S., 2015. Tracing Sediment Sources Using Strontium Isotopes in a Pond Draining an Agricultural Catchment (Loire River Basin, France). *Procedia Earth and Planetary Science* 13, 30-34.
- Lee, J.O., Kang, I.M., Cho, W.J., 2010. Smectite alteration and its influence on the barrier properties of smectite clay for a repository. *Applied Clay Science* 47, 99-104.

- Li, G., Chen, Y., Tang, X., 2009. Geosynthetics in Civil and Environmental Engineering: Geosynthetics Asia 2008 Proceedings of the 4th Asian Regional Conference on Geosynthetics in Shanghai, China. Springer Berlin Heidelberg.
- Lal, R., 2006. Encyclopedia of Soil Science. Taylor & Francis, Boca Raton.
- Lottermoser, B., 2007. Mine Wastes: Characterization, Treatment and Environmental Impacts. Springer Berlin Heidelberg.
- Lottermoser, B., 2010. Mine Wastes: Characterization, Treatment and Environmental Impacts. Springer Berlin Heidelberg.
- Mackey, R.E., von Maubeuge, K., 2004. Advances in Geosynthetic Clay Liner Technology: 2nd Symposium. ASTM International.
- Marques Fernandes, M., Baeyens, B., Dähn, R., Scheinost, A.C., Bradbury, M.H., 2012. U(VI) sorption on montmorillonite in the absence and presence of carbonate: A macroscopic and microscopic study. *Geochimica et Cosmochimica Acta* 93, 262-277.
- Merkel, B.J., Arab, A., 2014. Uranium - Past and Future Challenges: Proceedings of the 7th International Conference on Uranium Mining and Hydrogeology. Springer International Publishing.
- Merkel, B.J., Hasche-Berger, A., 2008. Uranium, Mining and Hydrogeology. Springer Berlin Heidelberg.
- Merkel, B.J., Schipek, M., 2011. The New Uranium Mining Boom: Challenge and lessons learned. Springer Berlin Heidelberg.
- Metcalfe, R., Rochelle, C.A., London, G.S.o., 1999. Chemical Containment of Waste in the Geosphere. Geological Society.
- Missana, T., García-Gutiérrez, M., 2007. Adsorption of bivalent ions (Ca(II), Sr(II) and Co(II)) onto FEBEX bentonite. *Physics and Chemistry of the Earth, Parts A/B/C* 32, 559-567.
- Missana, T., García-Gutiérrez, M., Alonso, Ú., 2004. Kinetics and irreversibility of cesium and uranium sorption onto bentonite colloids in a deep granitic environment. *Applied Clay Science* 26, 137-150.
- Nicholson, P.G., 2014. Soil Improvement and Ground Modification Methods. Elsevier Science.
- Norris, S., Bruno, J., Cathelineau, M., Delage, P., Fairhurst, C., Gaucher, E.C., Höhn, E.H., Kalinichev, A., Lalieux, P., Sellin, P., 2014. Clays in Natural and Engineered Barriers for Radioactive Waste Confinement. Geological Society of London.
- United States Nuclear Regulatory Commission (NRC), 2002. Radioactive Waste: Production, Storage, Disposal (NUREG/BR-0216, Revision 2). United States Nuclear Regulatory Commission, Washington DC, p. 34.
- United States Nuclear Regulatory Commission (NRC), 2007. Committee to Assess the Performance of Engineered Barriers, "Assessment of the performance of engineered waste containment barriers" National Academies Press, Washington, D.C..
- Ochs, M., Mallants, D., Wang, L., 2015. Radionuclide and Metal Sorption on Cement and Concrete. Springer International Publishing.
- The Organizing Committee of the 14th International Conference on Tailings and Mine Waste, 2010. Tailings and Mine Waste 2010, International Conference on Tailings and Mine Waste. CRC Press, Colorado, p. 484.
- Tournassat, C., Steefel, C.I., Bourg, I.C., Bergaya, F., 2015. Natural and Engineered Clay Barriers. Elsevier Science.
- Pan, D.-q., Fan, Q.-h., Li, P., Liu, S.-p., Wu, W.-s., 2011. Sorption of Th(IV) on Na-bentonite: Effects of pH, ionic strength, humic substances and temperature. *Chemical Engineering Journal* 172, 898-905.
- Popov, V., Itoh, H., Brebbia, C.A., 2012. Waste Management and the Environment VI. WIT Press.

- Poschl, M., Nollet, L.M.L., 2006. Radionuclide Concentrations in Food and the Environment. CRC Press.
- Pusch, R., Yong, R.N., 2006. Microstructure of Smectite Clays and Engineering Performance. Taylor & Francis.
- Qian, X., Koerner, R.M., Gray, D.H., 2002. Geotechnical Aspects of Landfill Design and Construction. Prentice Hall.
- Rahman, F., 2000. Hydraulic Conductivity and chemical Compatibility of some Victorian Soils used as Liners for Waste Containment, School of the Built Environment. Victoria University of Technology, Melbourne, Australia.
- Rihs, S., Gaillard, C., Reich, T., Kohler, S.J., 2014. Uranyl sorption onto birnessite: A surface complexation modeling and EXAFS study. *Chemical Geology* 373, 59-70.
- Rowe, R.K., 1998. Geosynthetics and minimization of contaminant migration through barrier system beneath solid waste, *Proceedings of 6th International Conference in Geosynthetics* pp. 27-103.
- Sato, T., Murakami, T., Watanabe, T., 1996. Change in layer change of smectites and smectite layers in illite/smectite during diagenetic alteration. *Clays and Clay Minerals* 44, 460-469.
- Shan, H.Y., Daniel, D.E., 1991. Results of laboratory tests on a geotextile/bentonite liner material. *Proc. Geosynthetics* 91, 517-535.
- Shultis, J.K., Faw, R.E., 2007. *Fundamentals of Nuclear Science and Engineering Second Edition*. Taylor & Francis.
- Sparks, D.L., 1999. Kinetics and mechanism of chemical reactions at the soil mineral/water interface. CRC press, Boca Raton, FL.
- Sylwester, E.R., Hudson, E.A., Allen, P.G., 2000. The structure of uranium (VI) sorption complexes on silica, alumina, and montmorillonite. *Geochimica et Cosmochimica Acta* 64, 2431-2438.
- Toll, D.G., Augarde, C.E., Gallipoli, D., Wheeler, S.J., 2008. Unsaturated Soils. *Advances in Geo-Engineering: Proceedings of the 1st European Conference, E-UNSAT 2008, Durham, United Kingdom, 2-4 July 2008*. CRC Press.
- Van Olphen, H., 1965. Thermodynamics of interlayer adsorption of water in clays. I.— Sodium vermiculite. *Journal of Colloid Science* 20, 822-837.
- Well, L.W., 1997. *Testing and Acceptance Criteria for Geosynthetic Clay Liners*. ASTM.
- Walther, J.V., 2013. *Earth's Natural Resources*. Jones & Bartlett Learning.
- White, W.M., 2013. *Geochemistry*. Wiley, Blackwell.
- Wise, D.L., 1994. *Remediation of Hazardous Waste Contaminated Soils*. Taylor & Francis.
- Yilmaz, G., Yetimoglu, T., Arasan, S., 2008. Hydraulic conductivity of compacted clay liners permeated with inorganic salt solutions. *Waste Management & Research* 26, 464-473.
- Zhao, D.L., Feng, S.J., Chen, C.L., Chen, S.H., Xu, D., Wang, X.K., 2008. Adsorption of thorium(IV) on MX-80 bentonite: Effect of pH, ionic strength and temperature. *Applied Clay Science* 41, 17-23.

## 2. Mineralogy and geology of bentonite rocks in Portugal

### 2.1. Clay Minerals: A brief introduction.

Clay minerals are among the most important minerals used by manufacturing and environmental industries. The basic structural units of clay minerals involve the combination of tetrahedral and di- or trioctahedral sheets bounded by shared oxygen atoms that form the aluminosilicate layers (Fig.1) (Brigatti and Mottana, 2011). The tetrahedral sheet consists of a sequence of tetrahedrons which are connected by shared oxygen atoms, whose single structure is characterized by four oxygen atoms bonded together with an internal silicon (Si) and/or aluminium (Al). In the octahedral sheet four apical oxygens and two hydroxyl ions are shared by aluminium (Al), magnesium (Mg) and iron (Fe) atoms to form octahedrons (Fig.1) (Meurant, 2011; Walther, 2013). The dioctahedral structures are characterized by almost exclusively a gibbsite layer, whereas the trioctahedral structures by a brucitic layer (Velde, 2013).

Clay minerals can be classified depending on the arrangement of the tetrahedral and octahedral sheets that form their structural layers (Fig.1): 1:1 layer is assigned to one octahedral layer sitting on the apices of a single tetrahedral layer and 2:1 layer corresponds to one octahedral layer sandwiched between two tetrahedral layers (Yotsumoto, 2011).

The clay minerals can be classified on the basis of variations of chemical composition and atomic structure into nine groups: (1) kaolin-serpentine, (2) talc-pyrophyllite, (3) illite (4) mica, (5) vermiculite, (6) smectite, (7) chlorite, (8) sepiolite-palygorskite and (9) interstratified clay minerals (Huang et al., 2011). The more relevant clay minerals and groups of clay minerals are characterized synthetically as follows (Table 1):

- Kaolinite ( $\text{Si}_4\text{Al}_4\text{O}_{10}(\text{OH})_8$ ; 47%  $\text{SiO}_2$ , 39%  $\text{Al}_2\text{O}_3$  and 14%  $\text{H}_2\text{O}$ ) is included in the kaolin-serpentine group. It is the most refractory of the clay minerals and has several industrial applications due to their low cost, low conductivity of heat and electricity, high plasticity, high-temperature stability and it is chemically inert over a wide range of pH (Allegretta et al., 2015; Murray, 2006; Orbovic and Huang, 2012). Single tetrahedral sheets of silica combine with single octahedral sheets of alumina to form a kaolin 1:1 layer, where two-thirds of oxygen atoms (-O) are shared. In this case,

the charge distribution is balanced in the dioctahedral structure and there is no net layer charge (Reeves et al., 2006).

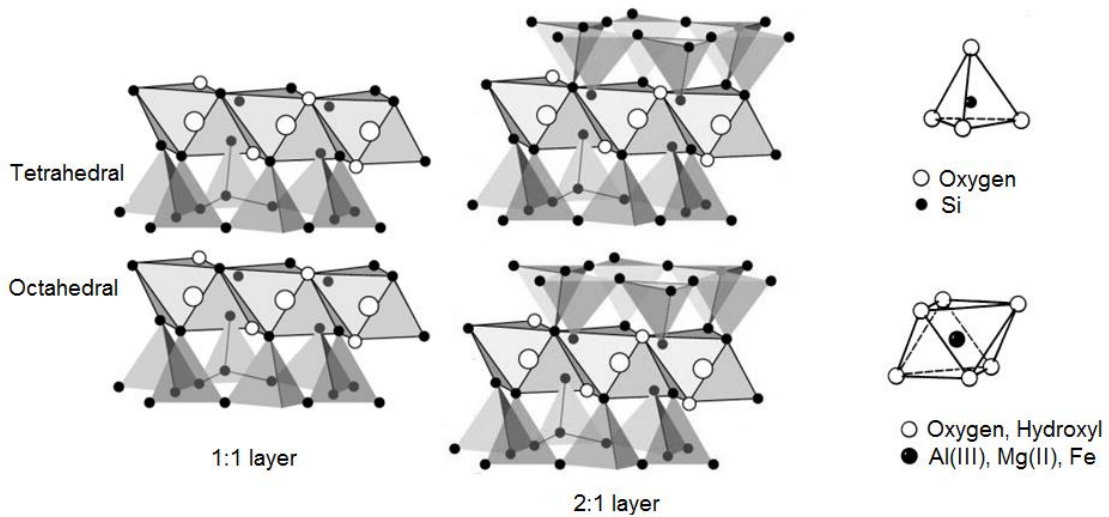


Fig.1 - Schematic representation of both configurations 1:1 layer and 2:1 layer that form clay minerals structures.

- Pyrophyllite ( $\text{Al}_2\text{Si}_4\text{O}_{10}(\text{OH})_2$ ) is a 2:1 phyllosilicate mineral that consists of an octahedral sheet sandwiched by two tetrahedral sheets (Huang et al., 2011; Kogel et al., 2006). It is used as raw material for glass fibers and has several agricultural applications (Kogel et al., 2006). Pyrophyllite has no layer charge and bonding between layers is characterized by weak hydrogen or Van der Waals bonds between oxygen or hydroxide atoms (Strawn et al., 2015).
- Smectite and interstratified clay minerals have special attention in this thesis and will be described in detail in the next chapter.
- Vermiculite is a 2:1 aluminosilicate clay mineral characterized by the chemical formula  $\text{Mg}(\text{SiAl})_4(\text{Al})_2\text{O}_{10}(\text{OH})_2 \cdot 4\text{H}_2\text{O}$ , higher Si:Al ratio (3:1) and higher net layer charge ( $x \sim 0.6-0.9/\text{O}_{10}(\text{OH})_2$ ), which results in higher cation exchange capacity (Lal, 2006). It is an important industrial mineral due to their physicochemical properties. When submitted to high temperature their structural water is readily converted into steam, involving a significant increase of interlayer expansion (8 to 12 times), usually known as thermal exfoliation (Walther, 2013). The product formed is used in several

industrial applications, as well as, in agricultural, horticultural and construction products (Kogel et al., 2006).

- Illite is a dioctahedral 2:1 clay mineral that was originally proposed as a group name to represent all clay-size micas. It is composed by 12% K<sub>2</sub>O, 45% SiO<sub>2</sub>, 38% Al<sub>2</sub>O<sub>3</sub> and 5% H<sub>2</sub>O, and the chemical formula is described by K(Si<sub>3</sub>Al)Al<sub>2</sub>O<sub>10</sub>(OH)<sub>2</sub> (Chesworth, 2007; Meunier and Velde, 2013). Illite is one of the most abundant clay minerals in common clay resources and, more recently, it has attracted more attention as fertilizer for the use in agriculture applications, while its use in industrial applications has been declining (Ke and Stroeve, 2005). The net layer charge of illite ranges between 0.6 and 1.0 per unit cell, resulted from isomorphous substitutions in the tetrahedral sheets (Al for Si) and is counterbalanced by K<sup>+</sup> (Velde and Meunier, 2008).
- Chlorite is a large group of minerals represented by the chemical formula [(M<sup>2+</sup>,M<sup>3+</sup>)<sub>3</sub>(Si,Al)<sub>4</sub>Al<sub>2</sub>O<sub>10</sub>(OH)<sub>2</sub>]<sup>x-</sup>[(M<sup>2+</sup>,M<sup>3+</sup>)<sub>3</sub>(OH)<sub>6</sub>]<sup>x+</sup> and characterized by common properties (Lal, 2006). It is called a 2:1:1 layer mineral since their structure comprises tri-octahedral mica-like layers interspersed with brucite-like layers (Brigatti and Mottana, 2011). The thickness of the chlorite layer is 1.4 nm. The negative charge resulted from the isomorphous substitution of Si<sup>4+</sup> by Al<sup>3+</sup> in the mica-like layer is compensated by brucite-like layer as a result of the substitution of Mg<sup>2+</sup> by Al<sup>3+</sup> (Barnard, 2008). Chlorite may be classified as tri,triocahedral or di,triocahedral whether both 2:1 layer and interlayer hydroxide sheet have a triocahedral structure or a dioctahedral 2:1 layer and a triocahedral interlayer hydroxide sheet, respectively (Sparks, 2003).
- Sepiolite-palygorskite minerals group are distinguished by their fibrous macro- and micro-morphologies, containing ribbons along to the fiber length (Pasbakhsh and Churchman, 2015). They have a 2:1 phyllosilicate structure which include a continuous two-dimensional SiO<sub>4</sub> tetrahedral sheet, where the ribbons are linked each other by the inversion of this tetrahedral structures through Si-O-Si bonds (Burzo, 2009). The oxygen atoms of the octahedral sheet are only coordinated to cations on the ribbon side and the charge balance is compensated by protons, water molecules and exchangeable cations through these channels (Galan, 1996). They have a wide range of industrial applications due to their physicochemical properties such as their crystal morphology, porosity, high surface area, structure and chemical composition (Galan, 1996; Singer and Galan, 2000).

Table 1 includes the groups, subgroups and species that are part of the clay minerals phyllosilicates.

Table 1. Classification of phyllosilicates with emphasis on clay minerals.

Layer Type	Group	Subgroup	Species	
1:1	Serpentine-kaolin (x-0)	Serpentines (Tr)	Chrysotile, antigorite, lizardite, berthierine	
		Kaolins (Di)	Kaolinite, dickite, nacrite, halloysite	
	Talc-pyrophyllite (x-0)	Talc (Tr)		
		Pyrophyllite (Di)		
	Smectite (x-0.2-0.6)	Tr smectites	Saponite, hectorite	
		Di smectites	Montmorillonite beidellite, nontronite	
		Vermiculite (x-0.6-0.9)	Tr vermiculites	
		Illite (x < 0.9 > 0.6)	Di vermiculites Tr illite? Di illite	
	2:1	Mica (x-1.0)	Tr micas	Biotite, phlogopite lepidolite
			Di micas	Muscovite, paragonite
Brittle mica (x-2.0)		Di brittle micas	Margarite	
Chlorite (x variable)		Tr, Tr chlorites	Common, name based on Fe <sup>2+</sup> , Mg <sup>2+</sup> , Mn <sup>2+</sup> , Ni <sup>2+</sup>	
		Di, Di chlorites	Donbassite	
		Di, Tr chlorites Tr, Di chlorites	Sudoite, cookeite (Li)	
2:1	Sepiolite-palygorskite	Inverted ribbons (with x variable)		

Tr = trioctahedral and Di = dioctahedral; x = charge per formula unit. Based on Bailey (1980a,b), Brindley (1981), Hower and Mowatt (1966), and Środoń (1984).

## 2.1.1. Smectite: The main clay mineral of bentonite rocks

### 2.1.1.1. Formation, physico-chemical properties and applications

Smectite is a group of expansible 2:1 phyllosilicate clay minerals which consists of an octahedral sheet, where trivalent ( $\text{Fe}^{3+}$  and  $\text{Al}^{3+}$ ) and divalent cations ( $\text{Mg}^{2+}$  and  $\text{Fe}^{2+}$ ) are octahedrally coordinated by oxygen and hydroxyl ions, sandwiched by two silica tetrahedral sheets through the sharing of the apical oxygen atoms (Bergaya and Lagaly, 2013; Murray, 2006; Sparks, 2013; Wilson, 2013). Smectite group includes a wide number of different minerals that are distinguished by the chemical composition of the octahedral and tetrahedral sheets (Sposito, 1995). Trioctahedral smectites including hectorite, saponite and stevensite are characterized by all three octahedral sites filled, whereas dioctahedral smectites including montmorillonite, nontronite and beidellite only have two-thirds of the total octahedral sites filled (Sparks, 2013). Montmorillonite is characterized by isomorphic substitutions only on the octahedral sheet ( $\text{Fe}$  and  $\text{Mg}^{2+}$  for  $\text{Al}^{3+}$ ) (Bergaya and Lagaly, 2013; Murray, 2006). Beidellite has only tetrahedral substitutions ( $\text{Al}^{3+}$  for  $\text{Si}^{4+}$ ) and nontronite is characterized by both tetrahedral ( $\text{Al}^{3+}$  for  $\text{Si}^{4+}$ ) and octahedral substitutions ( $\text{Fe}^{2+}$  for  $\text{Al}^{3+}$ ) (Wilson, 2013). Therefore, the chemical formula of these three dioctahedral minerals is described as follows (Wilson, 2013).

- Montmorillonite  $\text{M}_x\text{Si}_4(\text{Al}_{2-x}\text{Mg}_x\text{Fe}_x)\text{O}_{10}(\text{OH})_2.n\text{H}_2\text{O}$
- Beidellite  $\text{M}_x(\text{Si}_{4-x}\text{Al}_x)\text{Al}_2\text{O}_{10}(\text{OH})_2.n\text{H}_2\text{O}$
- Nontronite  $\text{M}_x(\text{Si}_{4-x}\text{Al}_x)(\text{Fe}_2^{3+})\text{O}_{10}(\text{OH})_2.n\text{H}_2\text{O}$

Smectite formation is highly dependent on the geological environment, including the environment of sedimentary, weathering and hydrothermal processes (van Breemen and Buurman, 2002). Weathering environment (low temperature) generally involves acidic conditions, with the exception of the case of weathering of mafic rocks, where alkaline conditions control the alteration processes to smectite (Al-Rawas and Goosen, 2006; Xie et al., 2012). The weathering processes comprise four main geological variables: rock type, climate (precipitation and temperature), water flow rate and time. Beidellite tends to be formed under low precipitation and tropical conditions, whereas Fe-montmorillonite and saponite are formed in weathering profiles of basic rocks (Xie et al., 2012). Smectites may also be formed by hydrothermal alteration products of volcanic glass under neutral to alkaline pH, with increasing selectivity for Ca as increasing of temperature. The

hydrothermal alteration of felsic rocks gives rise to smectite with higher content of Na and K, but less Mg and Fe, whereas the mafic rocks alteration produces smectite rich in Mg, Fe and Ca (Al-Rawas and Goosen, 2006; Xie et al., 2012). Nontronite, beidellite and hectorite are relatively rare whereas saponite and montmorillonite are more abundant. Ca-montmorillonite is more abundant than Na-montmorillonite and may be found in several World areas (Murray, 2006).

When compared to other clay minerals, smectite and vermiculite reveal the higher surface areas and higher CEC's (Table 2) (White, 2009). The smaller the clay particle size, the greater the ratio of its surface to volume and, consequently, greater is the specific surface area (Cresser et al., 1993; Lal, 2006). In the case of smectite and vermiculite, the surface area outside is increased by the surface area of the internal surface (Huang et al., 2011). However, vermiculite has lower basal spacing (14Å) and lower tendency to expand than smectite (9.8-1.8+Å), due to their higher layer charge mainly located in the tetrahedral sheet, which results into stronger force of bonding between cations and sheets (Table 2) (Laird, 2006; Sato et al., 1992). Illite presents the higher layer charge which contributes to fix K<sup>+</sup> ions in their structure and, therefore, to reduce significantly their CEC (Schaetzl and Thompson, 2015). Table 2 includes the main physicochemical parameters of phyllosilicates clay minerals.

Table 2. Physicochemical parameters of 1:1 and 2:1 clay minerals.

Clay mineral	Type	CEC (meq/100g)	Layer charge/hfu	Surface area (m <sup>2</sup> /g)	Basal spacing (Å)
Kaolinite	1:1 (non expandable)	3-15	<0.01	5-20	7.2
Vermiculite	2:1 (expandable)	100-150	0.6-0.9	500-700	14
Smectite	2:1 (expandable)	40-150	0.25-0.6	10-800	9.8-18 <sup>+</sup>
Illite	2:1 (non expandable)	10-40	0.7-1.0	50-200	10
Chlorite	2:1:1 (non expandable)	10-40	variable	----	14
Sepiolite /Palygorskite	----	10-45/5-30	----	150-900	----

- White (2009); Wilson (2013); Christidis (2011).

The scope of this thesis focuses on the study of 2:1 dioctahedral smectites where montmorillonite is the most common and important mineral (Ismadji et al., 2015). Montmorillonite is recognized by their structure, chemical composition, high cation exchange

capacity, good swelling properties, high surface area and small crystal size which give rise to several unique properties, including a great sorption capacity, important catalytic applications, interlamellar surfaces with important hydration properties, and the capacity to change the flow behaviour of liquids (Mohamed and Antia, 1998; Odom, 1984; Wilson, 2013). It is widely used as “buffer” barrier in engineered radioactive waste containment systems, owing to their low permeability and high sorption capacity (Chisholm-Brause et al., 2004; Emmerich, 2013; Korichi and Bensmaili, 2009; Turner et al., 1996), and it has also a wide range of industrial and chemical applications, particularly in the civil engineering, cosmetics, paint, medical, agricultural, iron foundry and well oil drilling industries (Al-Rawas and Goosen, 2006; Ciullo, 1996; Ismadji et al., 2015).

The structural data of montmorillonite was firstly provided by x-ray diffraction and electron diffraction studies, which revealed that montmorillonite has a 2:1 pyrophyllite-like structure characterized by isomorphic substitutions, mainly  $Mg^{2+}$  for  $Al^{3+}$ , in the octahedral sheet, which generates negative charge in their structure (Brigatti and Mottana, 2011; Vainshtein et al., 2013). It is also characterized by stacking disorder between the layers that results from physical effects (Wilson, 2013). The XRD pattern allow to identify the exact basal spacing between layers, depending on the exchangeable cation, through the information provided by the basal reflections obtained by diffraction from the (001) planes (Fig.2) (Carroll, 1970; Shah and Shroff, 2003). According to the XRD data, the unit cell of montmorillonite is described by the following parameters:  $a = 5.17 \text{ \AA}$ ,  $b = 8.94 \text{ \AA}$ ,  $c$  is variable according to the exchangeable cation (12-15 $\text{\AA}$ );  $\beta = 99.54^\circ$ ;  $Z = 1$ . The space group corresponds to C2/m or C2 (Vainshtein et al., 2013; Wilson, 2013). Fig.2 a) and b) shows Ca- and Na-montmorillonite structures. Ca-montmorillonite and Na-montmorillonite have significant differences in their properties. Na-montmorillonite has a layer spacing of about 12.5 $\text{\AA}$  and one water layer (1W), whereas Ca-montmorillonite has two water layers (2W) and a layer spacing of 14.2-14.5 $\text{\AA}$  (Murray, 2006). Therefore, Na-montmorillonite has higher swelling capacity and viscosity than Ca-montmorillonite (Ismadji et al., 2015). Na-montmorillonite has the higher cation exchange capacity in the group of dioctahedral smectite, 80-110 meq/100g, and a layer charge that ranges from 0.32 to 0.65 per half of unit cell (Murray, 2006). The total charge of montmorillonite and other dioctahedral smectite minerals is responsible and influences most of smectite properties (Giesecking, 2012).

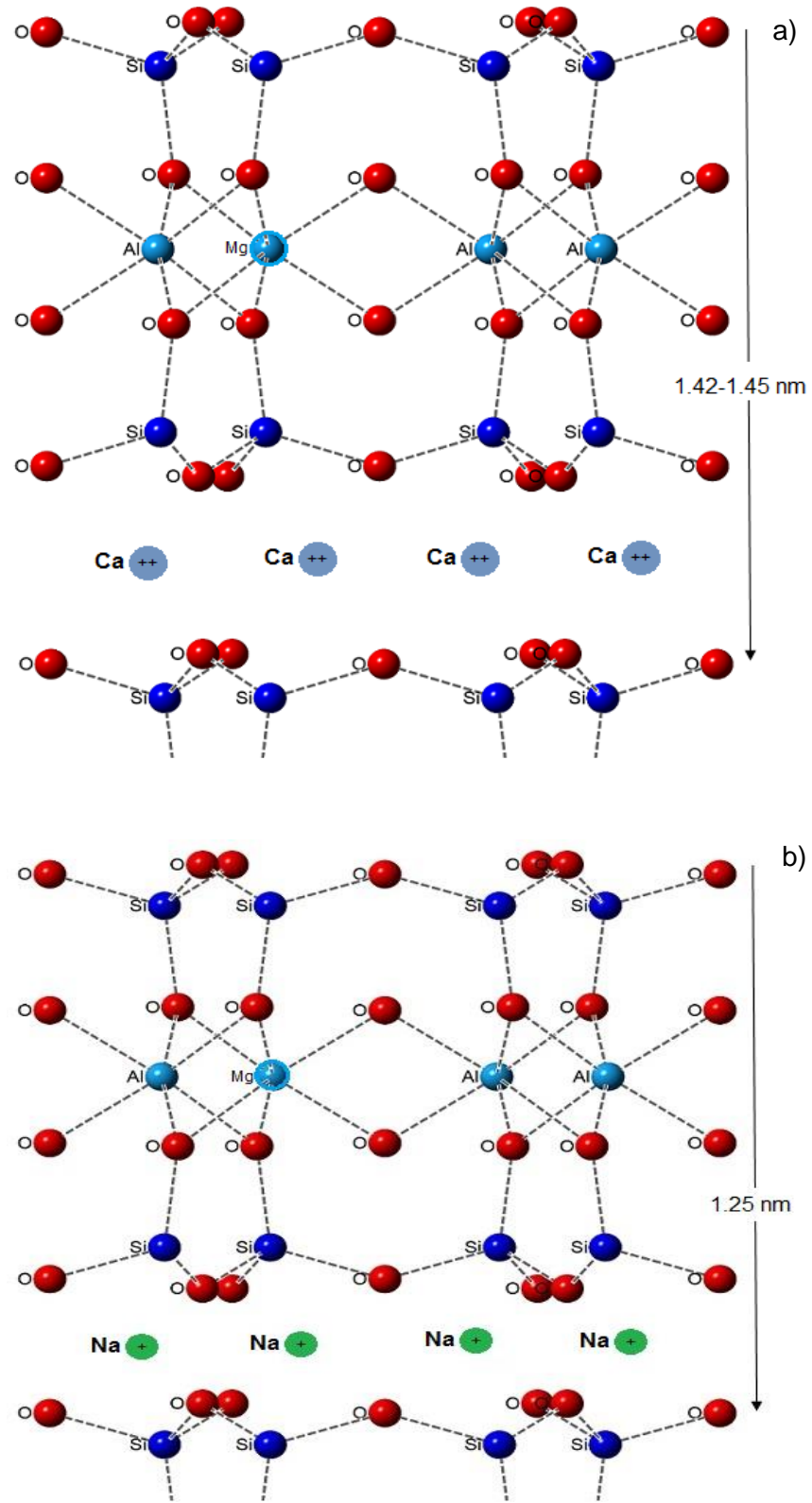


Fig.2 - Montmorillonite structure: a) Ca-montmorillonite and b) Na-montmorillonite.

### 2.1.1.2. Total negative charge of smectite: Permanent and variable charge

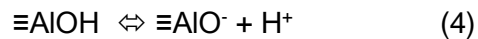
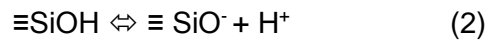
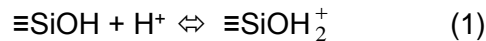
The permanent negative charge on the basal planes resulted by isomorphous substitutions, either in the octahedral sheet or in the tetrahedral sheet, is the main contribution to the surface charge of dioctahedral smectite minerals such as montmorillonite or beidellite (Bourg et al., 2007; Kaufhold and Dohrmann, 2013). This charge may be more diffuse or concentrated according to their location in the octahedral and/or in the tetrahedral sheets, respectively (Barany, 2012). The isomorphous substitutions create negative charge when these replacements are between atoms of distinct electrovalence and identical ionic radii (Essington, 2015). However, the electrovalence of the atom only differs one unity from the atom replaced (Mering, 1975). The negative charge acquired may be estimated based on smectite chemical formula, according to the equation deduced in Table 3 (Dobias, 1993; Sparks, 2013). This layer charge is compensated by exchangeable cations located in the interlayer region (Dobias, 1993; Somasundaran, 2006), according to the charge balance described in Table 3.

Table 3. Charge distribution on smectite clays for an ideal structure and when isomorphous substitutions occur. Determination of layer charge (general case).

	Ideal structure		Structure with Isomorphous substitutions	
	Ions	Charge	Ions	Charge
Interlayer	H <sub>2</sub> O + cations	<sup>+</sup> (variable)	H <sub>2</sub> O + cations	<sup>+</sup> (variable)
Tetrahedral sheet	6 O <sup>2-</sup>	-12	6 O <sup>2-</sup>	-12
	4 Si <sup>4+</sup>	+16	x <sub>1</sub> Si <sup>4+</sup> + y <sub>1</sub> M <sup>3+</sup>	x <sub>1</sub> *4 + y <sub>1</sub> *3 (+)
Contact layer	4 O <sup>2-</sup> + 2 OH <sup>-</sup>	-10	4 O <sup>2-</sup> + 2 OH <sup>-</sup>	-10
Octahedral sheet	4 Al <sup>3+</sup>	+12	x <sub>2</sub> Al <sup>3+</sup> + y <sub>2</sub> M <sup>2+</sup>	x <sub>2</sub> *3 + y <sub>2</sub> *2 (+)
Contact layer	4 O <sup>2-</sup> + 2 OH <sup>-</sup>	-10	4 O <sup>2-</sup> + 2 OH <sup>-</sup>	-10
Tetrahedral sheet	4 Si <sup>4+</sup>	+16	x <sub>3</sub> Si <sup>4+</sup> + y <sub>3</sub> M <sup>3+</sup>	x <sub>3</sub> *4 + y <sub>3</sub> *3 (+)
	6 O <sup>2-</sup>	-12	6 O <sup>2-</sup>	-12
Interlayer	H <sub>2</sub> O + cations	<sup>+</sup> (variable)	H <sub>2</sub> O + cations	<sup>+</sup> (variable)
Layer charge		0	-44+[(x <sub>1</sub> *4 + y <sub>1</sub> *3)+(x <sub>2</sub> *3 + y <sub>2</sub> *2)+(x <sub>3</sub> *4 + y <sub>3</sub> *3)]<0	
Total charge (layer+interlayer)		0	0	

The natural acidity of dioctahedral smectite are defined by the Brönsted and Lewis sites (Lewinsky, 2007; Misaelides, 1999). The Brönsted sites are related with the water molecules coordinated to the exchangeable cations, whereas the Lewis sites correspond to the  $\text{Al}^{3+}$  coordination centre when  $\text{Si}^{4+}$  is replaced by  $\text{Al}^{3+}$  in the tetrahedral sheet (Hubbard, 2002; Lewinsky, 2007; Nagy and Konya, 2009). The Brönsted acidity is defined as the surface capacity to donate protons and is quantified by the amount of exchangeable cations in the interlayer and by the polarization effect of coordinated waters (Yariv and Cross, 2001). For another hand, the Lewis sites have great affinity for a pair of electrons in an unoccupied orbital and, therefore, the internal acidity of smectite increases as increasing of isomorphous substitutions in their structure (Hubbard, 2002; Yariv and Cross, 2001).

The variable charge of smectite results from additionally amphoteric sites, mainly aluminol ( $\text{AlOH}$ ) and silanol ( $\text{SiOH}$ ) groups, which were formed by the hydrolysis of Al and Si atoms exposed to crystallite edges (Bourg et al., 2007; Kaufhold and Dohrmann, 2013; Tombácz and Szekeres, 2004). Silanol and aluminol sites may be protonated or deprotonated, depending on the pH, according to the following reactions (Tombácz and Szekeres, 2004; Zrinyi et al., 2004):



The point of zero net proton charge (PZNPC) corresponds to the pH where the number of sites positively charged equals the number of sites negatively charged ( $\sigma_{0,H}=0$ ) (Misaelides et al., 2012; Tombácz and Szekeres, 2004). Consequently, the net proton surface charge is positive ( $\sigma_{0,H}>0$ ) below the pH of the PZNPC, and negative ( $\sigma_{0,H}<0$ ) above this point (Lagaly and Dékány, 2013; Misaelides et al., 2012). The variable charge has no contribution to the intrinsic surface charge density ( $\sigma_{in}$ ) when  $\sigma_{0,H}=0$  and, therefore, it is only dependent of the permanent charge ( $\sigma_0$ ) (Tombácz and Szekeres, 2004). According to the following equation, the intrinsic surface charge density ( $\sigma_{in}$ ) results from the sum of the net proton surface charge ( $\sigma_{0,H}$ ) and the net permanent structural charge density ( $\sigma_0$ ) (Hoddinott et al., 1990; Tombácz and Szekeres, 2004; Tournassat et al., 2015).

$$\sigma_{in} = \sigma_0 + \sigma_{0,H} \quad (5)$$

The understanding of the influence of surface charge variation on smectite properties has awakened a great interest in the scientific community (Lagaly and Dékány, 2013). The surface charge of smectite, as well as, the electrolyte concentration, the dielectric constant of the electrolyte pore fluid, the valence and size of the cation and the temperature, affect different double-layer parameters including the double-layer thickness, the surface charge and surface potential (Sumner, 1999; Yu, 1997). The diffuse double-layer theory explains basic phenomena occurring in the clay-water-electrolyte system, including flocculation and dispersion, osmotic swelling and particles orientation depending on the range of repulsive and attractive forces (Fang, 2013; Fang and Daniels, 1997). The flocculation and dispersion states will define the behavior of smectite and other clay minerals in different industrial and environmental applications (Fang, 2013; Hoddinott et al., 1990; Ratta and Lal, 1998).

Other important investigations regarding to the influence of layer charge distribution in the physicochemical properties of smectite were also conducted by several authors (Dazas et al., 2015; Ferrage et al., 2005; Ferrage et al. 2007). It is well known that the increase of temperature induces the replacement of  $\text{Si}^{4+}$  by  $\text{Al}^{3+}$  in the tetrahedral sheet of smectite, increasing the tetrahedral layer charge and reducing the cation exchange capacity (CEC) and the swelling capacity of smectite (Inoue et al., 1992; Lee et al., 2010). The consequences of this phenomena may be observed when the performance of smectite as an engineered barrier in a high-level waste repository is affected. It results from the diagenetic alteration of smectite that triggers structural changes on their structure and tends to transform low charge montmorillonite into illite, through the formation of interstratified structures commonly designated by “mixed layers illite-smectite” (Cuadros and Linares, 1996; Inoue et al., 1992; Pytte and Reynolds, 1989). It was also reported that interstratified montmorillonite/beidellite minerals may be formed in the early stages of the illitization process. The assumption that a proportion of high charge layers are formed before  $\text{K}^+$  fixation and subsequent Illitization is admitted by several authors (Meunier et al., 2000; Sato et al., 1996).

Previous studies have also reported that the increase of tetrahedral charge enhances the electrostatic attraction between interlayer cations and smectite layers, reducing the interlayer distance and therefore the mobility of water molecules (Christidis et al., 2006; Dazas et al., 2015; Ferrage et al., 2005; Ferrage et al., 2007; Laird, 2006).

Previous studies have contradicted the conventional wisdom that high-charge layers are less hydrated than low-charge layers, since it was observed an increase of interlayer H<sub>2</sub>O molecules and their successive reorganization as layer charge increases (Dazas et al., 2015; Ferrage et al., 2005; Ferrage et al., 2007). Therefore, the increase of tetrahedral charge is associated with the higher stability of most hydrated layers and the more organized interlayer cation distribution, as well as, with the higher attraction between the interlayer cation and smectite surface and the lower capacity of smectite to swell (Laird, 2006).

Generally, the layer charge and charge distribution of smectite are evaluated through the solvation properties of the expandable K<sup>+</sup>-Smectite and Li<sup>+</sup>-Smectite in Ethylene Glycol (EG) and Glycerol (GLY), respectively (Christidis and Eberl, 2003; Mosser-Ruck et al., 2005). This subject will be addressed in detail in the third part of this thesis, where the layer charge and charge distribution of Portuguese smectite are studied.

### **2.1.2. Interstratified clay minerals**

Interstratified clay minerals or mixed-layer clay minerals are materials in which individual crystals are composed by basic unit layers of more than one clay mineral, where the octahedral and tetrahedral sheets have identical crystal chemical and geometrical characteristics (Meurant, 2011; Moore and Reynolds, 1997; Worden and Morad, 2009). They are also identified as intermediate products of natural environment reactions involving surface to low-grade metamorphic and hydrothermal conditions, which are highly influenced by the increase of temperature and pressure, time, shearing phenomena and fluid movements, associated with faults (Środoń, 1999). It is also important to note that micro- and macro-organisms may play an important role in the formation mixed-layer clay minerals (Masuda et al., 2001). This process is characterized by the slow transformation of smectite into illite and chlorite, during burial diagenesis, where intermediate mixed-layer phases such as illite-smectite and chlorite-smectite are formed (Kim et al., 2004). Fig.3 resumes the occurrence of mixed layers at different processes of rock cycle.

The identification of interstratified clay minerals depends on the type of layers involved, in which each basic unit may be represented as a layer of smectite, illite, vermiculite, chlorite, kaolinite, glauconite, talc, serpentine or biotite (Fiore et al., 2010). The most common are, however, smectite, illite, vermiculite and chlorite (Fiore et al., 2010). The nomenclature of mixed-layer clay minerals consists into introduce both clay mineral names

separated by hyphen (e.g. illite-smectite, mica-vermiculite, etc), in which the first mineral is chosen by the smaller d-spacing (Brindley and Brown, 1982; Fiore et al., 2010; Giesecking, 2012). In this chapter, the characterization of I-S mixed layer clay minerals will be highlighted.

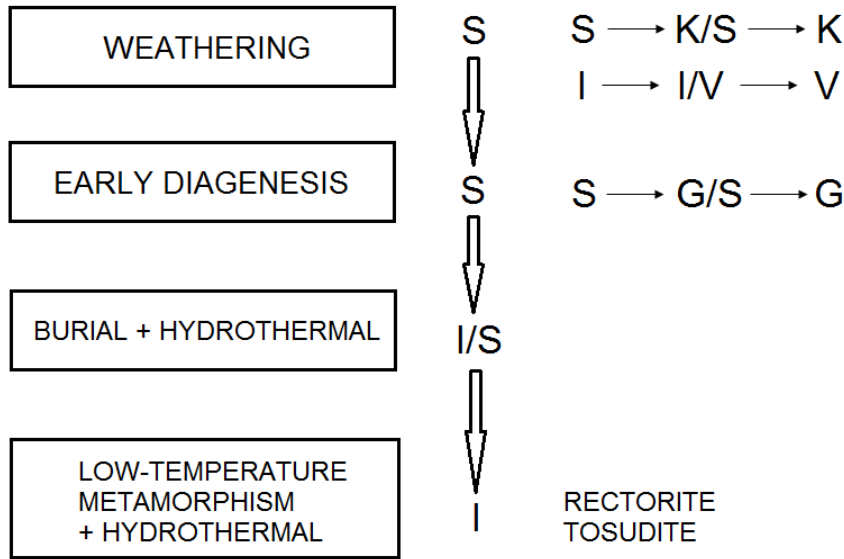


Fig.3 - Mixed layers formed at different stages of rock cycle: S-smectite, I-illite, K-kaolinite, V-vermiculite and G-glaucinite (Środoń, 1999).

Mixed-layer clay minerals may be randomly interstratified, when no discernible pattern occurs in the sequence of layer types, ordered, when it is observed a periodic stacking sequence, or partially ordered whether both conditions are identified (Bergaya and Lagaly, 2013; Inoue et al., 2005). According to Reynolds (1980), the probability of one type of layer occurring next to another is given by the grade of ordering “R” (Reichweite) of mixed layers. In this way, R0 is associated with mixed layers characterized by random interstratification and disorderly stack sequence (ABABBAAAABAAB...). R1 corresponds to mixed-layer clay minerals where the stack sequence is partially regular (ABABABABA...). R2 corresponds to a specific case where the existence of a layer B is determined by the two previous layers (AABAABAABAAB...), and R3 identifies mixed layers characterized by regular sequences of interstratification and long-range ordering (BAAABAAABAAA...)

(Inoue et al., 2005; Reynolds, 1980; Velde and Meunier, 2008).

### 2.1.2.1. I-S mixed-layer clay minerals

As previously described, the diagenetic alteration of smectite minerals during burial diagenesis is one of the most important source of I-S interstratified clay minerals (Larsen and Chilingar, 1983; Nieto and Livi, 2013; Środoń, 1999). The proportion of each type of layer in the I-S phases, as well as, the ordering of stacking sequence, provides important details about the progress of diagenesis process, including the depth and temperature involved in the illitization process (Fiore et al., 2010; Meunier and Velde, 2013). The use of X-ray diffraction method has been a key tool in the identification of clays and mixed-layered phases, and also to determine the proportion of each layer component and the ordering of layer stacking (Drits et al., 2012; Meunier, 2005). Previous XRD results have revealed that the proportion of contracted layers (illite layers -  $10\text{\AA}$ ) increases as increasing of depth of burial process (Eberl, 1978; Meurant, 2011). They also show that as increasing of temperature, there are more contracted layers and the layer stacking is subsequently more ordered (R0 to R3) (Drits et al., 2012; Moore and Reynolds, 1997; Potter et al., 2005; Reeves et al., 2006). According to Huggett and Cuadros (2005), the I-S mixed-layers may have a random distribution, during the burial diagenesis, even at high illite content. More specifically, the I-S R0 sequence is obtained between 0 and 60% of illite layers (Fiore et al., 2010). The R1 sequence corresponds to the range 60-75% of illite, and the R3 sequence is characterized by 75% to 100% of illite (Fiore et al., 2010). Fig.4 represents the transition process from smectite to illite via interstratified I-S layers. This transitions occurs progressively under increasing burial over the temperature range of  $50^{\circ}$  to  $200^{\circ}$  (Ryan, 2014).

### 2.1.2.2. X-ray diffraction in the identification of mixed-layer clay minerals

Mixed-layer clay minerals are mainly characterized by the distance between the layers of their components (Brigatti and Mottana, 2011). The XRD analysis takes into account their distinct swelling capacities which produce different d-spacing in the  $c^*$  direction of the two layer types within the diffraction domain (Drits et al., 2012). Mixed-layer minerals are prepared as oriented mounts in order to facilitate the analysis of the basal diffraction peaks (001) and improve their characterization (Fiore et al., 2010). These samples are previously treated with an organic compound that causes layer swelling to a very well defined d-spacing (Merlino, 1997). Ethylene glycol (EG) and glycerol (GLY) are the most frequent organic compounds used for this purpose (Fiore et al., 2010; Reeves et al., 2006; Wilson, 2013). The d-spacing is changed on solvation with EG and/or GLY and after heating

depending on the composition of the mixed-layer phase (Inoue et al., 2005; Reeves et al., 2006).

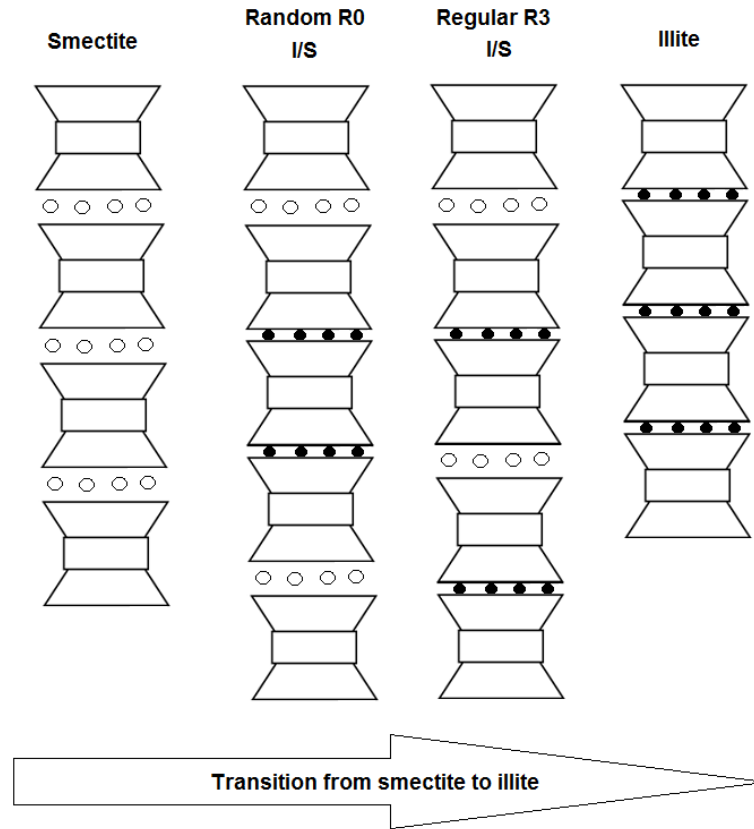


Fig.4 - Transition process from smectite to illite via interstratified I-S layers.

The mineral identification by XRD analysis consists on the direct comparison between the experimental diffractogram and those calculated for a structure model (Brigatti and Mottana, 2011; Reeves et al., 2006). This process is based in a trial-and-error procedure, where structure models include the number, the nature and proportions of the different layer types and information about layer stacking sequence (Brigatti and Mottana, 2011). When this sequences are identical to all XRD experimental profiles of the same sample, a consistent structure model is produced and it is observed a good agreement between the experimental and calculated XRD patterns. NEWMOD program was developed by Reynolds (1985) and is one of the most used programs to identify and quantify mixed-

layer clay minerals. The program simulates XRD patterns for mixed-layer clays which can be compared with the experimental XRD patterns (Reeves et al., 2006; Reynolds, 1985).

## **2.2. Geology of bentonite rocks from Portugal**

### **2.2.1. Bentonite**

The term “bentonite” is defined by geologists as a rock formed by highly colloidal and plastic clays composed mainly of montmorillonite, a clay mineral of the smectite group, which is produced by in situ devitrification of volcanic ash (Parker, 1988). The transformation of ash to bentonite apparently takes place only in water (certainly seawater, probably alkaline lakes, and possibly other fresh water) during or after deposition (Grim, 1968; Patterson and Murray, 1983). Bentonite term is based in Fort Benton (Wyoming, USA), the locality where it was first found. In addition to montmorillonite, bentonite may also contain feldspar, biotite, kaolinite, illite, cristobalite, pyroxene, zircon, and crystalline quartz (Parkes, 1982).

Usually, the term bentonite is applied commercially to any plastic, colloid, and swelling clay regardless of its geological origin.

### **2.2.2. Bentonite rocks from Porto Santo Island, Madeira Archipelago**

#### **2.2.2.1. Geology**

Porto Santo is located ca. 700 km off NW-Africa. Bathymetry shows that the island represents the partly eroded subaerial portion of a much larger submerged edifice (ca. 80 km<sup>2</sup> - 40 km) that rises from water depths of more than 3,000 m. The edifice has a flat top at ca. 100 m below sea level (b.s.l) and is star-shaped in plan view with a prominent NW–SE oriented rift zone. Volcanic rocks comprise dominantly alkali basalts, with minor mugearites, benmoreites, trachytes, and rhyolites (Schmincke and Weibel 1972). Most rocks exposed on the island are submarine in origin. The submarine series can be divided into an older, trachytic series (intrusions, flows, and related hyaloclastites) unconformably overlain by a basaltic-hawaiitic submarine to subaerial series (pillow lavas, associated hyaloclastite

breccias, and intercalated fossil-bearing calcarenites grading into subaerial lava flows towards the top of the section).

Submarine rocks occur at least as high as 300 m above sea level, indicative of uplift of the island, lowering of sea level, or both (Schmincke and Staudigel 1976; Feraud et al. 1981). Fossiliferous limestones intercalated with volcanic deposits are of mid-Miocene (ca. 14 Ma) age (Lietz and Schwarzbach 1970). K/Ar ages indicate that most of the exposed volcanic rocks were emplaced between 12.5 and 13.8 Ma (Macedo et al. 1974; Feraud et al. 1981). Our new age data from subaerially exposed rocks of Porto Santo, discussed more fully elsewhere, indicate that this part of the volcano was formed between ca. 14 and 10 Ma (Geldmacher et al.; 2000). First emergence of the volcano occurred around 14 Ma, whereas younger rocks are subaerially erupted and submarine and/or subaerially emplaced.

#### 2.2.2.2. Bentonite deposits from Porto Santo Island

Porto Santo has several bentonite deposits, located in the oriental part of the island of Porto Santo, which are characterized by unique properties in the Portuguese territory. The deposits occur above and below the sea level and were probably formed by the alteration of volcanic tuffs rich in glass, which were deposited successively on the island platform during the activity of explosive volcanism (Miocene) (Ferreira and Serrano, 1971).

Bentonite rocks used in the sorption experiments were collected from the Serra de Dentro area of Porto Santo Island. The geological map of the N-E region of the Porto Santo area is shown in Fig. 5., and the area with bentonite rocks is delimited by the square contour.

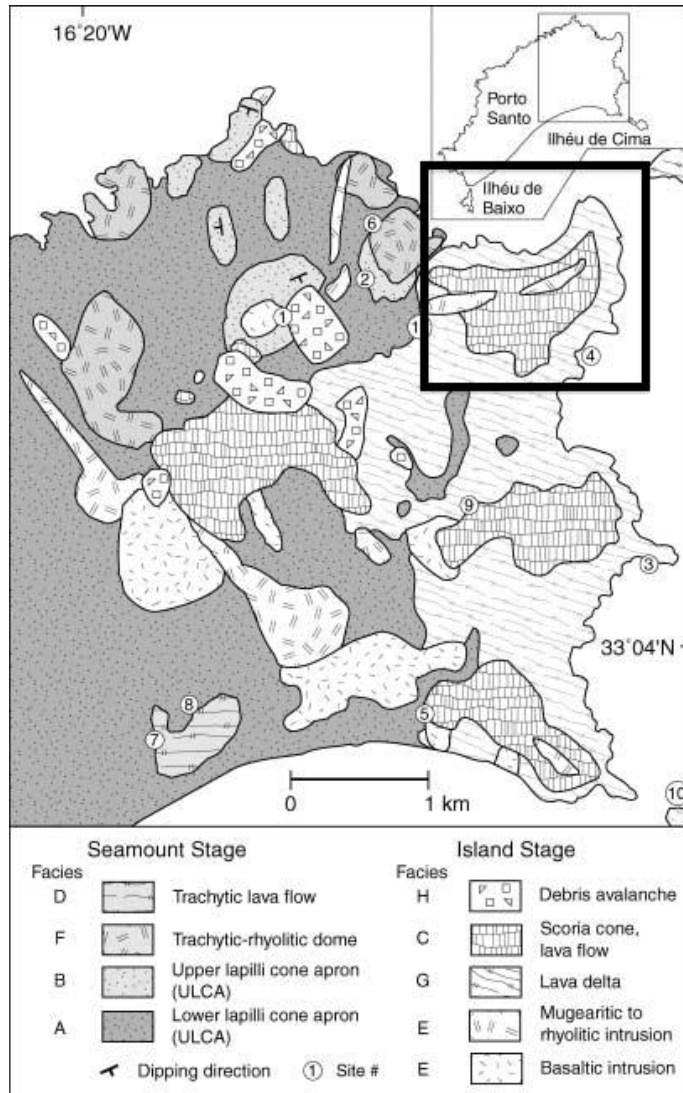


Fig.5 – Geological map of the N-E Porto Santo Island (after Schmidt and Schmincke et al., 2002).

### 2.2.3. Bentonite rocks from Avis

The igneous outcrop of Benavila is located along the Ribeira de Sede, southeast of Ponte de Sôr, implanted in the lower Silurian rocks. The contact of these rocks is only viewed from the East and West, because is partly covered by Tertiary deposits of the Tagus basin. These deposits are constituted by greenish loamy clay of continental facies probably of Miocene age (Carvalho et al., 1980). Petrographic characteristics of Benavila rocks lead to consider them similar to the rocks neighbour to Ervedal, Frontier and Santa Eulalia. However, this region rocks such as Sta Eulalia are more diverse than the first two mentioned

ranges, by checking if also the presence of gabbros (Goncalves, 1978). The massif is cut by several NW- SE lodes, which mostly are of granitic rock.

Benavila bentonite, collected from the Hercynian Massif, was considered an alteration product of granodiorite rocks (Benavila Massif, Torrejana area), which can be dated as a paleogenic deposit (Dias et al. 2004; Rebelo et. al, 2010). The composition of the weathering product is highly influenced by the chemistry and mineralogy of the granodiorite rock, as well as, by the topography, biological activity, and climate. In this case, the weathering product is mainly composed by Fe-rich smectite and different proportions of typical associated minerals (mainly calcite) (Rebelo et. al, 2010). The Geological and Mining Institute of Portugal refers to these clay materials as very pure bentonites with relevant technological characteristics and exposure conditions (Rebelo et al., 2011; SFM, 1993). However, it requires previous laboratory treatment, due to their specific properties.

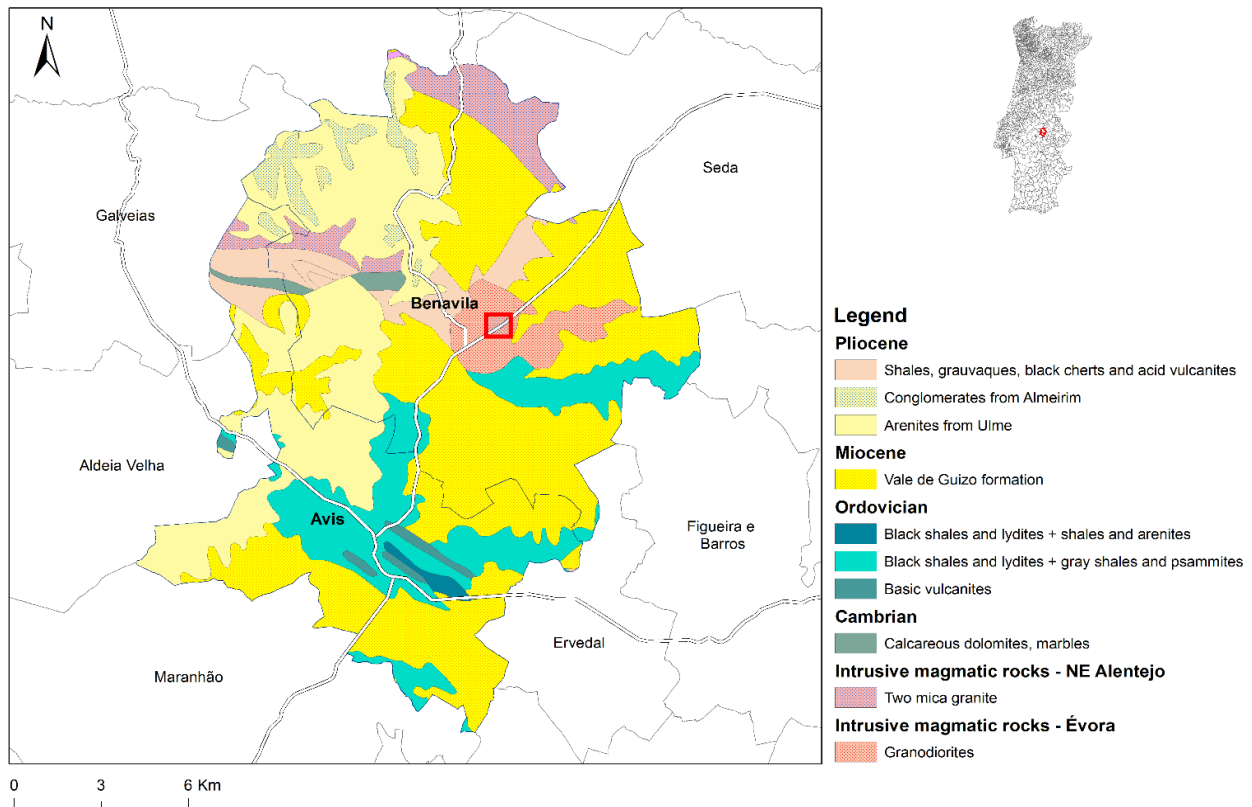


Fig.6 - Geological map of Benavila region: the location of Bentonite rocks is delimited by the square contour (Piçarra et al., 2009).

The last data obtained from previous prospection studies, developed by “*Serviço de Fomento Mineiro*” (SFM), indicated the presence of important resources, about  $3 \times 10^6 \text{ m}^3$  (SFM, 1993), making this bentonite deposit one of the most important clay deposits in Portugal (Dias et al., 2004). The geological map of Benavila region, including the location of bentonite rocks, is represented in Fig. 6.

## 2.2.4. References

- Al-Rawas, A.A., Goosen, M.F.A., 2006. *Expansive Soils: Recent Advances in Characterization and Treatment*. Taylor & Francis Group, p. 546.
- Allegretta, I., Eramo, G., Pinto, D., Kilikoglou, V., 2015. Strength of kaolinite-based ceramics: Comparison between limestone- and quartz-tempered bodies. *Applied Clay Science* 116–117, 220-230.
- Barany, S., 2012. *Role of Interfaces in Environmental Protection*. Springer Netherlands.
- Barnard, H., 2008. *Eastern Desert Ware: Traces of the Inhabitants of the Eastern Deserts in Egypt and Sudan During the 4th-6th Centuries Ce*. Archaeopress.
- Bergaya, F., Lagaly, G., 2013. *Handbook of Clay Science*. Elsevier Science.
- Bourg, I.C., Sposito, G., Bourg, A.C.M., 2007. Modeling the acid–base surface chemistry of montmorillonite. *Journal of Colloid and Interface Science* 312, 297-310.
- Brigatti, M.F., Mottana, A., 2011. *Layered Mineral Structures and their Application in Advanced Technologies*. European Mineralogical Union.
- Brindley, G.W., Brown, G., 1982. *Crystal Structures of Clay Minerals and their X-Ray Identification*. Mineralogical Society.
- Carroll, D., 1970. *Clay Minerals: A Guide to Their X-ray Identification*. Geological Society of America.
- Carvalho, A.M.G., Alegria, M.F., Azevedo, T.M., 1980. Aspectos de alteração em rochas dioríticas de Benavila. *Com. Serv Geol. Portugal, Lisboa*, p. 49.
- Chesworth, W., 2007. *Encyclopedia of Soil Science*. Springer, Netherlands.
- Chisholm-Brause, C.J., Berg, J.M., Little, K.M., Matzner, R.A., Morris, D.E., 2004. Uranyl sorption by smectites: spectroscopic assessment of thermodynamic modeling. *Journal of Colloid and Interface Science* 277, 366-382.
- Christidis, G.E., Blum, A.E., Eberl, D.D., 2006. Influence of layer charge and charge distribution of smectites on the flow behaviour and swelling of bentonites. *Applied Clay Science* 34, 125-138.
- Christidis, G.E., Eberl, D.D., 2003. Determination of layer-charge characteristics of smectites. *Clays and Clay Minerals* 51, 644-655.
- Ciullo, P.A., 1996. *Industrial Minerals and Their Uses: A Handbook and Formulary*. Elsevier Science.
- Cresser, M., Killham, K., Edwards, T., 1993. *Soil Chemistry and its Applications*. Cambridge University Press.
- Cuadros, J., Linares, J., 1996. Experimental kinetic study of the smectite-to-illite transformation. *Geochimica et Cosmochimica Acta* 60, 439-453.
- Dazas, B., Lanson, B., Delville, A., Robert, J.-L., Komarneni, S., Michot, L.J., Ferrage, E., 2015. Influence of Tetrahedral Layer Charge on the Organization of Interlayer Water and Ions in Synthetic Na-Saturated Smectites. *The Journal of Physical Chemistry C* 119, 4158-4172.

- Dias M., Suarez Barrios M., Prates S., 2004. Bentonites from Benavila (Portugal). Mineralogical characterization and properties. *Geogaceta*, 35, 99-102.
- Dobias, B., 1993. Coagulation and Flocculation: Theory and Applications. CRC Press.
- Drits, V.A., Besson, G., Setton, R., Guinier, A., Bookin, A.S., Tchoubar, C., Rousseaux, F., Sakharov, B.A., Tchoubar, D., 2012. X-Ray Diffraction by Disordered Lamellar Structures: Theory and Applications to Microdivided Silicates and Carbons. Springer Berlin Heidelberg.
- Emmerich, K., 2013. Chapter 2.13 - Full Characterization of Smectites, in: Faïza, B., Gerhard, L. (Eds.), *Developments in Clay Science*. Elsevier, pp. 381-404.
- Essington, M.E., 2015. *Soil and Water Chemistry: An Integrative Approach*, Second Edition. CRC Press.
- Fang, H.Y., 2013. *Foundation Engineering Handbook*. Springer US.
- Fang, H.Y., Daniels, J., 1997. *Introduction to Environmental Geotechnology*. Taylor & Francis.
- Feraud, G., Schmincke, H-U., Lietz, J., Gastaud, J., Pitchard, G., Bleil, U., 1981. New K-Ar ages, chemical analyses and magnetic data of rocks from the islands of Santa Maria (Azores), Porto Santo and Madeira (Madeira Archipelago) and Gran Canaria (Canary Islands). *Bull Volcanol* 44:359–375.
- Ferrage, E., Lanson, B., Sakharov, B.A., Drits, V.A., 2005. Investigation of smectite hydration properties by modeling experimental X-ray diffraction patterns: Part I: Montmorillonite hydration properties. *American Mineralogist* 90, 1358-1374.
- Ferrage, E., Lanson, B., Sakharov, B.A., Geoffroy, N., Jacquot, E., Drits, V.A., 2007. Investigation of dioctahedral smectite hydration properties by modeling of X-ray diffraction profiles: Influence of layer charge and charge location. *American Mineralogist* 92, 1731-1743.
- Ferreira, M. and Serrano, L., 1971. O Problema das Esmectites da Ilha de Porto Santo, *Actas do I Congresso Hispano-Luso-Americano de Geologia Económica*, Lisboa, P-6-3, 255-244.
- Fiore, S., Cuadros, J., Huertas, F.J., 2010. *Interstratified Clay Minerals: Origin, Characterization & Geochemical Significance*. Digilabs.
- Galan, E., 1996. Properties and Applications of Palygorskite-Sepiolite Clays. *Clay Minerals* 31, 443-453.
- Geldmacher, J., Bogaard, P.V.D., Hoernle, K., Schmincke, H-U., 2000. 40Ar/39Ar age dating of the Madeira Archipelago and hotspot track (eastern North Atlantic). *G3 Geochem. Geophys. Geosyst.*1.
- Giesecking, J.E., 2012. *Soil Components: Vol. 2: Inorganic Components*. Springer Berlin Heidelberg.
- Grim, R.E., 1968. *Clay Mineralogy*, McGraw-Hill Book Company, p. 568.
- Hodinnott, K.B., Lamb, R.O., Soil, A.C.D.-o., Soils, R.S.D.o.P.-C.P.o., Rocks, 1990. *Physico-chemical Aspects of Soil and Related Materials*. ASTM.
- Huang, P.M., Li, Y., Sumner, M.E., 2011. *Handbook of Soil Sciences: Properties and Processes*, Second Edition. CRC Press.
- Hubbard, A.T., 2002. *Encyclopedia of Surface and Colloid Science*. Taylor & Francis.
- Huggett, J.M., Cuadros, J., 2005. Low-temperature illitization of smectite in the late Eocene and early Oligocene of the Isle of Wight (Hampshire basin), UK. *American Mineralogist* 90, 1192-1202.
- Inoue, A., Lanson, B., Marques-Fernandes, M., Sakharov, B.A., Murakami, T., Meunier, A., Beaufort, D., 2005. Illite-smectite mixed-layer minerals in the hydrothermal alteration of volcanic rocks: I. One dimensional XRD structure analysis and characterization of component layers. *Clays and Clay Minerals* 53, 423-439.

- Inoue, A., Utada, M., Wakita, K., 1992. Smectite-to-illite conversion in natural hydrothermal systems. *Applied Clay Science* 7, 131-145.
- Ismadji, S., Soetaredjo, F.E., Ayucitra, A., 2015. *Clay Materials for Environmental Remediation*. Springer International Publishing.
- Kaufhold, S., Dohrmann, R., 2013. The variable charge of dioctahedral smectites. *Journal of Colloid and Interface Science* 390, 225-233.
- Ke, Y.C., Stroeve, P., 2005. *Polymer-Layered Silicate and Silica Nanocomposites*. Elsevier Science.
- Kim, J., Dong, H., Seabaugh, J., Newell, S.W., Eberl, D.D., 2004. Role of microbes in the smectite-to-illite reaction. *Science of The Total Environment* 303, 830-832.
- Kogel, J.E., Society for Mining, M., Exploration, 2006. *Industrial Minerals & Rocks: Commodities, Markets, and Uses*. Society for Mining, Metallurgy, and Exploration.
- Korichi, S., Bensmaili, A., 2009. Sorption of uranium (VI) on homoionic sodium smectite experimental study and surface complexation modeling. *Journal of Hazardous Materials* 169, 780-793.
- Lagaly, G., Dékány, I., 2013. Chapter 8 - Colloid Clay Science, in: Faïza, B., Gerhard, L. (Eds.), *Developments in Clay Science*. Elsevier, pp. 243-345.
- Laird, D.A., 2006. Influence of layer charge on swelling of smectites. *Applied Clay Science* 34, 74-87.
- Lal, R., 2006. *Encyclopedia of Soil Science*. Taylor & Francis, Boca Raton.
- Larsen, G., Chilingar, G.V., 1983. *Diagenesis in Sediments and Sedimentary Rocks*. Elsevier Scientific Publishing Company.
- Lee, J.O., Kang, I.M., Cho, W.J., 2010. Smectite alteration and its influence on the barrier properties of smectite clay for a repository. *Applied Clay Science* 47, 99-104.
- Lewinsky, A.A., 2007. *Hazardous Materials and Wastewater: Treatment, Removal and Analysis*. Nova Science Publishers.
- Lietz, J., Schwarzbach, M., 1970. Neue Fundstellen von marinem Tertiär auf der Atlantik-Insel Porto Santo (Madeira-Archipel). *Neues Jahrb Geol Palaeontol Monatsh* 5:270-282.
- Macedo, C.R., Costa, V., Ferreira, M., 1974. K/Ar ages on the central Atlantic islands. *Int. Meet. Geochronol. Cosmochronol. Isotope Geol.*, Paris.
- Masuda, H., Peacor, D.R., Dong, H., 2001. Transmission electron microscopy study of conversion of smectite to illite in mudstones of the Nankai Trough: Contrast with coeval bentonites. *Clays and Clay Minerals* 49 109-118.
- Mering, J., 1975. Smectites, in: Gieseking, J.E. (Ed.), *Soil Components: Vol. 2: Inorganic Components*. Springer Berlin Heidelberg, Berlin, Heidelberg, pp. 97-119.
- Merlino, S., 1997. *Modular Aspects of Minerals*. Eötvös University Press.
- Meunier, A., Lanson, B., Beaufort, D., 2000. Vermiculitization of smectite interfaces and illite layer growth as a possible dual model for illite-smectite illitization in diagenetic environments: a synthesis. *Clay Minerals* 35, 573-586.
- Meunier, A., Velde, B.D., 2013. *Illite: Origins, Evolution and Metamorphism*. Springer Berlin Heidelberg.
- Meurant, G., 2011. *The chemistry of clay minerals*. Elsevier Science.
- Misaelides, P., 1999. *Natural Microporous Materials in Environmental Technology*. Springer Netherlands.
- Misaelides, P., Macásek, F., Pinnavaia, T.J., Colella, C., 2012. *Natural Microporous Materials in Environmental Technology*. Springer Netherlands.
- Mohamed, A.M.O., Antia, H.E., 1998. *Geoenvironmental Engineering*. Elsevier Science.
- Moore, D.M., Reynolds, R.C., 1997. *X-ray diffraction and the identification and analysis of clay minerals*. Oxford University Press, Oxford and New York.

- Mosser-Ruck, R., Devineau, K., Charpentier, D., Cathelineau, M., 2005. Effects of ethylene glycol saturation protocols on XRD patterns: a critical review and discussion. *Clays and Clay Minerals* 53, 631-638.
- Murray, H.H., 2006. *Applied Clay Mineralogy: Occurrences, Processing and Applications of Kaolins, Bentonites, Palygorskitesepiolite, and Common Clays*. Elsevier Science.
- Nagy, N.M., Konya, J., 2009. *Interfacial Chemistry of Rocks and Soils*. CRC Press.
- Nieto, F., Livi, K.J.T., 2013. *Minerals at the Nanoscale*. Mineralogical Society of Great Britain & Ireland.
- Odom, I.E., 1984. Smectite clay Minerals: Properties and Uses. *Philosophical Transactions of the Royal Society of London. Series A, Mathematical and Physical Sciences* 311, 391-409.
- Orbovic, V., Huang, Z., 2012. *Kaolinite: Occurrences, Characteristics, and Applications*. Nova Science Publishers.
- Parker, S.P., 1988. *McGraw-Hill encyclopedia of the geological sciences*, 2nd ed. New York, McGraw-Hill, 32–33, 69–72, 400–401.
- Parkes, W.R., 1982. Occupational lung disorders. London, Butterworths, 310-318.
- Pasbakhsh, P., Churchman, G.J., 2015. *Natural Mineral Nanotubes: Properties and Applications*. Apple Academic Press.
- Patterson, S.H. and Murray, H.H., 1983. Clays. In: Lefond SI ed. *Industrial minerals and rocks*, 5th ed. New York, American Institute of Mining, Metallurgical, and Petroleum Engineers, p. 585–651.
- Piçarra, J.M., Dias, R.P., Ribeiro, M.L., Solá, R., Barbosa, B., Pais, J., 2009. Nota explicativa da folha 32-C Avis, Unidade de Geologia e Cartografia Geológica. Laboratório Nacional de Energia e Geologia, Lisboa.
- Potter, P.E., Maynard, J.B., Depetris, P.J., 2005. *Mud and Mudstones: Introduction and Overview*. Springer Berlin Heidelberg.
- Pytte, A.M., Reynolds, R.C., 1989. The Thermal Transformation of Smectite to Illite, in: Naeser, N., McCulloh, T. (Eds.), *Thermal History of Sedimentary Basins*. Springer New York, pp. 133-140.
- Ratta, R., Lal, R., 1998. *Soil Quality and Soil Erosion*. Taylor & Francis, U.S.A. p. 337.
- Rebello M., Rocha F., Ferreira da Silva E., 2010. Mineralogical and physicochemical characterization of selected Portuguese Mesozoic-Cenozoic muddy/clayey raw materials to be potentially used as healing clays. *Clay Minerals*, 229-240.
- Rebello, M., Viseras, C., López-Galindo, A., Rocha, F., da Silva, E.F., 2011. Characterization of Portuguese geological materials to be used in medical hydrology. *Applied Clay Science* 51, 258-266.
- Reeves, G.M., Sims, I., Cripps, J.C., London, G.S.o., 2006. *Clay Materials Used in Construction*. Geological Society.
- Reynolds, R.C., 1980. Interstratified clay minerals, *Crystal Structures of Clay Minerals and Their X-ray Identification* (Brindley G.W. and Brown G. eds.) Mineralogical Society, London, pp. 249-303.
- Reynolds, R.C., 1985. NEWMOD a computer program for the calculation of one-dimensional diffraction patterns of mixed-layer clays. R. C. Reynolds, Jr. 8 Brook Dr., Hanover, NH 03755.
- Ryan, P., 2014. *Environmental and Low Temperature Geochemistry*. Wiley.
- Sato, T., Murakami, T., Watanabe, T., 1996. Change in layer change of smectites and smectite layers in illite/smectite during diagenetic alteration. *Clays and Clay Minerals* 44, 460-469.

- Sato, T., Watanabe, T., Otsuka, R., 1992. Effects of layer charge, charge location, and energy change on expansion properties of dioctahedral smectites. *Clays and Clay Minerals* 40, 103-113.
- Schaetzl, R., Thompson, M.L., 2015. *Soils: Genesis and Geomorphology*. Cambridge University Press.
- Schmidt, R. and Schmincke, H.U., 2002. From seamount to oceanic island, Porto Santo, central East-Atlantic. *Int. J. Earth Sci.*, 91, 594-614.
- Schmincke, H-U., Staudigel, H., 1976. Pillow lavas on central and eastern Atlantic islands (La Palma, Gran Canaria, Porto Santo, Santa Maria). (Preliminary report). *Bull. Soc. Géol. Fr.* 7:871– 883.
- Schmincke, H-U., Weibel, M., 1972. Chemical study of rocks from Madeira, Porto Santo, and São Miguel, Terceira (Azores). *Neues Jahrb Mineral Abh* 117:253–281.
- SFM, 1993. *Estudos, notas e trabalhos*. Serviço de Fomento Mineiro, Portugal.
- Shah, D.L., Shroff, A.V., 2003. *Soil Mechanics and Geotechnical Engineering*. Taylor & Francis.
- Singer, A., Galan, E., 2000. *Palygorskite-Sepiolite: Occurrences, Genesis and Uses*. Elsevier Science.
- Somasundaran, P., 2006. *Encyclopedia of Surface and Colloid Science*. Taylor & Francis.
- Sparks, D.L., 2013. *Environmental Soil Chemistry*. Elsevier Science, USA, p.267.
- Sparks, D.L., 2003. *Environmental Soil Chemistry* (2nd ed.). Academic Press., Elsevier Science, USA.
- Sposito, G., 1995. *The Environmental Chemistry of Aluminum*, Second Edition. Taylor & Francis.
- Środoń, J., 1999. Nature and of Mixed Layer Clays and Mechanism of their Formation and Alteration. *Annu. Rev. Earth Planet. Sci.* 27, 19-53.
- Strawn, D.G., Bohn, H.L., O'Connor, G.A., 2015. *Soil Chemistry*. Wiley.
- Sumner, M.E., 1999. *Handbook of Soil Science*. Taylor & Francis.
- Tombácz, E., Szekeres, M., 2004. Colloidal behavior of aqueous montmorillonite suspensions: the specific role of pH in the presence of indifferent electrolytes. *Applied Clay Science* 27, 75-94.
- Tournassat, C., Steefel, C.I., Bourg, I.C., Bergaya, F., 2015. *Natural and Engineered Clay Barriers*. Elsevier Science.
- Turner, G.D., Zachara, J.M., McKinley, J.P., Smith, S.C., 1996. Surface-charge properties and UO<sub>2</sub><sup>2+</sup> adsorption of a subsurface smectite. *Geochimica et Cosmochimica Acta* 60, 3399-3414.
- Vainshtein, B.K., Feigl, E., Spink, J.A., 2013. *Structure Analysis by Electron Diffraction*. Elsevier Science.
- van Breemen, N., Buurman, P., 2002. *Soil Formation*. Springer, Netherlands.
- Velde, B., 2013. *Origin and Mineralogy of Clays: Clays and the Environment*. Springer Berlin Heidelberg.
- Velde, B.B., Meunier, A., 2008. *The Origin of Clay Minerals in Soils and Weathered Rocks*. Springer Berlin Heidelberg.
- Walther, J.V., 2013. *Earth's Natural Resources*. Jones & Bartlett Learning.
- White, R.E., 2009. *Principles and Practice of Soil Science: The Soil as a Natural Resource*. Wiley.
- Wilson, M.J., 2013. *Rock-forming Minerals: Clay Minerals. Sheet silicates. Volume 3C*. Geological society.
- Worden, R., Morad, S., 2009. *Clay Mineral Cements in Sandstones* (Special Publication 34 of the IAS). Wiley.
- Xie, M., Reaktorsicherheit, G.f.A.-u., Miehe, R., Kasbohm, J., Herbert, H.J., Meyer, L., Ziesche, U., 2012. *Bentonite Barriers - New Experiments and State of the Art*:

Bentonite as Barrier Material for the Sealing of Underground Disposal Sites : Final Report. GRS.

Yariv, S., Cross, H., 2001. Organo-Clay Complexes and Interactions. Taylor & Francis.

Yotsumoto, H., 2011. Electron micrographs of clay minerals. Elsevier Science.

Yu, T.R., 1997. Chemistry of Variable Charge Soils. Oxford University Press.

Zrinyi, M., Hórvölgyi, Z., Hórvölgyi, Z.D., Egyesülete, M.K., Egyetem, B.M.é.G., 2004. From Colloids to Nanotechnology. Springer.



## 3. Materials and Methods

### 3.1. Clay minerals selection and preparation

Three selected bentonite rocks (BA1, PS2 and PS3) were collected from two different regions of Portugal: Benavila region (BA1) and Porto Santo Island, Madeira archipelago (PS2 and PS3). Adsorption experiments were preceded by separation and purification process, where carbonate was removed from the selected samples according to Jackson's method (1975).

The <2 µm fractions were previously obtained by sedimentation from the purified samples, according to Stokes law. It establishes the relationship between the sedimentation time (t) and a spherical particle of radius (r), increasing to radius r + Δr by adsorption of a fluid (Cornell and Hoveling, 1998). The following equation was used to predict the time of settling for particles >2µm:

$$t = \frac{18\eta h}{gd^2(\rho_p - \rho_w)} \quad (1)$$

where *t* corresponds to the settling time (sec.); *η* is the water dynamic viscosity (close to 1 in 20 °C); *h* is the height of water column (m) (0.1 or 0.2 m); *g* is gravitational acceleration (9.81 m/s<sup>2</sup>); *d* is the equivalent spherical diameter (2\*10<sup>-6</sup> m); *ρ<sub>p</sub>* and *ρ<sub>w</sub>* are the particle density (quartz density– 2650 kg/m<sup>3</sup>) and water density (20 °C), respectively.

The settling time calculated corresponded to about 15 hours, considering that *h*=0.2 m and *d*=2x10<sup>-6</sup> m.

Before sorption experiments, the <2 µm clay fractions were studied by X-ray diffraction (XRD), infrared-spectroscopy and electron microprobe analysis. The <2 µm clay fractions were analysed by XRD in air-dried and ethylene-glycol conditions. The structural behavior of smectite samples was verified using several well-known protocols used to differentiate high- from low-charge smectite (Barshad, 1960; Harward, 1968; Jackson and Barak, 2005) and to distinguish beidellite from montmorillonite (Greene-Kelly, 1952).

*Structural characterization of the <2 μm clay fractions.* Sample BA1 corresponds to an interstratified structure composed of beidellite/(Ca,Na)-montmorillonite (2-waters). Sample PS2 corresponds to K-illite/beidellite/(Na,Ca)-montmorillonite (R0, 85-90%S). Sample PS3 corresponds to a randomly interstratified structure of K-illite/(Na,Ca)-montmorillonite (R=0; 70%S), where no beidellitic layers did occur.

*Chemical characterization.* The crystal chemistry composition of the <2 μm clay fractions obtained by electron microprobe is given in Table 4.

Table 4. Physicochemical properties of clay minerals.

Sample	Structural Formula	S <sub>BET</sub> (m <sup>2</sup> /g)	CEC (meq/g)	Charge Def./Uc
BA1	Ca <sub>0.53</sub> Na <sub>0.40</sub> (Al <sub>2.61</sub> Fe <sub>0.73</sub> Mg <sub>0.66</sub> )(Si <sub>7.28</sub> Al <sub>0.72</sub> )O <sub>20</sub> (OH) <sub>4</sub>	12	0.96	- 1.38 48%O 52%T
PS2	Ca <sub>0.27</sub> Na <sub>0.74</sub> K <sub>0.16</sub> (Al <sub>2.52</sub> Fe <sub>0.67</sub> Mg <sub>0.78</sub> )(Si <sub>7.50</sub> Al <sub>0.50</sub> )O <sub>20</sub> (OH) <sub>4</sub>	26	1.04	- 1.31 62%O 38%T
PS3	Ca <sub>0.30</sub> Na <sub>0.59</sub> K <sub>0.28</sub> (Al <sub>2.33</sub> Fe <sub>0.81</sub> Mg <sub>0.85</sub> )(Si <sub>7.40</sub> Al <sub>0.60</sub> )O <sub>20</sub> (OH) <sub>4</sub>	84	0.81	- 1.45 50%O 50%T

## 3.2. Analytical techniques and Methods

### 3.2.1. Cation exchange capacity

The <2 μm clay fractions were saturated with Sr<sup>2+</sup> and prepared in order to determine the cation exchange capacity (CEC). The experiments were carried out by adding 0.050 grams of smectite into the polypropylene centrifuge tubes with 14.00 mL of different stock solutions at different Sr<sup>2+</sup> concentrations, ranged between 5×10<sup>-4</sup> M and 1.50 × 10<sup>-2</sup> M. Suspensions were shaken for 34 hours, then centrifuged, separated and the solutions resulted were preserved by adding HNO<sub>3</sub> (65%) and stored at 4 °C for subsequent chemical analyses. The CEC was determined by Sr<sup>2+</sup> adsorption tests at pH 4. The <2μm clay fractions the Sr<sup>2+</sup>-aqueous solutions were analysed by atomic absorption spectrometry (AAS) after Sr<sup>2+</sup> saturated. The CEC value was estimated from the maximum amount of Sr<sup>2+</sup>

adsorbed in these conditions, taking into account the following relation:  
 $CEC(\text{meq/g}) = q_{\text{Sr}^{2+}}(\text{mmol/g}) \times 2$ .

### 3.2.2. Brunauer-Emmett-Teller specific surface area (BET)

The Brunauer-Emmett-Teller specific surface area (BET) of the <2 $\mu\text{m}$  clay fractions was characterized by nitrogen adsorption-desorption measurements at -196 °C with a Micromeritics Tristar II analyser. The samples were degassed at 200 °C overnight before the measurements were taken. The surface area was calculated based on the adsorption data in the relative partial pressure range of 0.05-0.2, and the pore size distributions were determined based on the Barrett-Joyner-Halender (BJH) adsorption curve.

### 3.2.3. X-ray Diffraction Spectroscopy

The structural characterization of the <2  $\mu\text{m}$  clay fractions was performed by X-ray diffraction (XRD) using a Siemens D500 machine equipped with a  $\text{CuK}_\alpha$  radiation and a scanning speed of  $1^\circ 2\theta/\text{min}$  in the range  $2-50^\circ 2\theta$ . The <2  $\mu\text{m}$  clay fractions prepared as oriented specimens on glass slide were X-ray run in air-dried (AD) condition and then, saturated during 24 h with ethylene-glycol vapour. Prior to XRD analysis, the smectite heterogeneity was studied using several chemical treatments. To differentiate high- from low-charge smectite and to study the layer charge distribution, different clay fractions were saturated with KCl (1M) (Barshad and Kishk, 1970) and with  $\text{MgCl}_2$  (1M) (Harward et al., 1968) during 24 hours (S:L=3.57 g/L). The clay samples saturated were analysed by XRD in air-dried (AD) conditions. After X-ray run in AD, the K-saturated clay fractions were heated at 300 °C during 2 h, solvated with ethylene glycol (EG) and then analysed by XRD. By contrast, the  $\text{Mg}^{2+}$ -saturated clay fractions followed a glycerol treatment before XRD analysis. The Greene-Kelly test (Greene-Kelly, 1952) allows to distinguished beidellite from montmorillonite. The test started with  $\text{Li}^+$  saturation of <2  $\mu\text{m}$  clay fractions, adding 0.050 g of clay into 14 mL of LiCl (1M) solution, during 24 h, followed by heating at 300 °C during 6h, and glycerol treatment. The  $\text{Li}^+$  irreversible migrated to the octahedral sheet converts montmorillonite to a non-expandable structure upon treatment with glycerol. In this case, the XRD analyses were carried out after heating and glycerol treatment.

The XRD method is based on the observation that XRD peaks are broadened regularly as a function of decreasing crystallite size. This effect permits accurate

measurement of mean crystallite sizes for periodic crystals that range from about 2 nm to about 100 nm. The Bertaut-Warren-Averbach (BWA) analysis was performed in the 3 to 6 °2θ range using the MudMaster computer program (Drits et al., 1998). The program includes corrections of the diffracted intensity ( $I(\theta)$ ) for the Lorentz-polarization (Lp) and the structural (G) factors, which are necessary for clays. A combined LpG2 factor was calculated for each sample accounting for its Fe content.

### 3.2.4. Infrared absorption spectroscopy

The infrared (FTIR) spectra of Li-, Na- and K-smectite were obtained by using KBr pellets, which were firstly prepared by mixing 1 mg smectite with 200 mg KBr. The powder mixtures were then inserted in molds and pressed at 10 tons/cm<sup>2</sup> to obtain the transparent pellets. The samples were analyzed with a Bruker Tensor 27 spectrometer. The infrared spectra in transmission mode were recorded in the 4000–400 cm<sup>-1</sup> frequency region. The measurements of the adsorption bands integrated intensity were made using OPUS software supplied by the Bruker instrument.

### 3.2.5. Electron microprobe analysis

Polished sample surfaces were prepared from the <2 μm clay fractions, which were previously pressed in pellets with diameter of 3 mm with a PIKE Hand Press Kit 161-1024 (Pike technologies). The epoxy resin was prepared using the Araldite EAY 103-1 and a HY956-KG hardener (9:1 ratio) and then dispersed in a holder of 13 mm. The pellets were located in the epoxy resin, dried during 24 h and subsequently polished using the 30, 10 and 2 μm micro-finishing films under dry conditions. The major elements of minerals were determined using a Jeol Hyperprobe JXA-8500F electron microprobe operated at 15 kV accelerating voltage and 10 nA beam current. Detection limits (3σ) above mean background were 0.03 wt.% for most oxides with counting times of 80 s. Standards used include albite (NaKα), orthoclase (AlKα, SiKα, KKα), apatite (CaKα, PKα), MgO (MgKα), MnTiO<sub>3</sub> (MnKα), TiO<sub>2</sub> (TiKα), Fe<sub>2</sub>O<sub>3</sub> (FeKα).

### 3.2.6. Atomic absorption spectroscopy

Chemical analyses of  $\text{Sr}^{2+}$  aqueous solutions were carried out by atomic absorption spectroscopy using a flame absorption spectrometer Perkin Elmer, AAnalyst 200 model with a Strontium hollow cathode lamp, wavelength 460.73 nm, air flow 5.2 L/min and acetylene flow 2.5 L/min. The 5 mL of the acidified strontium solution was mixed with 750  $\mu\text{L}$  of lanthanum chloride ( $\text{LaCl}_3 \cdot 7\text{H}_2\text{O}$ ) solution previously prepared (176 g of  $\text{LaCl}_3 \cdot 7\text{H}_2\text{O}$  and 19.1 g of KCl diluted in 1000 mL of deionised water).

### 3.2.7. Inductively coupled plasma-mass spectrometry

The  $\text{UO}_2^{2+}$  aqueous solutions obtained after batch experiments were analysed by inductively coupled plasma-mass spectrometry (ICP-MS). The uranium concentrations in acidified solutions were determined by external standard calibration method using an inductively coupled plasma-mass spectrometry (ICP-MS) (THERMO X series ELEMENT2 and Amiga series, JobinYvon equipments). Calibration was done in each analytical session by the external standard method. Also, major elements of smectite and composite material were analyzed by ICP-MS.

### 3.2.8. X-ray photoelectron spectroscopy

Uranyl-clay samples obtained after batch experiments were analysed by X-ray photoelectron spectroscopy (XPS). XPS spectra were recorded using a Physical Electronics PHI 5701 spectrometer with a non-monochromatic Al  $K\alpha$  radiation (300 W, 15 kV,  $h\nu = 1486.6$  eV) as the excitation source. Spectra were recorded at  $45^\circ$  take-off angle by a concentric hemispherical analyzer operating in the constant pass energy mode at 25.9 eV, using a 720 mm diameter analysis area. Under these conditions the Au  $4f_{7/2}$  line was recorded with 1.16 eV FWHM at a binding energy of 84.0 eV. The spectrometer energy scale was calibrated using Cu  $2p_{3/2}$ , Ag  $3d_{5/2}$  and Au  $4f_{7/2}$  photoelectron lines at 932.7, 368.3 and 84.0 eV, respectively. Charge referencing was done against adventitious carbon (C1s 284.8 eV). Powdered solids were mounted on a sample holder without adhesive tape and kept overnight in high vacuum in the preparation chamber before they were transferred to the analysis chamber of the spectrometer. Each region was scanned with several sweeps until a good signal to noise ratio was observed. The pressure in the analysis chamber was

maintained lower than  $10^{-9}$  Torr. A PHI ACCESS ESCA-V6.0 F software package was used for acquisition and data analysis. A Shirley-type background was subtracted from the signals. Recorded spectra were always fitted using Gauss–Lorentz curves in order to determine more accurately the binding energy of the different element core levels. The accuracy of binding energy (BE's) values was within  $\pm 0.1$  eV.

### 3.2.9. References

- Barshad, I., 1960. X-ray analysis of soil colloids by a modified salted paste method. Proceedings 7<sup>th</sup> Nat. Conf. Clays 5, 350-364.
- Barshad, I., Kishk, F.M., 1970. Factors affecting potassium fixation and cation exchange capacities of soil vermiculite clays. Clay and Clay Minerals 18, 122-137.
- Cornell, H., Hoveling, A.W., 1998. Wheat: Chemistry and Utilization. Taylor & Francis.
- Harward, M.E., Carstea, D., Sayegh, A., 1968. Properties of vermiculite and smectites: Expansion and collapse. Clays and Clay Minerals 15, 179.
- Greene-Kelly, R., 1952. Irreversible dehydration in montmorillonite. Clay Minerals Bull. 1, 221.
- Drits, V., Eberl, D.D., Środoń, J., 1998. XRD measurement of mean thickness, thickness distribution and strain for illite and illite-smectite crystallites by the Bertaut-Warren-Averbach technique. Clays and Clay Minerals 46, 38-50.
- Jackson, M.L.R., Barak, P., 2005. Soil Chemical Analysis: Advanced Course. Parallel Press, University of Wisconsin-Madison Libraries.

## 4. Clay liners reactivity and behavior during metal and actinide sorption experiments at variable pH, ionic strength and concentrations

### 4.1. Introduction

Natural and inexpensive materials, such as bentonite rocks, having the right physical and chemical properties to act as liner/backfill/buffer, can be useful as additional barriers to stabilize the surrounding environment, restrict the access of groundwater to the waste packages and reduce by sorption the rate of eventual radionuclide migration from the waste. To qualify the layer silicates as candidate buffer material few major criteria are requested such as: high swelling pressure, good sorption and fixation and long-term stability under repository conditions. The results obtained on layer silicates collected from several Portuguese geological formations confirm the presence of interstratified structures having two or three components, including smectite and illite.

### 4.2. Metal and actinide selected in this study

The radioactive wastes produced in Portugal result from the use of radioactive materials in the medicine, industry, research and education. The main radionuclides (sealed sources) present in these wastes are:  $^{137}\text{Cs}$ ,  $^{60}\text{Co}$ ,  $^{55}\text{Fe}$ ,  $^{90}\text{Sr}$ ,  $^{241}\text{Am}$ ,  $^{238}\text{U}$  and  $^{226}\text{Ra}$ .

#### 4.2.1. Strontium

Safety assessment of low and intermediate level waste (LILW) repositories requires the understanding of radionuclides sorption–desorption mechanisms, mainly the degree of interaction between radionuclides and mineral surfaces.

Among the different radionuclides that are part of the Portuguese radwastes inventory the  $^{137}\text{Cs}$  and  $^{90}\text{Sr}$  are the most important from the radiological point of view due to its high radiotoxicity.

## 4.2.2. Uranium

### 4.2.2.1. Uranium mining operations as source of radioactive contamination

The recovery of uranium using physical and chemical processes, such as the conventional mining processes (open pit and underground) to excavate the ore and the acid leaching to separate uranium from the host rock, released large quantities of solid and liquid materials (waste piles, mill tailings, acid mine drainage and sludge from acid water neutralization) that are potential radiation sources (Merkel and Arab, 2014; Nero et al., 2005). Several studies have confirmed that the high level of radiation impact is mainly caused by the hydrological system contamination, either by radionuclides and heavy metals leaching from the uranium ore or by the percolation of radioactive particles from the mining tailings (IAEA, 1999; Lollar, 2005; Merkel et al., 2012). After the closure of uranium mines, the groundwater level is gradually restored, representing an additional source of radionuclide contamination resulted from the contact between the mineralized rocks, which kept dried during the mining activities, and groundwater (Committee on Uranium Mining in Virginia et al., 2012). The radioactive contamination of hydrological systems is a source of especial concern once it could end up in drinking water or could be accumulated in the food chain, representing a serious risk for the public health (Campbell, 2009). Fig.7 shows the different sources of contamination of hydrological systems.

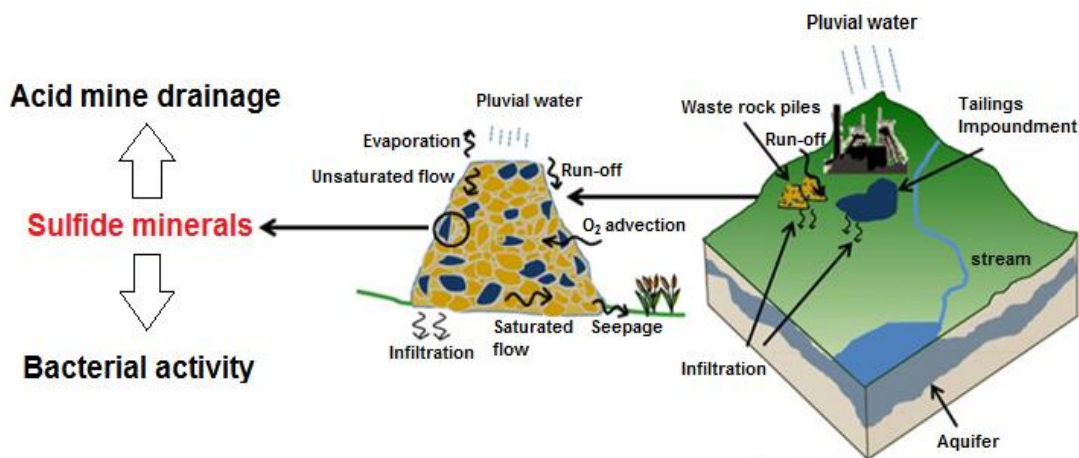


Fig.7 - Different sources of contamination of hydrological systems caused by mining activities.

#### 4.2.2.2. Uranium properties and their mobility in the environment

Uranium fuel is one of the main four worldwide energy resources and is mainly used to produce energy and nuclear weapons (Murray and Holbert, 2015). There are three natural uranium isotopes  $^{238}\text{U}$  ( $t_{1/2}=4.5 \times 10^9$  y),  $^{235}\text{U}$  ( $7.0 \times 10^8$  y) and  $^{234}\text{U}$  ( $2.5 \times 10^5$  y), whose radioactive decay is characterized by alpha emission and weak gamma radiation. The  $^{238}\text{U}$  and  $^{234}\text{U}$  isotopes are dominant in natural waters (L'Annunziata, 2012), whereas the abundance of  $^{235}\text{U}$  in the environment is only 0.75%.

Discharges of U, either by their exploitation or by nuclear industries, generated a global concern in the environmental authorities due to the serious risk of surface water and groundwater contamination (Falck, 2015; Kayzar et al., 2014; Zachara et al., 2013). Exposure to U is associated to chemical and radiological toxicity, and the risks to human health were investigated by many researchers (Gupta and Singh, 2003; Janardhan and Fesmire, 2010; Keith et al., 2015; Merkel et al., 2012; Siegel and Bryan, 2014; Yang and Zaoui, 2013). It was generally concluded that when ingested, uranium may cause severe damage to the kidney cells (Nordberg et al., 2014). Uranium was considered the only radionuclide for which the chemical toxicity has been identified to be comparable to or greater than their radiotoxicity (Jiang and Aschner, 2015; Lagauzère et al., 2009). Thus, EPA has established a concentration of  $30\mu\text{g/L}$  as the maximum contaminant level (MCL) for uranium in drinking water (Campbell and Ingram, 2014; Merkel et al., 2012).

The mobility of uranium in aqueous systems is highly dependent on chemical, physical and biological processes (Campbell, 2009). Uranium occurs in valences of III, IV, V and VI but only U(IV) and U(VI) are dominant in the environment, where their solubility is influenced by the oxidation state. The uranium mobility is higher at oxidative conditions (U(VI)), once it tends to be converted into uranyl ions ( $\text{UO}_2^{2+}$ ) which in contact with water form cationic, anionic and neutral complexes with high solubility (Merkel and Hasche-Berger, 2008). When U(VI) is reduced to U(IV), either by abiotic (chemical) or biotic (microbiological) processes, it tends to precipitate as uraninite ( $\text{UO}_2$ ). The biological actions involved in this process are triggered by several metal reducing and sulphate-reducing bacteria (e.g. *Geobacter*, *Shewanella*) (Campbell, 2009).

The water pH conditions also affect the uranium mobility as it controls the  $\text{UO}_2^{2+}$  aqueous species formed. In acidic conditions ( $\text{pH} < 4$ )  $\text{UO}_2^{2+}$  is the dominant species in solution, whereas from near neutral pH conditions  $\text{UO}_2^{2+}$  polynuclear species (e.g.  $[(\text{UO}_2)_3(\text{OH})_5]^+$ ) start to form and are dominant at pH 6-7. (Chisholm-Brause et al., 1994). From neutral to alkaline conditions and in the presence of carbonates or atmospheric  $\text{CO}_2$

(g), it tends to form cationic, anionic and neutral  $\text{UO}_2^{2+}$ -carbonate complexes which increase the U(VI) mobility in water (Sukla et al., 2015). Depending on the U(VI) concentration and the pH conditions in solution, schoepite and other U(VI) oxide precipitates may be formed, reducing the U(VI) mobility (Guillaumont et al., 2003).

It is also necessary take into account that the adsorption of  $\text{UO}_2^{2+}$ , especially in acidic conditions, on the organic matter, silicates, clays and/or iron and manganese oxy(hydroxides), and the composition of natural waters may delay significantly the U(VI) transport (Campbell, 2009). In the presence of carbonates and phosphates in solution,  $\text{UO}_2^{2+}$  may precipitate (e.g.  $\text{Ca}(\text{UO}_2)_2(\text{PO}_4)_2 \cdot n\text{H}_2\text{O}$ , autunite), contributing to reduce their mobility in the environment (Selim, 2015). Depending on the environmental conditions and the sediments composition, the concentration of U(VI) in the sediments and suspended solids may be several orders of magnitude higher than in the surrounding water, due to the higher tendency of U(VI) be adsorbed on the surface of the sediments and colloidal particles (Merkel and Hasche-Berger, 2008). These solid phases present their higher adsorption capacity between pH 5 and 7, whereas at  $\text{pH} < 3$  and  $\text{pH} > 7$  the adsorption capacity is reduced (Atwood, 2013).

The U(VI) mobility restrictions due to physical processes are frequently ignored. However, it is important to take into account that the physical properties of soil, such as the particles size, hydraulic conductivity and lithology, also have great implications in the U(VI) transport in the environment (Iskandar and Kirkham, 2001).

#### 4.2.2.3. Uranium contamination in Portugal

The uranium exploitation in Portugal has undergone a significant development after world war two, when the nuclear fission chain reaction was controlled and the price of uranium was valued in the international market (Duarte et al., 2005). A total of 60 mines (45 open pits and 15 underground operations) located in the granite massif of the Iberian Meseta and its edge, in the centre-north regions of Portugal, were explored between 1907 with the Urgeiriça ore discovery and 2001 with the closure of the uranium mines that still remained in activity (Sevilha and Quinta do Bispo mines) (Batista and Martins, 2008; Carvalho, 2014). According to Cerveira (1951), the uraniferous Portuguese veins approached the more productive uranium ore deposits of the world, which justifies their high economic interest at that time. The uraniferous ore deposits of greater economic value are associated with (1) epithermal quartz veins from Beira Baixa and Beira Alta regions that

occur within Hercynian calc-alkaline granites and metamorphosed schists and greywackes, near the margins of the granites; (2) supergene impregnation along faults and sheared zones throughout quartz, aplite and pegmatite veins, and also the basement granitic and perigranitic zones and dolerite dykes; (3) lacustrine deposits composed mainly by sandstones where uranium phosphates occurred (Cerveira, 1951).

Most of Portuguese uranium deposits that were exploited and later abandoned were not subject to any recovery intervention. After uranium mining activities has ceased in Portugal, about 4370 tons of  $U_3O_8$  and 60 Mtons of solid waste (15 Mtons in Urgeiriça – milling tailings) were produced. The great number of abandoned uranium mines, as well as, the major threat to public health led the Portuguese government to assume the remediation actions for environment safety in the areas of major concern. The decree-law no. 198-A/2001 reveals the awareness of the current risk situation and the huge necessity in to find efficient methods to recover the environmental balance of the areas affected by the mining exploitation, mainly in Viseu and Guarda districts, which were in state of degradation and abandonment. According to the law No. 11/87 of 7 April, the objectives for the recovery and environmental monitoring of the degraded areas should be defined. It is intended to introduce a new life cycle of a uranium mine and processing facility, including, after the mining activities, two new crucial steps:

- Reclamation: Procedures adopted after the mining activities that comprise the decontamination and clean-up, the demolition of buildings and other facilities, and the waste disposal on-site and/or off-site.
- Long-term stewardship: The government is responsible for the enforcement of institutional controls or other restrictions in order to ensure maintenance and long-term protection of the environment and public health. It should include the maintenance of tailing covers and water treatment systems, or other clean-up technologies, and ensure the continuous monitoring of terrestrial, aquatic and atmospheric levels of contamination.

The “Empresa de Desenvolvimento Mineiro” (EDM) was nominated as the government agency responsible for the management of the recovery process in the mining areas. EDM has assumed the remediation work on 14 closed mine sites between 2002 and 2008, which involved an investment of more than 45 million euros. These interventions were mainly intended to demonstrate the agreement with the regulations (decree-law no. 34/92, 4 of December), ensuring that the environmental, radiological or chemical contamination was not exceeding the standards, and to control the ecosystems contamination and the

radiation exposed to the critical population. The obligation to environmental monitoring in the area of influence of mining of radioactive ore, including the phases of operation, closure and rehabilitation as provided in the Decree Law 165/2002, Arto 14, point o) is currently allocated to IST (Instituto Superior Técnico).

#### 4.2.2.3.1. Cases of Study: Urgeiriça, Cunha Baixa and Quinta do Bispo uranium mining areas

During several decades, the contamination of Mondego river tributary has occurred by successive discharges of radioactive wastewater that resulted primarily from the pH neutralization treatment of AMD. This process also generated large quantities of radioactive sludge with high concentrations of uranium, radium and lead (Urgeiriça mine: 50 kBq/kg), which were an additional and indirect source of water contamination. The higher contribution to the river contamination came from the Urgeiriça, Quinta da Bispo and Cunha Baixa uranium mines that produced more than 13 Mtons of mining and milling tailings and wastes, subsequently deposited near to the old mining sites. The Urgeiriça mine, located in the village of Canas de Senhorim, was the most important complex operating in Portugal, once most of the uranium exploited from the locally mined uranium or from the remaining radioactive mineral mining areas in the central-north region of the country, were processed and produced in its Chemical Treatment Facility (CTF). About 1.460.000 m<sup>3</sup> of mining tailings were deposited there and acted as a source of radiation, particularly from <sup>238</sup>U and <sup>230</sup>Th, which contributed to significant levels of contamination mainly in the stream sediments of the Ribeira da Pantanha, resulted by surface run-off and percolation of water through mining wastes. Therefore, the surface radiometry and external radiation before remediation process detected at some points 15,000 shocks per second (SPP2 scintillometer) and 7.5µGy/h (mini-instruments). Neves et al. (2012a, b), have also detected high concentrations of uranium in leaf vegetables like lettuce (5,373 µg/kg), cabbage (255 µg/kg), and potato with peel (589 µg/kg). At that point, the need for action was urgent and the remediation process took place in the Urgeiriça mine area between 2006 and 2008, with the main purpose of mitigate the radiological contamination of pluvial waters, due to the percolation of waste particles previously deposited, and surface and subterranean aquifers through run-offs. For this propose, the implementation of tailings management systems, usually denominated as engineered barriers or covers, was developed in order to isolate tailings from the

environment and control the mobility of metals and radioactive contaminants, for at least 200 years and possibly up to 1000 years. These waste containment structures are usually constructed from clay (clay liners) and their life time is highly dependent on the temperature, the natural forces that gradually degrade these structures and the chemical incompatibility that increases the hydraulic conductivity and is mainly influenced by three main factors: (1) the type and properties of the liquid, (2) the type and properties of the soil, and (3) the physical conditions imposed on the clay barrier. Before their application in the Urgeiriça mine area, the materials used for sealing proposes were tested and qualified. Fig.8 shows the cover system adopted in the containment and sealing project in the Urgeiriça mine.

The coverage of mining tailings and treatment of radioactive waste water, controlled the radon air surface contamination and prevented the discharges of radioactive AMD in surface stream (EDM, 2011). In general, it controlled the radiation exposure in the environment, reducing significantly the radiometry and external radiations measured to 300 cps and 0.35  $\mu\text{Gy/h}$ , respectively, after remediation process. An integrated project solution, which involved water measurement and control systems, in terms of levels and characteristics of its leaches, dust, and exhaled radon were also developed in order to ensure the continuous monitoring of terrestrial, aquatic and atmospheric levels of contamination/radiation. The analysis of water samples collected in 2008 in the stream of Ribeira da Pantanha have still detected high levels of contamination by thorium ( $^{230}\text{Th}$ ) and radon ( $^{222}\text{Rn}$ ), and high concentrations of  $^{238}\text{U}$  and  $^{222}\text{Rn}$  in the downstream of the waste piles. It continuous to be a situation of high concern since the remediation strategy did not avoid the continuous discharges of radioactive wastewater in Mondego river tributary. The vegetables from small agriculture productions, near to the Urgeiriça mine area, which were irrigated from Pantanha streams, also revealed higher radionuclide concentrations when compared to other agriculture productions that were irrigated with non-contaminated water sources. The impact of the contamination levels recorded after remediation in the public health of population living near to mine area, remains a subject of strong controversy and discussion.

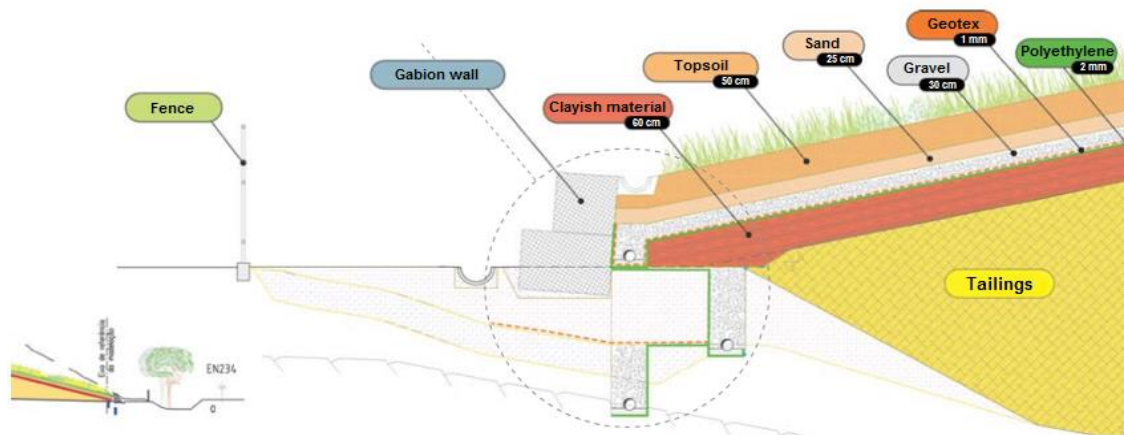


Fig.8 - Cover system adopted for sealing proposes in Urgeiriça mine.

Cunha Baixa village is located approximately 20 km southeast of Viseu. The uranium exploitation ceased in 1993 and a preliminary of its chemical environmental impact was started. In this case, it was concluded that the main contaminants in the surface and groundwater that were detected until 1-1.5 km from the contaminated mining sites (sulphate, manganese, aluminium and uranium) may cause serious health consequences to the Cunha Baixa village habitants (Neves and Matias, 2007). Therefore, these waters were not recommended for irrigation or livestock watering. The remediation process in the Cunha Baixa mine area mainly consisted in the recovery of contaminated soils through the deposition of organic matter (manure) in the soils, in order to reduce the bioavailability of contaminants. It was also constructed a dam to store rainwater in order to prevent the irrigation with contaminated water from private wells. The long-term stewardship was provided by the installation of dosimeters and dust meters near to the houses, in order to control the fluxes of radon gas, the potential alpha energy of the progeny of  $^{222}\text{Rn}$  and of thorium  $^{230}\text{Th}$  and the concentration of long-life radionuclides of the decay series of uranium and thorium in the dust particles (Pereira et al., 2013).

The Quinta do Bispo uranium mine has ceased the mining activities in 2001. As previously detected in the Urgeiriça and Cunha Baixa mining areas, it was also found in this area acid mine waters characterized by elevated radionuclide concentrations that reached to 170 Bq/L, resulted from the use of sulphuric acid for in situ leaching of uranium from the

host rock (Carvalho et al., 2005a). Although the remediation actions in this area did not start yet, a chemical treatment plant is currently running to treat the AMD before releasing it in the environment (Pereira et al., 2013). The treatment adopted in Quinta do Bispo, such as in Urgeiriça and Cunha Baixa pretends to remove metals and other chemical compounds by means of physical and chemical processes that consist on decanting the precipitates previously formed after the addition of lime and barium chloride. This process is usually used to neutralize the acid effluents resulted from AMD and to remove sulphides, uranium, radium and other heavy metals commonly present in the mine water. EDM has followed this treatment system for six years, during which has noted significant reductions in uranium, radium and manganese concentrations in the neutralized waters. Nevertheless, nothing was mentioned regarding to the radioactive sludge that is characterized by high concentrations of uranium, radium and lead and is usually accumulated during these operations, representing an additional source of water contamination. Although we do not have access to recent water analysis in this area, it is expectable a similar situation as detected in the Urgeiriça mine area, once the same treatment procedure was adopted.

#### 4.2.2.3.2. Case of Study: The Old Senhora das Fontes Uranium mining area

The old Senhora das Fontes was an underground mine but open pit mining was carried out in the 1980s. The uranium was mainly processed in this mining area for 5 years, while the Urgeiriça mine has temporarily ceased their activities for maintenance (European Commission, 2011). It was in activity between 1967 and 1982 and remained abandoned for more than 25 years, where were left about 33.800m<sup>3</sup> of radioactive waste that was continuously exposed to the external geodynamic processes and released in the environment (European Commission, 2011; Neiva et al., 2015). The remediation activities took place between 2010 and 2011. The radioactive materials was covered and isolated by a geomembrane in order to ensure that no water was infiltrated or escaped to the surroundings (European Commission, 2011). The remobilization of mine dumps and pyrite and chalcopyrite exposures led to a relevant decrease of uranium concentration in the surface and groundwater at the north part of the mining area, whereas in the south and southeast parts there was an increase of contamination by uranium (Neiva et al., 2015). In general, after remediation process there was a decrease in pH and an increase in Eh of surface water and groundwater, and, at the same time, the concentration of uranium has increased from 83

$\mu\text{g/L}$  and  $116 \mu\text{g/L}$  in the surface water and groundwater, respectively, to  $183 \mu\text{g/L}$  and  $272 \mu\text{g/L}$  in the former and latter, respectively (Neiva et al., 2015). Considering these results, it may be necessary to review the main remediation proposals defined by EDM, in order to find an efficient solution that would definitely prevent the continuous radiation exposure to the near population. Neiva et al. (2015) have suggested a detailed study of the geochemical water spatial distribution and a radiological characterization, taking into account that after decades of abandon the materials distribution left around the mine was probably changed.

#### 4.2.2.3.3. Cases of Study: Pinhal do Souto e Vale de Abrutiga uranium mining areas

The Vale de Abrutiga (VA) uranium mine located in Tábua, Coimbra district, near to the Aguieira dam reservoir, was exploited by open pit mining between 1982 and 1989. This deposit occurs in quartz veins in the intersection of two faults systems, where the precipitation of saleeite and meta-saleeite in the intersection at the surface of iron minerals has contributed to uranium retention and to uranium phosphate mineralization (Cabral Pinto and Silva, 2007; Cabral Pinto et al., 2008). After mining operations, about  $462.000 \text{ m}^3$  of radioactive waste were produced (European Commission, 2011). The surface and groundwater were considered not appropriated for human consumption or irrigation, due to their acidic conditions and high concentrations of U,  $\text{SO}_4$ , Zn, Fe, Mn, Ra, Cu, Th and Pb. It was also concluded that the stream sediments had high geoaccumulation indices of U, Fe, Ag, Zn, Cr, Co, and Pb (Cabral Pinto et al., 2004).

The remediation process was carried out in 2008 and was mainly intended to the repackaging, stabilization and drainage of the mining tailings and landscape design, as well as, the environmental monitoring (LCW, 2008). A water treatment plant consisting in 3 agitator tanks were also installed, and, at periodic intervals, water is brought up and treated with barium sulphate and lime. Periodic measurements are carried out on the water sources across the rehabilitated mine by EDM's subcontractor (European Commission, 2011). The European Commission report of 2011 revealed that the verification team has detected several problems regarding to the sampling method and has requested the revision of these procedures and the work of EDM's subcontractor (European Commission, 2011).

The Pinhal do Souto (PS) uranium deposit located at the western end of the village of Tragos (Mangualde), Viseu district, was exploited underground between 1978 and 1989

and produced 93,091 kg  $U_3O_8$ . The mineralization is mainly characterized by autunite and torbernite formed in quartz veins that intersects two-mica granites containing 10 ppm of U and uraninite (Neiva et al., 2014). Previous research based on the analysis of soil and water samples collected in 2011, have revealed that soils, stream sediments and waters were contaminated and were not prepared for human exploitation or consumption (Neiva et al., 2014). The uranium concentrations detected in the mining area were up to 485.20 mg/kg in Fe-oxides precipitate, 336.79 mg/kg in soils, 35.68 mg/kg in stream sediments and, in the wet season, were up to 104.42  $\mu\text{g/L}$  in water. The total amount of radioactive waste produced was about 42.000  $\text{m}^3$  and no recovery operations have been developed so far (European Commission, 2011; Neiva et al., 2014).

Neiva et al. (2014) have compared both Pinhal do Souto and Vale de Abrutiga mine legacies. They were both closed down in 1989, but PS was exploited for four more years and produced more 3000 kg of  $U_3O_8$ , but significant less quantify of radioactive waste (42,000  $\text{m}^3$ ), when compared to the same produced by VA mining activities (462,000  $\text{m}^3$ ). The environment impact in the water and stream sediments cause by VA mining activities was more significant due to the higher proportion of sulphides in the quartz veins, which in contact with water is oxidized to  $\text{SO}_4^{2-}$ , reducing significantly the water pH conditions and contributing to the AMD consequences.

The open pit exploitation in the VA area have favoured more the alteration than the underground exploitation in the PS area (Neiva et al., 2014). Therefore, secondary uranium minerals that tend to retain acidity and metals should be more abundant in the VA quartz veins and may have been dissolved in the water streams, mainly in the wet season, contributing to the higher level of contamination in the VA area. According to the chemical analysis results provided by Neiva et al. (2014), the water from VA area contain higher concentration of U (Surface water – 74.83  $\mu\text{g/L(U)}$ ; groundwater – 104.42  $\mu\text{g/L(U)}$ ), Pb and Cu than that from PS area (Surface water – 18,660  $\mu\text{g/L(U)}$ ; groundwater – 1000  $\mu\text{g/L(U)}$ ), as well as, elevated concentrations of  $\text{SO}_4^{2-}$ , Mn, Fe and Ra and is not recommended for human consumption or irrigation, whereas from PS area is also contaminated with  $\text{NO}_2^-$ , Cr, As, Cd and Ni and is not recommended for human consumption (Neiva et al., 2014; Portuguese Decree, 2007).

### 4.3. Interaction between radionuclides and smectite surface

Smectite play an important role in the retardation of radionuclides in the natural environment due to their capacity to adsorb metals ions either by ion-exchange at the permanent-charge sites or by surface complexation at the amphoteric or surface-hydroxyl sites (Atwood, 2013; Sparks, 2003).

Sorption mechanisms involving physical and chemical processes, such as, adsorption, surface precipitation and polymerization are common in the interaction between contaminants and mineral surfaces (Bauer and Velde, 2014). Generally, adsorption refers to the process through which a chemical substance reacts at the interface between two contiguous phases (Sposito, 2004). This process is described by adsorption isotherms, which are defined by the relation between the amount of adsorbate on the surface and the equilibrium concentration of the adsorptive at constant temperature (Maurer, 2000; Sparks, 2003). According to the IUPAC recommendations (Thommes et al., 2015), based on the Brunauer et al. (1940) classification, six different types of isotherms may be identified (Fig.9): The type I isotherm is associated with the chemical adsorption of microporous solids, in which the maximum adsorption capacity corresponds to the formation of a monolayer (Lowell et al., 2012); The type II and III isotherms are represented by multi-layer adsorption and the adsorbed quantity tends to  $\infty$ , when  $p/p_0$  ratio tends to 1 (Suzuki, 1993); The type IV isotherm is associated with mesoporous and macroporous solids and is described by the increased uptake of adsorbate as the pores are being filled, resulted by the increase of pressure (Hubbard, 2002); The type V isotherm corresponds to microporous and mesoporous solids and is characterized by an inflection point at relatively high pressure, and type VI isotherm is described by layer-by-layer adsorption onto non-porous solids with uniform surface (Aligizaki, 2005; Hubbard, 2002; Thommes et al., 2015). The adsorption of metals on unmodified clay minerals are usually described by type I and type II isotherms, from which different adsorption isotherms/models were developed to describe in detail this process: Langmuir isotherm assumes a monolayer adsorption where all the sorption sites are energetically equivalent. It predicts a maximum adsorption capacity, as the saturation point approaches, and is characterized by the linear behavior between the dissolved and sorbed concentrations for lower concentrations range (Langmuir, 1916); Freundlich isotherm assumes multi-layer formation on heterogeneous sites (Brebbia and Popov, 2011). It is described by the linear calibration that represents the logarithm of the sorption concentration as function of the logarithm of the dissolved concentration; Sips isotherm

combines both Langmuir and Freundlich isotherms and is characterized by heterogeneous adsorption. At lower sorption concentrations it behaves as Freundlich isotherm, and as the saturation point approaches it predicts a maximum adsorption capacity characteristic of the Langmuir isotherm (Maurer, 2000; Toth, 2002).

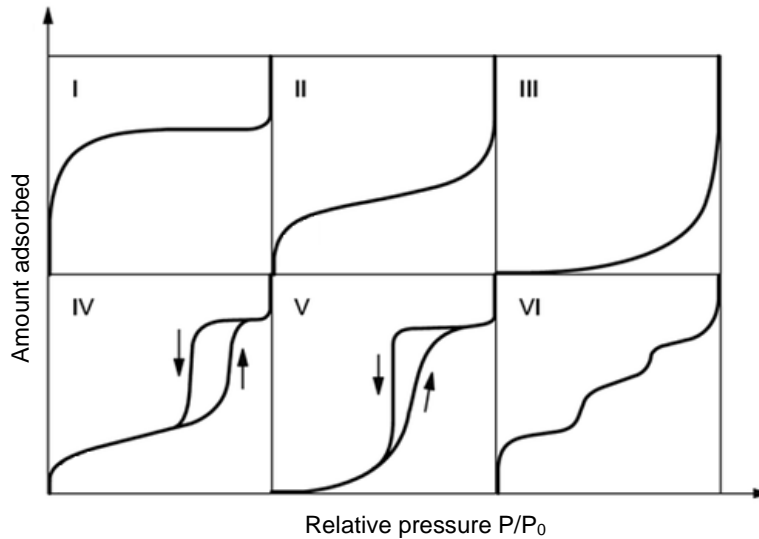


Fig.9 - Six main types of adsorption isotherms according to the IUPAC classification.

### 4.3.1. Mechanisms of adsorption of radionuclides on clay minerals

Radionuclides and metals may be retained on clay through five main processes: 1) adsorption, 2) surface precipitation, 3) surface cluster formation, 4) coprecipitation or 5) diffusion into an existing mineral structure (Lal, 2006). Regarding to the adsorption process, three distinct mechanisms may be identified: outer-sphere complexation, inner-sphere complexation, and adsorption of diffusion-layer ions (Lal, 2006; White, 2013). The outer-sphere complexation is characterized by weak electrostatic interactions which include a water molecule positioned between the metal and the clay surface, whereas inner-sphere complexation involves strong and direct bonding to the surface oxygens previously ionized (Bergaya and Lagaly, 2013; Sparks, 2003). The outer-sphere complexation is a rapid and reversible process, whereas inner-sphere complexation is an irreversible process characterized by covalent and electrostatic bondings (Brantley et al., 2007; Chorover and Brusseau, 2008). The adsorption of diffuse-layer ions are associated with the accumulated

ions away from the surface that does not interact directly with the clay surface, but are permanently moving on the diffuse double layer (Lal, 2006).

Specifically, the adsorption of radionuclides may occur at different sites on smectite particles surface by means of different mechanisms of complexation, depending on the pH and ionic strength conditions as well as the type of metal and species involved (Wypych and Satyanarayana, 2004). Generally, the adsorption by ion-exchange is characterized by weak electrostatic interactions between the exchangeable cations and the permanently charged sites (outer-sphere complexation), which makes the radionuclide adsorption reversible and contributes to the strong competition between cations for the exchangeable sites (Bauer and Velde, 2014). The preference of smectite for cations absorbed by ion-exchange depends on the size and the charge of the ion. The affinity increases as smaller is the ion size and higher is the ion charge, due to the greater density of charge per unit volume of ions with smaller ionic radii (Bohn et al., 2015). Regarding to the adsorption of radionuclides on the external sites (Hydroxyl groups) of smectite, there is major contribution from the pH and ionic strength conditions, and the bonding strength is highly dependent of the type of radionuclide involved in the surface complexation (Selim and Sparks, 2001). The type of sites involved, as well as, the mechanism of surface complexation are following described for both  $\text{Sr}^{2+}$  and  $\text{UO}_2^{2+}$  on smectite:

- Previous extended X-ray absorption fine structure (EXAFS) studies of  $\text{Sr}^{2+}$  adsorbed on smectite have confirmed that  $\text{Sr}^{2+}$  retains its primary hydration sheath and only forms outer-sphere complexes with the surface hydroxyl sites of smectite, regardless the solution pH and ionic strength (Jenne, 1998). Identical experiments of  $\text{Sr}^{2+}$  adsorbed on illite have also confirmed that at  $\text{pH} < 12.5$  it remains forming outer-sphere complexes, which suggests that the increase of layer charge does not influence the mechanism of adsorption in this specific case (Fuller et al., 2016). In the case of Illite,  $\text{Sr}^{2+}$  was only forming inner-sphere complexes with the surface hydroxyl sites at  $\text{pH} > 12.5$ . It was also observed in this experiments that the amount of  $\text{Sr}^{2+}$  adsorbed, at moderate pH conditions, decreased as increasing of ionic strength, due to competition between the  $\text{Na}^+$  and  $\text{Sr}^{2+}$  for the sorption sites (Fuller et al., 2016). However, the amount of  $\text{Sr}^{2+}$  adsorbed remained high as increasing of pH and ionic strength, suggesting that the increase of ionic strength, as increasing of pH, is less significant (Fuller et al., 2016; Galamboš et al., 2013; Galamboš et al., 2009; Missana and García-Gutiérrez, 2007).

- EXAFS studies of  $\text{UO}_2^{2+}$  sorbed on Ca-smectite indicated that the mechanism of adsorption and the coordination geometry of  $\text{UO}_2^{2+}$  depends on the surface coverage. In this study, different surface binding sites were found as increasing of  $\text{UO}_2^{2+}$  concentration (Chisholm-Brause et al., 1994). The EXAFS results have also revealed that at low pH and low ionic strength  $\text{UO}_2^{2+}$  is adsorbed by ion exchange through the formation of outer-sphere complexes with the fixed charge sites in the interlayer region of smectite, whereas at higher pH and ionic strength an inner-sphere coordination through specific coordination at silanol and aluminol sites was observed (Sylwester et al., 2000). More recently, additional spectroscopic information also suggested the presence of different surface complexes on smectite (outer-sphere and inner-sphere complexation) as increasing of pH and ionic strength and for distinct  $\text{UO}_2^{2+}$  concentrations (Chisholm-Brause et al., 2001; Marques Fernandes et al., 2012).

#### 4.3.1.1. Surface complexation modeling

A more detailed interpretation of the behavior of radionuclide sorption on smectite may be provided by the surface complexation modeling, which consists on the formation of surface complexes between the radionuclide and the surface groups of smectite (Poinssot and Geckeis, 2012). The development of surface complexation models (SCM) predicts the behavior of radionuclides sorption on smectite through the optimization of different surface complexation constants, previously published and obtained for these specific reactions, and the use of non-adjustable parameters (protolysis reactions, site capacities, selectivity coefficients) that were previously determined for smectite (Kim, 2001; Zachara and McKinley, 1993). This simplifications have been adopted in order to reduce the complexity of the modelling process. It is pretended the standardization of SCM, developing a “unique model” that is based on thermodynamic approaches and parameter optimization (Tabatabai and Sparks, 2005; Turner et al., 1996). In this way, it is possible to reduce the number of adjustable parameters and provide a set of uniform parameters based on common reference values.

Generally, the surface complexation models combined both cation exchange and surface complexation on the hydroxyl groups of smectite, considering the protonation and deprotonation of the edge amphoteric sites of smectite. The cation exchange on the permanently charge planar sites (low pH) are usually modeled taking into account the

adsorbent CEC (eq/kg) and the selectivity coefficient for each ion exchange process occurring on the planar sites. For another hand, the surface complexation modeling assumes that metal uptake on the edge surface sites, occurs on two types of surface sites, named aluminol (AlOH) and silanol (SiOH) sites (McKinley et al., 1995; Turner et al., 1996; Zachara and McKinley, 1993). Previous studies have demonstrated satisfactory modelling of the  $UO_2^{2+}$  sorption on low charge smectite from near neutral pH to alkaline conditions, in the presence and absence of  $CO_2$  (g) (Korichi and Bensmaili, 2009; Marques Fernandes et al., 2012; Zachara and McKinley, 1993).

Models based on surface complexation reactions have been intensively studied (Frimmel et al., 2007). Electric double-layer models (EDL models) such as constant-capacitance model (CCM), diffuse double-layer model (DLM) and triple-layer model (TLM) are used to describe the adsorption of different contaminants on clay minerals surface, and assume that the particle surface charge and electrical potential result from surface complexation of protons and other sorbates (Sparks, 1998). The different EDL models are characterized by the stated relationships between surface potential and surface charge, and are distinguished by the position of the adsorbed species in the double-layer (Jenne, 1998). The diffuse-layer and constant capacitance models assume that the adsorbed species are positioned at the shear plane, whereas triple-layer model assumes that the cations are adsorbed at the shear plane or in a more distant plane (Jenne, 1998). The three models assume that the surface charge ( $\sigma_0$ ) is balanced by counterions charge. The DLM considers that the counterions charges ( $\sigma_d$ ) are located in the diffuse part of the EDL and the electroneutrality constrain is  $\sigma_0 + \sigma_d = 0$  (Toth, 2002). In the case of CCM the electrical potential relationship is linear ( $\sigma_0 = \epsilon_0 \cdot \epsilon_r \cdot k \cdot \psi_0$ ) (Toth, 2002).

## References

- Aligizaki, K.K., 2005. Pore Structure of Cement-Based Materials: Testing, Interpretation and Requirements. Taylor & Francis.
- Bachmaf, S., Merkel, B., 2011. Sorption of uranium(VI) at the clay mineral–water interface. *Environmental Earth Sciences* 63, 925-934.
- Batista, M.J., Martins, L.P., 2008. Preliminary Results of a Risk Assessment Study for Uranium Contamination in Central Portugal, in: Pasman, H.J., Kirillov, I.A. (Eds.), *Resilience of Cities to Terrorist and other Threats: Learning from 9/11 and further Research Issues*. Springer Netherlands, Dordrecht, pp. 69-84.
- Bauer, A., Velde, B.D., 2014. *Geochemistry at the Earth's Surface: Movement of Chemical Elements*. Springer Berlin Heidelberg.

- Bergaya, F., Lagaly, G., 2013. Handbook of Clay Science. Elsevier Science.
- Bohn, H.L., Strawn, D.G., O'Connor, G.A., 2015. Soil Chemistry. Wiley.
- Bradl, H.B., 2002b. Adsorption of heavy metal ions on clays, Encyclopedia of Surface and Colloid Science. Marcel Dekker, New York, pp. 373-384.
- Brantley, S., Kubicki, J., White, A., 2007. Kinetics of Water-Rock Interaction. Springer.
- Brebbia, C.A., Popov, V., 2011. Water Resources Management VI. WIT Press.
- Brunauer, S., Deming, L.S., Deming, W.E., Teller, E., 1940. On a theory on the van der Waals adsorption of gases. Journal of American Chemical Society 62, 1723-1732.
- Burzo, E., 2009. Sepiolite and palygorskite group of silicates, in: Wijn, H.P.J. (Ed.), Magnetic Properties of Non-Metallic Inorganic Compounds Based on Transition Elements. Springer Berlin Heidelberg, Berlin, Heidelberg, pp. 353-452.
- National Research Council, Committee to Assess the Performance of Engineered Barriers, Board on Earth Sciences and Resources, Division on Earth and Life Studies, 2007. Assessment of the Performance of Engineered Waste Containment Barriers. National Academies Press.
- Committee on Uranium Mining in Virginia, Committee on Earth Resources, Board on Earth Sciences and Resources, Division on Earth and Life Studies, National Research Council, 2012. Uranium Mining in Virginia: Scientific, Technical, Environmental, Human Health and Safety, and Regulatory Aspects of Uranium Mining and Processing in Virginia. National Academies Press, United States.
- Cabral Pinto, M., Silva, M., 2007. The Vale de Abrutiga Uranium Phosphates Mine, Central Portugal. 67, 251-252.
- Cabral Pinto, M., Silva, M., Neiva, A., 2004. Pollution of Water and Stream Sediments Associated with the Vale De Abrutiga Uranium Mine, Central Portugal. Mine Water and the Environment 23, 66-75.
- Cabral Pinto, M., Silva, M., Neiva, A., 2008. Geochemistry of U-bearing minerals from the Vale de Abrutiga uranium mine area, Central Portugal N. Jb. Miner. Abh 158, 183-198.
- Campbell, N.R., Ingram, J.C., 2014. 4 - Characterization of  $^{234}\text{U}/^{238}\text{U}$  Activity Ratios and Potential Inorganic Uranium Complexation Species in Unregulated Water Sources in the Southwest Region of the Navajo Reservation, in: Ahuja, S. (Ed.), Water Reclamation and Sustainability. Elsevier, Boston, pp. 77-94.
- Carvalho, F.P., 2014. The National Radioactivity Monitoring Program for the Regions of Uranium Mines and Uranium Legacy Sites in Portugal. Procedia Earth and Planetary Science 8, 33-37.
- Carvalho, F.P., Madruga, M.J., Reis, M.C., Alves, J.G., Oliveira, J.M., Gouveia, J., Silva, L., 2005a. Radioactive survey in former uranium mining areas in Portugal, International Workshop on Environmental Contamination from Uranium Production Facilities and Remediation Measures. International Atomic Energy, Lisbon, pp. 29-40.
- Cerveira, A., 1951. Sobre a metalogenia do urânio em Portugal. Boletim Sociedade Geológica de Portugal 8, 141-182.
- Chisholm-Brause, C., Conradson, S.D., Buscher, C.T., Eller, P.G., Morris, D.E., 1994. Speciation of uranyl sorbed at multiple binding sites on montmorillonite. Geochimica et Cosmochimica Acta 58, 3625-3631.
- Chisholm-Brause, C.J., Berg, J.M., Matzner, R.A., Morris, D.E., 2001. Uranium(VI) Sorption Complexes on Montmorillonite as a Function of Solution Chemistry. J Colloid Interface Sci 233, 38-49.
- Chorover, J., Brusseau, M.L., 2008. Kinetics of Sorption—Desorption, in: Brantley, S.L., Kubicki, J.D., White, A.F. (Eds.), Kinetics of Water-Rock Interaction. Springer New York, pp. 109-149.
- Christidis, G.E., 2011. Advances in the Characterization of Industrial Minerals. European Mineralogical Union.

- Churchman, G., Fitzpatrick, R., Eggleton, R., 1995. *Clays: Controlling the Environment*. CSIRO PUBLISHING.
- Duarte, P., Machado, L., Reis, M.J., 2005. Radon survey in old Uranium mines in the region of Sabugal, Portugal, International Workshop on Environmental Contamination from Uranium Production Facilities and their Remediation. International Atomic Energy Agency, Lisbon, pp. 71-79.
- Eberl, D.D., 1978. The reaction of montmorillonite to mixedlayer clay: The effect of interlayer alkali and alkaline earth cations. *Geochim. Cosmochim. Acta* 42, 1-7.
- European Commission, 2011. Environmental Radioactivity and Discharge Monitoring and part of National Monitoring System for Environmental Radioactivity in Portugal. Nuclear Energy Radiation Protection, Belgium, p. 40.
- Falck, W.E., 2015. 1 - Radioactive and other environmental contamination from uranium mining and milling, in: Velzen, L.v. (Ed.), *Environmental Remediation and Restoration of Contaminated Nuclear and Norm Sites*. Woodhead Publishing, pp. 3-34.
- Farrah, H., Pickering, W.F., 1979. pH effects in the adsorption of heavy metal ions by clays. *Chemical Geology* 25, 317-326.
- Frimmel, F.H., von der Kammer, F., Flemming, H.C., 2007. *Colloidal Transport in Porous Media*. Springer.
- Fuller, A.J., Shaw, S., Peacock, C.L., Trivedi, D., Burke, I.T., 2016. EXAFS Study of Sr sorption to Illite, Goethite, Chlorite, and Mixed Sediment under Hyperalkaline Conditions. *Langmuir* 32, 2937-2946.
- Galamboš, M., Krajňák, A., Roskopfová, O., Viglašová, E., Adamcová, R., Rajec, P., 2013. Adsorption equilibrium and kinetic studies of strontium on Mg-bentonite, Fe-bentonite and illite/smectite. *Journal of Radioanalytical and Nuclear Chemistry* 298, 1031-1040.
- Galamboš, M., Kufčáková, J., Roskopfová, O.g., Rajec, P., 2009. Adsorption of cesium and strontium on natrified bentonites. *Journal of Radioanalytical and Nuclear Chemistry* 283, 803-813.
- Geological Society of London, 2006. 3. Formation and alteration of clay materials. *Engineering Geology Special Publications* 21, 29-71.
- Guerra, F.D.C., Tavares, A.A.S., Tavares, J.M.R.S., 2016. Palliative treatment of metastatic bone pain with radiopharmaceuticals: A perspective beyond Strontium-89 and Samarium-153. *Applied Radiation and Isotopes* 110, 87-99.
- Guillaumont, R., Fanghänel, T., Fuger, J., Grenthe, I., Neck, V., Palmer, D.A., Rand, M.H., 2003. *Update on the Chemical Thermodynamics of Uranium, Neptunium, Plutonium, Americium and Technetium*. Elsevier Science.
- Gupta, C., Singh, H., 2003. *Uranium Resource Processing: Secondary Resources*. Springer.
- IAEA, 1999. *Technical options for the remediation of contaminated groundwater*. Waste Technology Section: International Atomic Energy Agency, Vienna.
- International Atomic Energy Agency (IAEA), 2012. *International status and prospects for nuclear power 2012*. IAEA, Vienna.
- Iskandar, I.K., Kirkham, M.B., 2001. *Trace Elements in Soil: Bioavailability, Flux, and Transfer*. CRC Press.
- Janardhan, V., Fesmire, B., 2010. *Energy Explained: Conventional Energy and Alternative*. Rowman & Littlefield Publishers.
- Jenne, E.A., 1998. *Adsorption of Metals by Geomedia: Variables, Mechanisms, and Model Applications*. Academic Press.
- Jiang, G.C.T., Aschner, M., 2015. Chapter 33 - Depleted Uranium, in: Gupta, R.C. (Ed.), *Handbook of Toxicology of Chemical Warfare Agents (Second Edition)*. Academic Press, Boston, pp. 447-460.
- Kayzar, T.M., Villa, A.C., Lobaugh, M.L., Gaffney, A.M., Williams, R.W., 2014. Investigating uranium distribution in surface sediments and waters: a case study of contamination

- from the Juniper Uranium Mine, Stanislaus National Forest, CA. *Journal of Environmental Radioactivity* 136, 85-97.
- Keith, L.S., Faroon, O.M., Fowler, B.A., 2015. Chapter 59 - Uranium\*, in: Nordberg, G.F.N.A.F. (Ed.), *Handbook on the Toxicology of Metals (Fourth Edition)*. Academic Press, San Diego, pp. 1307-1345.
- Kim, S.J., 2001. Sorption mechanism of U(VI) on a reference montmorillonite: Binding to the internal and external surfaces. *Journal of Radioanalytical and Nuclear Chemistry* 250, 55-62.
- L'Annunziata, M.F., 2012. *Handbook of Radioactivity Analysis*. Elsevier Science.
- Lagauzère, S., Terrail, R., Bonzom, J.-M., 2009. Ecotoxicity of uranium to Tubifex tubifex worms (Annelida, Clitellata, Tubificidae) exposed to contaminated sediment. *Ecotoxicology and Environmental Safety* 72, 527-537.
- Laird, D.A., 1999. Layer Charge Influences on the Hydration of Expandable 2:1 Phyllosilicates. *Clays and Clay Minerals* 47, 630-636.
- Langmuir, I., 1916. The Constitution and Fundamental Properties of Solids and liquids. Part I. Solids. *Journal of the American Chemical Society* 38, 2221-2295.
- Larsen, D., Egenhoff, S.O., Fishman, N.S., 2015. *Paying Attention to Mudrocks: Priceless!* Geological Society of America, Incorporated.
- LCW, 2008. Environmental remediation works of the Vale da Abrutiga old mining area. <http://www.lcwconsult.com/>.
- Liu, X., Hicher, P., Muresan, B., Saiyouri, N., Hicher, P.-Y., 2016. Heavy metal retention properties of kaolin and bentonite in a wide range of concentration and different pH conditions. *Applied Clay Science* 119, Part 2, 365-374.
- Laboratório Nacional de Energia e Geologia (LNEG), 1998. Mineral Potential of Portugal. [http://www.lneg.pt/CienciaParaTodos/edicoes\\_online/diversos/potential/texto](http://www.lneg.pt/CienciaParaTodos/edicoes_online/diversos/potential/texto).
- Lollar, B.S., 2005. *Environmental Geochemistry*. Elsevier.
- Lowell, S., Shields, J.E., Thomas, M.A., Thommes, M., 2012. *Characterization of Porous Solids and Powders: Surface Area, Pore Size and Density*. Springer Netherlands.
- Marques Fernandes, M., Baeyens, B., Dähn, R., Scheinost, A.C., Bradbury, M.H., 2012. U(VI) sorption on montmorillonite in the absence and presence of carbonate: A macroscopic and microscopic study. *Geochimica et Cosmochimica Acta* 93, 262-277.
- Maurer, S., 2000. *Prediction of Single Component Adsorption Equilibria*. Utz, Wiss.
- McKinley, J.P., Zachara, J.M., Smith, S.C., Turner, G.D., 1995. The influence of uranyl hydrolysis and multiple site-binding reactions on adsorption of U(VI) to montmorillonite. *Clays and Clay Minerals* 43, 586-598.
- Merkel, B., Planer-Friedrich, B., Wolkersdorfer, C., 2012. Uranium in the Aquatic Environment: Proceedings of the International Conference Uranium Mining and Hydrogeology III and the International Mine Water Association Symposium Freiberg, Germany, 15-21 September 2002. Springer Berlin Heidelberg.
- Merkel, B.J., Arab, A., 2014. *Uranium - Past and Future Challenges: Proceedings of the 7th International Conference on Uranium Mining and Hydrogeology*. Springer International Publishing.
- Meunier, A., 2005. *Clays*. Springer.
- Missana, T., García-Gutiérrez, M., 2007. Adsorption of bivalent ions (Ca(II), Sr(II) and Co(II)) onto FEBEX bentonite. *Physics and Chemistry of the Earth, Parts A/B/C* 32, 559-567.
- Mukherjee, S., 2013. *The Science of Clays: Applications in Industry, Engineering, and Environment*. Springer Netherlands.
- Murray, R.L., Holbert, K.E., 2015. Chapter 19 - Reactor theory introduction, in: Holbert, R.L.M.E. (Ed.), *Nuclear Energy (Seventh Edition)*. Butterworth-Heinemann, Boston, pp. 315-329.

- Nuclear Energy Agency (NEA), 2014. Managing Environmental and Health Impacts of Uranium Mining. OECD/Nuclear Energy Agency, Paris, p. 139.
- Neiva, A.M.R., Carvalho, P.C.S., Antunes, I.M.H.R., Silva, M.M.V.G., Santos, A.C.T., Cabral Pinto, M.M.S., Cunha, P.P., 2014. Contaminated water, stream sediments and soils close to the abandoned Pinhal do Souto uranium mine, central Portugal. *Journal of Geochemical Exploration* 136, 102-117.
- Neiva, A.M.R., Carvalho, P.C.S.d., Antunes, I.M.H.R., Santos, A.C.T.d., Cabral-Pinto, M.M.d.S., 2015. Spatial and temporal variability of surface water and groundwater before and after the remediation of a Portuguese uranium mine area. *Chemie der Erde - Geochemistry* 75, 345-356.
- Nero, J.M.G., Dias J.M.M., Pereira, A.J.S.C., Neves, L.J.P.F., Torrinha, J., 2005. Environmental evaluation and remediation methodologies of abandoned radioactive mines in Portugal, International Workshop on Environmental Contamination from Uranium Production Facilities and Remediation. International Atomic Energy Agency, Measuresheld in Lisbon
- Neves, O., Matias, M.J., 2007. Assessment of groundwater quality and contamination problems ascribed to an abandoned uranium mine (Cunha Baixa region, Central Portugal). *Environmental Geology* 53, 1799-1810.
- Nordberg, G.F., Fowler, B.A., Nordberg, M., 2014. Handbook on the Toxicology of Metals. Elsevier Science.
- Pan, D.-q., Fan, Q.-h., Li, P., Liu, S.-p., Wu, W.-s., 2011. Sorption of Th(IV) on Na-bentonite: Effects of pH, ionic strength, humic substances and temperature. *Chemical Engineering Journal* 172, 898-905.
- Pereira, R., Barbosa, S., Carvalho, F.P., 2013. Uranium mining in Portugal: a review of the environmental legacies of the largest mines and environmental and human health impacts. *Environmental Geochemistry and Health* 36, 285-301.
- Poinssot, C., Geckeis, H., 2012. Radionuclide Behaviour in the Natural Environment: Science, Implications and Lessons for the Nuclear industry. Elsevier Science.
- Portuguese Decree, 2007. Portuguese Legislation on Water Quality. *Diário da República I-A*, Lisbon. pp. 5747–5765.
- Rafferty, J.P., 2011. Minerals. Britannica Educational Pub.
- Selim, H.M., 2015. Phosphate in Soils: Interaction with Micronutrients, Radionuclides and Heavy Metals. CRC Press.
- Selim, H.M., Sparks, D.L., 2001. Heavy Metals Release in Soils. CRC Press.
- Siegel, M.D., Bryan, C.R., 2014. 11.6 - Radioactivity, Geochemistry, and Health, in: Turekian, H.D.H.K. (Ed.), *Treatise on Geochemistry (Second Edition)*. Elsevier, Oxford, pp. 191-256.
- Sparks, D.L., 1998. *Soil Physical Chemistry*, Second Edition. Taylor & Francis.
- Sposito, G., 2004. *The Surface Chemistry of Natural Particles*. Oxford University Press.
- Sukla, L.B., Pradhan, N., Panda, S., Mishra, B.K., 2015. *Environmental Microbial Biotechnology*. Springer International Publishing.
- Suzuki, M., 1993. *Fundamentals of Adsorption*. Elsevier Science.
- Sylwester, E.R., Hudson, E.A., Allen, P.G., 2000. The structure of uranium (VI) sorption complexes on silica, alumina, and montmorillonite. *Geochimica et Cosmochimica Acta* 64, 2431-2438.
- Tabatabai, M.A., Sparks, D.L., 2005. *Chemical processes in soils*. Soil Science Society of America.
- Thommes, M., Kaneko, K., Neimark, A.V., Olivier, J.P., Rodriguez-Reinoso, F., Rouquerol, J., Sing, K.S.W., 2015. Physisorption of gases, with special reference to the evaluation of surface area and pore size distribution (IUPAC Technical Report), in: Gruyter, D. (Ed.). IUPAC Division of Physical and Biophysical Chemistry Division.

- Toth, J., 2002. Adsorption. Taylor & Francis.
- Wypych, F., Satyanarayana, K.G., 2004. Clay Surfaces: Fundamentals and Applications. Elsevier Science.
- Yang, W., Zaoui, A., 2013. Uranyl adsorption on (001) surfaces of kaolinite: A molecular dynamics study. *Applied Clay Science* 80–81, 98-106.
- Yu, S., Mei, H., Chen, X., Tan, X., Ahmad, B., Alsaedi, A., Hayat, T., Wang, X., 2015. Impact of environmental conditions on the sorption behavior of radionuclide  $^{90}\text{Sr}(\text{II})$  on Namontmorillonite. *Journal of Molecular Liquids* 203, 39-46.
- Zachara, J.M., Long, P.E., Bargar, J., Davis, J.A., Fox, P., Fredrickson, J.K., Freshley, M.D., Konopka, A.E., Liu, C., McKinley, J.P., Rockhold, M.L., Williams, K.H., Yabusaki, S.B., 2013. Persistence of uranium groundwater plumes: Contrasting mechanisms at two DOE sites in the groundwater–river interaction zone. *Journal of Contaminant Hydrology* 147, 45-72.
- Zachara, J.M., McKinley, J.P., 1993. Influence of hydrolysis on the sorption of metal cations by smectites: Importance of edge coordination reactions. *Aquatic Sciences* 55, 250-261.

## 4.4. Structural characterization and reactivity study of smectite from bentonite rocks of Portugal

Adapted from Vanessa Guimarães, Fernando Rocha, Iuliu Bobos

Submitted to Journal of Clay Minerals

### Abstract

The reactivity of smectite and the structural changes produced after thermal treatments (300°C) of Li<sup>+</sup>, K<sup>+</sup> and Na<sup>+</sup> saturated smectite, characterized by heterogeneous structures, were studied for smectite BA1, PS2 and PS3. The layer charge and charge distribution were also evaluated through the solvation properties of the expandable Li- and K-smectite samples in Glycerol (GLY) and Ethylene Glycol (EG), respectively. The XRD results revealed a partial-swelling to 13.63 Å, 13.48 Å and 14.30 Å, for samples BA1, PS2 and PS3, respectively, after K<sup>+</sup>-exchange and EG solvation, indicating the formation of only a monolayer EG complex (1-EG). It was expected for samples BA1 and PS2 considering the layer charges calculated by the chemical formula method (-1.38 and -1.31). However, the layer charge of sample PS3 was overestimated by the chemical formula method and re-predicted by the XRD results.

The infrared spectroscopy results indicated that only Li<sup>+</sup> ions had capacity to migrate and be fixed on the hexagonal holes in the octahedral sheet of smectite samples. The decrease of layer charge involved in this process was characterized by significantly structural changes that were mainly evidenced by changes in the Si-O stretching bands and -OH bending bands. This process was also confirmed by the XRD results which showed a total collapse of the basal spacings to ≈9.60 Å. After Glycerol solvation, the basal spacing of samples BA1 and PS2 have partially expanded, confirming that part of layer charge resides in the tetrahedral sheets, whereas the basal spacing of sample PS3 remained collapsed. Both Infrared spectroscopy and XRD results suggested that the layer charge of sample PS3 was neutralized by Li<sup>+</sup> ions.

**Keywords:** smectite, heterogeneous structure, X-ray diffraction Infrared spectroscopy, bentonite, Portugal

#### 4.4.1. Introduction

Smectite clay is widely used as “buffer” barrier in engineered radioactive waste containment systems, owing to their low permeability and high sorption capacity (Pusch 1994; Madsen 1998). The performance of the engineering barrier in a high-level waste repository is highly affected by structural changes caused by alteration of the original smectite (Meunier et al. 1992; Lee et al., 2010). One of the most unwanted reaction is the smectite illitization (Inoue et al., 1992), which may cause a negative impact on smectite buffer. The effect of temperature is reflected by increase of smectite surface charge, induced by silica for aluminium substitution in the tetrahedral sheet, affecting also the cation exchange capacity (CEC) and their swelling properties (Christidis et al., 2006 Ferrage et al., 2005; Ferrage et al., 2007; Laird, 2006). Long-term stability of smectite after waste emplacement is low because the buffer material will be exposed to a maximum temperature of 150 °C at the surface of the waste package, pressure in the range of 100 to 300 bars and groundwaters of various compositions depending of geological environment (Proust et al., 1990). Detailed studies of the reactivity of dioctahedral smectite have shown that under hydrothermal conditions imply the formation of high- and low-charge layers in different proportions from the smectite (Bouchet et al., 1988) and progressive formation of illite-montmorillonite mixed layers (Eberl, 1978; Inoue et al., 1992).

Smectite is the general term for swelling clay and can refer to either montmorillonite or beidellite. The structural features of smectites and illite-smectite (I-S) mixed layers from bentonite deposits have shown charge heterogeneities as revealed by K or alkylammonium saturation tests (Howard, 1981; Talibudeen and Goulding, 1983; Cetin and Huff, 1995). Structural heterogeneities are due to contrasting chemical composition of octahedral and tetrahedral sheets from one layer to the other (Cuadros and Altaner, 1998), which may also influence the expandability and total surface area of expandable layer silicates (Laird, 1999). Specifically, the distribution of high- and low-charge layers in the stacking may lead to mixed-layered sequences involving more than two layer types (Foscolos and Kodama, 1974; Cradwick and Wilson, 1978).

The layer charge and charge distribution of smectite has been studied by X-ray diffraction and infrared spectroscopy analyses by means of thermal treatments of smectite samples previously saturated with different inorganic ions ( $K^+$ ,  $Mg^{2+}$ ,  $Li^+$ ) and further saturated with organic solvents (Christidis and Eberl, 2003; Madejová et al., 1999).

The main aim of this work is to understand the structure of three smectite samples (BA1, PS2 and PS3) collected from the bentonite rocks of Portugal, in order to predict the possible changes on sorption mechanism caused by structural modification of smectite minerals during alteration. Smectite samples studied in this work were previously used for  $\text{Sr}^{2+}$  and  $\text{UO}_2^{2+}$  sorption experiments in batch and using a continuous stirred flow-through reactor at pH 4 and 6 (Guimarães et al. 2015, 2016a, 2016b).

## 4.4.2. Materials and Methods

### 4.4.2.1. Materials

*Clay minerals selection and preparation.* Three selected bentonite rocks (BA1, PS2 and PS3) were collected from two different regions of Portugal: Benavila region (BA1) and Porto Santo Island, Madeira archipelago (PS2 and PS3). The rocks were gently crushed and then, treated chemically following the Jackson's (1975) technique to removed carbonates and Fe and Al oxyhydroxides. The samples were treated with Na-acetate (NaOAc) to remove carbonate (pH = 5.5; 80 °C). Both Fe- and Al-oxyhydroxides were removed using Na-dithionite and Na-citrate (pH = 7; T = 80 °C). After each treatment the samples were washed three times with deionized water and dialyzed until no salts were identified.

The <2  $\mu\text{m}$  fractions were obtained by sedimentation according to Stocks law. The clay fractions were concentrated by centrifugation and re-dispersed with an ultrasonic probe. The <2  $\mu\text{m}$  clay fractions were studied by X-ray diffraction (XRD), infrared-spectroscopy and electron microprobe analysis. The <2  $\mu\text{m}$  clay fractions were prepared as oriented specimens on glass slide and then, were X-ray run in air-dried (AD) and saturated with ethylene-glycol (EG) vapor during 24 h.

### 4.4.2.2. Experimental Procedures

*K<sup>+</sup>- and Mg<sup>2+</sup>-saturation clay fractions.* The structural behaviour of smectite samples was verified using the well-known chemical protocol to differentiate high- from low-charge smectite and to distinguish beidellite from montmorillonite. The <2  $\mu\text{m}$  clay fractions were saturated with 1M KCl to differentiate high- from low-charge smectite (Barshad and Kishk, 1970). The X-ray diffraction analysis was carried out on K-saturated clay fractions heated to 300 °C during 2 hour and then solvated with ethylene glycol (EG).

Also, different aliquots with 1M MgCl<sub>2</sub> (S:L=3.57 g/L) during 24 hours were used for clay saturation (Harward et al., 1968). The Mg<sup>2+</sup>-saturated clay fractions were XRD analysed before and after glycerol treatment.

*Li<sup>+</sup>-saturation clay fractions.* The Greene-Kelly test (Greene-Kelly, 1952) allowed to distinguish beidellite from montmorillonite. The <2 μm clay fractions were Li<sup>+</sup> saturated by adding 0.050 g of clay into 14 mL of 1M LiCl solution during 24 hours and then heated at 300 °C during 6h. The XRD analysis were carried out on oriented specimens of <2 μm clay fractions after Li<sup>+</sup> saturation and heat at 300 °C, and after glycerol solvation.

*Ca<sup>2+</sup> and Na<sup>+</sup> homoionic exchange.* Behind these protocols, the <2 μm smectite samples were homoionic exchange with 1M CaCl<sub>2</sub> and 1M NaCl solutions, in order to remove the interlayer ion, where the salt excess was removed by washing with distilled water.

*Treatment of smectite clay fractions in alkaline and acid solutions.* The <2 μm clay fractions were saturated with acidic and alkaline solutions, where the pH was previously fixed using HCL 1M and NaOH 1M.

#### 4.4.2.3. Methods and analytical techniques

*Cation exchange capacity.* The <2 μm clay fractions were Sr<sup>2+</sup> saturated and prepared in order to determine the cation exchange capacity (CEC). The experiments were carried out by adding 0.050 grams of smectite into the polypropylene centrifuge tubes with 14.00 mL of different stock solutions at different Sr<sup>2+</sup> concentrations, ranged between 5x10<sup>-4</sup> M and 1.50x10<sup>-2</sup> M. Suspensions were shaken for 34 hours, then centrifuged, separated and the solutions resulted were preserved by adding HNO<sub>3</sub> (65%) and stored at 4 °C for subsequent chemical analyses. The CEC was determined by Sr<sup>2+</sup> adsorption tests at pH=4. After Sr<sup>2+</sup> saturated the <2μm clay fractions the Sr<sup>2+</sup>-aqueous solutions were analysed by atomic absorption spectrometry (AAS). The CEC value was estimated from the maximum amount of Sr<sup>2+</sup> adsorbed according with the following relation: CEC(meq/g)=qSr<sup>2+</sup>(mmol/g)\*2.

*The Brunauer-Emmett-Teller specific surface area (BET).* The BET surface area of the <2μm clay fractions was characterized by nitrogen adsorption-desorption measurements with a Micromeritics Tristar II analyser. The samples were degassed at 200 °C overnight before the measurements were taken. The surface area was calculated based on the adsorption data in the relative partial pressure range of 0.05–0.2, and the pore size

distributions were determined based on the Barrett–Joyner–Halender (BJH) adsorption curve.

*X-ray diffraction.* The structural characterization of the <2  $\mu\text{m}$  clay fractions was performed by X-ray diffraction (XRD) using a Rigaku Geigerflex machine equipped with a  $\text{CuK}\alpha$  radiation and a scanning speed of  $1^\circ 2\theta/\text{min}$  in the range  $2\text{--}50^\circ 2\theta$ . The oriented specimens of the <2  $\mu\text{m}$  clay fractions prepared on glass slide were X-ray diffraction analysed in air-dried (AD) condition and saturated in ethylene-glycol (EG) vapour during 24 h. Prior to XRD analysis, the smectite heterogeneity was studied using several chemical treatments previously described.

*Infrared Spectroscopy.* The infrared (IR) spectroscopy in transmission mode was carried out with a Bruker Tensor 27 spectrometer. The samples were firstly prepared by mixing 1 mg smectite with 200 mg KBr and then, the powder mixtures were inserted in a holder and pressed at  $10 \text{ tons}/\text{cm}^2$  to obtain the transparent pellet. The infrared spectra in transmission mode were recorded in the  $4000\text{--}400 \text{ cm}^{-1}$  frequency region. The measurements of the adsorption bands integrated intensity were made using OPUS software supplied by the Bruker instrument.

*Electron microprobe analysis.* The <2  $\mu\text{m}$  clay fractions, which were previously pressed in pellets with diameter of 3 mm with a PIKE Hand Press Kit 161 – 1024 (Pike technologies). The pellets were located in the epoxy resin, dried during 24 h and subsequently polished using the 30, 10 and 2  $\mu\text{m}$  microfinishing films under dry conditions. The epoxy resin was prepared using the Araldite EAY 103-1 and a HY956-KG hardener (9:1 ratio) and then dispersed in a holder of 13 mm. The major elements of minerals were determined using a Jeol Hyperprobe JXA-8500F electron microprobe operated at 15 kV accelerating voltage and 10 nA beam current. Detection limits ( $3\tau$ ) above mean background were 0.03 wt.% for most oxides with counting times of 80 s. Standards used include albite ( $\text{NaK}\alpha$ ), orthoclase ( $\text{AlK}\alpha$ ,  $\text{SiK}\alpha$ ,  $\text{KK}\alpha$ ), apatite ( $\text{CaK}\alpha$ ,  $\text{PK}\alpha$ ), MgO ( $\text{MgK}\alpha$ ),  $\text{MnTiO}_3$  ( $\text{MnK}\alpha$ ),  $\text{TiO}_2$  ( $\text{TiK}\alpha$ ),  $\text{Fe}_2\text{O}_3$  ( $\text{FeK}\alpha$ ).

*Atomic absorption spectrometry.* Chemical analyses of  $\text{Sr}^{2+}$  aqueous solutions were carried out by atomic absorption spectroscopy using a flame absorption spectrometer Perkin Elmer, AAnalyst 200 model with a Strontium hollow cathode lamp, wavelength 460.73 nm, air flow 5.2 L/min and acetylene flow 2.5 L/min. The 5 mL of the acidified strontium solution was mixed with 750  $\mu\text{L}$  of lanthanum chloride ( $\text{LaCl}_3 \cdot 7\text{H}_2\text{O}$ ) solution previously prepared (176 g of  $\text{LaCl}_3 \cdot 7\text{H}_2\text{O}$  and 19.1 g of KCl diluted in 1000 mL of deionised water).

### 4.4.3. Results and Discussion

#### 4.4.3.1. Physical properties and crystal chemistry of smectite samples

Cation exchange capacity, BET and crystal chemistry corresponding to the three selected samples are shown in Table 5. The influence of charge distribution of selected smectite samples was evaluated taking into account the ratio between the CEC values and the respective layer charge deficits (Table 5).

Table 5. Chemical composition, crystal chemistry, cation exchange capacity and BET of smectite samples.

Oxides	Mass (%)		
	BA1	PS2	PS3
SiO <sub>2</sub>	52.26	51.18	55.34
Al <sub>2</sub> O <sub>3</sub>	20.33	17.51	18.57
Fe <sub>2</sub> O <sub>3</sub>	6.96	6.10	8.08
MnO	---	0.22	0.08
MgO	3.17	3.57	4.26
CaO	3.58	1.78	2.07
Na <sub>2</sub> O	1.48	2.65	2.28
K <sub>2</sub> O	---	0.85	1.64
H <sub>2</sub> O	12.22	16.13	7.70
Total	100.00	100.00	100.00
	N° atoms/O <sub>10</sub> (OH) <sub>2</sub>		
Si	3.64	3.75	3.70
Al	1.30	1.26	1.16
Al	0.36	0.25	0.30
Fe	0.36	0.34	0.41
Mg	0.33	0.39	0.43
Ca	0.27	0.14	0.15
Na	0.20	0.37	0.30
K	---	0.08	0.14
Charge deficit/O <sub>10</sub> (OH) <sub>2</sub>	-0.69 (48%O;52%T)	-0.66 (62%O;38%T)	-0.73 (59%O;41%T)
CEC (meq/g)	0.96	1.04	0.81
S <sub>BET</sub> (m <sup>2</sup> /g)	12	26	84

Different charge layers reveal different compositions regarding to the degree of octahedral and tetrahedral substitutions occurring on smectite layers. Higher proportions of tetrahedral substitution ( $-0.37/(\text{Si,Al})_4\text{O}_{10}$ ) correspond to sample BA1, whereas the lower tetrahedral charge deficit and higher octahedral substitutions were found in samples PS2 ( $-0.26/(\text{Si,Al})_4\text{O}_{10}$ ) and PS3 ( $-0.30/(\text{Si,Al})_4\text{O}_{10}$ ). Sample BA1 has higher charge than PS2 but lower CEC. The lower proportion of tetrahedral substitutions of PS2 improved the adsorption on interlayer sites, contrary to what is observed for sample PS3 (CEC=0.81 meq/g). Usually, a decrease of CEC does occur as the percentage of illite layers increases in the randomly interstratified structure of I/S formed. Sample PS3 has higher proportion of illite interstratified layers into a randomly 2W/1W-smectite with a montmorillonitic character.

#### 4.4.3.2. X-ray diffraction

*Air-dried and EG solvation.* The  $<2\mu\text{m}$  fractions of samples BA1, PS2 and PS3 were X-ray run in AD and after EG solvation conditions (Figs. 10a, 11a and 12a).

*Sample BA1.* The 001 reflection occurs at 14.47 Å in AD and expanded to 16.29 Å after the EG treatment confirming the presence of a lower proportion of one-water smectite (1WS) layers interstratified with two-water smectite (2WS) layers (15 Å) (Fig. 10a).

*Sample PS2.* The XRD pattern shows a 001 reflection at 12.45 Å and after EG the 001 peak expanded to 15.10 Å. This reveals a higher content of 1WS layers interstratified with 2WS layers (Fig. 2a).

*Sample PS3.* The 001 peak occurs at 13.90 Å, and expanded to 16.50 Å after EG saturation (Fig. 3a).

*K<sup>+</sup>-saturation.* The XRD patterns of K<sup>+</sup>-saturated smectite samples and heated at 300 °C show the 001 peak collapse at 10.07 Å (BA1), 10.12 Å (PS2) and 10.25 Å (PS3) (Figs. 10c, 11c and 12c). Smectite samples were further EG solvated during 24 hours at 60 °C, in order to study the swelling properties of distinct K<sup>+</sup> saturated smectite. The XRD patterns reveal a partial swelling to 13.63 Å, 13.48 Å and 14.30 Å for samples BA1, PS2 and PS3, respectively. A monolayer EG complex (1-EG) was formed after K<sup>+</sup>-exchange, heated at 300 °C and EG solvation, revealing that the 2:1 layers failed to form 2-EG layer complex, as usually observed for low-charge montmorillonite.

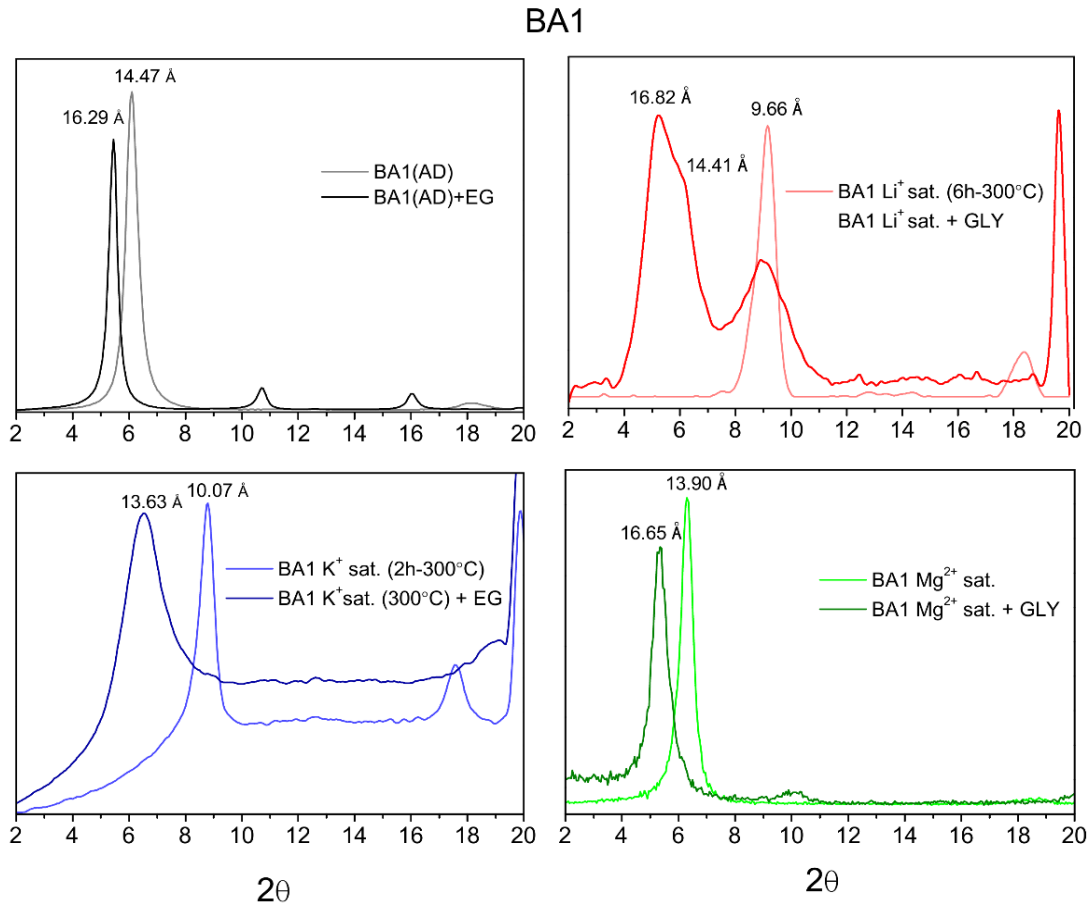


Fig.10 - XRD patterns of samples BA1. a) air-dried and ethylene glycol solvation; b) Li-saturation (Greene-Kelly test); c) K-saturation and heat at 300 °C; d) Mg-saturation and glycerol solvation.

Three different layers at  $17 \text{ \AA}$ ,  $14 \text{ \AA}$  and  $10 \text{ \AA}$  may be formed if the layer charge corresponds to  $-0.28$ ,  $-0.60$  and  $-1.00 \text{ eq./O}_{10}(\text{OH})_2$ , respectively (Tettenhorst and Johns, 1966). In this way, the presence of only one fraction at the 001 reflection (1-EG layer complex), for each K-smectite, suggests that their different 2:1 layers have similar charges.

**Mg<sup>2+</sup>-saturation.** After Mg<sup>2+</sup> saturation and glycerol solvation, the basal spacing expanded to  $16.65 \text{ \AA}$  (BA1) and to  $17.31 \text{ \AA}$  (PS2 and PS3) (Figs. 10d, 11d and 12d). The Mg-saturation test confirmed that no vermiculite layers are present in smectite structures.

**Greene-Kelly test.** The most used method to distinguish beidellite from montmorillonite is based on the Hofmann-Klemen effect which consists on the reduction of the octahedral layer charge compromising the hydration, solvation and expansion properties

of smectite (Greene-Kelly, 1952). The XRD patterns (Figs.10b, 11b and 12b) show changes of the 001 basal spacing of smectite samples after Li<sup>+</sup> saturation and heating to 300 °C.

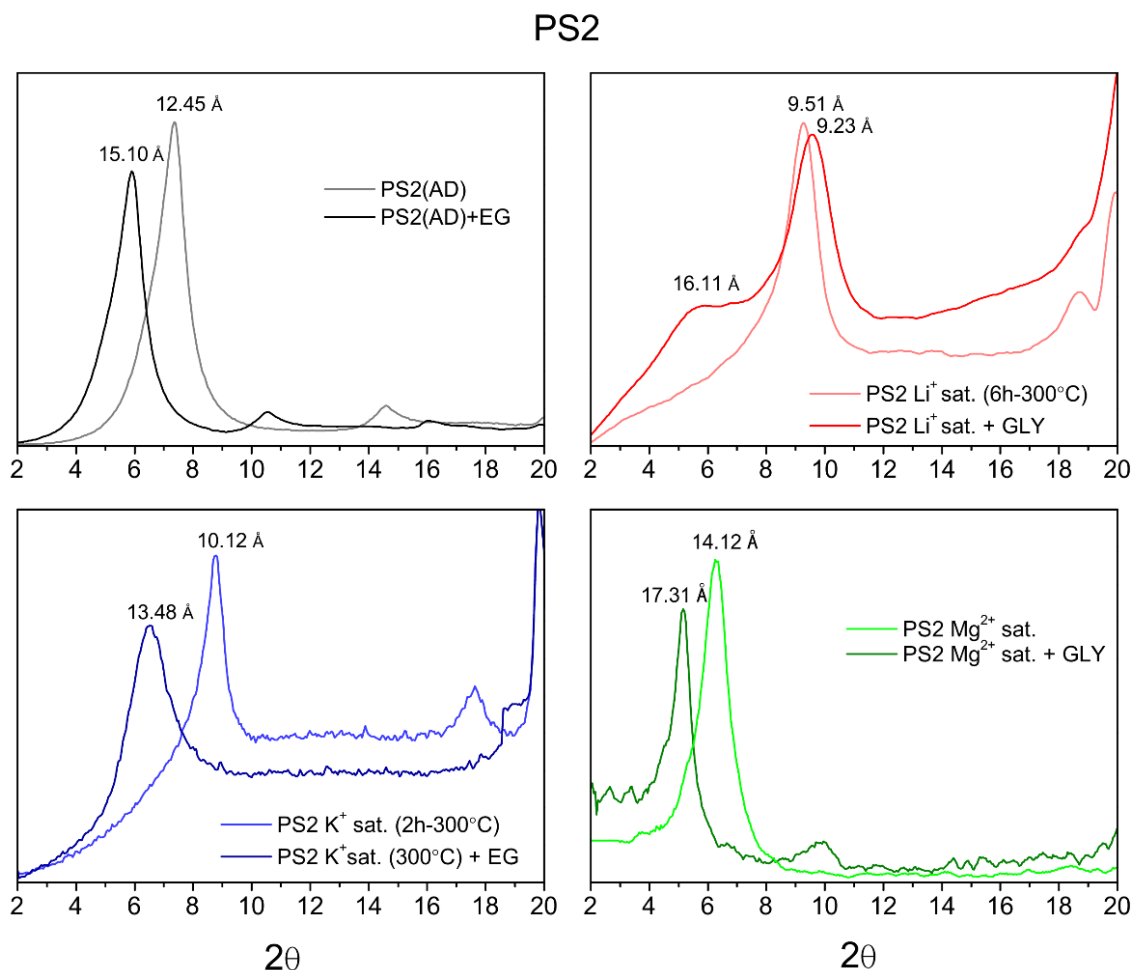


Fig.11 - XRD patterns of sample PS2. a) air-dried and ethylene glycol solvation; b) Li-saturation (Greene-Kelly test); c) K-saturation and heat at 300 °C; d) Mg-saturation and glycerol solvation.

The 001 basal plane spacing collapsed to 9.66 Å, 9.51 Å and 9.55 Å for samples BA1, PS2 and PS3 (Figs.10b, 11b and 12b), which suggests that the Li<sup>+</sup> ions have been attracted to the negative charges sites. The magnitude of octahedral and tetrahedral substitutions affects the glycerol solvation process, once the re-expansion until 16.5-17 Å will only occur if the layer charge is mainly concentrated on the tetrahedral sheet. The thermal treatment of smectite saturated by cations of small radius triggers the migration of

Li<sup>+</sup> ions from the interlayer positions to the vacant octahedral sites, resulting into a marked decrease of its net layer charge and its cation exchange capacity. According to Schultz (1969), the percentage of re-expansion peak ratios (18:9.6 Å) may be divided in three different classes in the montmorillonite-beidellite series: <30% re-expansion, montmorillonite is dominant; 30-60% re-expansion, an interstratified structure montmorillonite-beidellite is dominant; >60% re-expansion, beidellite is dominant.

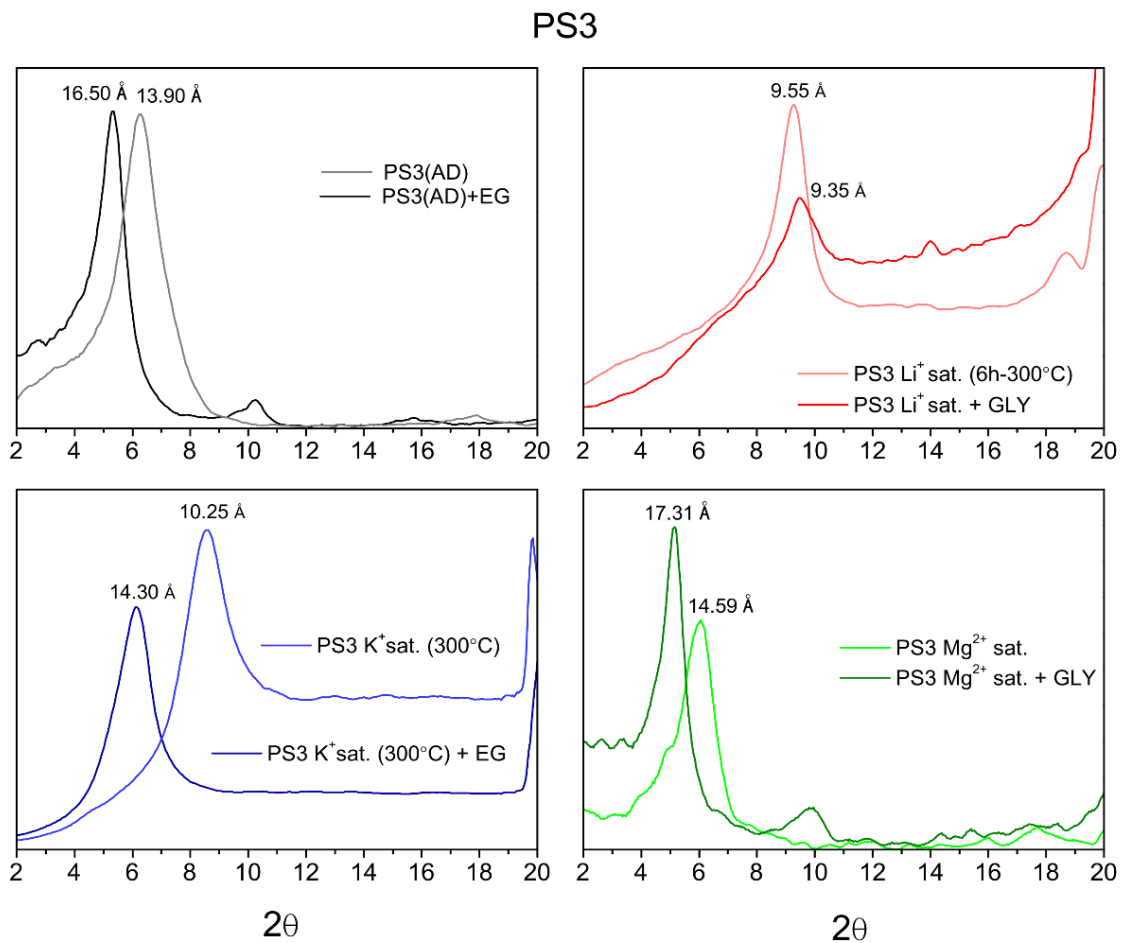


Fig.12 - XRD patterns of sample PS3. a) air-dried and ethylene glycol solvation; b) Li-saturation (Green-Kelly test); c) K-saturation and heat at 300 °C; d) Mg-saturation and glycerol solvation.

After Glycerol solvation, the presence of a beidellitic component (16.82 Å = beidellite) interstratified with 2W/1W-smectite (9.66 Å = 2W smectite) was identified for Sample BA1.

The peak at 14.41 Å represents a mixed structure between beidellite (16.82Å) and montmorillonite (9.66 Å), assumed as 1W-beidellite, characterized by isomorphic substitutions on the octahedral and tetrahedral sheets. Part of smectite layers is of beidellite-like character (16.82 Å) with predominance of net layer charge located in the tetrahedral sheet (Fig.10). The existence of these layers is attributed to the heterogeneous distribution of layer charge on smectite structure (Lagaly, 1979; Malla and Douglas, 1987; Petit et al., 1998).

After Glycerol solvation most of layers remained collapsed at 9.40 Å for Sample PS2, and few layers expanded to 16.50 Å (Fig.11), confirming the presence of beidellite-like layers, where the layer charge on tetrahedral sheet is dominant. The basal spacing of Sample PS3 did not expand after Glycerol treatment, suggesting a 2W-smectite structure (Ca,Na-montmorillonite) with a net layer charge on the octahedral sheet that was totally compensated by Li<sup>+</sup> ions (Fig.12). In this case, the tetrahedral charge calculated by the chemical formula method was compensated by the presence of illite interstratified, where K<sup>+</sup> ions were fixed into the hexagonal cavities.

Assuming that the octahedral charge was neutralized by Li<sup>+</sup> ions and the remaining charge is located in the tetrahedral sheet, it is possible to segregate the tetrahedral charge according to the results obtained after Glycerol solvation process. According to Calvet and Prost (1971), when the remaining tetrahedral charge is higher than 0.38/O<sub>20</sub>(OH)<sub>4</sub> smectite expands to 16.5-17 Å after Glycerol treatment. If the tetrahedral charge is between 0.23 and 0.38/O<sub>20</sub>(OH)<sub>4</sub>, smectite has a random interstratified structure with collapsed, expanded to 14 Å, and expanded to 16.5-17 Å layers. Contrary, smectite has only collapsed layers (≈9.6 Å) after Glycerol solvation whether the tetrahedral layer charge is <0.23/O<sub>20</sub>(OH)<sub>4</sub>. Considering it, the interstratified structure of smectite BA1 is characterized by the presence of tetrahedral sheets with charges between 0.23 and 0.38/O<sub>20</sub>(OH)<sub>4</sub>, with higher proportion of expanded layers, whereas smectite PS2 has a lower proportion of expanded layers to 16.5 Å, with tetrahedral charges >0.38/O<sub>20</sub>(OH)<sub>4</sub>. Smectite PS3 has no expanded layers, which means that the tetrahedral charges are lower than 0.23/O<sub>20</sub>(OH)<sub>4</sub> (Fig.12).

Acid and alkaline treatment. The <2µm fractions of sample BA1 were chemical treated in acid and alkaline solution and then XRD run. The intensity of the 001 peak decreased and expanded few Å in both acid (pH = 2) and alkaline (pH = 11) environment (Fig.13).

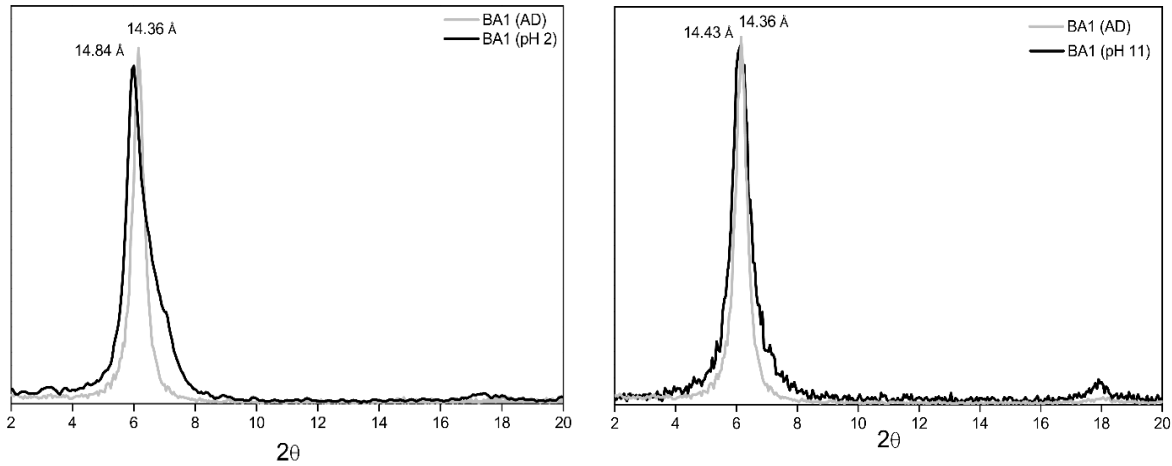


Fig.13 - XRD patterns of sample BA1 treated at acid (pH = 2) and alkaline (pH=11) conditions.

The expansion observed is related with the particle charge. At both extreme pH conditions, the clay mineral particles acquire total positive (pH=2) or negative charge (pH=11), depending on the solution pH, which contributes to increase the repulsion between subsequent layers, and therefore, to increase their interlayer distances. The structure of smectite is conserved and no structural damage were observed. Also the samples PS2 and PS3 revealed the same behaviour.

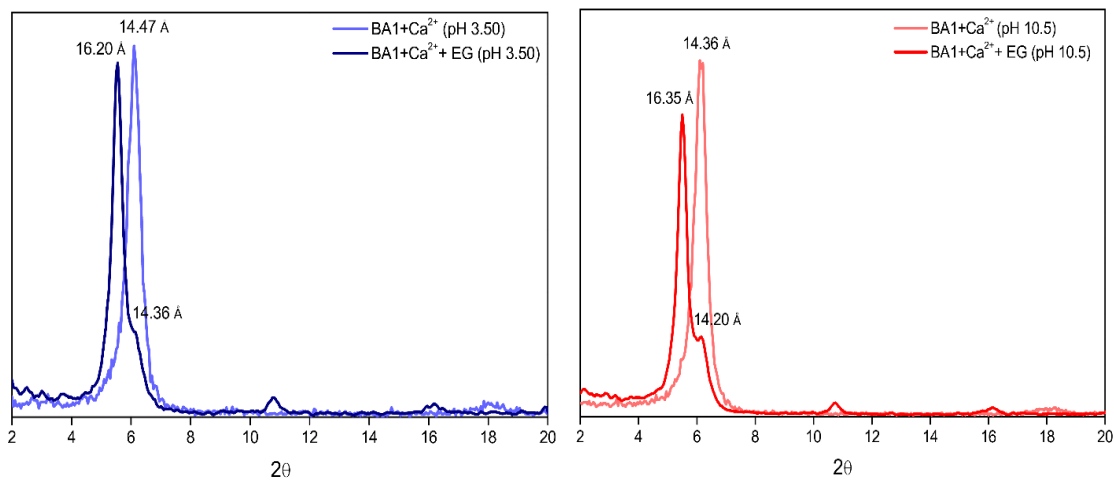


Fig.14 - XRD patterns of Ca-saturated smectite sample (BA1) treated at acid (pH = 2) and alkaline (pH=11) conditions.

Also, Ca-saturated smectite sample was treated with acid and alkaline solutions. In this case, the XRD patterns (Fig.14) does not show additional expansion in acidic and alkaline conditions, when compared to the results obtained after  $\text{Ca}^{2+}$  saturation at neutral pH (Fig.15), probably due to the presence of more  $\text{Ca}^{2+}$  in the interlayer which may have restricted the swelling capacity. A shoulder of the 001 peak is well evidenced in these samples after EG salvation. The shoulder at 14 Å is probably associated with some unexpandable smectite layers.

$\text{Ca}^{2+}$ - and  $\text{Na}^+$ -saturation. The XRD patterns obtained in AD conditions and after EG solvation of oriented specimens of the Ca- and Na-saturated smectite samples are shown in Fig. 14. The 001 peak of the XRD patterns of  $\text{Ca}^{2+}$ -saturated samples (BA1, PS2 and PS3) in air-dried conditions occurs at 14.60 Å, 14.47 Å and 14.40 Å, whereas after EG treatment expanded to 16.20 Å, 16.20 Å and 16.35 Å. The 001 peak of Ca-smectite occurs at 15 Å for 100% Ca-exchange, and we noted that few smectite layers remain inaccessible after subsequent Ca-exchange.

$\text{Na}^+$ -saturated samples show the 001 peak at 12.61 Å, 12.45 Å and 12.75Å, which expanded after EG solvation to 17.76 Å, 17.15 Å and 16.86 Å. Contrary to what was observed for Ca-smectite samples, Na-exchange is 100% for the three smectite samples. The 001 peak of Ca-saturated smectite solvated with EG corresponding to samples PS2 and PS3 is very broad confirming an interstratification between 2W-smectite and K-I. By contrast, the 001 peak of sample BA1 is sharp confirming a pure smectite, but with distinct layers (montmorillonite and beidellite).

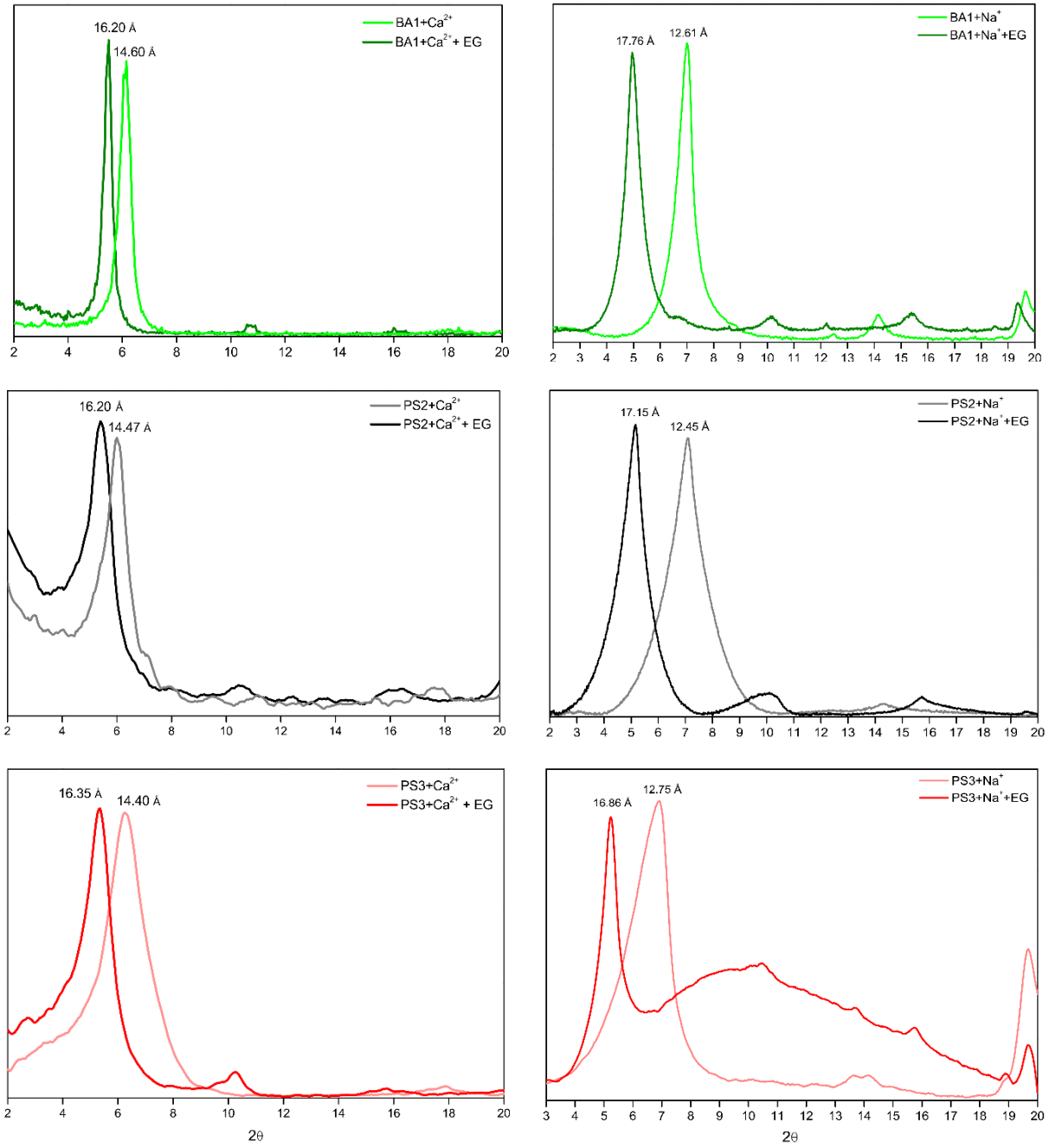


Fig.15 - XRD patterns of Ca<sup>2+</sup> and Na<sup>+</sup>-saturated smectite samples (BA1, PS2 and PS3) in air-dried conditions and after ethylene glycol solvation.

#### 4.4.3.2.1. Interpretation

Sample BA1. The crystal chemical composition of the  $<2\mu\text{m}$  clay fraction confirmed the presence of  $\text{Na}^+$  as exchangeable cation, where the presence of few Na-montmorillonite layers interstratified with Ca-montmorillonite is confirmed by the position of 001 peak in air-dried at  $14.47 \text{ \AA}$  and not to  $15 \text{ \AA}$  typical for 100 % Ca-montmorillonite. Two-waters (2W) smectite (Ca-montmorillonite) interstratified with 1-water (1W) smectite (Na-montmorillonite) characterizes sample BA1.

The 001 peak collapsed to  $10.07 \text{ \AA}$  after  $\text{K}^+$  saturation and heat at  $300 \text{ }^\circ\text{C}$  (2h), and partially expanded to  $13.63 \text{ \AA}$  after EG solvation, confirming a 2W/1W-smectite randomly interstratified structure. The Mg-saturation test confirmed no vermiculite layers in smectite structure. The Green-Kelly test confirms the presence of a beidellitic component ( $16.82 \text{ \AA} =$  beidellite) interstratified with 2W/1W-smectite ( $9.66 \text{ \AA} =$  2W smectite). The peak at  $14.41 \text{ \AA}$  represents a mixed structure between beidellite ( $16.82 \text{ \AA}$ ) and 2W-smectite ( $9.66 \text{ \AA}$ ), assumed as 1W-beidellite. Part of smectite layers is of beidellitic character ( $16.80 \text{ \AA}$ ) with more than 50% of net layer charge location in the tetrahedral sheet. Similar experimental conditions were reported by Schultz (1969) and by Sato et al. (1992), whose results revealed that the basal spacings have expanded between  $13 \text{ \AA}$  and  $16 \text{ \AA}$ , when the layer charge was higher than  $0.43 \text{ eq./O}_{10}(\text{OH})_2$ , and to  $14 \text{ \AA}$  for layer charges ranging between  $0.57 - 0.63 \text{ eq./O}_{10}(\text{OH})_2$ , with tetrahedral charge higher than  $0.70 \text{ eq./O}_{20}(\text{OH})_4$ .

Sample PS2. The  $12.45 \text{ \AA}$  peak which expanded at  $15.10 \text{ \AA}$  corresponds to a randomly mixed layers K-illite/2W/1W-smectite or K-illite/(Na,Ca)-montmorillonite (R0, 85-90%S). After K-saturation the 001 peak collapsed to  $10.12 \text{ \AA}$  and expanded at  $13.48 \text{ \AA}$  after  $300 \text{ }^\circ\text{C}$  heated and EG solvation, where a randomly interstratified structure is formed with 2W/1W-smectite. The Mg-test confirms the absence of vermiculite layers. The smectite layers are of beidellitic and montmorillonitic character with net layer charge in both tetrahedral and octahedral sheets, as indicated by the Greene-Kelly test.

Sample PS2 seems to have the same smectite layers as sample BA1, excepted by the presence of K-illite layers randomly interstratified with 2W/1W-smectite with beidellitic character.

Sample PS3. XRD pattern corresponds to a randomly interstratified structure of K-I/1W/2W-smectite (R=0; 80%S), where no beidellitic layers did occur.

Conclusion. The XRD patterns of smectite samples studied correspond to a randomly interstratified structure with a tendency towards segregation into two components:

12 Å Na-smectite and 15 Å Ca-smectite layers. The low-charge and high-charge smectite layers may be distinguished by their swelling and collapse behavior after saturation with K<sup>+</sup> and EG solvation (Schultz, 1969). After K<sup>+</sup> saturation at heat at 300°C (2h) there is a collapse to 10 Å, which is shifted to near 14 Å after EG solvation if the layer charge is less than 0.57/(Si,Al)<sub>4</sub>O<sub>10</sub>. The tetrahedral layer charge measured in samples analyzed ranges from -0.37 to 0.30 and -0.26/(Si,Al)<sub>4</sub>O<sub>10</sub>. The Mg-saturation test confirmed the absence of vermiculite layers in the samples studied.

Montmorillonite was distinguished from beidellite layers taking into account their swelling properties after octahedral neutralization with Li<sup>+</sup> and heat treatment (Greene-Kelly, 1952). The samples BA1 and PS2 correspond to 2W-smectite with beidellitic character interstratified with 1W-smectite. Few K-I layers are also randomly interstratified with 2W/1W-smectite in sample PS2. Sample PS3 is a randomly interstratified I/S structure (R=0), where smectite is constituted by a randomly 2W/1W smectite with a montmorillonitic character (substitutions on the octahedral sheet).

Considering the previous characterization, smectite structures are represented in Fig.16, where the different types of layers described above are randomly interstratified. The calculated amount of negative layer charge was estimated from the crystal chemistry information of each clay.

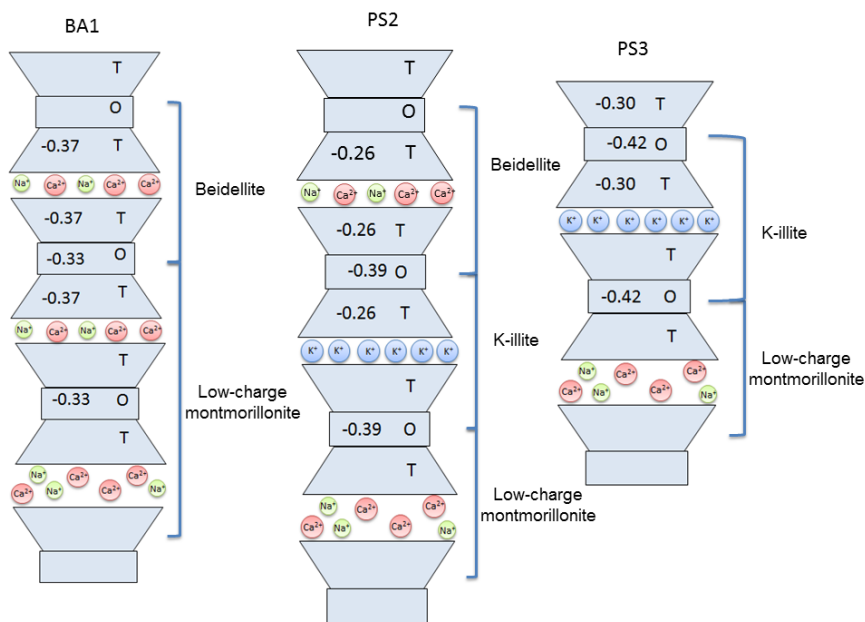


Fig.16 - Idealization of smectite structure samples used in sorption experiments: a) BA1: beidellite and low-charge montmorillonite interstratified structure; b) PS2: beidellite, illite and low-charge montmorillonite randomly interstratified structure; c) PS3: illite and low-charge montmorillonite randomly interstratified structure.

### 4.4.3.3. Infrared spectroscopy

#### 4.4.3.3.1. Characterization of vibrational planes of smectite samples

The following vibrational planes are discussed in this work: i) The OH<sup>-</sup> stretching vibrations occur in the frequency range between 3700 cm<sup>-1</sup> and 3500 cm<sup>-1</sup>; ii) The Si-O stretching vibrations and M-OH bending modes and lattice deformations are between 1100 cm<sup>-1</sup> and 550 cm<sup>-1</sup>. The bending modes associated with the Al<sub>2</sub>OH, AlFeOH and AlMgOH, depend on the degree of isomorphic substitutions on the octahedral sheet and are usually present in the IR spectrum of smectite. The vibration frequencies ranges vary between 912 and 935 cm<sup>-1</sup> for the Al<sub>2</sub>OH band and correspond to 868-890 cm<sup>-1</sup> and to 832-848 cm<sup>-1</sup> for the AlFeOH and AlMgOH vibration modes; iii) The bending vibrations assigned to the Si-O are represented in the range between 600 cm<sup>-1</sup> to 400 cm<sup>-1</sup>, where the Al-O-Si bending frequencies appears between 515 cm<sup>-1</sup> and 525 cm<sup>-1</sup> and the Si-O-Si mode occurs at about 465 cm<sup>-1</sup>.

Vibrational planes of air-dried samples. The OH<sup>-</sup> and Si-O stretching vibrations and M-OH bending vibrations are close for the three smectite samples. However, the bending vibrations assigned to Si-O, Al-O-Si and Si-O-Si show different in-plane vibration frequencies, caused probably by different proportions of isomorphic substitutions on the tetrahedral sheets. These substitutions affected the Al-O-Si and Si-O-Si bending modes, which decreased their frequencies as increasing of Al<sup>3+</sup> for Si<sup>4+</sup> in the tetrahedral sheet. The Al-O-Si band occurs at 515 cm<sup>-1</sup> (BA1), 522 cm<sup>-1</sup> (PS2) and 519 cm<sup>-1</sup> (PS3), whereas the Si-O-Si band arises at 459 cm<sup>-1</sup> (BA1), 467 cm<sup>-1</sup> (PS2) and 465 cm<sup>-1</sup> (PS3). The interatomic distances and bond strengths are changed for structures where isomorphic substitutions occur, increasing the distortion in the local bonding environment and decreasing the vibration frequencies (Gates, 2005). The stretching vibration and bending modes of air-dried smectite samples are resumed in Table 6.

Vibrational planes of specimens in acid and alkaline environment. No structural modifications were observed than the vibrational planes previously discussed in air-dried.

Table 6. Vibration planes of smectite in the region 1100 - 400  $\text{cm}^{-1}$ .

Vibration modes	Wavenumber ( $\text{cm}^{-1}$ )		
	BA1	PS2	PS3
Si-O	1030	1030	1030
Al <sub>2</sub> OH	915	915	916
AlFeOH	873	872	875
AlMgOH	840	835	838
M-O	625	624	624
Al-O-Si	515	522	519
Si-O-Si	459	467	465

*Vibrational planes of Li-smectite and K-, Na-smectite after thermal treatment at 300*

°C. The charge neutralization and irreversible collapse of smectite layers depend on the size of the interlayer cation (Karakassides et al., 1999; Madejová et al., 1996). The IR spectra obtained for Li-smectite revealed structural modifications in the region between 1200  $\text{cm}^{-1}$  and 400  $\text{cm}^{-1}$  after the heating treatment. The  $\text{Li}^+$  (1.80 Å) has capacity to migrate and to be fixed into the hexagonal holes of the octahedral sheet (2.52 Å). The main structural changes occurred on different smectite samples after heated at 300 °C are shown in Fig.17. In the case of K- and Na-smectite there are no structural modifications.

The structural changes of Li-smectite are clearly evidenced by the vibrations corresponding to the M-OH and Si(Al)-O-Si bending modes and the Si-OH stretching modes (Figs. 17 and 18), which suggests that both octahedral and tetrahedral layers were influenced. The IR spectra reveal a shift of the main M-OH bending vibrations to higher frequencies due to the movement of dehydrated  $\text{Li}^+$  on the hexagonal holes. The IR spectrum of sample BA1 show that the Al-OH band shifted from 915  $\text{cm}^{-1}$  to 923  $\text{cm}^{-1}$ , involving a significant decrease of vibration intensity. The same behaviour is observed for the AlFeOH and AlMgOH bending vibrations, which shifted from 873  $\text{cm}^{-1}$  to 877  $\text{cm}^{-1}$  and from 840  $\text{cm}^{-1}$  to 849  $\text{cm}^{-1}$ , respectively. The decrease of intensity of the OH<sup>-</sup> bending vibrations was especially observed in the IR spectra of samples PS2 and PS3, which hampered the analysis of structural changes. In the case of sample PS3, the AlMgOH band shifted from 838  $\text{cm}^{-1}$  to 848  $\text{cm}^{-1}$ , whereas the Al<sub>2</sub>OH and AlFeOH bands are not distinguished after  $\text{Li}^+$  fixation. The decrease of intensity of the OH<sup>-</sup> bending vibrations of sample PS2 was even more pronounced and only the shift from 835  $\text{cm}^{-1}$  to 846  $\text{cm}^{-1}$ , assigned to the AlMgOH bending mode, was slightly detected. A new band was detected at

800  $\text{cm}^{-1}$  for all smectite samples and was assigned to the AlMgLiOH bending mode (Madejová et al., 2000).

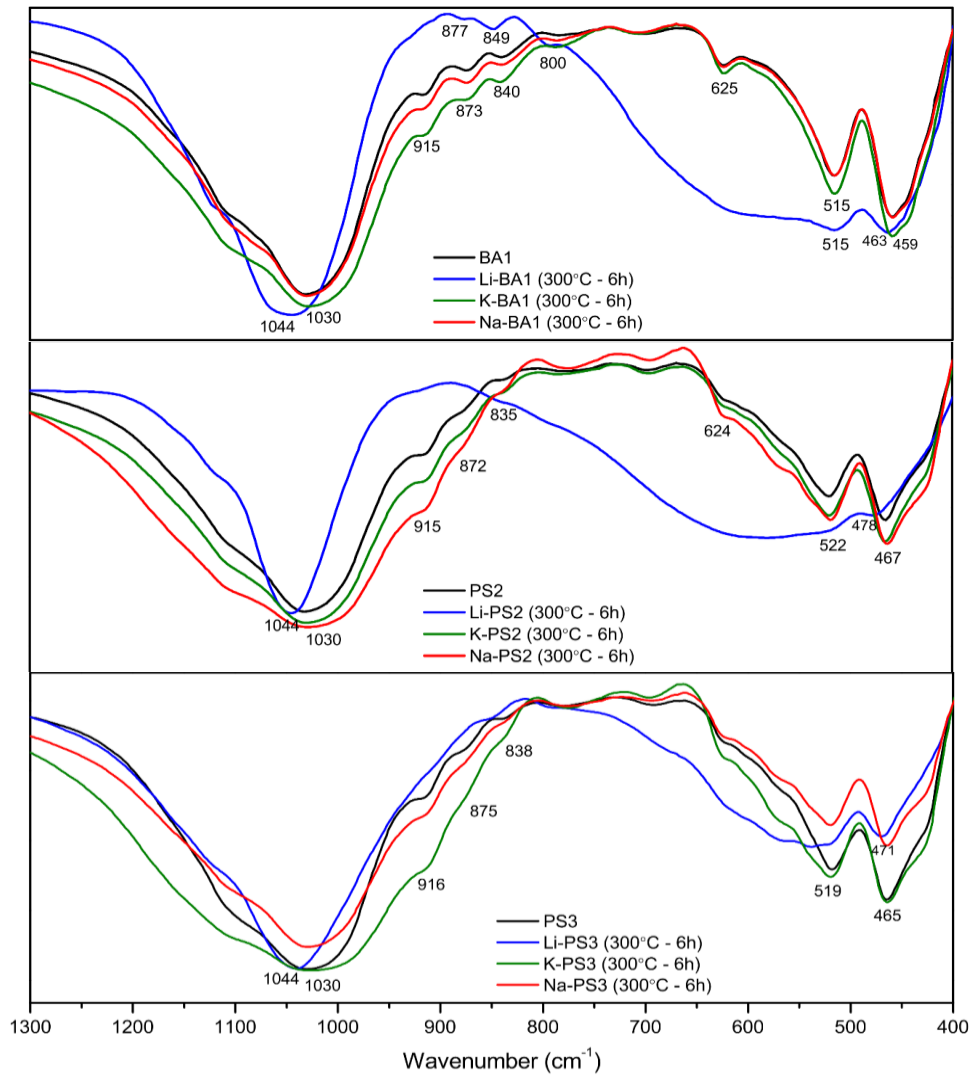


Fig.17 - Infrared spectra of Li-, K- and Na-smectite (BA1, PS2 and PS3) after heating at 300°C during 6 hours. The black lines correspond to the IR spectra of air dried smectite.

The wavenumbers of  $\text{Al}_2\text{OH}$  and  $\text{AlMgOH}$  increase as decreasing of layer charge in the charge reduced-montmorillonite, involving a decrease in the respective intensities as increase of  $\text{Li}^+$  fixed on the hexagonal holes of the octahedral sheets (Calvet and Prost, 1971; Madejová et al., 1996). These conclusions are in agreement with our results, once samples PS2 and PS3 have the higher proportions of negative charge on the octahedral

sheet, 62% and 59%, respectively, and probably the higher proportion of  $\text{Li}^+$  fixed, which justifies the lower intensities observed in the  $\text{OH}^-$  bending vibrations.

The structural changes occurred in the tetrahedral sheet are described by the increase of vibration frequencies of Si-O stretching modes, traduced by the shifts from  $1030\text{ cm}^{-1}$  to  $1044\text{ cm}^{-1}$  and from  $1105\text{ cm}^{-1}$  to  $1120\text{ cm}^{-1}$  observed for all Li-smectite samples after heating process (Fig.18). The vibration band associated with Si-O-Si bending mode has also shifted from  $459\text{ cm}^{-1}$  to  $463\text{ cm}^{-1}$  for sample BA1, whereas for samples PS2 and PS3 shifted from  $467\text{ cm}^{-1}$  to  $478\text{ cm}^{-1}$  and from  $465\text{ cm}^{-1}$  to  $471\text{ cm}^{-1}$ , respectively. In this case, the higher variation observed for sample PS2, may be also related with the higher proportion of  $\text{Li}^+$  probably fixed on the hexagonal holes in the octahedral sheet, once it was previously admitted that the presence of  $\text{Li}^+$  ions either in the hexagonal holes (octahedral) and/or in the ditrigonal cavities on tetrahedral sheets triggers structural changes in the Si-OH groups, affecting the Si-O vibration frequencies.

The  $\text{Li}^+$  fixation caused changes in the electric field surrounded the apical oxygens that connect the octahedral and tetrahedral sheets, influencing the Si-O bond distances and the respective IR vibration frequencies (Gates et al. 2000). During this process, the layer charge is reduced and the mineral structure becomes more pyrophyllite-like. The IR spectra obtained after the  $\text{Li}^+$  saturation and  $300^\circ\text{C}$  heated (6h) was compared with the IR spectrum of pyrophyllite ( $\text{Al}_2(\text{Si}_4\text{O}_{10})(\text{OH})_2$ ) (Fig.18). The shifted bands corresponding to the stretching and bending vibration of Si-O show identical frequencies as those of pyrophyllite ( $1120\text{ cm}^{-1}$ ,  $1044\text{ cm}^{-1}$  and  $475\text{ cm}^{-1}$ ). New bands assigned to the Al-O-Si bending modes of pyrophyllite appeared also in the IR spectra of smectite between  $350$  and  $650\text{ cm}^{-1}$ . The similar vibrations were confirmed by other investigators, who claimed that smectite structure become to a pyrophyllite-like structure after  $\text{Li}^+$  fixation process (Gates, 2005; Gournis et al., 2008; Karakassides et al., 1999; Komadel et al., 2005; Madejová et al., 1996; Mavedová et al., 2000).

The heating process of Li-smectite samples was followed during 6 hours. The samples were analysed after 30 minutes, 3 hours and 6 hours. The IR spectra of sample BA1 confirm that the structural changes have occurred successively. The Si-O stretching and bending bands and the  $\text{OH}^-$  bending bands were successively shifted for Sample BA1, whereas it is observed a total shift of the same vibration bands in the IR spectra of samples PS2 and PS3. The higher proportion of tetrahedral charge of smectite BA1 may have influenced this process, making the  $\text{Li}^+$  migration process slower. The evolution of the heating process on Li-smectite samples also shows that the AlMgOH band had a strongly

decrease of intensity after 30 minutes, among the other OH- bending modes, but after 3h and 6h it is evidenced a successively increase of their intensity. It is also observed a successively increase of intensity of Al-Mg-Li-OH band at  $800\text{ cm}^{-1}$ , as increasing of  $\text{Li}^+$  migration and fixation (Fig.18).

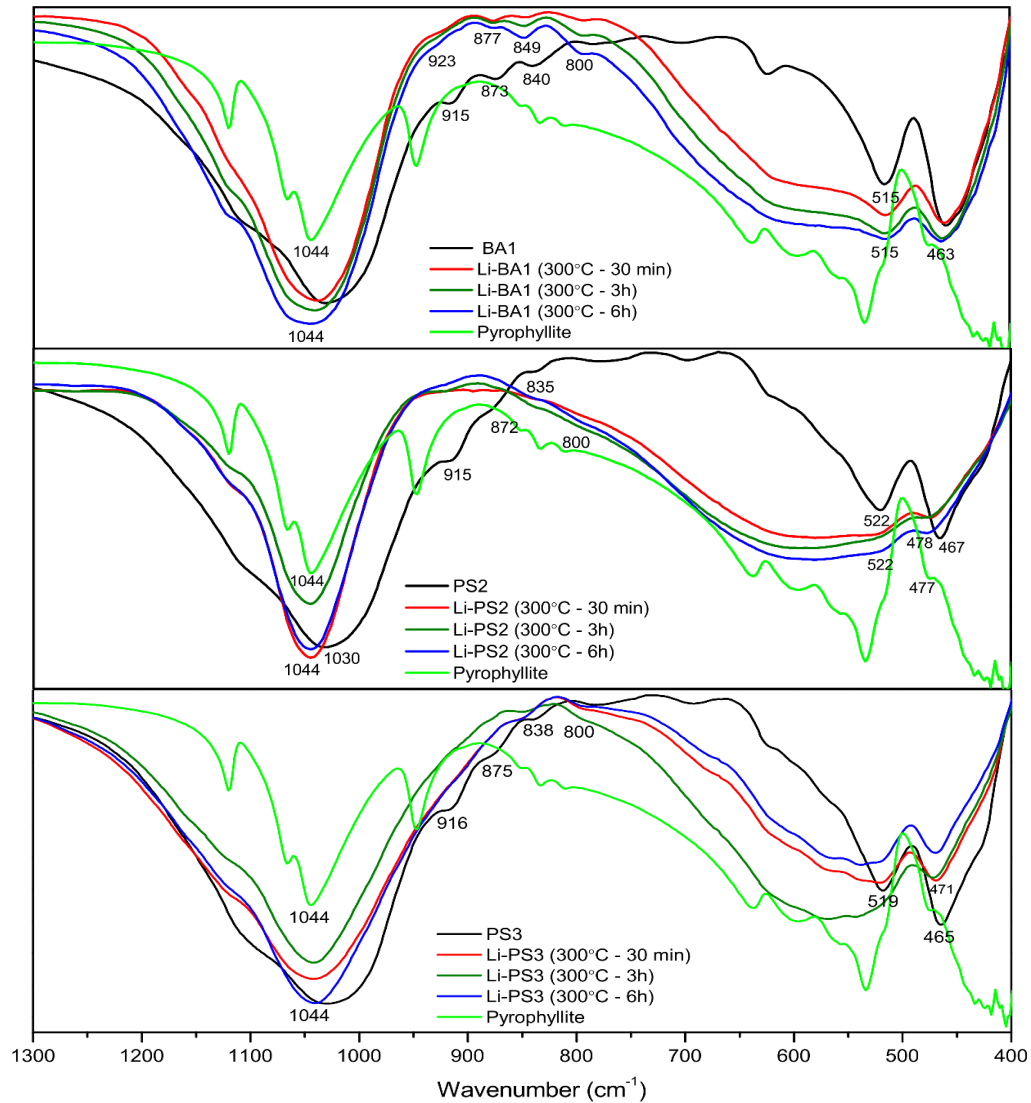


Fig.18 - Infrared spectra of Li-smectite (BA1, PS2 and PS3) after 30 min., 3h and 6 h of heating at  $300^{\circ}\text{C}$ . Comparing with pyrophyllite IR spectra. The black lines correspond to the IR spectra of air dried smectite.

*Vibrational planes of glycerol solvated smectite.* The glycerol solvation of smectite samples was also followed by FTIR spectroscopy (Fig.19).

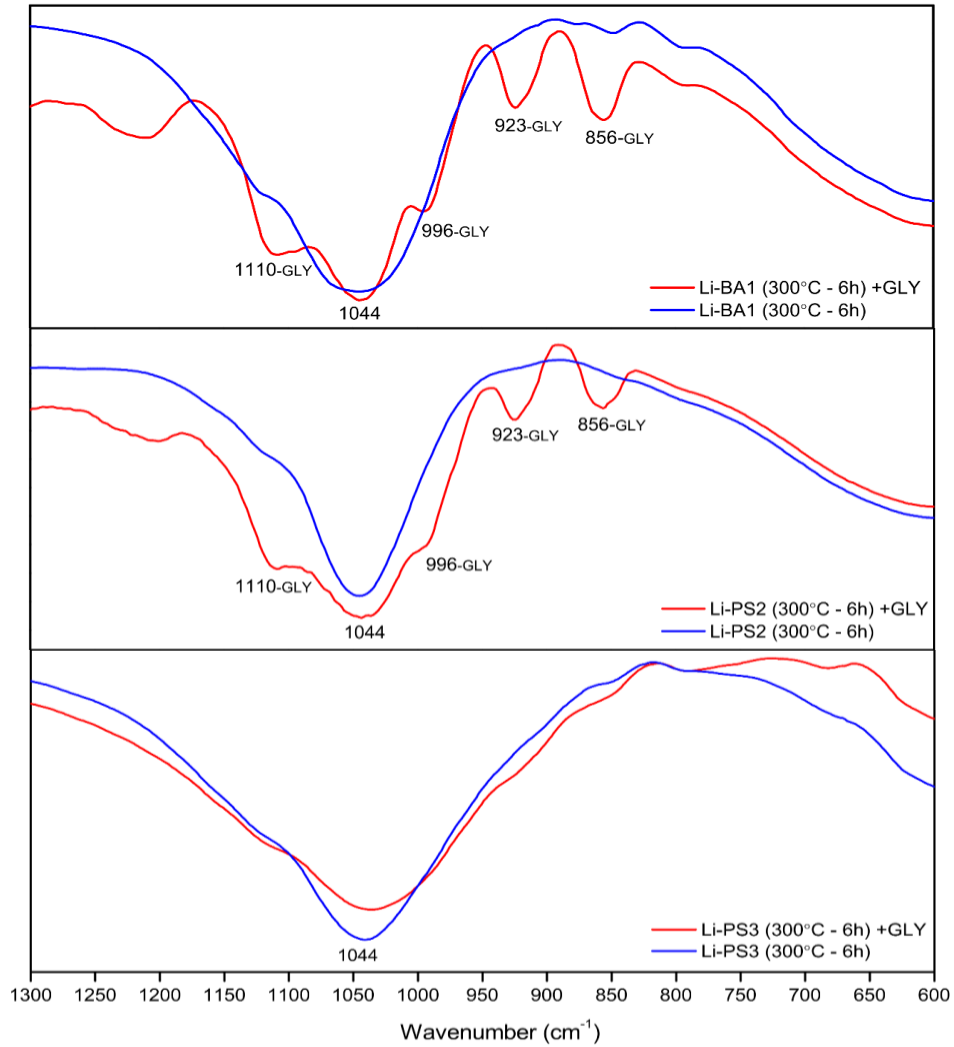


Fig.19 - Infrared spectra of Li-smectite (BA1, PS2 and PS3) after heating at 300°C during 6 h before and after glycerol solvation.

After this process, the Si-OH stretching vibration, at 1044 cm<sup>-1</sup>, did not suffer any alteration in all smectite spectra, suggesting that the structural changes occurred on smectite after Li<sup>+</sup> fixation are irreversible.

The IR spectra of samples BA1 and PS2 show characteristic bands of glycerol that confirms their adsorption in the interlayer of smectite, whereas the IR spectra of sample PS3 does not reveal the presence of glycerol on smectite structure (Fig.19). These results are in agreement with our previous XRD results, which revealed that sample PS3 was the only smectite that did not expand after  $\text{Li}^+$  saturation (300 °C) and Glycerol solvation, confirming the total charge neutralization promoted by  $\text{Li}^+$  fixation. This behaviour is identical with the observed for pyrophyllite, where there is no charge deficit, once Glycerol will only be adsorbed if the tetrahedral charge is higher  $0.23/\text{O}_{10}(\text{OH})_2$ .

#### 4.4.3.4. Conclusion

The reactivity of smectite and the structural changes generated after saturation with  $\text{K}^+$ ,  $\text{Mg}^{2+}$ ,  $\text{Ca}^{2+}$  and  $\text{Na}^+$ , and Green-Kelly test reflect heterogeneous structures consisting of beidellite interstratified with 2W/1W-montmorillonite (sample BA1), 2W/1W-montmorillonite randomly interstratified with K-I (sample PS2) and were studied for smectite. The XRD results revealed the basal spacing collapse to 10.07 Å (BA1), 10.12 Å (PS2) and 10.25 Å (PS3) after  $\text{K}^+$  saturation and heating process, indicating the total dehydration of smectite. They expanded to 13.63 Å, 13.48 Å and 14.30 Å, for samples BA1, PS2 and PS3, respectively, after EG solvation, indicating the formation of only a monolayer EG complex (1-EG). It suggests that the different 2:1 layers have similar layer charges and uniform charge distribution. The infrared spectroscopy results indicated that only  $\text{Li}^+$  ions had capacity to migrate and be fixed on the hexagonal holes in the octahedral sheet of smectite samples. This process was also confirmed by the XRD results which showed a total collapse of the basal spacings to  $\approx 9.60$  Å after heating process. The decrease of layer charge involved in this process was characterized by significantly structural changes that were mainly evidenced by changes in the Si-O stretching bands and  $\text{OH}^-$  bending bands. The wavenumbers of  $\text{Al}_2\text{OH}$  and  $\text{AlMgOH}$  increase as decreasing of layer charge in the charge reduced-smectite, involving a decrease in the respective band intensities, mainly for samples PS2 and PS3, which were associated with the higher proportions of negative charge on the octahedral sheets, 62% and 59%, respectively.

During  $\text{Li}^+$  fixation process, the layer charge was reduced and the mineral structure became more pyrophyllite-like. Changes in the electric field surrounded the apical oxygens influenced the Si-O bond distances and the respective IR vibration frequencies. The IR spectra obtained after thermal process revealed that the shifted bands, corresponding to the

stretching and bending vibration of Si-OH groups, have identical frequencies when compared to the same obtained for pyrophyllite ( $1120\text{ cm}^{-1}$ ,  $1044\text{ cm}^{-1}$  and  $475\text{ cm}^{-1}$ ).

After Glycerol solvation of Li-smectite, the Si-OH stretching vibration ( $1044\text{ cm}^{-1}$ ) did not suffer any alteration in all smectite spectra, suggesting that the structural changes occurred on smectite after  $\text{Li}^+$  fixation are irreversible. The IR spectra of samples BA1 and PS2 showed characteristic bands of Glycerol that confirmed their adsorption in the interlayer of smectite, whereas the IR spectra of sample PS3 did not reveal the presence of Glycerol on smectite structure. These results are in agreement with our previous XRD results, which revealed that sample PS3 did not expand after  $\text{Li}^+$  saturation ( $300^\circ\text{C}$ ) and Glycerol solvation, confirming the total charge neutralization promoted by  $\text{Li}^+$  fixation.

The XRD results also revealed that the basal spacing of samples BA1 and PS2 have partially expanded, after Glycerol solvation, confirming that part of layer charge resides in the tetrahedral sheets, whereas the basal spacing of sample PS3 remained collapsed. The interstratified structure of smectite BA1 is characterized by the presence of tetrahedral sheets with charges between 0.23 and  $0.38/\text{O}_{10}(\text{OH})_2$ , with higher proportion of expanded layers, whereas smectite PS2 has a lower proportion of expanded layers to  $16.5\text{ \AA}$ , with tetrahedral charges  $>0.38/\text{O}_{10}(\text{OH})_2$ . Smectite PS3 has no expanded layers, which means that the tetrahedral charges are lower than  $0.23/\text{O}_{10}(\text{OH})_2$ .

### Acknowledgements

The first author benefited a PhD scholarship (Ref. SFRH/BD/79969/2011) financed by Fundação para a Ciência e Tecnologia (FCT), Portugal. This work was funded by FEDER fund through the Operational Program Competitiveness Factors e COMPETE and by National funds through FCT.

### 4.4.4. References

- Alvero, R., Alba, M.D., Castro, M.A., Trillo, J.M., 1994. Reversible Migration of Lithium in Montmorillonites. *The Journal of Physical Chemistry* 98, 7848-7853.
- Barshad, I., Kishk, F.M., 1970. Factors affecting potassium fixation and cation exchange capacities of soil vermiculite clays. *Clay and clay minerals* 18, 122-137.

- Bauer, A., Lanson, B., Ferrage, E., Emmerich, K., Taubald, H., Schild, D., Velde, B., 2006. The fate of smectite in KOH solutions. *American Mineralogist* 91, 1313-1322.
- Besson, G., Drits, B.A., 1997a. Refined relationship between chemical composition of dioctahedral fine-grained mica minerals and their infrared spectra within the OH stretching region. Part1. Identification of the OH stretching bands. *Clays and Clay Minerals* 45, 158-169.
- Brindley, G.W., Brown, G., 1982. *Crystal Structures of Clay Minerals and their X-Ray Identification*. Mineralogical Society.
- Calvet, R., Prost, R., 1971. Cation Migration into Empty Octahedral Sites and Surface Properties of Clays. *Clays and Clay Minerals* 19, 175-186.
- Chang, F.-R.C., Skipper, N.T., Sposito, G., 1998. Monte Carlo and Molecular Dynamics Simulations of Electrical Double-Layer Structure in Potassium-Montmorillonite Hydrates. *Langmuir* 14, 1201-1207.
- Christidis, G.E., Blum, A.E., Eberl, D.D., 2006. Influence of layer charge and charge distribution of smectites on the flow behaviour and swelling of bentonites. *Applied Clay Science* 34, 125-138.
- Christidis, G.E., Eberl, D.D., 2003. Determination of layer-charge characteristics of smectites. *Clays and Clay Minerals* 51, 644-655.
- Cicel, B., Machajdik, D., 1981. Potassium- and ammonium-treated montmorillonites; I, Interstratified structures with ethylene glycol and water. *Clays and Clay Minerals* 29, 40-46.
- Farmer, V.C., 1968. Infrared spectroscopy in clay mineral studies. *Clay minerals* 7, 373-387.
- Galán, E., 2006. Chapter 14 Genesis of Clay Minerals, in: Faïza Bergaya, B.K.G.T., Gerhard, L. (Eds.), *Developments in Clay Science*. Elsevier, pp. 1129-1162.
- Gates, W.P., 2005. Infrared spectroscopy and the chemistry of dioctahedral smectites. IN: T. Kloprogge (Ed.) *Vibrational spectroscopy of layer silicates and hydroxides*. CMS Workshop Lectures. The Clay Minerals Society, Aurora, CO. 13, 125-168.
- Gates, W.P., Komadel, P., Madejová, J., Bujdák, J., Stucki, J.W., Kirkpatrick, R.J., 2000. Electronic and structural properties of reduced-charge montmorillonites. *Applied Clay Science* 16, 257-271.
- Gournis, D., Lappas, A., Karakassides, M.A., Töbrens, D., Moukarika, A., 2008. A neutron diffraction study of alkali cation migration in montmorillonites. *Physics and Chemistry of Minerals* 35, 49-58.

- Greathouse, J., Sposito, G., 1998. Monte Carlo and Molecular Dynamics Studies of Interlayer Structure in Li(H<sub>2</sub>O)<sub>3</sub>-Smectites. *The Journal of Physical Chemistry B* 102, 2406-2414.
- Greene-Kelly, R., 1952. Irreversible dehydration in montmorillonite. *Clay Minerals Bulletin* 1, 221-225.
- Harward, M.E., Carstea, D., Sayegh, A., 1968. Properties of vermicullite and smectites: Expansion and Collapse. *Clays and clay minerals* 15, 179.
- Karakassides, M.A., Gournis, D., Petridis, D., 1999. An infrared reflectance study of Si-O vibrations in thermally treated alkali-saturated montmorillonites. *Clay Minerals* 34, 429-438.
- Kaufhold, S., Dohrmann, R., Stucki, J.W., Anastácio, A.S., 2011. Layer charge density of smectites – closing the gap between the structural formula method and the alkylammonium method. *Clays and Clay Minerals* 59, 200-211.
- Komadel, P., Madejová, J., Bujdák, J., 2005. Preparation and properties of reduced charge smectites-a review. *Clays and Clay Minerals* 53, 313-334.
- Lagaly, G., 1979. The "layer charge" of regular interstratified 2:1 clay minerals. *Clays and Clay Minerals* 27, 1-10.
- Larsen, D., Egenhoff, S.O., Fishman, N.S., 2015. *Paying Attention to Mudrocks: Priceless!* Geological Society of America, Incorporated.
- Madejová, J., Arvaiová, B., Komadel, P., 1999. FTIR spectroscopic characterization of thermally treated Cu<sup>2+</sup>, Cd<sup>2+</sup>, and Li<sup>+</sup> montmorillonites. *Spectrochimica Acta Part A: Molecular and Biomolecular Spectroscopy* 55, 2467-2476.
- Madejová, J., Bujdák, J., Gates, W.P., Komadel, P., 1996. Preparation and Infrared Spectroscopy Characterization of reduced-charge monmorillonite with various Li contents. *Clay Minerals* 31, 233-241.
- Madejová, J., Bujdák, J., Petit, S., Komadel, P., 2000. Effects of chemical composition and temperature of heating on the infrared spectra of Li-saturated dioctahedral smectites. (I) Mid-infrared region. *Clay Minerals* 35, 739-751.
- Malla, P.B., Douglas, L.A., 1987. Problems in identification of montmorillonite and beidellite. *Clays and Clay Minerals* 35, 232-236.
- Mavedová, J., Bujdák, J., Petit, S., Komadel, P., 2000. Effects of chemical composition and temperature of heating on the infrared spectra of Li-saturated dioctahedral smectites. (I) Mid-infrared region. *Clay Minerals* 35, 739-751.

- Meunier, A., Lanson, B., Beaufort, D., 2000. Vermiculitization of smectite interfaces and illite layer growth as a possible dual model for illite-smectite illitization in diagenetic environments: a synthesis. *Clay Minerals* 35, 573-586.
- Meunier, A., Velde, B.D., 2013. *Illite: Origins, Evolution and Metamorphism*. Springer Berlin Heidelberg.
- Mosser-Ruck, R., Devineau, K., Charpentier, D., Cathelineau, M., 2005. Effects of ethylene glycol saturation protocols on XRD patterns: A critical review and discussion. *Clays and Clay Minerals* 53, 631-638.
- Petit, S., Righi, D., Madejová, J., Decarreau, A., 1998. Layer charge estimation of smectites using infrared spectroscopy. *Clay Minerals* 33, 579-591.
- Reynolds, R.C., 1985. NEWMOD a computer program for the calculation of one-dimensional diffraction patterns of mixed-layer clays. R. C. Reynolds, Jr. 8 Brook Dr., Hanover, NH 03755.
- Ross, C.S., Hendricks, S.B., 1945. Minerals of the montmorillonite group, their origin and relation to soils and clays, Professional Paper, - ed.
- Sato, T., Watanabe, T., Otsuka, R., 1992. Effects of layer charge, charge location, and energy change on expansion properties of dioctahedral smectites. *Clays and Clay Minerals* 40, 103-113.
- Schultz, L.G., 1969. Lithium and potassium absorption, dehydroxylation temperature, and structural water content of aluminous smectites. *Clays and Clay Minerals* 17, 115-149.
- Somasundaran, P., 2006. *Encyclopedia of Surface and Colloid Science*. Taylor & Francis.
- Sparks, D.L., 2013. *Environmental Soil Chemistry*. Elsevier Science.
- Sposito, G., 1984. *The Reactive Solid Surfaces in Soils*. Oxford University Press, New York.
- Stackhouse, S., Coveney, P.V., 2002. Study of Thermally Treated Lithium Montmorillonite by Ab Initio Methods. *The Journal of Physical Chemistry B* 106, 12470-12477.
- Suquet, H., Calle, C., Pezerat, H., 1975. Swelling and Structural Organization of Saponite. *Clays and Clay Minerals* 23, 1-9.
- Suter, J.L., Boek, E.S., Sprik, M., 2008. Adsorption of a Sodium Ion on a Smectite Clay from Constrained Ab Initio Molecular Dynamics Simulations. *The Journal of Physical Chemistry C* 112, 18832-18839.
- Tettenhorst, R., Johns, W.D., 1966. Interstratification in montmorillonite. *Clays and Clay Minerals* 15, 85-93.

- Tsutomu, S., Takashi, M., Takashi, W., 1996. Change in Layer Charge of Smectites and Smectite Layers in Illite/Smectite during Diagenetic Alteration. *Clays and Clay Minerals* 44, 460-469.
- Wilson, M.J., 2013. *Rock-forming Minerals: Clay Minerals. Sheet silicates. Volume 3C.* Geological society.
- Zemanová, M., Link, G., Takayama, S., Nüesch, R., Janek, M., 2006. Modification of layer charge in smectites by microwaves. *Applied Clay Science* 32, 271-282.

## 4.5. Influence of pH, concentration and ionic strength during batch and flow-through continuous stirred reactor experiments of Sr<sup>2+</sup>-adsorption onto montmorillonite

Adapted from Vanessa Guimarães, Manuel Azenha, Fernando Rocha, Fernando Silva, Iuliu Bobos

Journal of Radioanalytical and Nuclear Chemistry (2015), 303(3), 2243-2255

### ABSTRACT

The adsorption experiments using the <2 µm clay fractions of montmorillonite were carried out in batch and continuous flow-through stirred reactor. Flow-through experiments were carried out at different pH (4 and 8), concentrations (7.00 mgSr<sup>2+</sup>/L, 27.00 mgSr<sup>2+</sup>/L and 34 mgSr<sup>2+</sup>/L) and ionic strengths ([KNO<sub>3</sub>]=1011 mg/L and [KNO<sub>3</sub>]=101.1 mg/L). Also, distinct pH (4 and 8) and variable solution concentrations (15 mgSr<sup>2+</sup>/L and 860 mgSr<sup>2+</sup>/L) were used for batch experiments. The amount of Sr<sup>2+</sup> adsorbed increased as increasing of Sr<sup>2+</sup> concentration during the flow-through experiments. The gradient of concentration acted as an increasing driving force resulting in an increasing equilibrium sorption until the steady-state equilibrium was reached. The Sr<sup>2+</sup> amount desorbed at pH 4 is only half of the amount desorbed at pH 8, revealing that at pH 4 enhanced the retention of Sr<sup>2+</sup> onto montmorillonite.

The largest adsorption value was obtained at pH 8.0 ([KNO<sub>3</sub>]=101.1 mg/L) with q<sub>0</sub>=41.49 mgSr<sup>2+</sup>/g from the Langmuir and Freundlich adsorption isotherms. The pseudo-first order model fitted better our experimental data.

These findings allow a better prediction of the hazardous trace elements sorption in compacted clay liners used for environmental protection.

**Keywords:** Montmorillonite; Strontium ion; Batch and flow-through experiments; Breakthrough curves; Sorption vs. desorption; Kinetics models.

### 4.5.1. Introduction

Strontium is the fifteenth most abundant element present in the earth's crust and the 10<sup>th</sup> most abundant element in seawater (Chegrouche et al., 2009; Dimović et al., 2009).

The 16 isotopes of strontium are well known, where four of them are stable, while twelve others are radioactive. The  $^{90}\text{Sr}$  is a by-product of the fission of uranium and plutonium in nuclear reactors and in nuclear weapons, being considered by the U.S. Environmental Protection Agency as the most important radioactive isotope present in the environment (Başçetin and Atun, 2006; Dimović et al., 2009; Khan et al., 1995; Sureda et al., 2010). Due to its high mobility, the  $^{90}\text{Sr}$  is one of the most hazardous radionuclides having a long term radiation hazard (Zhu and Shaw, 2000). The  $^{90}\text{Sr}$  with a half-life of 28 years emits  $\beta$  radiation, being employed as a radioactive tracer in medical (eye diseases and bone cancer) and agricultural studies (EPA, 2009).

The problem of environmental protection is the safety storage of radioactive waste of nuclear power plants in geological repositories, using multibarrier concept to ensure the convenient protection (Chorover et al., 2003; Ahmad, S., 1995; Nemes et al., 2005; Mahoney and Langmuir, 1991; Rafferty et al., 1981).

Montmorillonite has a great potential as adsorbent, being a subject of interest in several research areas, due to its large specific surface area, chemical and mechanical stability, high cation exchange capacity (CEC) and low cost (Başçetin and Atun, 2006; Chorover et al., 2003; Khan et al., 1995; Ahmad, S., 1995). Previous kinetic studies of  $\text{Sr}^{2+}$  adsorption onto montmorillonite were performed using batch and column experiments (Mahoney and Langmuir, 1991; Nemes et al., 2005; Rafferty et al., 1981). However, some drawbacks are associated with these techniques, concerning to “particle concentration effect” associated to the dependence on the solid concentration, which contributes to insufficient prewashing of the soil with the background electrolyte solution. Other disadvantage is the incomplete removal of pre-adsorbed ions, which triggers a major source of error in sorption processes. To avoid these problems and to identify the factors responsible for deviations in sorption parameters under different experimental conditions, we used in this study a simple flow-through reactor that provides an intensive prewashing procedure and a convenient stirring during all the adsorption process.

Several experimental conditions were taken into account in this work to evaluate the adsorption and desorption of  $\text{Sr}^{2+}$  onto montmorillonite, such as: contact time, pH,  $\text{Sr}^{2+}$  concentrations and ionic strength. The adsorption and desorption of  $\text{Sr}^{2+}$  onto montmorillonite surfaces with high deficit charge was carried out in extreme pH conditions and different ionic strength and concentrations. The kinetic data were achieved using a continuously stirred flow-through reactor (CSTR) that facilitates an intensive pre-washing and a good preconditioning of montmorillonite, providing an appropriate control of the

chemical conditions imposed during our experiments (Grolimund et al., 1995). Breakthrough studies were carried out to evaluate the effect of pH, concentration and ionic strength during adsorption-desorption on the shape of breakthrough curves. Several models were used to test the kinetic behavior of  $\text{Sr}^{2+}$  adsorption onto montmorillonite, where batch experiments were performed to obtain the sorption equilibrium data, examining the  $\text{Sr}^{2+}$  sorption behavior onto montmorillonite under equilibrium and isothermal conditions.

## 4.5.2. Experimental

### 4.5.2.1. Materials and Techniques

Adsorption experiments were carried out on the  $<2\mu\text{m}$  clay fractions extracted by sedimentation from bentonite rocks (Madeira Arquipelago, Portugal). The pH was measured with a pH meter (Corning 240) calibrated with buffer solutions (pH 4, 7, and 10 Merck). Cation exchange capacity (CEC) of selected samples was determined using ammonia as exchanged cation and an ammonia-specific electrode (Davis and Worrall, 1971). BET multipoint surface area (Gemini 2370 V5, Micromeritics) of selected samples was also carried out by measuring the volume of a mixture of  $\text{He}/\text{N}_2$  adsorbed at five different pressures. Prior to  $\text{He}/\text{N}_2$  adsorption, the samples were de-aired at  $200\text{ }^\circ\text{C}$  for 10 h (Brunauer et al., 1938).

The  $<2\text{ }\mu\text{m}$  clay fractions were analyzed by X-ray diffraction (XRD) using a Philips X'Pert machine equipped with a  $\text{CuK}\alpha$  radiation and a scanning speed of  $1^\circ\text{ }2\theta/\text{min}$ .

Chemical analysis were carried out by atomic absorption spectroscopy using a flame absorption spectrometer Perkin Elmer, AAnalyst 200 model with a Strontium hollow cathode lamp, wavelength  $460.73\text{ nm}$ , air flow  $5.2\text{ L/min}$  and acetylene flow  $2.5\text{ L/min}$ . The  $5\text{ mL}$  of the acidified strontium solution was mixed with  $750\text{ }\mu\text{L}$  of lanthanum chloride ( $\text{LaCl}_3 \cdot 7\text{H}_2\text{O}$ ) solution previously prepared ( $176\text{ g}$  of  $\text{LaCl}_3 \cdot 7\text{H}_2\text{O}$  and  $19.1\text{ g}$  of  $\text{KCl}$  diluted in  $1000\text{ mL}$  of deionised water).

### 4.5.2.2. Kinetics Experiments

The adsorption kinetic studies were carried out on montmorillonite suspension at different  $\text{Sr}^{2+}$  concentrations ( $7.00\text{ mgSr}^{2+}/\text{L}$ ,  $27.00\text{ mgSr}^{2+}/\text{L}$  and  $34.00\text{ mgSr}^{2+}/\text{L}$ ) and variable pH (4 and 8) using a continuous stirred flow through reactor with a volume of  $37.3$

cm<sup>3</sup> and loaded with 0.50 g of clay. Strontium solutions were prepared from Sr(NO<sub>3</sub>)<sub>2</sub> (p.a., Merck), by dissolving the exact quantities of salt in distilled water. The initial pH values of the solutions in the sorption experiments were adjusted by adding HNO<sub>3</sub> (1M) or KOH (1M).

Input solution flowed through 0.45 μm Millipore membranes (Merck KGaA) at room temperature with a flow rate of 0.8 mL/min during 34 hours (28 pore volumes) and some samples were collected at time intervals for further chemical analysis. The system was previously preconditioned with a solution of KNO<sub>3</sub> ([KNO<sub>3</sub>]=1011 mg/L; pH 4 or 8) until the system reached a steady state. After this, the Sr<sup>2+</sup> solution was pumped into the reactor until the clay system became saturated and then, reverted to the original blank solution for desorption experiments. In this last step, the experiments were followed for 10 hours, where the samples were collected at time intervals for further chemical analysis. The collected samples were preserved by adding HNO<sub>3</sub> (65%) and stored at 4 °C.

The adsorption and kinetics experiments were carried out in equilibrium conditions with the atmospheric CO<sub>2</sub> (pCO<sub>2</sub>=10<sup>-3.5</sup> bar).

#### 4.5.2.2.1. Modeling of mass balance

The continuously stirred flow technique used in this work has several advantages over the continuously flow techniques, because it avoids problems related to sample dispersion and significant transport effects. Under these conditions, the concentration of the adsorptive in the reactor is equal to the effluent concentration (Sparks, 2003). The efficiency of the mixing conditions may be tested by comparing the metal concentrations obtained in the end of the process, when no montmorillonite is loaded into the reactor, with the values predicted by the theoretical curve for an inert specie in a continuously stirred flow-through reactor obtained, as a function of time, by Eq. 1(Tertre et al., 2013):

$$\frac{[Sr^{2+}]_{n-M}}{C_{0-Sr}} = 1 - \exp^{-Qt/V_R} \quad (1)$$

where  $[Sr^{2+}]_{n-M}$  is the concentration of the output solution at time  $t$  in the absence of montmorillonite,  $C_{0-Sr}$  is the Sr<sup>2+</sup> concentration of the input solution that is pumped through

the reactor during the adsorption process.  $Q$  is the flow rate,  $t$  is the time and  $V_R$  is the volume of the reactor.

The amount of  $\text{Sr}^{2+}$  adsorbed, or desorbed, was obtained by taking into account the area between the breakthrough curve measured with montmorillonite and the theoretical curve measured in the absence of montmorillonite. This amount was calculated according to the following equation [22]:

$$q_{\text{Sr}^{2+}} = V_R \cdot \frac{\sum_{i=1}^n (NV_R^{i+1} - NV_R^i) \cdot \left( \left[ \text{Sr}^{2+} \right]_M^{i+1} + \left[ \text{Sr}^{2+} \right]_M^i \right) - \left( \left[ \text{Sr}^{2+} \right]_{n-M}^{i+1} + \left[ \text{Sr}^{2+} \right]_{n-M}^i \right)}{m} \quad (2)$$

where  $NV_R^i$  and  $NV_R^{i+1}$  are the numbers of pore volumes at times  $t_i$  and  $t_{i+1}$ , calculated by the ratio between the total volume of solution pumped through the reactor during each time period and the volume of the reactor ( $V_R$ ). In this case, one pore volume corresponds to 80 minutes.

The  $\left[ \text{Sr}^{2+} \right]_M^i$  and  $\left[ \text{Sr}^{2+} \right]_M^{i+1}$  correspond to the output  $\text{Sr}^{2+}$  concentration of each sample collected successively at times  $t_i$  and  $t_{i+1}$ . The  $\left[ \text{Sr}^{2+} \right]_{n-M}^i$  and  $\left[ \text{Sr}^{2+} \right]_{n-M}^{i+1}$  represent the concentrations of the output solution at time  $t_i$  and time  $t_{i+1}$  in the absence of montmorillonite.  $V_R$  is the reactor volume ( $37.3 \text{ cm}^3$ ) and  $m$  is the mass of montmorillonite in the reactor ( $0.5 \text{ g}$ ).

#### 4.5.2.2.2. Kinetic models

The adsorption is one of the most applied methods for environmental remediation, where the kinetics models were applied to describe adsorption reaction and diffusion processes. The adsorption mechanism is described using the following reaction-controlled models: pseudo-first order model or pseudo-second order model, where the interaction between  $\text{Sr}^{2+}$  and the binding sites controls the rate of the process. Also the transport-controlled models, such as liquid-film diffusion, parabolic diffusion and intra-particle diffusion, are used to describe the kinetic phenomenon of ion-exchange (time independent) depending of (1) ions diffusion in the aqueous solution, (2) film diffusion at the solid-liquid interface, (3) intra-particle diffusion on pore surfaces and (4) inter-particle diffusion along the solid particles (Selim, 2012; Sparks, 2003).

The pseudo-first order model (Ho and McKay, 1999) curves was obtained by plotting  $\log(q_0 - q_t)$  vs. time using Eq. 3:

$$\log\left(1 - \frac{q_t}{q_\infty}\right) = K_1' t \quad (3)$$

where  $q_t$  is the amount of  $\text{Sr}^{2+}$  on clay at time  $t$  (mg/g), obtained by eq. 2,  $q_\infty$  is the amount of  $\text{Sr}^{2+}$  on clay at equilibrium (mg/g) and  $k_1$  ( $\text{min}^{-1}$ ) is the first order adsorption rate constant and is obtained by Eq. 4:

$$K_1 = \frac{K_1'}{2.3} \quad (4)$$

Pseudo-second order model (Ghaedi et al., 2012; Rahman et al., 2010; Zhang and Hou, 2008) is derived on the basis of the sorption capacity of the solid and could be expressed by the linear Eq. 5:

$$\frac{t}{q_t} = \frac{1}{K_2 q_\infty^2} + \frac{1}{q_\infty} t \quad (5)$$

where  $q_t$  is the amount of  $\text{Sr}^{2+}$  on clay at time  $t$  (mg/g),  $q_\infty$  is the amount of  $\text{Sr}^{2+}$  on clay at equilibrium (mg/g) and  $k_2$  is the constant rate of pseudo-second order adsorption (g/mg min).

The kinetic intra-particle model has been extensively used to describe sorption rates in various types of materials (Baral et al., 2008; Mall et al., 2006; Rahman et al., 2010). In this case, uptake varies with  $t^{1/2}$  rather than with the contact time, according to Eq. 6:

$$q_t = K_j t^{1/2} \quad (6)$$

where  $K_i$  is the intra-particle diffusion rate constant ( $\text{mg/gmin}^{1/2}$ ) and  $q_t$  is the amount of  $\text{Sr}^{2+}$  on clay at time  $t$  ( $\text{mg/g}$ ). In the adsorption mechanism following the intra-particle diffusion process, the plot of  $q_t$  versus  $t^{1/2}$  should be a straight line passing through the origin with a slope  $K_i$ .

The liquid film diffusion model (Eq. 7) describes the kinetic phenomenon when the flow of the reactants through the liquid film surrounding the adsorbent particles is the slowest process determining kinetics of the rate process (Ames, 1962; Bhattacharyya and Gupta, 2006, 2008; Rahman et al., 2008; Susmita Sen and G, 2009; Zhang and Hou, 2008).

$$\ln(F) = -K_{fd}t \quad (7)$$

where  $F$  is the fractional attainment of equilibrium ( $=q_t/q_\infty$ ) and  $K_{fd}$  is the film diffusion rate constant (Bhattacharyya and Gupta, 2008; Ekpete, 2012).

#### *Batch Experiments*

Batch experiments were carried out to investigate  $\text{Sr}^{2+}$  adsorption onto montmorillonite surface under different pH conditions (4 and 8), concentrations and ionic strength. The experiments were carried out by adding 0.050 grams of montmorillonite into the polypropylene centrifuge tubes with 14.00 mL of different stock solutions at different  $\text{Sr}^{2+}$  concentrations, ranged between 15  $\text{mgSr}^{2+}/\text{L}$  and 860  $\text{mgSr}^{2+}/\text{L}$ .

Suspensions were shaken for 34 hours, then centrifuged, separated and the solutions resulted were preserved by adding  $\text{HNO}_3$  (65%) and stored at 4 °C for subsequent chemical analysis.

#### *Modeling of the isotherms*

The Langmuir theoretical model can be represented in several ways. Langmuir isotherm could be arranged in its linear form using Eq. 8:

$$\frac{1}{q_e} = \frac{1}{K_L q_m C_e} + \frac{1}{q_m} \quad (8)$$

where  $q_e$  (mg/g) and  $C_e$  (mg/L) are the equilibrium concentrations of  $Sr^{2+}$  in the solid and the liquid phase, respectively,  $q_m$  (mg/g) is the maximum sorption capacity, and  $K_L$  (L/g) is the Langmuir constant related to the energy of adsorption.  $q_e$  is obtained according to Eq. 9:

$$q_e = (C_i - C_f) * \frac{V}{m} \quad (9)$$

where  $C_i$  and  $C_f$  are the concentrations of  $Sr^{2+}$  in the beginning and the end of the adsorption process,  $V$  is the solution volume used during batch experiments (14.00 mL) and  $m$  is the mass of clay used (0.050 g).

The equilibrium parameter constant ( $R_L$ ) used as an indicator to assess the extent of adsorption was calculated using the Langmuir constant (Dimović et al., 2009; Eba, 2010; Kannan and Sundaram, 2001; Rahman et al., 2010) according with Eq. 10:

$$R_L = \frac{1}{1 + K_L C_0} \quad (10)$$

where  $C_0$  (mg/L) is the initial concentration. Depending on the  $R_L$  value, there are four possibilities for adsorption: (1) favorable adsorption if  $0 < R_L < 1$ , (2) unfavorable adsorption when  $R_L > 1$ , (3) linear adsorption for  $R_L = 1$  and (4) irreversible adsorption for  $R_L = 0$ .

The linear equation of Freundlich sorption isotherm (Jinsheng et al., 2010) is expressed as Eq. 11:

$$\ln(q_e) = \ln(K_f) + \frac{1}{n} \ln(C_e) \quad (11)$$

where  $K_f$  and  $n$  are Freundlich adsorption isotherm constants, being indicative of the extent of the adsorption and the degree of nonlinearity between solution concentration and adsorption.

## 4.5.3. Results and Discussions

### 4.5.3.1. Surface properties and mineralogy of selected material

Mineralogy of clay fractions was studied by XRD and chemical analyses. The X-ray pattern identified only montmorillonite in the  $<2\mu\text{m}$  clay fractions. Crystal chemistry of montmorillonite show a negative total charge of - 0.12 to - 0.15 per  $\text{O}_{10}(\text{OH})_2$ . BET surface area ranges from 128 to 136  $\text{m}^2\text{g}^{-1}$  and CEC measurement gave values from 96 to  $114 \pm 1.6$  meq  $100\text{g}^{-1}$ .

### 4.5.3.2. Continuous stirred flow-through experiments

The influence of pH and  $\text{Sr}^{2+}$  concentration during the adsorption and desorption processes was evaluated by the flow-through experiments. The breakthrough curves (BTC's) were obtained at different  $\text{Sr}^{2+}$  concentrations during the input solutions and different pH conditions (pH 4 and pH 8) (Fig.20). The S-shaped BTC's represent a typical plot of the ratio of outlet to inlet solute concentration in the fluid as a function of time. For each experiment there are two different BTC's corresponding to the adsorption process followed by the desorption process. Both phases were separated by an equilibrium period, when the saturation did occurred. To achieve the amounts of  $\text{Sr}^{2+}$  adsorbed or desorbed, the area between the theoretical BTC and each experimental BTC was taken into account. The results show that the amount of  $\text{Sr}^{2+}$  retained on the surface of montmorillonite increased as increasing the  $\text{Sr}^{2+}$  concentration at both pH conditions (Fig.20). Increasing concentration gradient acts as increasing driving force, which results in increasing equilibrium sorption until the saturation of montmorillonite.

Despite the amount of  $\text{Sr}^{2+}$  adsorbed on clay is higher at elevated initial  $\text{Sr}^{2+}$  concentrations, a higher amount of  $\text{Sr}^{2+}$  remained in solution during the continuous flow process, which didn't contribute to the  $\text{Sr}^{2+}$  retardation. The input amount of  $\text{Sr}^{2+}$  adsorbed on clay surface and the variation of the distribution coefficient ( $K_d$ ) during the adsorption process are shown in Fig.21, where the  $K_d$  parameter is related with the  $\text{Sr}^{2+}$  partitioning between the solid and the aqueous phase. A faster decrease of  $K_d$  values occur when the  $\text{Sr}^{2+}$  concentration increased and the pH decreased. We assumed that the adjustment of concentration and pH is critical for the retention and longer control of contaminant. The best

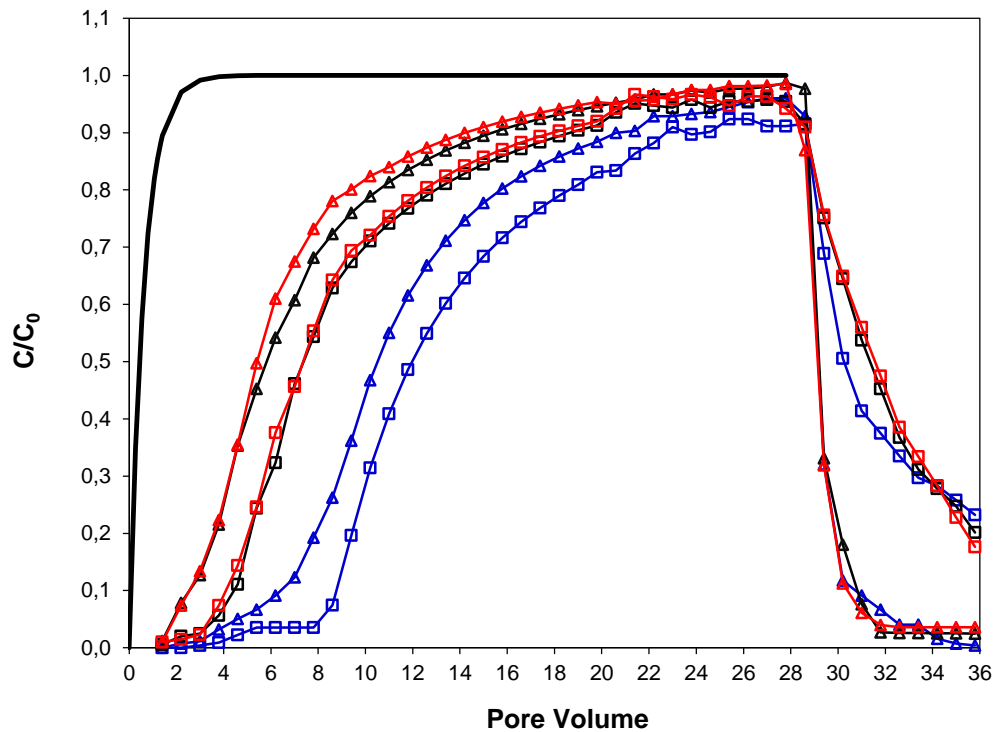
performance was obtained with lower  $\text{Sr}^{2+}$  concentration (7.00 mg  $\text{Sr}^{2+}/\text{L}$ ) and higher pH (pH=8), where the  $\text{Sr}^{2+}$  retention was between 95% and 100% during 9 hours.

The effect of pH on  $\text{Sr}^{2+}$  adsorption onto montmorillonite (Fig.20) under identical conditions shows that the amounts of  $\text{Sr}^{2+}$  adsorbed at pH 4 was 80% of the amounts adsorbed at pH 8 after 34 hours (28 pore volumes). The main contribution was attributed to the high permanent negative charge on the basal planes of montmorillonite. However, additional polar sites situated at the broken edges of octahedral and tetrahedral sheets are conditionally charged by direct  $\text{H}^+$  or  $\text{OH}^-$  transferred from aqueous phase, depending on the pH, influencing the adsorption process. Therefore, the adsorption is higher as increasing the pH and more negative sites are available for metal uptake. There is a less competition between the hydrogen ions and the metal ions on the clay surface sorption sites. The results obtained are shown in Fig. 20.

Table 7. Amounts of  $\text{Sr}^{2+}$  adsorbed/desorbed and total amounts of  $\text{Sr}^{2+}$  retained by montmorillonite.

pH	$C_{in}$ (mg $\text{Sr}^{2+}/\text{L}$ )	$q_{ads}$ (mg $\text{Sr}^{2+}/\text{g}$ )	$q_{des}$ (mg $\text{Sr}^{2+}/\text{g}$ )	Desorbed (%)	$q_{retained}$ (mg $\text{Sr}^{2+}/\text{g}$ )
8	7.00	13.89	1.82	13.10	12.07
	27.00	33.36	7.30	21.88	26.06
	34.00	42.13	9.65	22.91	32.48
4	7.00	11.53	0.670	5.81	10.86
	27.00	27.13	2.77	10.21	24.36
	34.00	31.89	3.21	10.07	28.68

Montmorillonite was submitted to desorption after the previous adsorption process. The behavior of desorption breakthrough curves at pH 4 and 8 is shown in Fig.20. The amounts of  $\text{Sr}^{2+}$  desorbed after 10 hours (36 pore volumes) are shown in Table 7. A significant amount of  $\text{Sr}^{2+}$  is still released by clay at pH 8 toward the end of the desorption process. At pH 4, the desorbed amounts are significantly lower from 32 pore volumes (300 min) and approximately half of that at 36 pore volumes. Thus, the  $\text{Sr}^{2+}$  amount retained on clay surface was slightly lower at pH 4 after desorption period studied with tendency to increase since the desorption process was incomplete at pH 8.

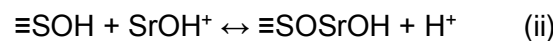


—□— pH 8 - 7 mg/L Sr(II)    —△— pH 4 - 7 mg/L Sr(II)    —■— pH 8 - 27 mg/L Sr(II)    —▲— pH 4 - 27 mg/L Sr(II)  
 —□— pH 8 - 34 mg/L Sr(II)    —△— pH 4 - 34 mg/L Sr(II)    ——— Blank curve

Fig.20 - Break-through curves corresponding to adsorption processes at different  $\text{Sr}^{2+}$  concentrations and different pH.

Despite the interlayer sites being more abundant than edge surface sites, the adsorption properties of montmorillonite are connected with the edge surface sites. Therefore, two possible situations are accounted during the adsorption/desorption processes:

Edge surface sites of silanol and aluminol sheets are the dominant adsorption sites at pH 8, where the ionic reaction occurs between the surface edges and the structure forming the double-layer at the solution-solid interface. The edges sites (SOH) are partially hydrolyzed to  $\text{SO}^-$  and different surface reactions may occur on the "O" plane (Eslinger and Pevear, 1988; Marimon, 2002; Parker and Rae, 1998):





Permanent-charge sites of the interlayer basal planes are also evolved in the adsorption process at pH 8. The  $\text{Sr}^{2+}$  cations adsorbed by silanol may be envisaged as an ion exchange between a hydrated cation (*i.e.*,  $\text{Ca}^{2+}$ ) and a hydrated proton held in the outer Helmholtz layer (Malatti et al., 1974).

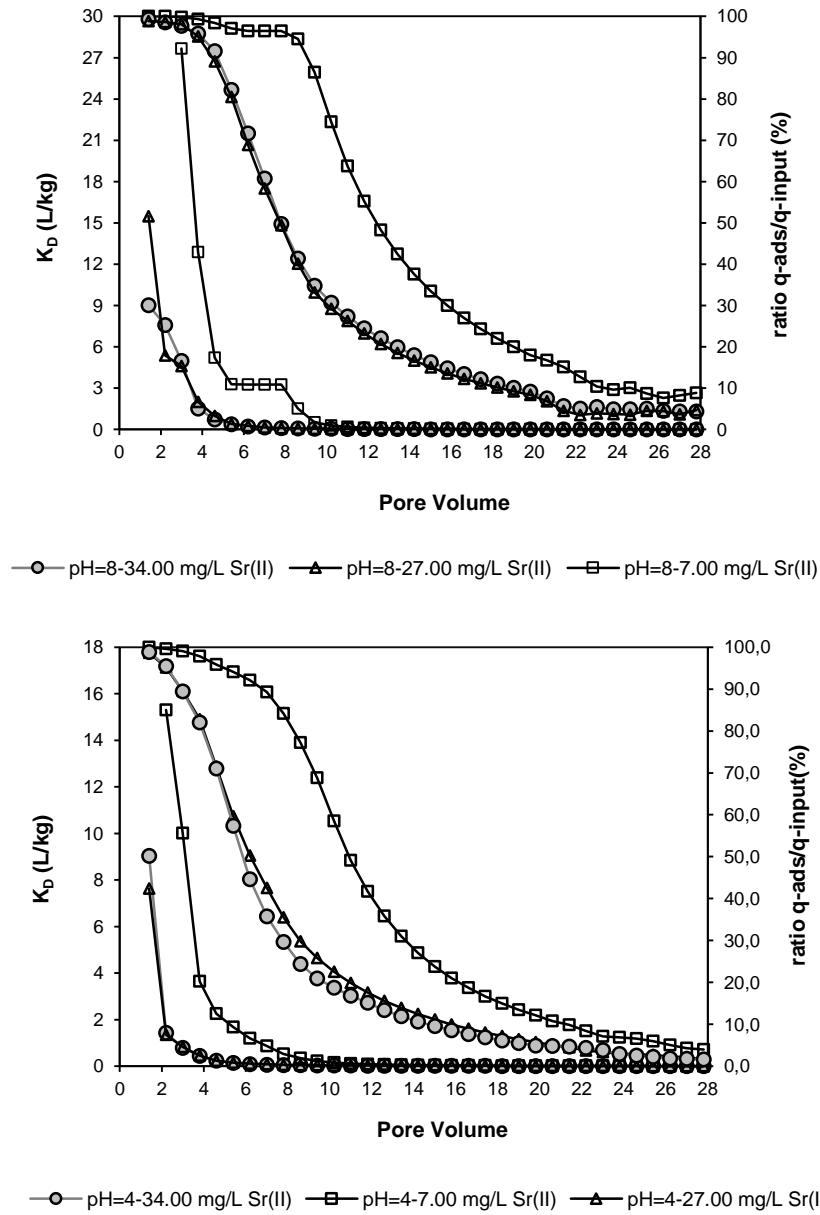


Fig.21 - Distribution Coefficients and ratio qads/qinput (%), during the adsorption process.

The inner-sphere complexes, formed on the “O” plane, are strongly linked to surface and are more difficult to be removed from that. During the desorption process the  $K^+$  is adsorbed onto surface sites and the  $Sr^{2+}$  ions that form outer-sphere complexes on the “O” plane and  $\beta$  plane are more easily replaceable by  $K^+$  due to their lower bonding energies associated to weak electrostatic interactions with the surface sites.  $K^+$  is preferentially adsorbed on montmorillonite over other common cations since it loses more easily their hydrated water, being more strongly fixed (Eslinger and Pevear, 1988; Parker and Rae, 1998).

The adsorption is mainly on the interlayer sites at pH 4, since the charge deficit on clay surface is essentially due to permanent charge.  $Sr^{2+}$  has a low hydration enthalpies and small ionic radius, being strongly bonded to water molecules forming complexes that are weakly bonded to basal oxygens (Velde and Meunier, 2008).

The ionic concentration is higher at pH 4 and there is a less tendency for the cations to diffuse away from the surface, which contributes to double layer compression and, therefore, to approach clay layers due to less repulsion on double layer. It was assumed that the entry of  $K^+$  ions into the structure is hampered (Eslinger and Pevear, 1988; Parker and Rae, 1998). Otherwise, the ionic radius of  $K^+$  is higher than  $Sr^{2+}$  and  $Ca^{2+}$ , and their hydration sphere is smaller. Thus, the cation exchange between  $Sr^{2+}$ ,  $Ca^{2+}$  and  $K^+$  triggers the collapse of structure, hindering the entry of more  $K^+$  and contributing to  $Sr^{2+}$  retention in the interlayer (Howard, 1981).

#### 4.5.3.3. Sorption kinetics

The results achieved during the adsorption process were used to test the  $Sr^{2+}$  adsorption kinetics onto montmorillonite and to determine the kinetic parameters.

According to experimental data (Fig.20) two phases of reaction are distinguished: an initial rapid phase, where large amount of  $Sr^{2+}$  ions was uptaken by montmorillonite, followed by a long plateau phase extended to several hours. These different behavior is commonly observed in similar experimental kinetic studies, which shows that adsorption of  $Sr^{2+}$  onto mineral surface is a complex process that may be associated with more than one mechanism of multiple chemical and physical processes. Thus, the previous described kinetic models were applied in order to achieve the mechanism/s that control/s the kinetics of sorption process.

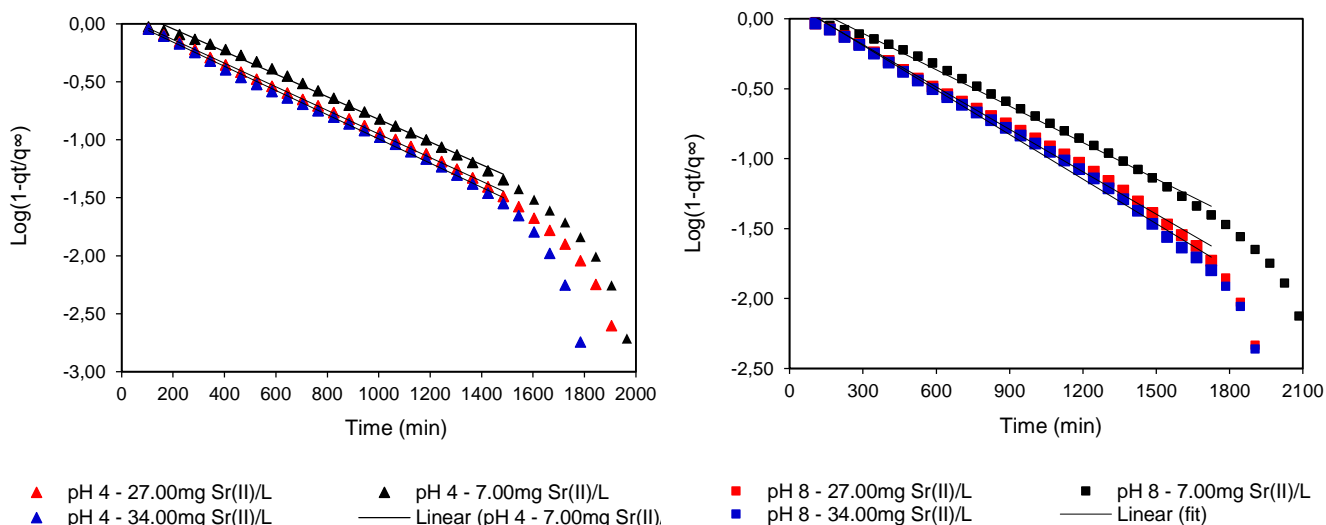


Fig.22 - Kinetic modeling of the sorption of Sr<sup>2+</sup> onto montmorillonite. Pseudo-first order model for adsorption process at pH 4 and pH8, at different Sr<sup>2+</sup> concentrations.

Pseudo-first order model used to describe the adsorption of liquid-solid systems based on the adsorption capacity assumes that the reaction rate is limited by only one process or mechanism on a single class of sorbing sites and all sites are time dependent (Bhattacharyya and Gupta, 2006; Rahman et al., 2010).

The pseudo-first order model curves were obtained by plotting  $\log\left(1 - \frac{q_t}{q_\infty}\right)$  vs. time (Fig.22) using Eq. 3 (Ho and McKay, 1998). The graphic representation should give a linear trace from which the values of  $k_1$  and  $q_0$  can be determined from the slope and intercept. It's common to describe the "goodness-of-fit" of both linear and nonlinear regressions in terms of square of correlation coefficient ( $r^2=1$ ; perfect "goodness-of-fit").

The results show that the pseudo-first order model presents the best overall goodness-of-fit of experimental data (Tables 8 and 9), confirming that the interaction between Sr<sup>2+</sup> and the binding sites has an important role in the rate of the process. The model was employed under different pH conditions and concentrations in order to evaluate the influence of these variables on sorption rates. It was found that there is an increase of sorption rates with an increase of Sr<sup>2+</sup> concentration and a decrease of pH from 8 to 4. The competition between H<sup>+</sup> and Sr<sup>2+</sup> is higher at pH 4 and the variation of Sr<sup>2+</sup> adsorbed over

the time is greater, contributing to higher sorption rates. It was also concluded that the good fit performed by pseudo-first order model is not modified by the change of  $\text{Sr}^{2+}$  concentration.

Table 8. Kinetic models parameters for  $\text{Sr}^{2+}$  adsorption onto montmorillonite at pH 8.

Model	Time scale	Parameter	Strontium concentration (mg/L)		
			7.00	27.00	34.00
Pseudo-first-order	To 1365 min (18.2 pore volumes)	$K_1$ ( $\text{min}^{-1}$ )	0.0019	0.0022	0.0023
		$R^2$	0.995	0.999	0.999
		Equation	$y=-0.00084x+0.141$	$y=-0.00094x+0.0782$	$y=-0.000979x+0.0812$
Pseudo-second-order	Entire range	$K_2$ (g/mgmin)	24921	20944	14598
		$R^2$	0.406	0.834	0.845
		Equation	$y=0.0252x+79.25$	$y=-0.0185x+19.68$	$y=0.0151x+14.85$
	From 825 min (11.0 pore volumes)	$K_2$ (g/mgmin)	2280	4050	2600
		$R^2$	0.996	0.999	0.999
		Equation	$y=0.0542x+35.15$	$y=0.0250x+10.062$	$y=0.0201x+7.2296$
Intra-particle Model	To 705 min (9.4 pore volumes)	$K_i$	0.508	1.44	1.84
		$R^2$	0.986	0.996	0.996
		Equation	$y=0.508x-5.14$	$y=1.436x-12.73$	$y=1.841x-16.15$
Liquid Film Diffusion	To 285 min (3.7 pore volumes)	$K_{fd}$	0.0085	0.0084	0.0084
		$R^2$	0.958	0.957	0.956
		Equation	$y=0.0085x-3.81$	$y=0.0084-3.37$	$y=0.0084x-3.35$

Consistently a good goodness-of-fit is obtained with the first order model, and a worst goodness-of-fit was observed for the pseudo-second order model (Fig.23) when entire range was considered. There is a linear behavior from  $t=825$  min, suggesting that the second order model may be appropriate to explain the kinetics of the second phase of the adsorption process.

The intra-particle model assumes the transport from the aqueous phase to the surface of the solid. The relatively high values of linear correlation coefficients suggest a large amount of  $\text{Sr}^{2+}$  diffused into the sorbent pores, until  $t=705$  min (Fig.24). However, there is a deviation of straight lines from the origin for all the concentration level, caused by the difference of mass transfer rate between the initial and final stage of adsorption. This situation indicates that the intra-particle diffusion is not the main controlling mechanism (Bhattacharyya and Gupta, 2006; Mall et al., 2006).

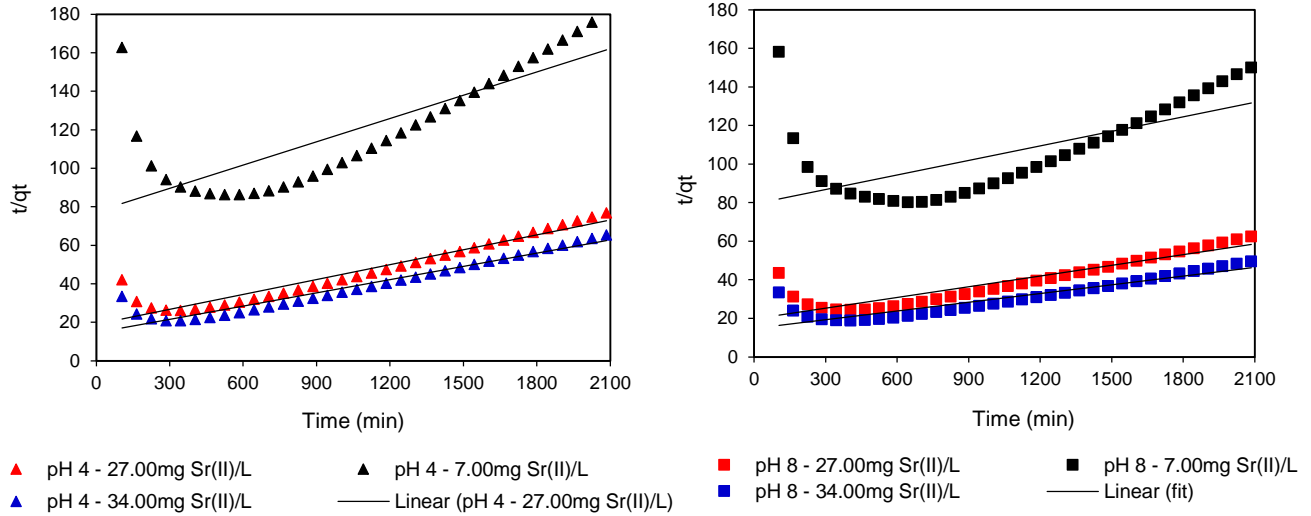


Fig.23 - Kinetic modelling of the sorption of Sr<sup>2+</sup> onto montmorillonite. Pseudo-second order model for adsorption process at pH 4 and pH 8, at different Sr<sup>2+</sup> concentrations.

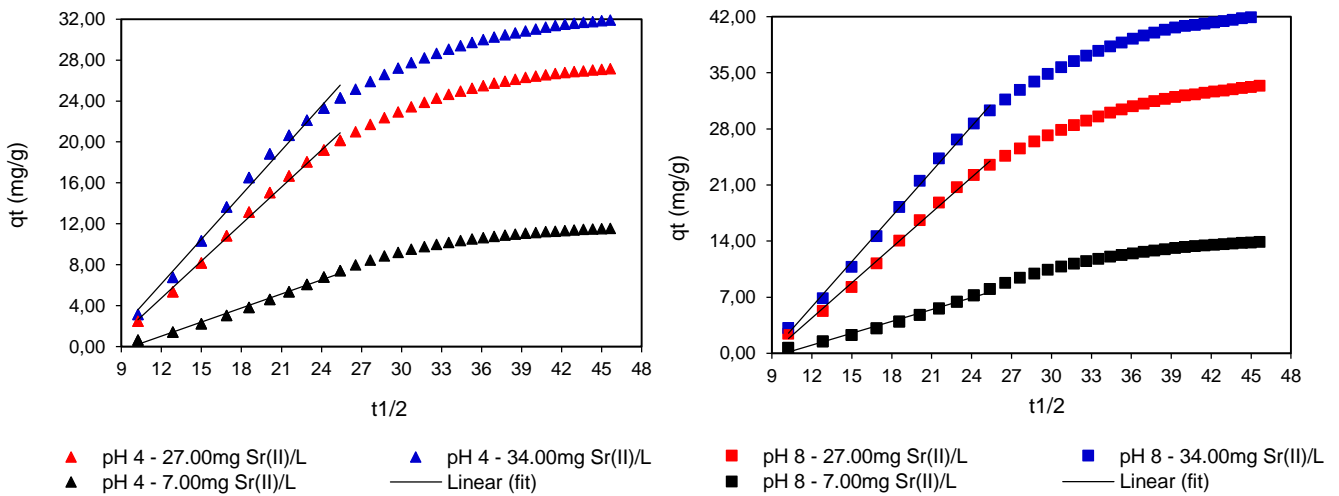


Fig.24 - Kinetic modelling of the sorption of Sr<sup>2+</sup> onto montmorillonite. Intra-particle model for adsorption process at pH 4 and pH 8, at different Sr<sup>2+</sup> concentrations.

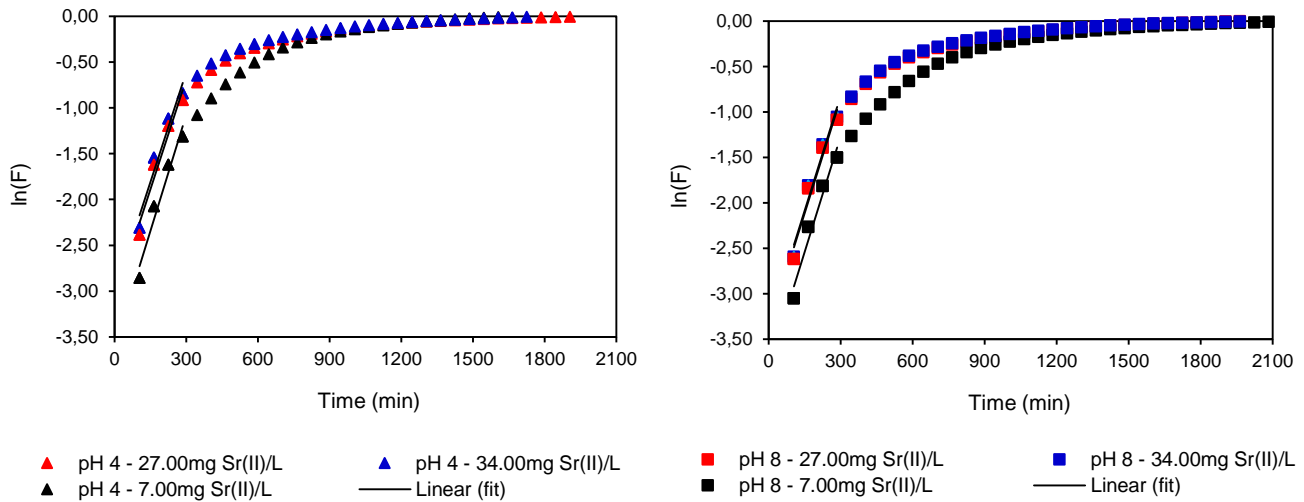


Fig.25 - Kinetic modelling of the sorption of  $\text{Sr}^{2+}$  onto montmorillonite. Film diffusion model for adsorption process at pH 4 and pH8, at different  $\text{Sr}^{2+}$  concentrations.

Table 9. Kinetic models parameters for  $\text{Sr}^{2+}$  adsorption onto montmorillonite at pH 4.

Model	Time scale	Parameter	Strontium concentration (mg/L)		
			7.00	27.00	34.00
Pseudo-first-order	To 1365 min (18.2 pore volumes)	$K_1$ ( $\text{min}^{-1}$ )	0.0020	0.0023	0.0024
		$R^2$	0.995	0.999	0.998
		Equation	$y=-0.00096x+0.142$	$y=-0.00100x+0.0592$	$y=-0.00104x+0.0422$
Pseudo-second-order	Entire range	$K_2$ (g/mgmin)	149602	13941	9320
		$R^2$	0.609	0.920	0.936
		Equation	$y=0.0402x+77.55$	$y=-0.0258x+18.97$	$y=0.0229x+14.61$
Pseudo-second-order	From 825 min (11.0 pore volumes)	$K_2$ (g/mgmin)	14622	3160	2436
		$R^2$	0.998	0.999	1.000
		Equation	$y=0.0703x+32.06$	$y=0.0318x+10.025$	$y=0.0273x+8.155$
Intra-particle Model	To 705 min (9.4 pore volumes)	$K_i$	0.465	1.173	1.396
		$R^2$	0.992	0.992	0.986
		Equation	$y=0.465x-4.58$	$y=1.173x-9.21$	$y=1.396x-10.40$
Liquid Film Diffusion	To 285 min (3.7 pore volumes)	$K_{fd}$	0.0085	0.0081	0.0080
		$R^2$	0.957	0.951	0.950
		Equation	$y=0.0085x-3.62$	$y=0.0081x-3.10$	$y=0.0080x-3.02$

Liquid diffusion becomes the rate controlling cation exchange mechanism, when diffusion of the cation across the surrounding film is slower than cation diffusion within the particle (Ames, 1962). In order, the liquid film diffusion model was applied to investigate the influence of transporting the  $\text{Sr}^{2+}$  ions from the liquid phase up to the solid phase boundary and their role in the adsorption process (Ames, 1962; Bhattacharyya and Gupta, 2006, 2008; Susmita Sen and G, 2009; Zhang and Hou, 2008).

A linear plot of  $\ln(F)$  vs. *time* with zero intercept suggests that the kinetic of the sorption process is controlled by diffusion through the liquid surrounding the solid sorbent (Bhattacharyya and Gupta, 2008; Ekpete, 2012). The reasonable linear ( $R^2=0.950$  to  $R^2=0.958$  until  $t=285$  min) behavior observed, with the goodness-of-fit improving as  $\text{Sr}^{2+}$  concentration decreases at both pH's (Tables 8 and 9), shows that diffusion from the liquid phase might have a considerable role on the adsorption until  $t=285$  min of the interaction process (Fig.25).

#### 4.5.3.4. Sorption isotherm analysis

Batch equilibrium experiments were used to measure the  $\text{Sr}^{2+}$  uptake by montmorillonite under different pH and ionic strength conditions. The amount of  $\text{Sr}^{2+}$  removed from the solution was plotted as a function of the  $\text{Sr}^{2+}$  concentration remained in solution (Coles and Yong, 2006). The results of the sorption experiments achieved for different  $\text{Sr}^{2+}$  concentrations are shown in Fig.26. The sorption isotherm shows an increase of the amount of  $\text{Sr}^{2+}$  adsorbed with the increase of initial  $\text{Sr}^{2+}$  concentration until the steady state of equilibrium is reached. No considerable effect on the  $\text{Sr}^{2+}$  amount adsorbed has been achieved due to a full occupancy of available active sites onto montmorillonite surface.

The adsorption isotherms of Langmuir and Freundlich were applied to describe the adsorption equilibrium (Mall et al., 2006). The equilibrium is obtained when occur a monolayer formation on the sorbent and all the sorption sites are considered identical and energetically equivalent due to its homogeneous structure (Dimović et al., 2009; Kütahyalı et al., 2012; Mall et al., 2006; Oubagaranadin and Murthy, 2010; Piccin et al., 2012; Sdiri et al., 2011). The slope ( $1/K_L q_m C_e$ ) and the intercept ( $1/q_m$ ) of the plot  $1/q_e$  vs.  $1/C_e$ , sorption capacity and Langmuir constant are shown in Table 10. The linear fit of the  $\text{Sr}^{2+}$  sorption using Langmuir isotherm is shown in Fig.27.

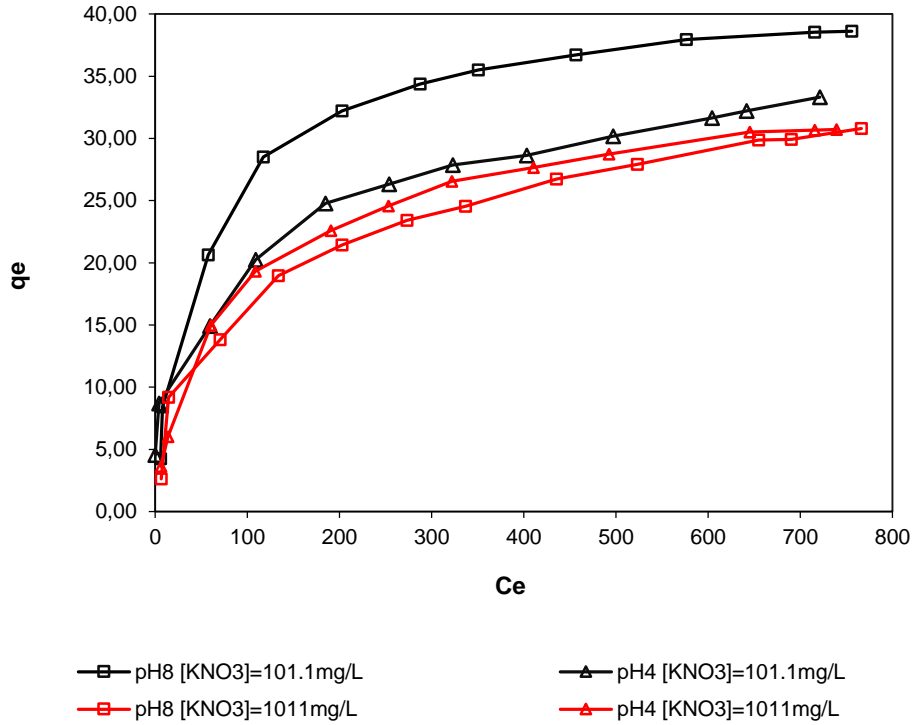


Fig.26 - Behavior of experimental isotherm data for sorption of Sr<sup>2+</sup>.

Table 10. Isothermic models parameters for Sr<sup>2+</sup> adsorption onto Montmorillonite.

Model	Parameter	pH 8		pH 4	
		[KNO <sub>3</sub> ]=101.1mg/L	[KNO <sub>3</sub> ]=1011mg/L	[KNO <sub>3</sub> ]=101.1mg/L	[KNO <sub>3</sub> ]=1011mg/L
Langmuir Isotherm	q <sub>m</sub>	41.49	33.22	35.59	32.89
	K <sub>L</sub>	17.37	9.910	12.10	13.45
	R <sup>2</sup>	0.998	0.990	0.996	0.990
	Equation	y=1.39x+0.0241	y=3.04x+0.0301	y=2.32x+0.0281	y=2.26x+0.0304
Freundlich Isotherm	n	4.64	3.14	3.38	3.61
	K <sub>F</sub>	9.64	3.82	4.89	5.14
	R <sup>2</sup>	0.915	0.982	0.961	0.976
	Equation	y=0.215x+2.266	y=0.318x+1.339	y=0.296+1.588	y=0.277x+1.638

The “goodness-of-fit” of experimental data towards the linear form of Langmuir model illustrate higher values of the correlation coefficients ( $R^2$ ), between 0.990 and 0.998, showing a good representation of experimental data. The  $R_L$  values determined are lesser than 1 and greater than 0, indicating a favorable  $Sr^{2+}$  sorption isotherms onto montmorillonite.

Two relevant data were obtained from the Langmuir isotherm: *i*) the maximum amount of  $Sr^{2+}$  adsorbed by montmorillonite is closely the same (from 33.22  $mgSr^{2+}/g$  – pH=8 to 32.89  $mgSr^{2+}/g$  – pH=4) at higher ionic strength ( $[KNO_3]=1011$  mg/L) and different pH (4 and 8); *ii*) there is a decrease in the amount of metal adsorbed at pH 4 (from 41.49  $mgSr^{2+}/g$  – pH=8 to 35.59  $mgSr^{2+}/g$  – pH=4), at lower ionic strength ( $[KNO_3]=10^{-3}$  M), which means that with an increase of ionic strength the amount of  $Sr^{2+}$  adsorbed decreased, and the difference between the amounts of  $Sr^{2+}$  ions adsorbed at different pH is less significant. This situation could be explained by the competition between  $K^+$  and  $Sr^{2+}$  for sorption sites. At pH 8, the edge sites will be occupied by  $K^+$ , due to their lower bonding energies and their higher capacity to lose more easily their hydrated water. Thus,  $Sr^{2+}$  was probably adsorbed by ionic exchange mechanism in the interlayer space, showing an identical behavior to the adsorption at pH 4 (Eslinger and Pevear, 1988; Parker and Rae, 1998).

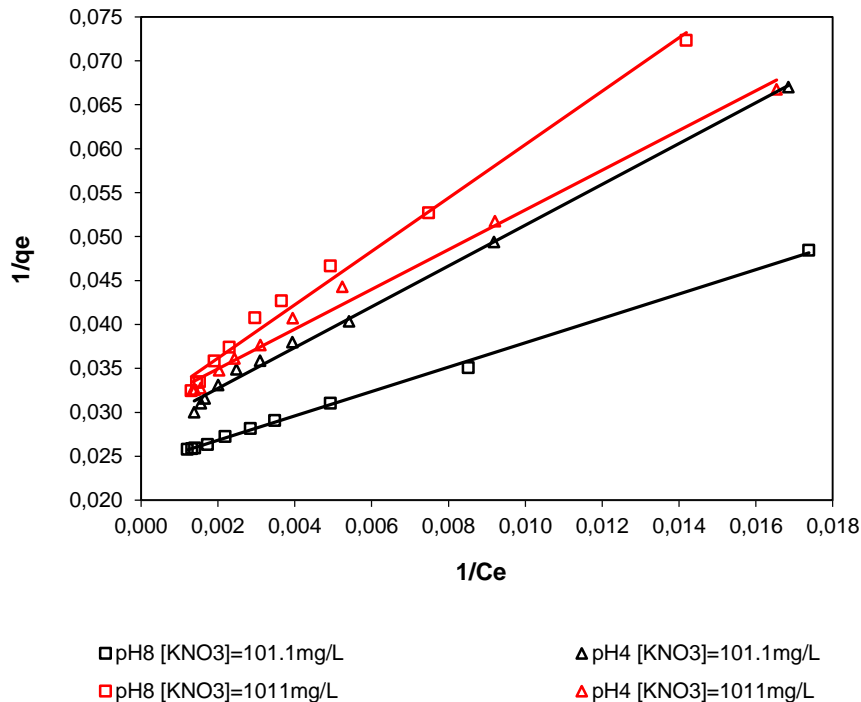


Fig.27 - Langmuir isotherms for  $Sr^{2+}$  adsorption onto montmorillonite under different experimental conditions.

The Freundlich sorption model describes the sorption of solutes from liquid to solid surfaces. Adsorbents that follow the Freundlich isotherm equation are assumed to have a heterogeneous surface consisting of sites with different exponential distribution and energies (Akar et al., 2009; Inglezakis and Pouloupoulos, 2006; Oladoja, 2008). The Freundlich isotherm is linear if  $1/n=1$  and, as  $1/n$  decreases the isotherm becomes more nonlinear (Atun and Kaplan, 1996; Coles and Yong, 2006).

The linear fit of the  $\text{Sr}^{2+}$  sorption experimental data obtained using Freundlich isotherm is shown in Fig.28. The calculated correlation factors (Table 10) confirm a poor agreement between theoretical model and our experimental results, compared to Langmuir model, indicating that the sorbent structure seems to be homogeneous, with similar and energetically equivalent sorption sites. The adsorption intensity given by the Freundlich coefficient ( $n$ ) is  $>1$  in the cases studied and the Freundlich coefficient lies between 3.82 ( $\text{Lg}^{-1}$ ) and 9.64 ( $\text{Lg}^{-1}$ ).

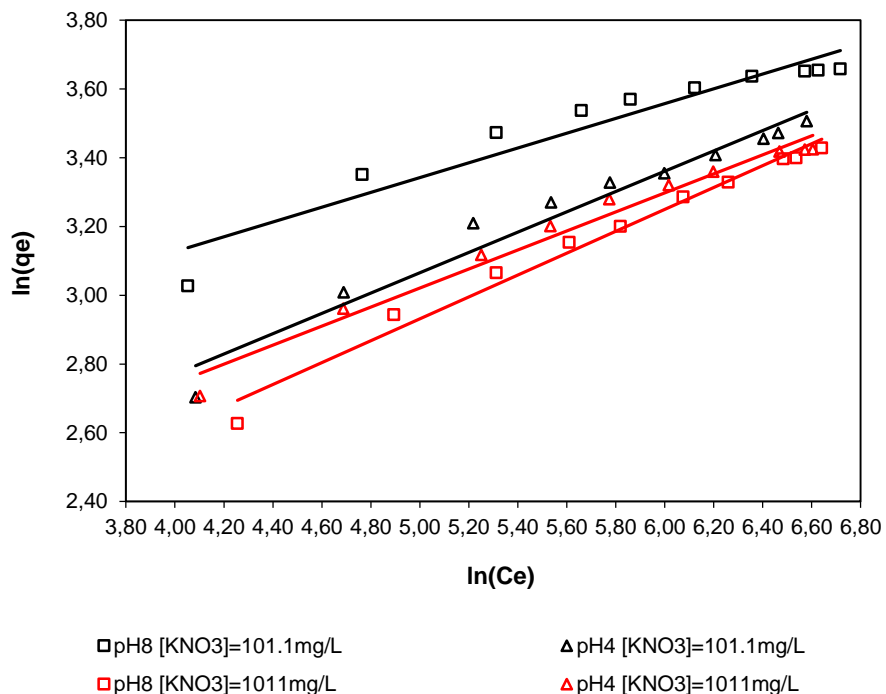


Fig.28 - Freundlich isotherms for  $\text{Sr}^{2+}$  adsorption onto montmorillonite under different experimental conditions.

#### 4.5.4. Conclusion

The results obtained proved that sorption-desorption behavior of montmorillonite depend on the solid/solution ratio, where more negative sites become available for the  $\text{Sr}^{2+}$  ions sorption as pH increases. The amount of  $\text{Sr}^{2+}$  adsorbed increased as increasing the  $\text{Sr}^{2+}$  concentration during the flow-through experiments. The gradient of concentration acted as an increasing driving force resulting in an increasing of equilibrium sorption until the steady-state equilibrium was reached. The  $\text{Sr}^{2+}$  amount desorbed at pH 4 was about half of the amount desorbed at pH 8, revealing that at pH 4 enhanced the retention of  $\text{Sr}^{2+}$  onto montmorillonite.

The pseudo-first order model has the best fit of experimental data during all the adsorption process, confirming that the interaction between  $\text{Sr}^{2+}$  and the binding sites has an important role in the rate of the process.

The effect of pH and ionic strength was evaluated during batch experiments, under equilibrium and isothermal conditions. The adsorption was higher at pH 8 and lower ionic strength ( $[\text{KNO}_3]=101.1 \text{ mg/L}$ ) with a maximum adsorption capacity of  $41.49 \text{ mgSr}^{2+}/\text{g}$ . However, the effect of pH in adsorption becomes less significant as ionic strength increases (from  $33.22 \text{ mgSr}^{2+}/\text{g}$  – pH=8 to  $32.89 \text{ mgSr}^{2+}/\text{g}$  – pH=4, at higher ionic strength ( $[\text{KNO}_3]=1011 \text{ mg/L}$ ) and different pH (4 and 8)). The correlation coefficients indicated that the Langmuir model fits better the experimental data than the Freundlich model, indicating that sorbent structure seems to be homogeneous, with similar and energetically equivalent sorption sites.

The results obtained prove a better prediction of the hazardous trace elements sorption in compacted clay rocks liners in competition with the variation of chemical environment.

#### Acknowledgements

This is a contribution of KADRWaste PTDC/CTE-GEX/82678/2006 with financial support of FCT-Lisbon, Portugal. First author thank to FCT-Lisbon for the PhD scholarship (SFRH / BD /79969 / 2011).

#### 4.5.5. References

- EPA, 2009. Contaminant Occurrence Support Document for Category 2 Contaminants for the Second Six- Year Review of National Primary Drinking Water Regulations.
- Akar, S.T., Yetimoglu, Y., Gedikbey, T., 2009. Removal of chromium (VI) ions from aqueous solutions by using Turkish montmorillonite clay: effect of activation and modification. *Desalination* 244, 97-108.
- Ames, L.L.J., 1962. Kinetics of Cesium Reactions with Some Inorganic Cation Exchange Materials. *Journal Name: Am. Mineralogist; Journal Volume: Vol: 47; Other Information: HW-SA-2343. Orig. Receipt Date: 31-DEC-63, Medium: X; Size: Pages: 1067-1078.*
- Atun, G., Kaplan, Z., 1996. Influences of salt concentration, loading and pH on strontium adsorption. *Journal of Radioanalytical and Nuclear Chemistry* 211, 425-434.
- Baral, S.S., Das, S.N., Chaudhury, G.R., Swamy, Y.V., Rath, P., 2008. Adsorption of Cr(VI) using thermally activated weed *Salvinia cucullata*. *Chemical Engineering Journal* 139, 245-255.
- Başçetin, E., Atun, G., 2006. Adsorption behavior of strontium on binary mineral mixtures of Montmorillonite and Kaolinite. *Applied Radiation and Isotopes* 64, 957-964.
- Bhattacharyya, K.G., Gupta, S.S., 2006. Adsorption of Fe(III) from water by natural and acid activated clays: Studies on equilibrium isotherm, kinetics and thermodynamics of interactions. *Adsorption* 12, 185-204.
- Bhattacharyya, K.G., Gupta, S.S., 2008. Influence of acid activation on adsorption of Ni(II) and Cu(II) on kaolinite and montmorillonite: Kinetic and thermodynamic study. *Chemical Engineering Journal* 136, 1-13.
- Brunauer, S., Emmett, P.H., Teller, E., 1938. Adsorption of Gases in Multimolecular Layers. *Journal of the American Chemical Society* 60, 309-319.
- Chegrouche, S., Mellah, A., Barkat, M., 2009. Removal of strontium from aqueous solutions by adsorption onto activated carbon: kinetic and thermodynamic studies. *Desalination* 235, 306-318.
- Chorover, J., Choi, S., Amistadi, M.K., Karthikeyan, K.G., Crosson, G., Mueller, K.T., 2003. Linking Cesium and Strontium Uptake to Kaolinite Weathering in Simulated Tank Waste Leachate. *Environmental Science & Technology* 37, 2200-2208.
- Coles, C.A., Yong, R.N., 2006. Use of equilibrium and initial metal concentrations in determining Freundlich isotherms for soils and sediments. *Engineering Geology* 85, 19-25.
- Davis, G.A., Worrall, W.E., 1971. The adsorption of water by clays. *Trans. Brit. Ceramic Soc.* 70, 71-75.
- Dimović, S., Smičiklas, I., Plećaš, I., Antonović, D., 2009. Kinetic Study of Sr<sup>2+</sup> Sorption by Bone Char. *Separation Science and Technology* 44, 645-667.
- Eba, F.G., S.; A. Eya'A-Mvongbote ;Ondo, J. A. ; Yao, B. K. ; Ndong Nlo J. ; Kouya Biboutou R., 2010. Evaluation of the absorption capacity of the natural clay from Bikougou (Gabon) to remove Mn (II) from aqueous solution. *International Journal of Engineering Science and Technology* Vol. 2(10), 5001-5016.
- Ekpete, O.A.H.J., M.; Spiff A.I., 2012. Kinetics of Chlorophenol Adsorption onto Commercial and Fluted Pumpkin Activated Carbon in Aqueous Systems. *Asian Journal of Natural & Applied Sciences* 1.
- Eslinger, E., Pevear, D.R., 1988. Clay minerals for petroleum geologists and engineers. SEPM.

- Ghaedi, M., Jah, A.H., Khodadoust, S., Sahraei, R., Daneshfar, A., Mihandoost, A., Purkait, M.K., 2012. Cadmium telluride nanoparticles loaded on activated carbon as adsorbent for removal of sunset yellow. *Spectrochimica Acta Part a-Molecular and Biomolecular Spectroscopy* 90, 22-27.
- Grolimund, D., Borkovec, M., Federer, P., Sticher, H., 1995. Measurement of Sorption Isotherms with Flow-Through Reactors. *Environmental Science & Technology* 29, 2317-2321.
- Ho, Y.S., McKay, G., 1998. A Comparison of Chemisorption Kinetic Models Applied to Pollutant Removal on Various Sorbents. *Process Safety and Environmental Protection* 76, 332-340.
- Ho, Y.S., McKay, G., 1999. Pseudo-second order model for sorption processes. *Process Biochemistry* 34, 451-465.
- Howard, J.J., 1981. Lithium and potassium saturation of illite/smectite clays from interlaminated shales and sandstones. *Clays and Clay Minerals* 29, 136-142.
- Inglezakis, V.J., Pouloupoulos, S.G., 2006. 2 - Adsorption, Ion Exchange, and Catalysis. Elsevier, Amsterdam.
- Jinsheng, W., Rui, Z., Yanguo, T., QinHong, H., Zongjian, S., 2010. Sorption of strontium and fractal scaling of the heterogeneous media in a candidate VLLW disposal site. *Journal of Radioanalytical & Nuclear Chemistry* 283, 319-328.
- Kannan, N., Sundaram, M.M., 2001. Kinetics and mechanism of removal of methylene blue by adsorption on various carbons—a comparative study. *Dyes and Pigments* 51, 25-40.
- Khan, S.A., Riaz ur, R., Khan, M.A., 1995. Sorption of strontium on bentonite. *Waste Management* 15, 641-650.
- Kütahyalı, C., Çetinkaya, B., Acar, M.B., Işık, N.O., Cireli, T., 2012. Investigation of strontium sorption onto Kula volcanics using Central Composite Design. *Journal of Hazardous Materials* 201-202, 115-124.
- Mahoney, J.J., Langmuir, D., 1991. Adsorption of Sr on kaolinite, illite and montmorillonite at high ionic strengths. *Radiochim. Acta* 54, 139-144
- Malatti, M.A., Mazza, R.J., Sheren, A.J., Tomkins, D.R., 1974. The mechanism of adsorption of alkali metal ions on silica. *Powder Technology* 9, 107-110.
- Mall, I.D., Srivastava, V.C., Agarwal, N.K., 2006. Removal of Orange-G and Methyl Violet dyes by adsorption onto bagasse fly ash—kinetic study and equilibrium isotherm analyses. *Dyes and Pigments* 69, 210-223.
- Marimon, M.M., 2002. On the Sorption and Diffusion of Radionuclides in Bentonite Clay, Department of Chemistry / Nuclear Chemistry Royal Institute of Technology, Sweden.
- Nemes, Z., Nagy, N.M., Kónya, J., 2005. Kinetics of strontium ion adsorption on natural clay samples. *Journal of Radioanalytical and Nuclear Chemistry* 266, 289-293.
- Oladoja, N.A.A., C.O.; Oladimeji, Y.B., 2008. Kinetics and isotherm studies on methylene blue adsorption onto ground palm kernel coat. *Turk. J. Engg. Environ. Sci.* 32 303.
- Oubagaranadin, J.U.K., Murthy, Z.V.P., 2010. Isotherm modeling and batch adsorber design for the adsorption of Cu(II) on a clay containing montmorillonite. *Applied Clay Science* 50, 409-413.
- Parker, A., Rae, J.E., 1998. *Environmental Interactions of Clays: Clays and the Environment*. Springer.
- Piccin, J.S., Gomes, C.S., Feris, L.A., Gutterres, M., 2012. Kinetics and isotherms of leather dye adsorption by tannery solid waste. *Chemical Engineering Journal* 183, 30-38.
- Rafferty, P., Shiao, S.Y., Binz, C.M., Meyer, R.E., 1981. Adsorption of Sr(II) on clay minerals: Effect of salt concentration, loading and pH. *Journal of Inorg. Nucl. Chem.* 43, 797-806.

- Rahman, I., Iwakabe, K., Kawasaki, J., 2008. Laterite-A Potential Alternative for Removal of Groundwater Arsenic. *J. Appl. Sci. Environ. Manage* 12, 93-100
- Rahman, R.O.A., Ibrahim, H.A., Hanafy, M., Monem, N.M.A., 2010. Assessment of synthetic zeolite Na A–X as sorbing barrier for strontium in a radioactive disposal facility. *Chemical Engineering Journal* 157, 100-112.
- Sdiri, A., Higashi, T., Hatta, T., Jamoussi, F., Tase, N., 2011. Evaluating the adsorptive capacity of montmorillonitic and calcareous clays on the removal of several heavy metals in aqueous systems. *Chemical Engineering Journal* 172, 37-46.
- Selim, H.M., 2012. *Competitive Sorption and Transport of Heavy Metals in Soils and Geological Media*. CRC Press.
- Sparks, D.L., Sparks, D.L., 2003. *Environmental Soil Chemistry*. Academic Press.
- Sureda, R., Martínez-Lladó, X., Rovira, M., de Pablo, J., Casas, I., Giménez, J., 2010. Sorption of strontium on uranyl peroxide: Implications for a high-level nuclear waste repository. *Journal of Hazardous Materials* 181, 881-885.
- Gupta, S.S., Bhattacharyya, K.G., 2009. Treatment of water contaminated with Pb(II) and Cd(II) by adsorption on kaolinite, montmorillonite and their acid-activated forms. *Indian Journal of Chemical Technology* 16, 457-470.
- Ahmad, S., 1995. Competitive adsorption of  $^{90}\text{Sr}$  on soil sediments, pure clay phases and feldspar minerals. *Applied Radiation and Isotopes* 46, 287-292.
- Tertre, E., Hubert, F., Bruzac, S., Pacreau, M., Ferrage, E., Prêt, D., 2013. Ion-exchange reactions on clay minerals coupled with advection/dispersion processes. Application to  $\text{Na}^+/\text{Ca}^{2+}$  exchange on vermiculite: Reactive-transport modeling, batch and stirred flow-through reactor experiments. *Geochimica et Cosmochimica Acta* 112, 1-19.
- Velde, B.B., Meunier, A., 2008. *The Origin of Clay Minerals in Soils and Weathered Rocks: With 23 Tables*. Springer.
- Zhang, S.Q., Hou, W.G., 2008. Adsorption behavior of Pb(II) on montmorillonite. *Colloids and Surfaces A: Physicochemical and Engineering Aspects* 320, 92-97.
- Zhu, Y.G., Shaw, G., 2000. Soil contamination with radionuclides and potential remediation. *Chemosphere* 41, 121-128.

## 4.6. Kinetics of uranyl ions sorption on heterogeneous smectite structure at pH 4 and 6 using a continuous stirred flow-through reactor

Adapted from Vanessa Guimarães, Enrique Rodríguez-Castellón, Manuel Algarra, Fernando Rocha, Iuliu Bobos

Accepted by Journal of Applied Clay Science at 22 March 2016

DOI: doi:10.1016/j.clay.2016.03.028

### ABSTRACT

The  $<2 \mu\text{m}$  clay fractions of three smectite samples (BA1, PS2 and PS3) were submitted to  $\text{UO}_2^{2+}$  sorption experiments at pH 4 (0.1 mM) and pH 6 (0.2M) in a continuous stirred flow-through reactor. The aim was to evaluate the influence of heterogeneous structure of smectite during the adsorption and desorption processes, where the breakthrough curves (BTCs) were used to model the mass balance. Kinetic models were applied to describe the adsorption – desorption kinetics for a liquid-solid system. Sample PS2 (K-Illite/beidellite/Na,Ca-montmorillonite) adsorbed at pH 4 more 34% and 138% of  $\text{UO}_2^{2+}$  than samples BA1 (beidellite/Ca,Na-montmorillonite) and PS3 (K-illite/Na,Ca-montmorillonite) where the dominant mechanism was the ion-exchange (outer-sphere complexation). The  $\text{UO}_2^{2+}$  amount adsorbed at pH6 decreased significantly, indicating changes in the sorption mechanism. The desorption experiments at pH 4 suggested a complete reversibility of the  $\text{UO}_2^{2+}$  previously adsorbed, whereas lower reversibility of the  $\text{UO}_2^{2+}$  previously adsorbed and a stronger complexation occurred at pH 6. The kinetics was highly influenced by the structural properties of heterogeneous smectite and the surface complexation mechanism involved. Samples submitted to sorption experiments at pH 4 and 6 were analysed by XPS. Two binding energies were identified at pH 4,  $380.8 \pm 0.3 \text{ eV}$  and  $382.4 \pm 0.3 \text{ eV}$ , before and after desorption processes. The proportion of the higher binding energy component decreased after desorption process, suggesting that the  $\text{UO}_2^{2+}$  weakly adsorbed was previously desorbed. The results obtained at pH 6 show two different binding energies for smectite samples,  $380.3 \pm 0.3 \text{ eV}$  and  $381.8 \pm 0.3 \text{ eV}$ , whose proportions remained unchanged before and after desorption process, indicating the higher retention of  $\text{UO}_2^{2+}$  on smectite.

**Keywords:** Heterogeneous smectite, Continuous stirred flow-through reactor, Adsorption and desorption, X-photoelectron spectroscopy.

### 4.6.1. Introduction

The long-term storage and safe disposal of nuclear waste is successfully provided by the materials selected for engineering barriers in deep geological repositories (Apted and Ahn, 2010). The structural and physico-chemical changes of clay mineral properties due to thermal, chemical and biological factors may affect the performance of the engineered clay barriers in short- and long-term design life periods (Duro et al., 2014; Kaufhold and Dohrmann, 2010; Lee et al., 2010).

Smectite clay is widely used for sealing purposes in repositories owing to its low permeability and high sorption capacity (Lee et al., 2010; Parker and Rae, 1998; Pusch et al., 2015; Galamboš et al., 2011). A negative impact on smectite buffer is the smectite illitization (Inoue et al., 1992), being one of the most unwanted reactions. The reduction of hydration capacity and the welding of particle stacks affect the expandability and plasticity of smectite (Kaufhold and Dohrmann, 2010; Lee et al., 2010). Changes in the pH and ionic strength as a result of chemical and biological processes in the repository environment, will affect the aqueous speciation of radionuclides and the surface complexation process (Poinssot and Geckeis, 2012; Seaman and Roberts, 2012; Galamboš et al., 2011).

The  $\text{UO}_2^{2+}$  retardation is controlled by its interaction with smectite, depending to the  $\text{UO}_2^{2+}$  mobility in solution through the near-field adsorbent (Lujanienė et al., 2012; Miller et al., 2000). Two main mechanisms of  $\text{UO}_2^{2+}$  adsorption on smectite are reported in literature: ion-exchange through outer-sphere complexation at low pH and low ionic strength and inner-sphere complexation on the edge sites at near neutral pH and high ionic strength controls the sorption mechanism (Chisholm-Brause et al., 2001; Hennig et al., 2002; Korichi and Bensmaili, 2009; Marques Fernandes et al., 2012; Schindler et al., 2015; Sylwester et al., 2000). Free uranyl ion  $\text{UO}_2(\text{H}_2\text{O})_5^{2+}$  is the dominant specie up to  $\text{pH} \approx 5$ , whereas the  $\text{UO}_2^{2+}$  polynuclear species are dominant as pH increases (Bachmaf and Merkel, 2011).

The  $\text{UO}_2^{2+}$  sorption on smectite is governed by adsorption and desorption from multiple sites with different kinetics (Bachmaf and Merkel, 2011; Bachmaf et al., 2008; Campos et al., 2013; Missana et al., 2004; Wang et al., 2013). There is a lack of information relatively to the  $\text{UO}_2^{2+}$  desorption kinetics and the contaminant reversibility in different

environmental conditions, despite the kinetics of adsorption was well studied in batch conditions (Bachmaf and Merkel, 2011; Missana et al., 2004).

One of the main problems regarding to desorption experiments is the re-suspension of the solid particles that remains compacted at the bottom of the tube (Missana et al., 2004). This disadvantage is overcome by the continuous stirred tank reactors where the desorbed species are continuously removed from the system, avoiding reverse reactions and enhancing the study of desorption kinetics phenomena (Grolimund, 1998; Sparks, 1999). The continuous stirred flow-through method combines the advantages of batch and flow-through methods, which represents a powerful tool to identify the factors responsible for apparent deviations in sorption parameters measured under distinct environmental conditions (Brantley et al., 2007; Fernández-Calviño et al., 2010; Grolimund, 1998; Helfferich, 2004).

Several drawbacks were identified during  $\text{UO}_2^{2+}$  sorption in batch reactors regarding to the high dependency of the sorbent sorption behavior on the solid concentration (particle concentration effect) and the permanent accumulation of solutes, released by the adsorbent, which increases the risk of precipitation of secondary phases (Brantley et al., 2007; Grolimund, 1998).

The purpose of this study is to improve the characterization of the  $\text{UO}_2^{2+}$  retardation onto smectite through the adsorption and desorption experiments using a continuous stirred tank reactor. In our experiments three different smectite samples characterized by heterogeneous structures, with distinct proportions of tetrahedral and octahedral substitutions, were used. The kinetic of sorption process was interpreted by the reaction-controlled model (pseudo-first order and pseudo-second order) and diffusion-controlled model (intra-particle diffusion and liquid-film diffusion).

Previous studies revealed that multiple surface species are involved on the interaction between  $\text{UO}_2^{2+}$  and smectite, resulted from ion exchange on planar sites at acid pH and surface coordination reactions at the edge sites from near neutral pH at high ionic strengths (McKinley et al., 1995; Missana et al., 2004; Sylwester et al., 2000; Zachara and McKinley, 1993). In this way, different pH and ionic strengths were imposed during the flow-through experiments (pH 4,  $I=1 \times 10^{-4}$ ; pH=6,  $I=0.2$ ) to study the effect of each surface mechanism on the  $\text{UO}_2^{2+}$  reversibility. The influence of the structural changes of smectite during the adsorption and desorption processes were also taken into account. The results of the surface complexation mechanism in distinct environment conditions were supported by XPS data.

## 4.6.2. Materials and Methods

### 4.6.2.1. Materials

*Clay minerals selection and preparation.* Three selected bentonite rocks (BA1, PS2 and PS3) were collected from two different regions of Portugal: Benavila region (BA1) and Porto Santo Island, Madeira archipelago (PS2 and PS3). Adsorption experiments were preceded by separation and purification process, where carbonate was removed from the selected samples according to Jackson's method (1975). The <2  $\mu\text{m}$  fractions were obtained by sedimentation from the purified samples, according to Stocks law. Previously sorption experiments, the <2  $\mu\text{m}$  clay fractions were studied by X-ray diffraction (XRD), infrared-spectroscopy and electron microprobe analysis. The <2  $\mu\text{m}$  clay fractions were analysed by XRD in air-dried and ethylene-glycol conditions. Structural behavior of smectite samples was verified using several well-known protocols used to differentiate high- from low-charge smectite (Barshad, 1960; Harward, 1967; Jackson and Barak, 2005) and to distinguish beidellite from montmorillonite (Greene-Kelly, 1952). The detailed results of these experiments were discussed in Guimarães et al. (2015a-submitted).

*Structural characterization of the <2  $\mu\text{m}$  clay fractions.* Sample BA1 corresponds to an interstratified structure composed of beidellite/(Ca,Na)-montmorillonite (2-waters). Sample PS2 corresponds to K-illite/beidellite/(Na,Ca)-montmorillonite (R0, 85-90%S). Sample PS3 corresponds to a randomly interstratified structure of K-illite/(Na,Ca)-montmorillonite (R=0; 70%S), where no beidellitic layers did occur.

*Chemical characterization.* Crystal chemistry of the <2  $\mu\text{m}$  clay fractions obtained by electron microprobe is given in Table 11.

Table 11. Physicochemical properties of clay minerals.

Sample	Structural Formula	S <sub>BET</sub> (m <sup>2</sup> /g)	CEC (meq/g)	Charge Def./Uc
BA1	Ca <sub>0.53</sub> Na <sub>0.40</sub> (Al <sub>2.61</sub> Fe <sub>0.73</sub> Mg <sub>0.66</sub> )(Si <sub>7.28</sub> Al <sub>0.72</sub> )O <sub>20</sub> (OH) <sub>4</sub>	12	0.96	- 1.38 48%O 52%T
PS2	Ca <sub>0.27</sub> Na <sub>0.74</sub> K <sub>0.16</sub> (Al <sub>2.52</sub> Fe <sub>0.67</sub> Mg <sub>0.78</sub> )(Si <sub>7.50</sub> Al <sub>0.50</sub> )O <sub>20</sub> (OH) <sub>4</sub>	26	1.04	- 1.31 62%O 38%T
PS3	Ca <sub>0.30</sub> Na <sub>0.59</sub> K <sub>0.28</sub> (Al <sub>2.33</sub> Fe <sub>0.81</sub> Mg <sub>0.85</sub> )(Si <sub>7.40</sub> Al <sub>0.60</sub> )O <sub>20</sub> (OH) <sub>4</sub>	84	0.81	- 1.45 59%O 41%T

#### 4.6.2.1.1. Methods and analytical techniques

*Cation exchange capacity.* The  $<2\ \mu\text{m}$  clay fractions were  $\text{Sr}^{2+}$  saturated in order to determine the cation exchange capacity (CEC). The experiments were carried out by adding 0.050 grams of smectite into the polypropylene centrifuge tubes with 14.00 mL of different stock solutions at different  $\text{Sr}^{2+}$  concentrations, ranged between  $5 \times 10^{-4}\ \text{M}$  and  $1.50 \times 10^{-2}\ \text{M}$ . Suspensions were shaken for 34 hours, then centrifuged, separated and the solutions resulted were preserved by adding  $\text{HNO}_3$  (65%) and stored at  $4\ ^\circ\text{C}$  for subsequent chemical analyses. The CEC was determined by  $\text{Sr}^{2+}$  adsorption tests at  $\text{pH}=4$ . The  $\text{Sr}^{2+}$ -aqueous solutions of the  $<2\ \mu\text{m}$  clay fractions  $\text{Sr}^{2+}$  saturated were analysed by atomic absorption spectrometry (AAS). The CEC value was estimated from the maximum amount of  $\text{Sr}^{2+}$  adsorbed in these conditions, taking into account the following relation:  $\text{CEC}(\text{meq/g})=q_{\text{Sr}^{2+}}(\text{mmol/g}) \cdot 2$ .

*The Brunauer-Emmett-Teller specific surface area (BET).* The BET surface area of the  $<2\ \mu\text{m}$  clay fractions was carried out using nitrogen adsorption-desorption measurements with a Micromeritics Tristar II analyser. The samples were degassed at  $200\ ^\circ\text{C}$  overnight before the measurements were taken. The surface area was calculated based on the adsorption data in the relative partial pressure range of 0.05-0.2, and the pore size distributions were determined based on the Barrett–Joyner–Halender (BJH) adsorption curve.

*Electron microprobe analysis.* Polished sample surfaces were prepared from the  $<2\ \mu\text{m}$  clay fractions, which were previously pressed in pellets with diameter of 3 mm with a PIKE Hand Press Kit 161-1024 (Pike technologies). The epoxy resin was prepared using the Araldite EAY 103-1 and a HY956-KG hardener (9:1 ratio) and then dispersed in a holder of 13 mm. The pellets were located in the epoxy resin, dried during 24 h and subsequently polished using the 30, 10 and  $2\ \mu\text{m}$  micro-finishing films under dry conditions. The major elements of minerals were determined using a Jeol Hyperprobe JXA-8500F electron microprobe operated at 15 kV accelerating voltage and 10 nA beam current. Detection limits ( $3\sigma$ ) above mean background were 0.03 wt.% for most oxides with counting times of 80 s. Standards used include albite ( $\text{NaK}\alpha$ ), orthoclase ( $\text{AlK}\alpha$ ,  $\text{SiK}\alpha$ ,  $\text{KK}\alpha$ ), apatite ( $\text{CaK}\alpha$ ,  $\text{PK}\alpha$ ),  $\text{MgO}$  ( $\text{MgK}\alpha$ ),  $\text{MnTiO}_3$  ( $\text{MnK}\alpha$ ),  $\text{TiO}_2$  ( $\text{TiK}\alpha$ ),  $\text{Fe}_2\text{O}_3$  ( $\text{FeK}\alpha$ ).

*Atomic absorption spectrometry.* Chemical analyses of  $\text{Sr}^{2+}$  aqueous solutions were carried out by atomic absorption spectroscopy using a flame absorption spectrometer Perkin Elmer, AAnalyst 200 model with a Strontium hollow cathode lamp, wavelength 460.73 nm,

air flow 5.2 L/min and acetylene flow 2.5 L/min. The 5 mL of the acidified strontium solution was mixed with 750  $\mu\text{L}$  of lanthanum chloride ( $\text{LaCl}_3 \cdot 7\text{H}_2\text{O}$ ) solution previously prepared (176 g of  $\text{LaCl}_3 \cdot 7\text{H}_2\text{O}$  and 19.1 g of KCl diluted in 1000 mL of deionised water).

*Inductively coupled plasma-mass spectrometry.* The  $\text{UO}_2^{2+}$  aqueous solutions obtained after batch experiments were analysed by inductively coupled plasma-mass spectrometry (ICP-MS). The uranium concentrations in acidified solutions were determined by external standard calibration method using an inductively coupled plasma-mass spectrometry (ICP-MS) (THERMO X series ELEMENT2 and Amiga series, JobinYvon equipments). Calibration was done in each analytical session by the external standard method. Also, major elements of smectite and composite material were analyzed by ICP-MS.

*X-ray photoelectron spectroscopy.* Uranyl-clay samples obtained after batch experiments were analysed by X-ray photoelectron spectroscopy (XPS). XPS spectra were recorded using a Physical Electronics PHI 5701 spectrometer with a non-monochromatic Al  $\text{K}\alpha$  radiation (300 W, 15 kV,  $h\nu = 1486.6$  eV) as the excitation source. Spectra were recorded at  $45^\circ$  take-off angle by a concentric hemispherical analyzer operating in the constant pass energy mode at 25.9 eV, using a 720 mm diameter analysis area. Under these conditions the Au  $4f_{7/2}$  line was recorded with 1.16 eV FWHM at a binding energy of 84.0 eV. The spectrometer energy scale was calibrated using Cu  $2p_{3/2}$ , Ag  $3d_{5/2}$  and Au  $4f_{7/2}$  photoelectron lines at 932.7, 368.3 and 84.0 eV, respectively. Charge referencing was done against adventitious carbon (C1s 284.8 eV). Powdered solids were mounted on a sample holder without adhesive tape and kept overnight in high vacuum in the preparation chamber before they were transferred to the analysis chamber of the spectrometer. Each region was scanned with several sweeps until a good signal to noise ratio was observed. The pressure in the analysis chamber was maintained lower than  $10^{-9}$  Torr. A PHI ACCESS ESCA-V6.0 F software package was used for acquisition and data analysis. A Shirley-type background was subtracted from the signals. Recorded spectra were always fitted using Gauss–Lorentz curves in order to determine more accurately the binding energy of the different element core levels. The accuracy of binding energy (BE's) values was within  $\pm 0.1$  eV.

### 4.6.3. Kinetics of sorption processes

#### *Stirred flow-through reactor and flow-through experiments*

The sorption kinetic studies were carried out on smectite suspensions at pH 4 and pH 6 using a uranyl acetate solution  $[\text{UO}_2(\text{CH}_3\text{COO})_2 \cdot 2\text{H}_2\text{O}]$  with a concentration of  $1.00 \times 10^{-4}$  M, including different sodium chloride (NaCl) concentrations: 0.1 mM and 0.2 M, respectively. The continuous stirred tank reactor with a volume of  $37.3 \text{ cm}^3$  was previously loaded with 0.55 g of clay suspension pre-washed with a solution of NaCl (0.1 M), where the flux flowed during 24 h through the  $0.45 \text{ }\mu\text{m}$  Millipore membranes with a flow rate of 0.7 mL/min. The process assumes a perfect mixing when the chamber and effluent concentrations are equal and transport (diffusion) phenomena is minimized significantly (Denbigh and Turner, 1984). However, the use of sorbents (e.g. smectite, vermiculite) that contain internal sites for sorption that are not easily accessible may affect the diffusion process, and even using a continuous stirred system, diffusion may not be completely eliminated (Sparks, 1989). Washing was followed using a continuous flow-through sorption process during 34 hours where the  $\text{UO}_2^{2+}$  solution was pumped into the reactor at the same flow until the clay system became saturated. After this, the clay system was reverted to the blank solution with a concentration of 1 mM of NaCl for desorption experiments. In this last step, the experiments were followed for 10 hours, where the samples were collected at time intervals for further chemical analysis. The collected samples were preserved by adding  $\text{HNO}_3$  (65%) and then stored at  $4^\circ\text{C}$ . The adsorption and kinetics experiments were carried out in equilibrium conditions with the atmospheric  $\text{CO}_2$  ( $\text{pCO}_2 = 10^{-3.5}$  bar).

#### 4.6.3.1. Modelling of mass balance

The breakthrough experiments are used to measure the adsorption and desorption of contaminant species in the presence of suspended adsorbents (Grolimund et al., 1995). Assuming a perfect mixing, the concentration of the adsorptive in the reactor should be equal to the effluent concentration (Fernández-Calviño et al., 2010; Grolimund et al., 1995; Tertre et al., 2013). The efficiency of the mixing conditions may be tested by comparing the metal concentrations obtained in the end of the process, when no smectite is loaded into the reactor with the values predicted by the theoretical curve for an inert specie in a continuously stirred flow-through reactor. This represents the evolution in time of the outlet concentration,  $[\text{UO}_2^{2+}]_{n-M}$ , after a step-wise increase of the input concentration from 0 to  $C_0$ , obtained by Eq. 1 (Villermaux, 1985):

$$\frac{[UO_2^{2+}]_{n-M}}{C_{0-UO_2^{2+}}} = 1 - \exp^{-Qt/V_R} \quad (1)$$

where  $[UO_2^{2+}]_{n-M}$  is the concentration of the output solution at time  $t$  in the absence of smectite,  $C_{0-UO_2^{2+}}$  is the  $UO_2^{2+}$  concentration of the input solution that is pumped through the reactor during the adsorption process.  $Q$  is the flow rate,  $t$  is the time and  $V_R$  is the volume of the reactor.

The amount of  $UO_2^{2+}$  adsorbed, or desorbed, was obtained by taking into account the area between the breakthrough curve measured with smectite and the theoretical curve measured in the absence of smectite. This amount was calculated according to the mass balance proposed to stirred tank reactors, following Eq. 2 (Villiermaux, 1985).

$$q_{UO_2^{2+}} = V_R \cdot \frac{\sum_{i=1}^n (NV_R^{i+1} - NV_R^i) \cdot \left( \left( [UO_2^{2+}]_M^{i+1} + [UO_2^{2+}]_M^i \right) - \left( [UO_2^{2+}]_{n-M}^{i+1} + [UO_2^{2+}]_{n-M}^i \right) \right)}{m} \quad (2)$$

where  $NV_R^i$  and  $NV_R^{i+1}$  are the number of pore volumes at times  $t_i$  and  $t_{i+1}$ , calculated by the ratio between the total volume of solution pumped through the reactor during each time period and the volume of the reactor ( $V_R$ ). In this case, one pore volume corresponds to 58 minutes.

The  $[UO_2^{2+}]_M^i$  and  $[UO_2^{2+}]_M^{i+1}$  correspond to the output  $UO_2^{2+}$  concentration of each sample collected successively at times  $t_i$  and  $t_{i+1}$ . The  $[UO_2^{2+}]_{n-M}^i$  and  $[UO_2^{2+}]_{n-M}^{i+1}$  represent the concentrations of the output solution at time  $t_i$  and time  $t_{i+1}$  in the absence of smectite.  $V_R$  is the reactor volume ( $37.3 \text{ cm}^3$ ) and  $m$  is the mass of smectite in the reactor ( $0.55 \text{ g}$ ). The same analytical calculus was used by several authors in different sorption experiments using clay minerals (Fernández-Calviño et al., 2010; Guimarães et al., 2015; Tertre et al., 2013).

#### 4.6.3.2. Kinetic models

Several models are frequently applied to describe sorption kinetics for a liquid-solid system. Reaction-controlled models such as pseudo-first order model or pseudo-second order model assume that the interaction between  $UO_2^{2+}$  and the binding sites controls the rate of the process (Ismadji et al., 2015; Sparks, 2013). Both models were obtained by non-linear regression, given by Eqs. 3 and 4 (Ho and McKay, 1998; Lagergren, 1898):

$$q_t = q_e(1 - e^{-K_1 t}) \quad (3)$$

$$q_t = \frac{K_2 q_e^2 t}{1 + K_2 q_e t} \quad (4)$$

where  $q_t$  and  $q_e$  are the amount of solute adsorbed at time  $t$  and at equilibrium (mol/Kg), respectively, calculated according to Eq. 2.  $k_1$  is the rate constant of pseudo-first order in  $\text{min}^{-1}$  and  $k_2$  is the rate constant of pseudo-second order in  $\text{kg/mol}\cdot\text{min}$ .

Additionally, diffusion-controlled models, such as liquid-film diffusion and intra-particle diffusion, are also frequently used to describe the kinetic phenomenon of ion-exchange (time independent) depending of (1) ions diffusion in the aqueous solution, (2) film diffusion at the solid-liquid interface, (3) intra-particle diffusion on pore surfaces and (4) inter-particle diffusion along the solid particles (Selim, 2012; Sparks, 1989).

The kinetic intra-particle model has been extensively used to describe sorption rates in various types of materials (Tsai et al., 2005; Weber and Morris, 1963). In this case, uptake varies with  $t^{1/2}$  rather than with the contact time according to Eq. 5:

$$q_t = K_i t^{0.5} \quad (5)$$

where  $K_i$  is the intra-particle diffusion rate constant ( $\text{mol/kgmin}^{0.5}$ ) and  $q_t$  is the amount of  $UO_2^{2+}$  on clay at time  $t$  (mol/kg). In the adsorption mechanism following the intra-particle diffusion process, the plot of  $q_t$  versus  $t^{1/2}$  should be a straight line passing through the origin with a slope  $K_i$ .

The liquid film diffusion model (Eq. 6) describes the kinetic phenomenon when the flow of the reactants through the liquid film surrounding the adsorbent particles is the slowest process determining the kinetics of the rate process (Bhattacharyya and Gupta, 2008):

$$\ln(1 - F) = -K_{fd}t \quad (6)$$

where  $F$  is the fractional attainment of equilibrium ( $=q_t/q_e$ ) and  $K_{fd}$  is the film diffusion rate constant ( $\text{min}^{-1}$ ).

## 4.6.4. Results and Discussion

### 4.6.4.1. Influence of heterogeneous layers and layer charge location distributions

The effect of layer charge distributed between tetrahedral and/or octahedral sheets of smectite was taken into account in sorption experiment. Different charge layers reveal different compositions regarding to the degree of octahedral and tetrahedral substitutions occurring in smectite layers. Also, the influence of charge distribution of selected smectite samples was evaluated taking into account the ratio between the CEC values and the respective layer charge deficits (Table 11).

Higher proportions of tetrahedral substitution ( $-0.37/(\text{Si,Al})_4\text{O}_{10}$ ) attributed to beidellite layers correspond to sample BA1, whereas the lower tetrahedral charge deficits and higher octahedral substitutions were found in samples PS2 ( $-0.26/(\text{Si,Al})_4\text{O}_{10}$ ) and PS3 ( $-0.30/(\text{Si,Al})_4\text{O}_{10}$ ). Reduced interlayer distances induced by the increase of layer substitutions and by the proximity between the charge deficit of tetrahedral sheet and the contaminant, restrict the ion-exchanges process hampering the  $\text{UO}_2^{2+}$  uptake. Therefore, sample BA1 has higher charge than PS2 but lower CEC value (Table 11).

A hypothetic structure of smectite samples used in sorption experiments is shown in Fig.29, where both layer-types and charge layers are shown for each smectite sample used in sorption experiments according with structural and chemical data obtained by XRD and EMPA.

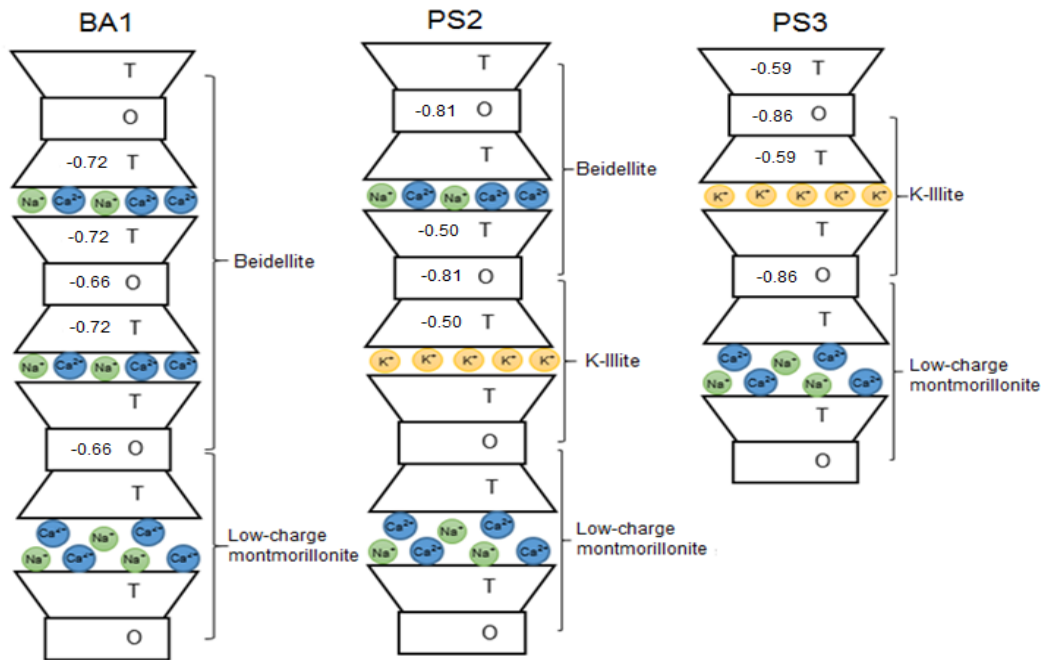


Fig.29 -Idealization of smectite structures: a) BA1 structure that results from interstratification between beidellite and low charge montmorillonite; b) PS2 interstratified structure that consists on Beidellite, Illite and low charge montmorillonite; c) PS3 structure composed by illite and low charge montmorillonite interstratified.

The lower proportion of tetrahedral substitutions of PS2 improved the adsorption on interlayer sites, contrary to what is observed for sample PS3 (CEC=0.81 meq/g). Usually, a decrease of CEC does occur as the percentage of illite layers increases in the randomly interstratified structure of I/S formed. Sample PS3 has higher proportion of illite interstratified layers into a randomly 2W/1W-smectite with montmorillonitic character. The lower number of available sites for ion-exchange favored the decrease of  $UO_2^{2+}$  adsorbed.

#### 4.6.4.2. Uranyl aqueous speciation

The aqueous speciation of  $UO_2^{2+}$  was calculated using PHREEQC 3.12-8538 code (Parkhurst and Appelo, 2013) taking into account the experimental conditions used in the acidic and alkaline range. The aqueous uranyl hydrolysis and carbonate complexation constants were implemented from the Nuclear Energy Agency (NEA-TDB). The distribution of aqueous species from pH 3 to pH 6, using  $1.00 \times 10^{-4} M$  of U(VI) and NaCl, and from pH 5 to pH 9, using  $1.00 \times 10^{-4} M$  of U(VI) and 0.2M of NaCl, is shown in Fig.30.

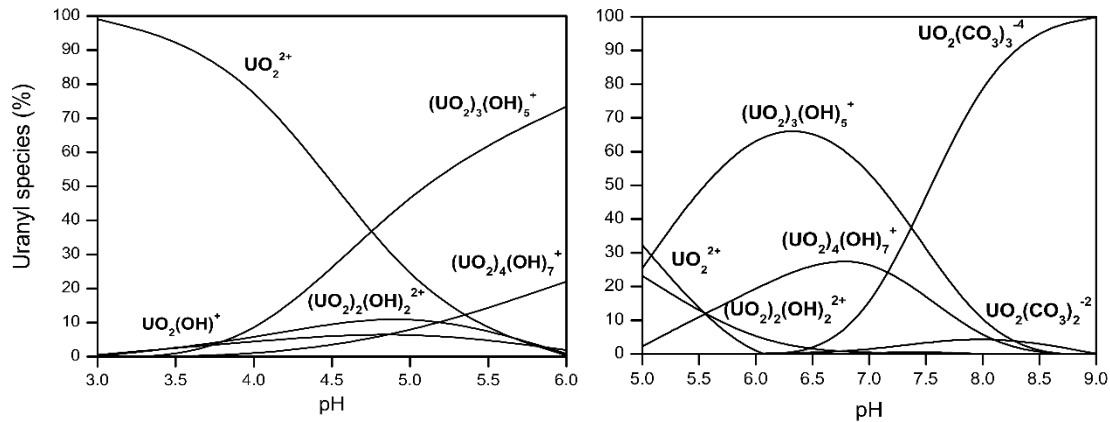


Fig.30 - Distribution of uranyl aqueous species: a) from pH 3 to pH 6, using  $1.00 \times 10^{-4} \text{M}$  ( $\text{UO}_2^{2+}$ ) and  $2.00 \times 10^{-2} \text{M}$  (NaCl) and b) from pH 5 to pH 9, using  $1.00 \times 10^{-4} \text{M}$  ( $\text{UO}_2^{2+}$ ) and  $2.00 \times 10^{-1} \text{M}$  (NaCl), considering the atmospheric  $\text{CO}_2$  effect ( $P=39 \text{ Pa}$ ).

The major specie up to pH 4.5 is  $\text{UO}_2^{2+}$ , whereas the polynuclear species are dominant at  $\text{pH} > 4.7$  and at near neutral pH. In the presence of  $\text{CO}_2$  (g), uranyl carbonate species start to be formed from near neutral pH, becoming the predominant species in alkaline conditions (Fig.30). The negative charge of uranyl carbonate complexes will compromise the adsorption on the partially ionized edge sites (Greathouse and Cygan, 2006; Pabalan and Turner, 1996). Under the imposed experimental conditions, the  $\text{UO}_2^{2+}$  is under-saturated in solution and precipitation did not occur.

#### 4.6.4.3. Continuous stirred flow-through experiments

Continuous stirred flow-through experiment was performed in order to investigate the kinetics of the  $\text{UO}_2^{2+}$  adsorption and desorption processes using different heterogeneous smectite samples, where the attention was focused on the  $\text{UO}_2^{2+}$  irreversibility. The experimental conditions imposed were: pH 4 and low ionic strength ( $[\text{NaCl}] = 1 \times 10^{-4}$ ) and pH 6 and high ionic strength ( $[\text{NaCl}] = 0.2$ ).

The S-shaped of BTCs represents a typical plot of the ratio of outlet to inlet solute concentration in the fluid as a function of pore volume. The theoretical BTC corresponds to the amount of  $\text{UO}_2^{2+}$  detected in the absence of smectite. Two different BTCs (for each

sample) corresponding to the adsorption - desorption process were obtained (Figs.31 and 32). Both phases are separated by an equilibrium period that started when the maximum adsorption capacity of smectite was reached. The BTCs are shifted down relatively to the theoretical curve (blank curve) indicating retention of  $UO_2^{2+}$  during the adsorption process. The amounts of  $UO_2^{2+}$  adsorbed or desorbed corresponding to the area between the theoretical BTC and each experimental BTC were calculated using Eq. 2, where the retention capacities are shown in Table 12.

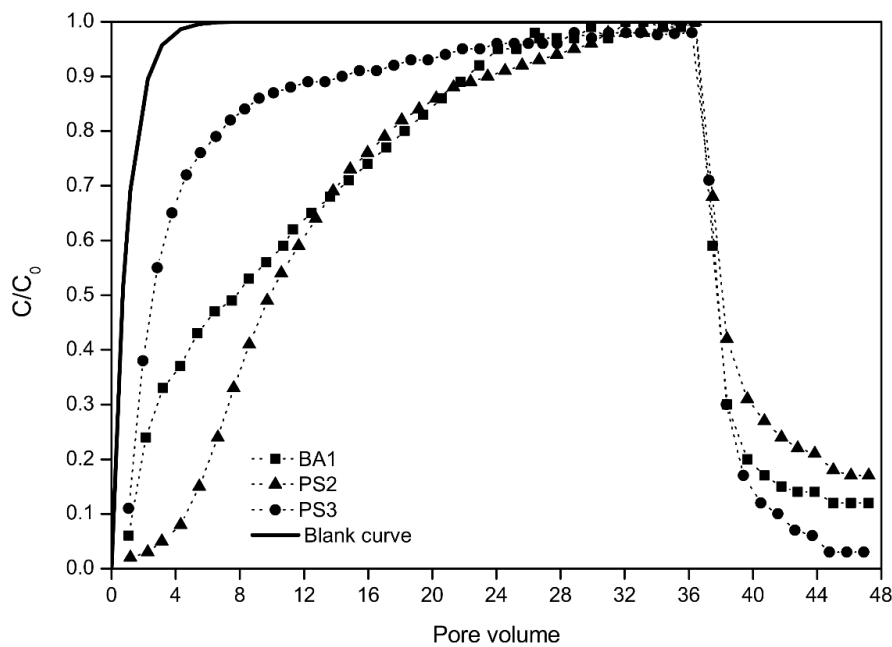


Fig.31 - Breakthrough curves corresponding to the flow-through reactor experiments occurred at pH 4 ( $[U(VI)]=1.0 \times 10^{-4} M$ ). The blank curve corresponds to the theoretical BTC for an inert specie. The pore volume corresponds to the number of reactor volumes that have passed through the reactor.

Table 12. Amounts of  $UO_2^{2+}$  adsorbed and desorbed from smectite samples and respective retention capacities.

Sample	$q_{\text{adsorbed}} \text{ (molKg}^{-1}\text{)}$		$q_{\text{desorbed}} \text{ (molKg}^{-1}\text{)}$		Retention (%)	
	pH 4	pH 6	pH 4	pH 6	pH 4	pH 6
BA1	0.18	0.05	0.02	0.02	87	68
PS2	0.23	0.08	0.04	0.02	85	80
PS3	0.10	0.06	0.02	0.02	82	71

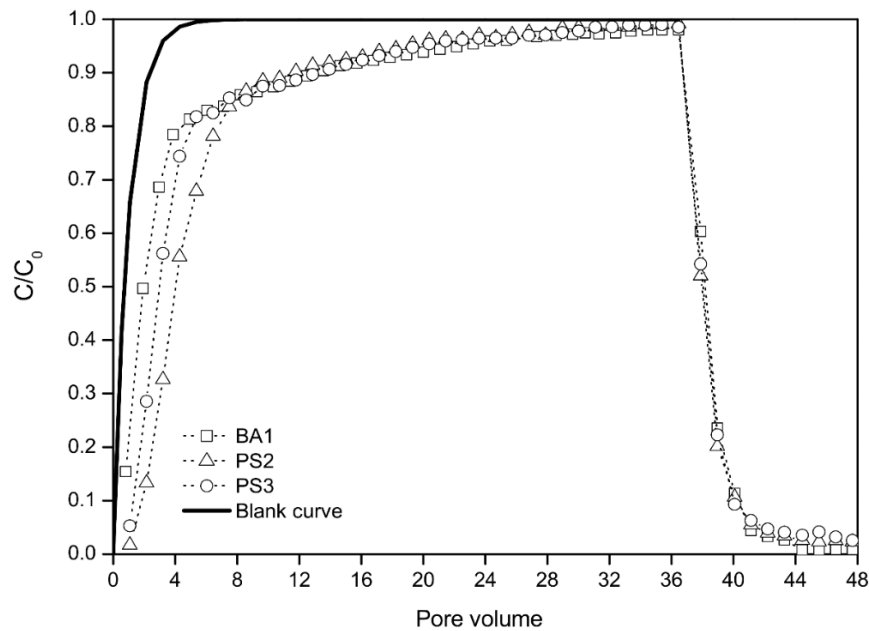


Fig.32 - Breakthrough curves corresponding to the flow-through reactor experiments occurred at pH 6 ( $[U(VI)]=1.00 \times 10^{-4} M$ ). The blank curve corresponds to the theoretical BTC for an inert specie. The pore volume corresponds to the number of reactor volumes that have passed through the reactor.

#### 4.6.4.3.1. Adsorption experiments

The kinetic sorption data obtained at pH 4 reveal a significant difference of the adsorbed amount by each smectite sample during the adsorption process, which affected directly the behavior of the BTCs. Different performances of smectite samples were observed until 5 pore volumes (300 min), where the  $UO_2^{2+}$  removal effectiveness was always above 90% for sample PS2 and from 91% to 62% for sample BA1 and 85% to 31% for sample PS3, respectively. The BTCs corresponding to samples BA1 and PS2 are identical from 12 pore volumes, where 40% of the  $UO_2^{2+}$  present in the input solution was adsorbed by both samples. By contrast, the sharpest BTC that describes the adsorption of sample PS2 reveals the lower effectiveness for  $UO_2^{2+}$  uptake, as compared with sample BA1 and PS3. The equilibrium was reached after 32 hours of adsorption for all smectite samples, where the amount of  $UO_2^{2+}$  adsorbed was calculated for each sample (Table 12). Higher adsorption capacity was found for PS2 at pH 4 (0.23 mol/kg), which adsorbed more 34%

and 138% than the amounts adsorbed by samples BA1 (0.18 mol/kg) and PS3 (0.10 mol/kg), respectively.

The amounts of  $\text{UO}_2^{2+}$  adsorbed correspond to 38% (BA1), 45% (PS2) and 24% (PS3) of the total CEC for each sample. The lower ratio obtained for PS3 suggests that the ion-exchange process is not only dependent of the adsorption capacity of smectite and, structural properties or chemical and physical mechanisms occurring during the uptake should be considered to explain the restricted adsorption. Sample PS3 consists of an interstratified structure (I/S) with about 30% of illite layers. The exchange and surface properties are affected by structural micro-organization, which is characterized by a high relative amount of external surface area as compared to internal surface area (intra-particle) (Huang et al., 2011; Robert et al., 1991). The higher external surface of sample PS3, when compared to BA1 and PS2, is confirmed by smectite BET surface areas (Table 11). In this case, the increase of the external to internal (interlayer) surface ratio may have enhanced the interaction between  $\text{UO}_2^{2+}$  and the edge sites, reducing the amount adsorbed.

The BTCs obtained at pH 6 show a quicker adsorption until 6 pore volumes ( $\approx 360$  min) for the three different smectite samples, where about 85% of the total amount of  $\text{UO}_2^{2+}$  adsorbed were uptaken until this point. The results reveal a significant decrease in the number of sites available for adsorption, which was expected taking into account the alteration of the adsorption mechanism from pH 4 to pH 6. The fast interaction observed was also expectable because the adsorption has mainly occurred in the external sites of smectite, where the edge groups are much more accessible for the interaction with the  $\text{UO}_2^{2+}$  polynuclear species. In this case, the equilibrium was reached after 25 hours of adsorption and the amounts adsorbed were calculated (Table 12).

Sample PS2 has also the highest adsorption capacity at pH 6, adsorbing 0.08 mol/kg, which means more 51% of the amount adsorbed by BA1 ( $0.05 \text{ mol kg}^{-1}$ ) and more 26% than PS3 (0.06 mol/kg). Assuming that the adsorption on the edge sites was the main adsorption mechanism at near neutral pH and high ionic strength ( $I=0.2$ ), two main factors may be responsible for the adsorption capacity:

(1) The reactivity of the surface groups is influenced by the degree of isomorphous substitutions. Thus, the octahedral substitution of  $\text{Al}^{3+}$  for  $\text{Fe}^{3+}$  increases the reactivity of the edge sites, whereas the  $\text{Al}^{3+}$  for  $\text{Mg}^{2+}$  has the opposite tendency (Avena et al., 2003; Bourg et al., 2007). No significant differences were found regarding to  $\text{Mg}^{2+}$  proportions in smectite samples. By contrast, higher proportion of  $\text{Fe}^{3+}$  (28%) in the octahedral sheet of sample PS3

was measured, comparing to samples BA1 and PS2 (18% of  $\text{Fe}^{3+}$ ), enhancing the  $\text{UO}_2^{2+}$  uptake.

(2) The increase of the attraction between the metal lattice and the surface oxygens enhances the ionization of the hydroxyl groups (Froideval et al., 2003). The charge density depends to the external surface area of smectite and influences the number of ionized hydroxyl groups due to repulsions between electrostatic charges (Papirer, 2000). The charge densities of our samples (BA1, PS2 and PS3) correspond to 4.82, 2.41 and 0.59 (sites/nm<sup>2</sup>). The higher charge density of sample BA1 suggests an increase of electrostatic repulsions, decreasing the surface groups stability, which infers on its ability to ionization and adsorption and explains the lower amount of  $\text{UO}_2^{2+}$  adsorbed as compared with samples PS2 and PS3.

The edge surface sites correspond to 10-20% of the total number of sites available for sorption (Anderson and Sposito, 1991; Bergaya and Lagaly, 2013), where the amounts of  $\text{UO}_2^{2+}$  adsorbed in these conditions correspond to 98-44% (BA1), 137%-61% (PS2) and 139-62% (PS3) of the edge sites capacity of smectite. In this case, the direct interaction adsorbent-adsorbate is controlled by inner-sphere and outer-sphere complexation, where inner-sphere complexation dominates when negative charge is situated directly at the surface. The excess of  $\text{UO}_2^{2+}$  adsorbed, mainly on PS2 and PS3, was attributed to diffuse-ion swarm adsorption that is characterized by ions free diffusion into and out of the interfacial region. Outer-sphere complexation and diffusion-ion swarm results from weak electrostatic interactions and it is presumable that part of the  $\text{UO}_2^{2+}$  adsorbed will be desorbed.

#### 4.6.4.3.2. Desorption experiments

The sorption irreversibility was evaluated by means of desorption experiments occurred during 10 h. The BTCs corresponding to the desorption process at pH 4 and pH 6 are shown in Figs.31 and 32. In acidic conditions, the desorption process was clearly incomplete after 10 hours for samples BA1 and PS2. The desorbed amount of  $\text{UO}_2^{2+}$  increased as increasing of  $\text{UO}_2^{2+}$  previously up-taken by ion-exchange at pH 4, which demonstrates an identical behavior between adsorption and desorption processes of BA1 and PS2, suggesting that the complete reversibility of adsorption process may occur. As previously described, the ion-exchange mechanism is characterized by weaker surface complexes (outer-sphere complexes) between  $\text{UO}_2^{2+}$  and smectite where a total reversibility

of adsorption is expected (Chorover and Brusseau, 2008). In this case, the higher proportion of tetrahedral charge of samples BA1 and PS2, does not seem to provide additional  $\text{UO}_2^{2+}$  retention.

After 10 h of desorption process, the amounts of  $\text{UO}_2^{2+}$  desorbed correspond to 0.04 mol/kg for PS2 and 0.02 mol/kg for BA1 and PS3 (Table 12). However, at this point, only 3% of the initial concentration  $\text{UO}_2^{2+}$  ( $C/C_0$ ) are being desorbed from PS3, and desorption process may be considered as concluded. The behavior of adsorption and desorption processes of sample PS3 clearly indicates that ion-exchange was not the only adsorption mechanism occurring. Moreover, a high retention capacity was obtained, 82 %, for sample PS3, indicating the irreversibility of the  $\text{UO}_2^{2+}$  previously adsorbed. This confirms the presence of stronger complexes probably formed on the edge sites of smectite. In this way, the assumption that the increase of the external to internal (interlayer) surface ratio enhanced the interaction between  $\text{UO}_2^{2+}$  and the edge sites of sample PS3 is reinforced.

The results obtained from desorption experiments at pH 6 and high ionic strength (0.2) suggest that ion-diffusion swarm and inner-sphere and outer-sphere complexation processes occurred on the external surface during the adsorption mechanism, which confirms that the extension of the  $\text{UO}_2^{2+}$  reversibility is highly influenced by the mechanism involved on the uptake process.

Desorption was concluded after 10 hours and the results indicate that more than 68% of  $\text{UO}_2^{2+}$  was fixed in all smectite samples at pH 6. In these conditions, the amount desorbed for all smectite samples was identical (i.e., 0.02 mol/kg), which indicates that there is no relationship between the amounts adsorbed and desorbed, as noted in the experiments occurred at pH 4. Assuming that the  $\text{UO}_2^{2+}$  was retained on the edge sites of smectite, its occupancy corresponds to 7.39%, 12.18 and 11.06% of their CEC capacities. The higher occupancy of the external sites as compared with similar experiments assigned in batch reactors (Guimarães et al., 2015b-submitted), revealed the importance of the continuous contact between the renewal contaminant solution and the adsorbent. According to the Eigen-Wilkins-Werner mechanism (Chorover and Brusseau, 2008), the conversion from outer-sphere to inner-sphere complexation occurs during the adsorption on the amphoteric sites of smectite. In this particular case, this process has been potentiated by the continuous solution flow, explaining the additional capacity to fix  $\text{UO}_2^{2+}$  (Brantley et al., 2007).

Comparing the experimental desorption curves and the predicted desorption curves (Fig.33), calculated assuming the total reversibility of the  $\text{UO}_2^{2+}$  previously adsorbed and

identical rates for the adsorption and desorption processes, it is possible to confirm an effective  $\text{UO}_2^{2+}$  retardation at pH 6 and high ionic strength, due to surface complexation.

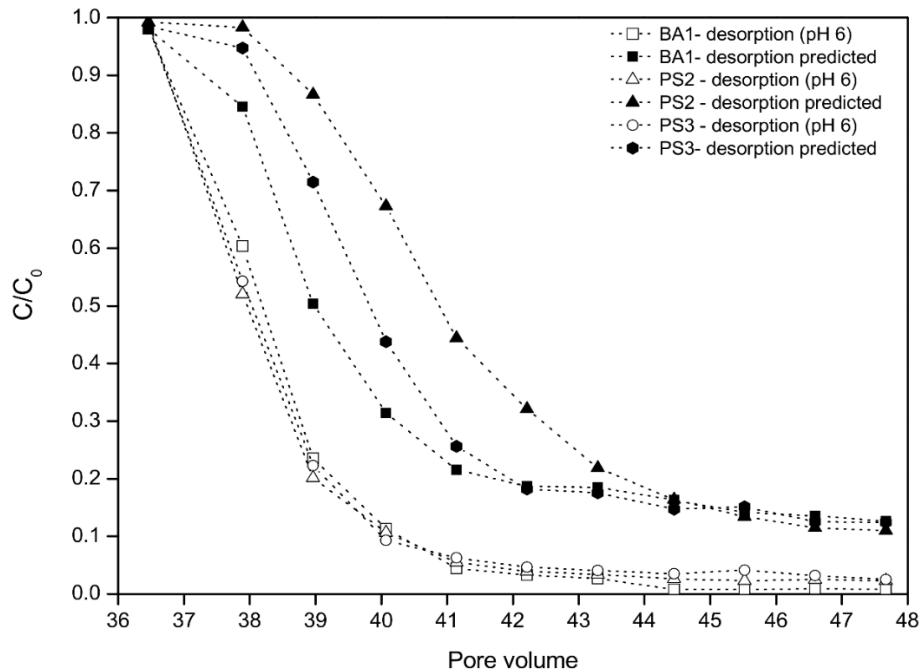


Fig.33 - Comparison between experimental desorption curves (pH6 – high I) and predicted desorption curves calculated assuming the total reversibility of the uranyl previously adsorbed and identical rates for de adsorption and desorption processes.

#### 4.6.4.4. Kinetics of Sorption-Desorption

The adsorption kinetics data were tested by pseudo-first order and pseudo-second order models and additionally, by diffusion controlled model for the experimental data obtained at pH 4 and low ionic strength. The diffusion effect was ignored at pH 6 and high ionic strength, because the main adsorption mechanism occurred in the accessible external sites of smectite where inner-sphere complexation prevailed. The experiments performed at pH 4 and low ionic strength reveal the most significant differences between the three sorbents (samples BA1, PS2 and PS3), suggesting different type of sites involved with different capacities and affinities to  $\text{UO}_2^{2+}$  sorption that affected the kinetic of adsorption.

Pseudo-first order and pseudo-second order models were obtained by non-linear regression (Eqs. 3 and 4), in order to avoid the distortion of model parameters (Table 13) when the non-linear equations are transformed into linear forms. The experimental data

were fitted to both models (Figs.34, 35 and 36). The pseudo-first order model provided the best fit of the kinetic adsorption data obtained at pH 4 for samples BA1 and PS2. The adsorption rate was higher for PS2 ( $K_1=2.02 \times 10^{-3}/\text{min}$ ) as compared with BA1 ( $K_1=1.76 \times 10^{-3}/\text{min}$ ), reflecting different surface properties of both smectite and the lower amount adsorbed by sample BA1. The limited expansibility of sample BA1, due to the higher proportion of tetrahedral substitutions, has probably reduced the rate of the hydrated  $\text{UO}_2^{2+}$  diffusion into the micro-porous interlayer of smectite particles (Brantley et al., 2007).

Considering the transport restrictions occurred during the uptake process, the kinetic of adsorption was additionally described by diffusion-controlled model. The liquid-film diffusion model revealed an unsatisfactory fit of the experimental data for both samples ( $R^2 < 0.97$ ). This suggests that the adsorption kinetic was not affected by film-diffusion and the mass transfer (diffusion) of the contaminant from the bulk fluid to the external surface of smectite was effectively eliminated by the continuous flow-through stirred system.

Table 13. Kinetic parameters obtained from the fit to the flow-through sorption data using different kinetic models.

Model	Parameter	Sample					
		BA1		PS2		PS3	
		pH 4	pH 6	pH 4	pH 6	pH 4	pH 6
Pseudo-first order	$q_e$ (mol/Kg)	0.244	0.121	0.304	0.151	0.11	0.131
	$K_1$ ( $\text{min}^{-1}$ )	$1.46 \times 10^{-3}$	$1.44 \times 10^{-3}$	$1.65 \times 10^{-3}$	$2.37 \times 10^{-3}$	$1.93 \times 10^{-3}$	$1.97 \times 10^{-3}$
	$R^2$	0.987	0.996	0.988	0.985	0.995	0.988
Pseudo -second order	$q_e$ (mol/Kg)	0.333	0.162	0.406	0.184	0.141	0.164
	$K_2$ ( $\text{kg}/\text{mol} \cdot \text{min}$ )	$3.69 \times 10^{-3}$	$7.89 \times 10^{-3}$	$3.57 \times 10^{-3}$	$1.40 \times 10^{-2}$	$1.33 \times 10^{-2}$	$1.22 \times 10^{-2}$
	$R^2$	0.975	0.999	0.974	0.990	0.998	0.996
Intra-particle diffusion	$K_i$ ( $\text{mol}/\text{kg} \cdot \text{min}^{1/2}$ )	$8.30 \times 10^{-3}$	$3.20 \times 10^{-3}$	$1.15 \times 10^{-2}$	$7.60 \times 10^{-3}$	$4.30 \times 10^{-3}$	$6.10 \times 10^{-3}$
	$R^2$	0.997	0.996	0.995	0.993	0.997	0.996
Film diffusion	$K_{fd}$	$1.35 \times 10^{-2}$	$1.80 \times 10^{-2}$	$1.45 \times 10^{-2}$	$1.37 \times 10^{-2}$	$1.34 \times 10^{-2}$	$1.26 \times 10^{-2}$
	$R^2$	0.956	0.916	0.9713	0.953	0.951	0.941

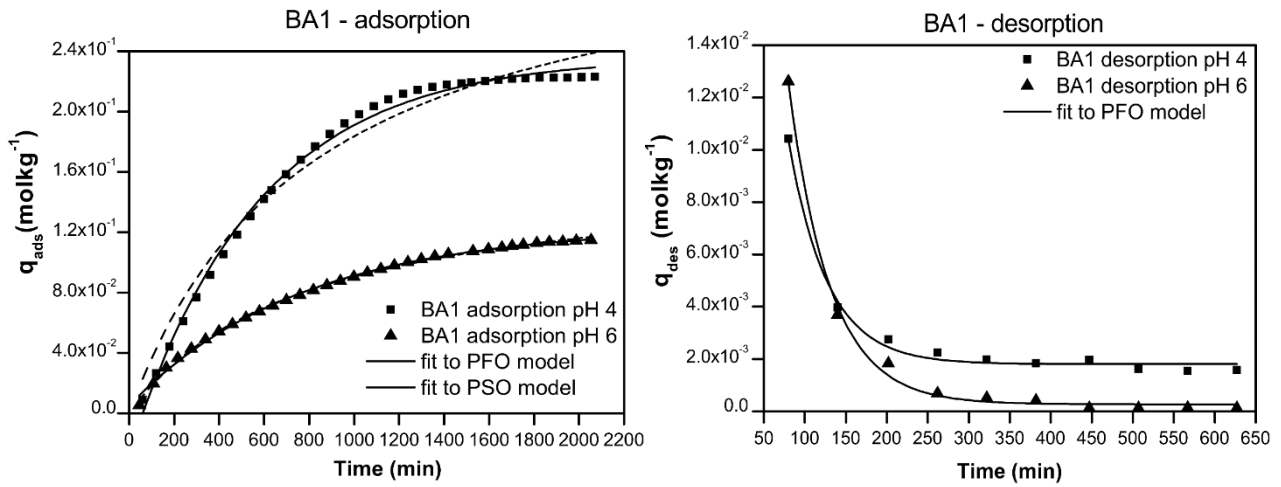


Fig.34 - Kinetics of adsorption and desorption processes of sample BA1 at pH 4 and 6: fit to PFO and PSO models.

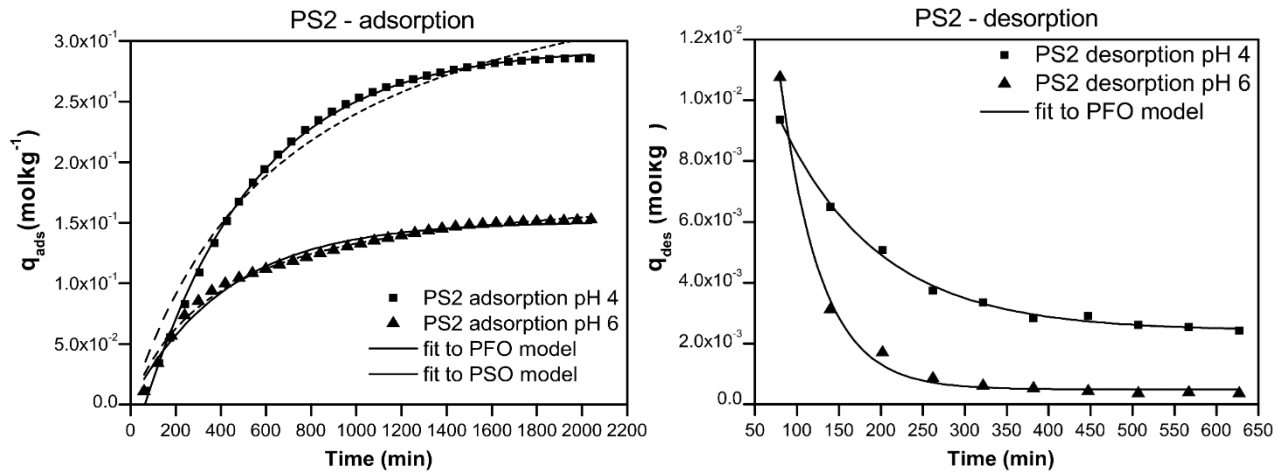


Fig.35 - Kinetics of adsorption and desorption processes of sample PS2 at pH 4 and 6: fit to PFO and PSO models.

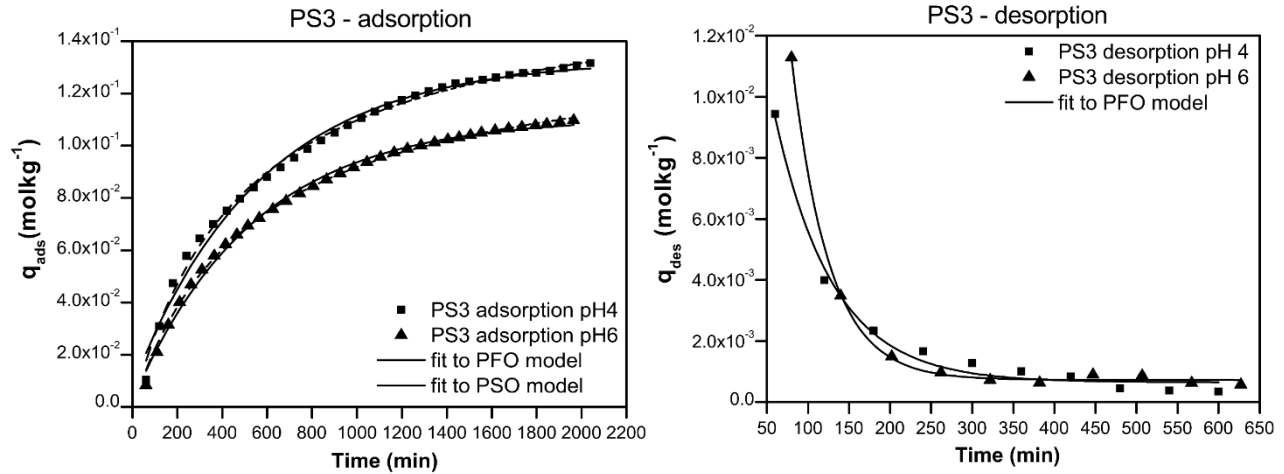


Fig.36 - Kinetics of adsorption and desorption processes of sample PS3 at pH 4 and 6: fit to PFO and PSO models.

The intra-particle diffusion model shows a good fit to the experimental data until 800 min (Fig.37), where the diffusion effect was probably more pronounced. The lower diffusion rate was obtained for sample BA1 ( $K_i=8.28 \times 10^{-3} \text{ mol/Kgmin}^{0.5}$ ), comparing with sample PS2 ( $K_i=1.15 \times 10^{-2} \text{ mol/Kg} \cdot \text{min}^{1/2}$ ), which is in agreement with our previous conclusions.

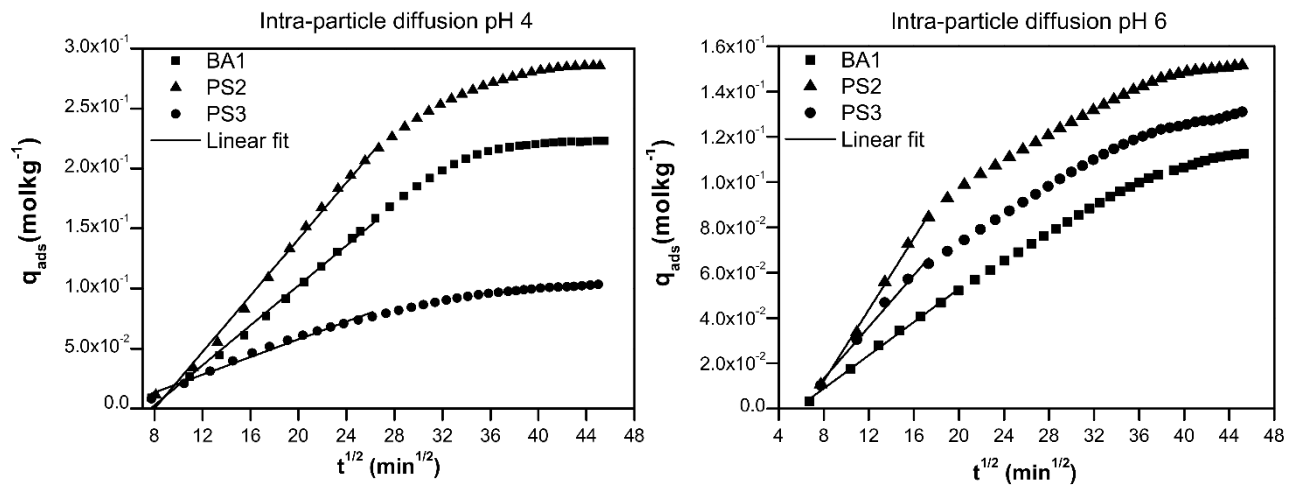


Fig.37 - Kinetics of adsorption at pH 4 and pH 6: fit to intra-particle diffusion model.

The results of desorption kinetic data at pH 4 are shown in Figs.34, 35 and 36. Desorption curves traduce the  $UO_2^{2+}$  desorbed amounts as a function of time, described satisfactorily by the pseudo-first order model (Table 14). The desorption processes associated with samples BA1 and PS2 were incomplete and revealed the same behavior: a faster desorption kinetic process until 200 min for sample BA1 ( $K_1=2.12 \times 10^{-2}/\text{min}^{-1}$ ) and until 260 min for sample PS2 ( $K_1=8.48 \times 10^{-3}/\text{min}$ ). A significant amount of  $UO_2^{2+}$  was desorbed from the lower affinity sites, followed by a much slower process (Table 14), which may be extended for several days until the  $UO_2^{2+}$  will be released.

The results also show that the amount of  $UO_2^{2+}$  previously adsorbed affects the kinetics of desorption. The desorption rate is slower as greater is the amount previously adsorbed. However, the reversible sorption concept assumes identical adsorption and desorption rates, which is not observed in this case for samples BA1 and PS2. In acid conditions, a total reversibility of the adsorption is expected as the mechanism of outer-sphere complexation prevailed during the ion-exchange process. The higher desorption rates obtained have resulted from the fact that desorption has been forced by a  $Na^+$ -solution with a concentration ten times higher (1mM) than the concentration of  $UO_2^{2+}$  used in the adsorption experiments (0.1 mM).

Table 14. Kinetic parameters obtained from the fit to the flow-through desorption data using the pseudo-first order model.

Model	Range	Parameter	Sample					
			BA1		PS2		PS3	
			pH 4	pH 6	pH 4	pH 6	pH 4	pH 6
Pseudo-first order	All range	$q_e$ (mol/Kg)	0.0018	0.0003	0.0024	0.0005	0.0006	0.0007
		$K_1$ ( $\text{min}^{-1}$ )	$2.12 \times 10^{-2}$	$1.98 \times 10^{-2}$	$8.48 \times 10^{-3}$	$2.10 \times 10^{-2}$	$1.41 \times 10^{-2}$	$2.22 \times 10^{-2}$
		$R^2$	0.992	0.996	0.997	0.995	0.988	0.999
	From 200 min	$q_e$ (mol/Kg)	0.0015	0.0003	0.0023	0.0004	0.000001	0.0007
		$K_1$ ( $\text{min}^{-1}$ )	$7.22 \times 10^{-3}$	$1.01 \times 10^{-2}$	$6.26 \times 10^{-3}$	$1.57 \times 10^{-2}$	$4.86 \times 10^{-3}$	$2.07 \times 10^{-2}$
		$R^2$	0.992	0.996	0.997	0.995	0.988	0.999

The results obtained for sample PS3, concerning the adsorption and desorption processes at pH 4 (Fig.36), indicate the existence of two distinct adsorption mechanism: ion exchange on the surface sites ( $\equiv X^-$ ) and surface complexation on edge sites ( $\equiv SOH$ ), which

contributed to the lower amount of  $\text{UO}_2^{2+}$  adsorbed and, to the greater retention capacities obtained. This confirms the differences of the kinetic of adsorption and desorption processes between sample PS3 and samples BA1 and PS2. A faster adsorption until 9 pore volumes ( $\approx 500$  min) corresponding to sample PS3 is followed by a very slow process that precedes the equilibrium point. The first step is characterized by a faster  $\text{UO}_2^{2+}$  diffusion ( $K_i=4\times 10^{-3}$  mol/Kg $\cdot$ min $^{0.5}$ ) followed by a slower diffusion step ( $K_i=2\times 10^{-3}$  mol/Kg $\cdot$ min $^{1/2}$ ). Both diffusion rates are lower than those obtained for samples BA1 and PS2, suggesting that the ion-exchange process was indeed hampered. Additionally, the kinetic sorption data was also perfectly fitted to pseudo-second order model, indicating a clear change of the kinetic mechanism.

This behavior was also found for the adsorption kinetic results obtained at pH 6 for smectite samples, where the best fit obtained correspond to the pseudo-second order model. The adsorption kinetic obtained at pH 6 reinforces the assumption that the  $\text{UO}_2^{2+}$  polynuclear species were mainly adsorbed by inner-sphere complexation on the edge sites of smectite. This also confirms the preference of smectite for adsorption on the external surface of sample PS3.

The kinetic model fit to the sorption data obtained at pH 6 is shown in Figs.34, 35 and 36. According to the model parameters (Table 13), the adsorption rates of samples PS2 and PS3 are very close, whereas the rate of adsorption of sample BA1 is about half comparing with samples PS2 and PS3. It was previously reported that the higher charge density, associated with electrostatic repulsions caused by the proximity of the surface hydroxyl groups of BA1, has probably influenced their lower adsorption capacity. The slower adsorption observed in this conditions confirmed the lower ability for sorption of smectite BA1.

Comparing desorption curves for all samples at pH 6, substantial desorption of the  $\text{UO}_2^{2+}$  weakly adsorbed was confirmed after 200 min. From this point, smectite revealed a great capacity to retain the  $\text{UO}_2^{2+}$  previously adsorbed, which resulted in a retention capacity higher than 68% for all smectite samples. The pseudo-first order model shows the best fit to desorption kinetic data (Figs.34, 35 and 36). Desorption rates obtained are similar for all the samples (Table 13), which suggests that the kinetic of desorption process is independent of the kinetic of adsorption where significant differences were observed.

Sample PS3 revealed the most identical behavior between desorption processes occurred at pH 4 and pH 6 (Fig.36). The kinetic of desorption was slower at pH 4 ( $K_{\text{des}}=1.40\times 10^{-2}/\text{min}$ ), which is in agreement with the assumption that a fraction of  $\text{UO}_2^{2+}$  was

adsorbed by ion-exchange in the interlayer space, in contrast with the dominant mechanism of adsorption occurred at pH 6, where the inner-sphere complexation on the edge sites of smectite was dominant.

Comparing the desorption processes in both pH conditions of samples BA1 and PS2, a more significant difference was found for sample PS2, considering their higher adsorption capacity at pH 4, when compared to the other samples, and their lower desorption rate (Fig.36).

#### 4.6.4.5. X-ray photoelectron spectroscopy

XPS analysis were carried out in order to obtain chemical information about the  $\text{UO}_2^{2+}$  surface complexes resulted from the interaction between the  $\text{UO}_2^{2+}$  ions and the internal and external surface of smectite (Fig.38). The relative atomic abundances in the samples were calculated from the area intensities of spectra, divided by the relative atomic sensitivity factors for the electron emission lines. The surface compositions of the three different smectite samples studied are resumed in Table 15.

It was previously demonstrated that  $\text{UO}_2^{2+}$  interact with different sites of smectite, depending on the pH and ionic strength conditions. At pH 4 and low ionic strength, we assume that  $\text{UO}_2^{2+}$  is adsorbed under different binding strengths through cation exchange and inner-sphere complexation on the edge sites of smectite. Our previous results, regarding to the  $\text{UO}_2^{2+}$  adsorption on smectite in similar conditions, but using a batch reactor (Guimarães et al., 2016), revealed that two binding energies at  $380.8 \pm 0.3$  eV and  $382.3 \pm 0.3$  eV (Fig.38) were obtained after the deconvolution of  $\text{U}4f_{7/2}$  peak. These two components are influenced by the sorption mechanism on smectite, where the  $\text{UO}_2^{2+}$  attraction will depend on the distance between the permanent negative charge and the  $\text{UO}_2^{2+}$ . In this way, the lower binding energy was assigned to the stronger attraction between  $\text{UO}_2^{2+}$  and smectite (inner-sphere complexation on the edge sites), whereas the other component corresponds to the weaker surface interaction (ion-exchange)\_which implies a lower electron density around U(VI) center that hampered the electron removal (Del Nero et al., 2004; Ilton and Bagus, 2011).

The smectite samples submitted to desorption experiments were also analyzed by XPS. The binding energies obtained at pH 4 and low ionic strength before and after desorption process are shown in Table 16. The results indicate identical binding energies

before and after desorption but clearly reveal a decrease in the proportion of component at  $382.4 \pm 0.3$  eV, suggesting that the  $\text{UO}_2^{2+}$  surface complexes more weakly adsorbed were also desorbed first, contributing to increase the proportion of the lower binding energy component.

The interaction between aluminol and silanol sites and  $\text{UO}_2^{2+}$  polynuclear species occurred at pH 6 and high ionic strength was also previously suggested (Guimarães et al., 2016), where two different components at  $\approx 380.3 \pm 0.3$  eV and  $\approx 381.8 \pm 0.3$  eV assigned to the adsorption of  $[\text{UO}_2(\text{H}_2\text{O})_5]^{2+}$  on aluminol and silanol sites were identified—after the deconvolution of the  $\text{U}4f_{7/2}$  peak. The data obtained are in agreement with the previous results obtained by Del Nero et al. (2004), Froideval et al. (2003), Drot et al. (2007) and Kowal-Fouchard et al. (2004). It was not identified any modification of the binding energies before and after desorption process at pH 6 (Table 16). The proportion of both components were not affected, indicating that  $\text{UO}_2^{2+}$  was retained on the external sites of smectite after desorption process.

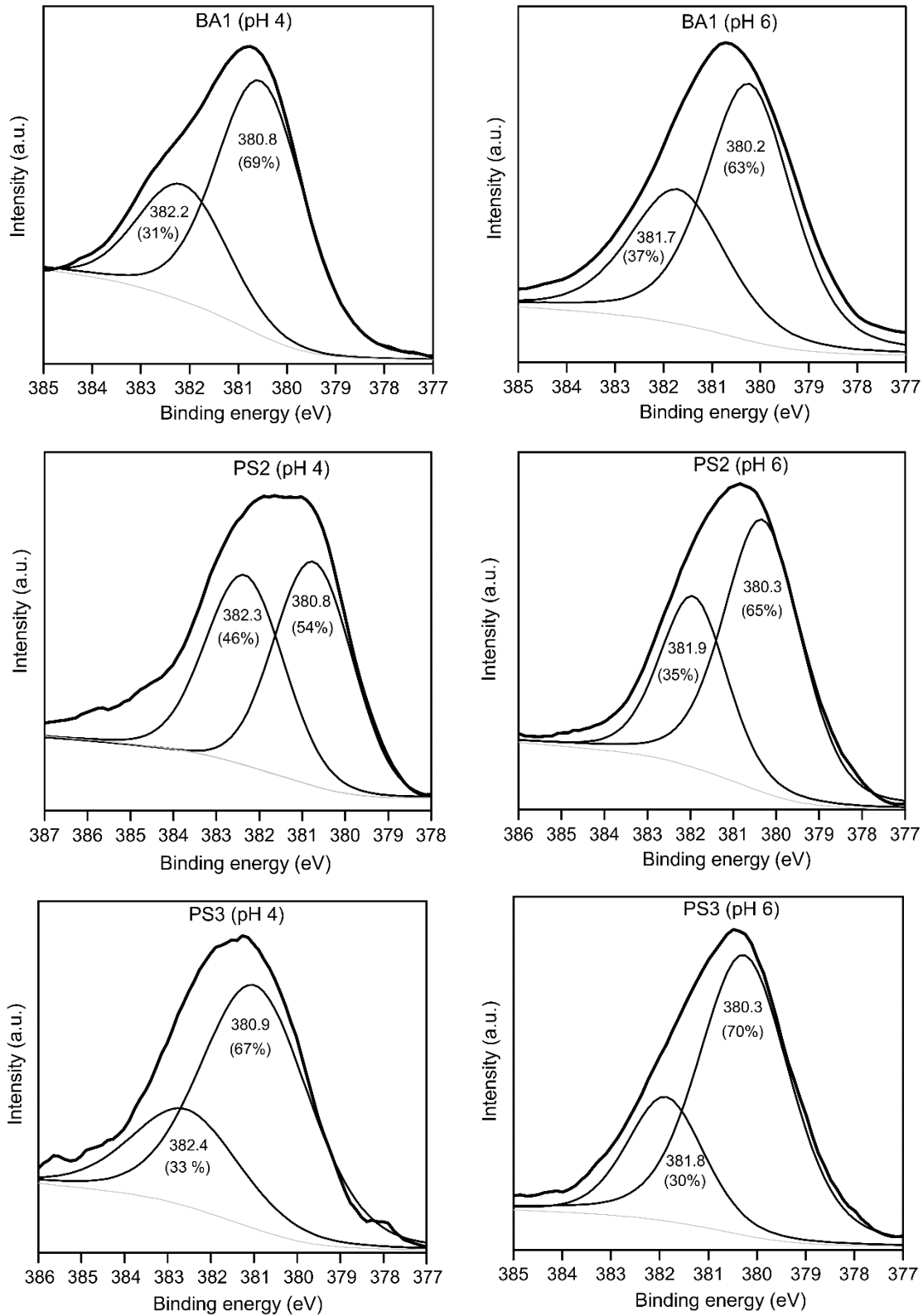


Fig.38 -  $U_{4f_{7/2}}$  XPS spectra of the U(VI)-smectite samples (BA1, PS2 and PS3), obtained from the flow-through reactor experiments at pH 4 (low I) and pH 6 (High I). Curve fit showing a contribution of two components for  $UO_2^{2+}$  ions.

Table 15. The element composition in atomic concentration (%) and the Si/U and Al/U atomic ratios of the studied samples after  $\text{UO}_2^{2+}$  sorption in flow-through conditions.

pH	Samples	Atomic concentration (%)						
		Si	O	Al	C	U	Si/U	Al/U
4	BA1	19.25	54.61	6.01	19.50	0.31	62	19
	PS2	19.08	55.69	7.62	17.13	0.28	68	27
	PS3	20.52	61.32	7.91	9.59	0.17	121	47
6	BA1	20.37	59.27	6.39	9.20	0.07	291	91
	PS2	19.06	61.70	7.92	7.85	0.10	190	79
	PS3	19.18	60.01	7.45	8.97	0.08	239	93

Table 16. Binding energies and relative proportions of the two components fitted to U4f Spectra, obtained from U(VI)-smectite samples.

Experiment	Smectite	BE (eV) and Relative proportions (%) – after desorption process			
		pH 4 (I=0.02M)		pH6 (I=0.2M)	
		Compnt. I	Compnt. II	Compnt. I	Compnt. II
Adsorption	BA1	382.3 (57%)	380.8 (43%)	381.9 (33%)	380.3 (67%)
	PS2	382.4 (77%)	380.8 (23%)	381.9 (27%)	380.3 (73%)
	PS3	382.3 (71%)	380.8 (29%)	381.7 (30%)	380.3 (70%)
Desorption	BA1	382.4 (34%)	380.8 (66%)	381.7 (36%)	380.3 (64%)
	PS2	382.3 (47%)	380.8 (53%)	381.7 (34%)	380.3 (66%)
	PS3	382.4 (37%)	380.8 (63%)	381.8 (35%)	380.3 (65%)

#### 4.6.5. Conclusion

The  $\text{UO}_2^{2+}$  adsorption and desorption experiments at pH 4 (low I) and pH 6 (high I) using a flow-through reactor were carried out in order to investigate the reversibility of the  $\text{UO}_2^{2+}$  on smectite and the kinetics of sorption processes when both ion-exchange and inner-sphere complexation mechanisms did occurred. The  $\text{UO}_2^{2+}$  sorption capacity is dependent on the pH conditions and the type of surface complexation of smectite. The ion-exchange (outer-sphere complexation) was the dominant mechanism at pH 4, where sample PS2 revealed the higher adsorption capacity, adsorbing more 34% and 138% of  $\text{UO}_2^{2+}$  than samples BA1 and PS3, respectively. The desorption experiments occurred at pH 4 were not

completed for samples BA1 and PS2 after 10 hours. However, the results obtained show higher reversibility in acidic conditions for both samples, suggesting that the  $\text{UO}_2^{2+}$  previously adsorbed may be completely desorbed. A different behavior was observed for sample PS3, which retained about 82% of the amount of  $\text{UO}_2^{2+}$  previously adsorbed. The results obtained demonstrated a great influence of the structural changes in the adsorption and reversibility of  $\text{UO}_2^{2+}$  on smectite.

The experiments conducted at pH 6 demonstrated a significant decrease of the  $\text{UO}_2^{2+}$  amount desorbed from the three smectite samples, indicating that the surface complexation process was changed. This confirmed that inner-sphere complexation on the edge sites of smectite is the dominant mechanism at near neutral pH and high ionic strength. Therefore, the number of sites available for sorption decreased, resulting into the lower amount adsorbed on all smectite samples. This is reinforced by the higher  $\text{UO}_2^{2+}$  retention capacities obtained in the end of desorption processes at pH 6, which revealed lower reversibility of the  $\text{UO}_2^{2+}$  previously adsorbed and stronger complexation.

The kinetic interpretation revealed that the  $\text{UO}_2^{2+}$  sorption on smectite is governed by the multiple sites with different kinetics. Pseudo-first order model provided the best fit to the experimental data obtained for samples BA1 and PS2 corresponding to the  $\text{UO}_2^{2+}$  adsorption at pH 4 and lower ionic strength, whereas pseudo-second order model fitted better the experimental results obtain during the adsorption at pH 6 and higher ionic strength, and the experimental data obtained for sample PS3 at pH 4. Distinct adsorption and desorption kinetics behavior of sample PS3 reinforces the assumption that the type of surface complexation involved and the different structural properties of smectite affected significantly the  $\text{UO}_2^{2+}$  irreversibility and the kinetics of sorption processes.

The XPS results confirm different sorption mechanism involved at both pH conditions. Before and after the desorption processes, two different binding energies at  $380.8 \pm 0.3$  eV and  $382.4 \pm 0.3$  eV were identified at pH 4. The proportion of the higher binding energy component decreased after desorption process, suggesting that the  $\text{UO}_2^{2+}$  weakly adsorbed was previously desorbed. The results obtained at pH 6 reveal two different binding energies for smectite samples,  $380.3 \pm 0.3$  eV and  $381.8 \pm 0.3$  eV, whose proportions remained unchanged before and after desorption process, indicating the higher retention of  $\text{UO}_2^{2+}$  on smectite surface.

## Acknowledgements

The first author benefited a PhD scholarship (Ref. SFRH/BD/79969/2011) financed by Fundação para a Ciência e Tecnologia (FCT), Portugal. This work was funded by FEDER funds through the Operational Program Competitiveness Factors e COMPETE and by National funds through FCT.

## 4.6.6. References

- Anderson, S.J., Sposito, G., 1991. Cesium-Adsorption Method for Measuring Accessible Structural Surface Charge. *Soil Sci. Soc. Am. J.* 55, 1569-1576.
- Apted, M., Ahn, J., 2010. 1 - Multiple-barrier geological repository design and operation strategies for safe disposal of radioactive materials, in: Ahn, J., Apted, M.J. (Eds.), *Geological Repository Systems for Safe Disposal of Spent Nuclear Fuels and Radioactive Waste*. Woodhead Publishing, 3-28.
- Avena, M.J., Mariscal, M.M., De Pauli, C.P., 2003. Proton binding at clay surfaces in water. *Appl. Clay Sci.* 24, 3-9.
- Bachmaf, S., Merkel, B., 2011. Sorption of uranium(VI) at the clay mineral–water interface. *Environ. Earth Sci.* 63, 925-934.
- Bachmaf, S., Planer-Friedrich, B., Merkel, B., 2008. Uranium sorption and desorption behavior on bentonite, in: Merkel, B., Hasche-Berger, A. (Eds.), *Uranium, Mining and Hydrogeology*. Springer Berlin Heidelberg, 515-524.
- Barshad, I., 1960. X-ray analysis of soil colloids by a modified salted paste method. *Proceedings 7th nat. Conf. Clays* 5, 350-364.
- Bergaya, F., Lagaly, G., 2013. *Handbook of Clay Science*. Elsevier Science.
- Bhattacharyya, K.G., Gupta, S.S., 2008. Influence of acid activation on adsorption of Ni(II) and Cu(II) on kaolinite and montmorillonite: Kinetic and thermodynamic study. *Chem. Eng. J.* 136, 1-13.
- Bourg, I.C., Sposito, G., Bourg, A.C.M., 2007. Modeling the acid–base surface chemistry of montmorillonite. *J. Colloid Interface Sci.* 312, 297-310.
- Brantley, S., Kubicki, J., White, A., 2007. *Kinetics of Water-Rock Interaction*. Springer.
- Campos, B., Aguilar-Carrillo, J., Algarra, M., Gonçalves, M.A., Rodríguez-Castellón, E., Esteves da Silva, J.C.G., Bobos, I., 2013. Adsorption of uranyl ions on kaolinite, montmorillonite, humic acid and composite clay material. *Appl. Clay Sci.* 85, 53-63.
- Chisholm-Brause, C.J., Berg, J.M., Matzner, R.A., Morris, D.E., 2001. Uranium(VI) Sorption Complexes on Montmorillonite as a Function of Solution Chemistry. *J. Colloid Interface Sci.* 233, 38-49.
- Chorover, J., Brusseau, M.L., 2008. Kinetics of Sorption—Desorption, in: Brantley, S.L., Kubicki, J.D., White, A.F. (Eds.), *Kinetics of Water-Rock Interaction*. Springer, New York, pp. 109-149.
- Del Nero, M., Froideval, A., Gaillard, C., Mignot, G., Barillon, R., Munier, I., Ozgümüs, A., 2004. Mechanisms of uranyl sorption. *Geological Society, London, Special Publications* 236, 545-560.
- Dorfner, K., 1991. *Ion Exchangers*. De Gruyter.
- Denbigh, K.G., Turner, J.C.R., 1984. *Chemical Reactor Theory: An Introduction*. Cambridge University Press.

- Drot, R., Roques, J., Simoni, É., 2007. Molecular approach of the uranyl/mineral interfacial phenomena. *Comptes Rendus Chimie* 10, 1078-1091.
- Duro, L., Bruno, J., Grivé, M., Montoya, V., Kienzler, B., Altmaier, M., Buckau, G., 2014. Redox processes in the safety case of deep geological repositories of radioactive wastes. Contribution of the European RECOSEY Collaborative Project. *Appl. Geochem.* 49, 206-217.
- Fernández-Calviño, D., Pérez-Novo, C., Bermúdez-Couso, A., López-Periago, E., Arias-Estévez, M., 2010. Batch and stirred flow reactor experiments on Zn sorption in acid soils: Cu competition. *Geoderma* 159, 417-424.
- Froideval, A., Del Nero, M., Barillon, R., Hommet, J., Mignot, G., 2003. pH dependence of uranyl retention in a quartz/solution system: an XPS study. *J. Colloid Interface Sci.* 266, 221-235.
- Galamboš, M., Roskopfová, O., Kufčáková, J., Rajec, P., 2011. Utilization of Slovak bentonites in deposition of high-level radioactive waste and spent nuclear fuel. *J. Radioanal. Nucl. Chem.* 288(3), 765-777.
- Galamboš, M., Suchánek, P., Roskopfová, O., 2012. Sorption of anthropogenic radionuclides on natural and synthetic inorganic sorbents. *J. Radioanal. Nucl. Chem.* 293(2), 613-633.
- Greathouse, J.A., Cygan, R.T., 2006. Water Structure and Aqueous Uranyl(VI) Adsorption Equilibria onto External Surfaces of Beidellite, Montmorillonite, and Pyrophyllite: Results from Molecular Simulations. *Environmental Science & Technology* 40, 3865-3871.
- Greene-Kelly, R., 1952. Irreversible dehydration in montmorillonite. *Clay Miner. Bulletin* 1, 221-225.
- Grolimund, D., 1998. Mobile colloidal particles in subsurface systems, Swiss Federal Institute of Technology Zürich.
- Grolimund, D., Borkovec, M., Federer, P., Sticher, H., 1995. Measurement of Sorption Isotherms with Flow-Through Reactors. *Environ. Sci. Technol.* 29, 2317-2321.
- Guimarães, V., Azenha, M., Rocha, F., Silva, F., Bobos, I., 2015. Influence of pH, concentration and ionic strength during batch and flow-through continuous stirred reactor experiments of Sr<sup>2+</sup>-adsorption onto montmorillonite. *J. Radioanal. Nucl. Chem.* 303, 2243-2255.
- Guimarães, V., Rocha, F., Bobos, I., 2015a. Reactivity of heterogeneous smectites from Portugal. *Clay miner.* - submitted.
- Guimarães, V., Rodríguez-Castellón, E., Algarra, M., Rocha, F., Bobos, I., 2016. Influence of pH, layer charge location and crystal thickness distribution on U(VI) sorption onto heterogeneous dioctahedral smectite. *Journal of Hazardous Materials* 317, 246-258.
- Harward, M.E., 1967. Properties of Vermiculites and Smectites: Expansion and Collapse. *Clays and Clay Miner.* 15, 179.
- Helferich, F.G., 2004. *Kinetics of Multistep Reactions.* Elsevier Science.
- Hennig, C., Reich, T., Dahn, R., Scheidegger, A.M., 2002. Structure of uranium sorption complexes at montmorillonite edge sites. *Radiochim. Acta* 90, 653-657.
- Ho, Y.S., McKay, G., 1998. A Comparison of Chemisorption Kinetic Models Applied to Pollutant Removal on Various Sorbents. *Process Saf. Environ.* 76, 332-340.
- Huang, P.M., Li, Y., Sumner, M.E., 2011. *Handbook of Soil Sciences: Properties and Processes, Second Edition.* Taylor & Francis.
- Ilton, E.S., Bagus, P.S., 2011. XPS determination of uranium oxidation states. *Surf. Interface Anal.* 43, 1549-1560.
- Inoue, A., Utada, M., Wakita, K., 1992. Clays and Hydrosilicate Gels in Nuclear Fields Smectite-to-illite conversion in natural hydrothermal systems. *Appl. Clay Sci.* 7, 131-145.

- Ismadji, S., Soetaredjo, F.E., Ayucitra, A., 2015. *Clay Materials for Environmental Remediation*. Springer International Publishing.
- Jackson, M.L., 1975. *Soil chemical analysis - Advanced Course*. Madison, Wisconsin, U.S.A., 895.
- Jackson, M.L.R., Barak, P., 2005. *Soil Chemical Analysis: Advanced Course*. Parallel Press, University of Wisconsin-Madison Libraries.
- Kaufhold, S., Dohrmann, R., 2010. Stability of bentonites in salt solutions: II. Potassium chloride solution - Initial step of illitization? *Appl. Clay Sci.* 49, 98-107.
- Korichi, S., Bensmaili, A., 2009. Sorption of uranium (VI) on homoionic sodium smectite experimental study and surface complexation modeling. *J. Hazard. Mater.* 169, 780-793.
- Kowal-Fouchard, A., Drot, R., Simoni, E., Ehrhardt, J.J., 2004. Use of Spectroscopic Techniques for Uranium(VI)/Montmorillonite Interaction Modeling. *Environmental Science & Technology* 38, 1399-1407.
- Lagergren, S., 1898. Zur theorie der sogenannten adsorption gelöster stoffe, *Kungliga Svenska Vetenskapsakademiens. Handlingar* 24, 1-39.
- Lee, J.O., Kang, I.M., Cho, W.J., 2010. Smectite alteration and its influence on the barrier properties of smectite clay for a repository. *Appl. Clay Sci.* 47, 99-104.
- Lujanienė, G., Beneš, P., Štamberg, K., Ščiglo, T., 2012. Kinetics of plutonium and americium sorption to natural clay. *J. Environ. Radioactiv.* 108, 41-49.
- Marques Fernandes, M., Baeyens, B., Dähn, R., Scheinost, A.C., Bradbury, M.H., 2012. U(VI) sorption on montmorillonite in the absence and presence of carbonate: A macroscopic and microscopic study. *Geochim. Cosmochim. Acta* 93, 262-277.
- McKinley, J.P., Zachara, J.M., Smith, S.C., Turner, G.D., 1995. The influence of uranyl hydrolysis and multiple site-binding reactions on adsorption of U(VI) to montmorillonite. *Clays Clay Miner.* 43, 586-598.
- Miller, W., Alexander, R., Chapman, N., McKinley, J.C., Smellie, J.A.T., 2000. *Geological Disposal of Radioactive Wastes and Natural Analogues*. Elsevier Science.
- Missana, T., García-Gutiérrez, M., Alonso, Ú., 2004. Kinetics and irreversibility of cesium and uranium sorption onto bentonite colloids in a deep granitic environment. *Appl. Clay Sci.* 26, 137-150.
- Pabalan, R.T., Turner, D.R., 1996. Uranium(6+) sorption on montmorillonite: Experimental and surface complexation modeling study. *Aquatic Geochemistry* 2, 203-226.
- Papirer, E., 2000. *Adsorption on Silica Surfaces*. Taylor & Francis.
- Parker, A., Rae, J.E., 1998. *Environmental Interactions of Clays: Clays and the Environment*. Springer.
- Parkhurst, D.L., Appelo, C.A.J., 2013. Description of input and examples for PHREEQC version 3-A computer program for speciation, batch- reaction, one-dimensional transport, and inverse geochemical calculations, Description of input and examples for PHREEQC version 3. *U.S. Geological Survey Techniques and Methods*, 497.
- Poinssot, C., Geckeis, H., 2012. *Radionuclide Behavior in the Natural Environment: Science, Implications and Lessons for the Nuclear industry*. Elsevier Science.
- Pusch, R., Kasbohm, J., Knutsson, S., Yang, T., Nguyen-Thanh, L., 2015. The Role of Smectite Clay Barriers for Isolating High-Level Radioactive Waste (HLW) In Shallow and Deep Repositories. *Proced. Earth Planet. Sci.* 15, 680-687.
- Robert, M., Hardy, M., Elsass, F., 1991. Crystallochemistry, Properties and Organization of Soil Clays Derived from Major Sedimentary-Rocks in France. *Clay Miner.* 26 (3).
- Schindler, M., Legrand, C.A., Hochella Jr, M.F., 2015. Alteration, adsorption and nucleation processes on clay-water interfaces: Mechanisms for the retention of uranium by altered clay surfaces on the nanometer scale. *Geochim. Cosmochim. Acta* 153, 15-36.

- Seaman, J., Roberts, K., 2012. Radionuclide fate and transport in terrestrial environments, in: Meyers, R. (Ed.), *Encyclopedia of Sustainability Science and Technology*. Springer New York, pp. 8597-8634.
- Selim, H.M., 2012. *Competitive Sorption and Transport of Heavy Metals in Soils and Geological Media*. CRC Press.
- Sparks, D.L., 1989. 3 - Kinetic Methodologies and Data Interpretation for Diffusion Controlled Reactions, in: Sparks, D.L. (Ed.), *Kinetics of Soil Chemical Processes*. Academic Press, San Diego, pp. 39-60.
- Sparks, D.L., 1999. *Kinetics and mechanism of chemical reactions at the soil mineral/water interface*. CRC press, Boca Raton, FL.
- Sparks, D.L., 2013. *Kinetics of Soil Chemical Processes*. Elsevier Science.
- Sylwester, E.R., Hudson, E.A., Allen, P.G., 2000. The structure of uranium (VI) sorption complexes on silica, alumina, and montmorillonite. *Geochim. Cosmochim. Acta* 64, 2431-2438.
- Tertre, E., Hubert, F., Bruzac, S., Pacreau, M., Ferrage, E., Prêt, D., 2013. Ion-exchange reactions on clay minerals coupled with advection/dispersion processes. Application to Na<sup>+</sup>/Ca<sup>2+</sup> exchange on vermiculite: Reactive-transport modeling, batch and stirred flow-through reactor experiments. *Geochim. Cosmochim. Acta* 112, 1-19.
- Tsai, W.T., Chang, Y.M., Lai, C.W., Lo, C.C., 2005. Adsorption of basic dyes in aqueous solution by clay adsorbent from regenerated bleaching earth. *Appl. Clay Sci.* 29, 149-154.
- Villiermaux, J., 1985. *Genie de la reaction chimique, conception et fonctionnement des réacteurs*, Lavoisier Technique et Documentation, Paris.
- Wang, Y., Miller, A., Matteo, E., Reimus, P., Ding, M., Dittrich, T., Zheng, L., Houseworth, J., 2013. *Experimental and Modeling Investigation of Radionuclide Interaction and Transport in Representative Geologic Media*. U.S. Department of Energy.
- Weber, W.J., Morris, J.C., 1963. Kinetics of adsorption on carbon from solution. *J. Sanit. Eng. Div.* 89, 31-60.
- Zachara, J., McKinley, J., 1993. Influence of hydrolysis on the sorption of metal cations by smectites: Importance of edge coordination reactions. *Aquat. Sci.* 55, 250-261.

## 4.7. Influence of pH, layer charge location and crystal thickness distribution of U(VI) sorption onto heterogeneous dioctahedral smectite

Adapted from Vanessa Guimarães, Enrique Rodríguez-Castellón, Manuel Algarra, Fernando Rocha, Iuliu Bobos

Journal of Hazardous Materials (2016), 317, 246-258

DOI: doi:10.1016/j.jhazmat.2016.05.060

### ABSTRACT

The  $\text{UO}_2^{2+}$  adsorption on smectite (samples BA1, PS2 and PS3) with a heterogeneous structure was investigated at pH 4 ( $I=0.02\text{M}$ ) and pH 6 ( $I=0.2\text{M}$ ) in batch experiments, with the aim to evaluate the influence of pH, layer charge and crystal thickness distribution. The sorption isotherms of Freundlich, Langmuir and SIPS were used to model the sorption experiments. The surface complexation and cation exchange reactions were modeled using PHREEQC-code to describe the  $\text{UO}_2^{2+}$  sorption on smectite. The amount of  $\text{UO}_2^{2+}$  adsorbed on smectite samples decreased significantly at pH 6 and higher ionic strength, where the sorption mechanism was restricted to the edge sites of smectite. The  $\equiv\text{AlOUO}_2^+$  and  $\equiv\text{SiOUO}_2^+$  were the major surface species involved. Two different binding energy components at  $380.8\pm 0.3$  and  $382.2\pm 0.3$  eV assigned to hydrate  $\text{UO}_2^{2+}$  adsorbed by cation exchange and by inner-sphere complexation on the external sites at pH 4 were identified by X-photoelectron spectroscopy after the  $\text{U}4f_{7/2}$  peak deconvolution. Two new binding energy components at  $380.3\pm 0.3$  and  $381.8\pm 0.3$  eV assigned to  $\equiv\text{AlOUO}_2^+$  and  $\equiv\text{SiOUO}_2^+$  surface species were observed at pH 6.

**Keywords:** Heterogeneous smectite structure, crystal thickness; batch sorption experiments, uranyl surface complexation model, X-ray photoelectron spectroscopy.

### 4.7.1. Introduction

Smectite clay is widely used as “buffer” barrier in engineered radioactive waste containment systems, owing to their low permeability and high sorption capacity (Pusch et

al., 2015). The performance of the engineering barrier in a high-level waste repository is highly affected by structural changes caused by alteration of the original smectite (Meunier et al., 1992; Lee et al., 2010). The effect of temperature is reflected by the increase of smectite surface charge, induced by silica for aluminium substitution in the tetrahedral sheet, affecting also the cation exchange capacity (CEC) and their swelling properties (Christidis et al., 2006; Dazas et al., 2015; Ferrage et al., 2005; Ferrage et al., 2007; Laird, 2006).

Long-term smectite stability after waste emplacement is low because buffer material will be exposed to a maximum temperature of 150 °C at the surface of the waste package, pressure in the range of 100-300 bars and groundwaters of various compositions depending to the geological environment (Proust et al., 1990). Detailed studies of the reactivity of dioctahedral smectite have shown that the hydrothermal conditions imply the formation of high- and low-charge layers in different proportions on smectite (Bouchet et al., 1988) and the progressive formation of illite-montmorillonite mixed layers (Eberl, 1978; Inoue et al., 1992).

Uranium (U) occurs as uranyl ( $\text{UO}_2^{2+}$ ) ions under oxidizing geochemical conditions and acidic aqueous solutions, forming monomers, dimers, and trimers at higher pH hydrolyses (Grenthe et al., 1992). The pH dependent adsorption behaviour under these conditions is similar to other metal oxides with a cationic adsorption on edge sites at pH 5-6 and an additional anionic adsorption on the edge sites around pH 8 in systems equilibrated with atmospheric  $\text{CO}_2$  (Chisholm-Brause et al., 2001). Despite the importance of this mechanism, there is a limited knowledge about the interaction between  $\text{UO}_2^{2+}$  ions and clay mineral surfaces (Hudson et al., 1999). The interaction of  $\text{UO}_2^{2+}$  ions with smectite clay minerals, as potential adsorbent materials with high surface area, were carried out with montmorillonite (Campos et al., 2013; Catalano and Brown Jr, 2005; Chisholm-Brause et al., 2001; Hennig et al., 2002; Hyun et al., 2001; Kim, 2001; Kowal-Fouchard et al., 2004; Marques Fernandes et al., 2012; McKinley et al., 1995; Pabalan and Turner, 1997; Schlegel and Descontes, 2009; Sylwester et al., 2000; Tsunashima et al., 1981), tri-smectite (Bauer et al., 2001; Giaquinta et al., 1997; Korichi and Bensmaili, 2009) or bentonite rocks (Olguin et al., 1997).

Uranyl sorption onto smectite involves multiple binding sites, including ion exchange and edge surface sites. Previous works reported that the adsorption of  $\text{UO}_2^{2+}$  on smectite follows two main mechanisms: ion-exchange through outer-sphere complexation at low pH and low ionic strength, whereas at near-neutral pH and high ionic strength through inner-sphere complexation on the edge sites controls the sorption mechanism (Chisholm-Brause

et al., 2001; Hennig et al., 2002; Korichi and Bensmaili, 2009; Schindler et al., 2015; Sylwester et al., 2000; Turner et al., 1996).

The development of surface complexation models (SCM) predicts the behavior of uranyl sorption on different clay minerals by fitting the thermodynamic data obtained from reference methods under different environmental conditions (Kim, 2001; Zachara and McKinley, 1993). The use of a “unique model” was developed to defend the standardization of SCM using thermodynamic approaches and parameter optimization in order to achieve the best fit to the experimental sorption data (Bradbury and Baeyens, 2000; Marques Fernandes et al., 2012; Pabalan and Turner, 1997; Turner et al., 1996). In this way, it was possible to reduce the number of adjustable parameters and provide a set of uniform parameters based on common reference values.

The main aim of this study is to understand the degree of interaction between  $\text{UO}_2^{2+}$  and dioctahedral smectite with a heterogeneous structure as a function of layer charge location and the type of interstratified layers, in order to predict the possible changes on sorption mechanism caused by structural modification of smectite during alteration. The heterogeneous smectite structure used in sorption experiments represents in fact the first alteration stage of smectite exposed to circulation of hydrothermal fluids or as backfilling materials in nuclear waste disposal (Meunier et al., 1992).

The kinetic of sorption-desorption experiments of the  $\text{UO}_2^{2+}$  retardation onto smectite samples (the same samples were used) using a continuous stirred tank reactor was previously interpreted by the reaction-controlled model (pseudo-first order and pseudo-second order) and diffusion-controlled model (intra-particle diffusion and liquid-film diffusion) (Guimarães et al. 2016, in press). The adsorption experiments in this work were carried out to evaluate the role of pH, charge location and the crystal thickness distribution of smectite on the  $\text{UO}_2^{2+}$  sorption mechanism. The pH variation influences the  $\text{UO}_2^{2+}$  aqueous speciation defining the species involved during the sorption mechanism. Also, it may play an important role in the surface sites distribution, controlling the adsorption capacity and the binding strength of surface complexes. The adsorption process on different smectite samples was simulated using the cation exchange and surface complexation model based on diffuse double layer (DDL) (Parkhurst and Appelo, 2013). The  $\text{UO}_2^{2+}$  surface species adsorbed on smectite at pH 4 and pH 6 were also identified by X-ray photoelectron spectroscopy (XPS) experiments.

## 4.7.2. Materials and methods

### 4.7.2.1. Clay minerals selection and preparation.

Three selected bentonite rocks (BA1, PS2 and PS3) were collected from two different regions of Portugal: Benavila region (BA1) and Porto Santo Island, Madeira archipelago (PS2 and PS3). The <2  $\mu\text{m}$  fractions were obtained by sedimentation according to Stocks law. Before sorption experiments, the <2  $\mu\text{m}$  clay fractions were studied by X-ray diffraction (XRD), infrared-spectroscopy and electron microprobe analysis. The structural behaviour of smectite samples was verified using several well-known protocols used to differentiate high- from low-charge smectite (Barshad, 1960; Harward, 1967; Jackson and Barak, 2005) and to distinguish beidellite from montmorillonite (Greene-Kelly, 1952). The detailed results of these experiments were discussed in recent work (Guimarães et al., 2015a). Sample BA1 corresponds to an interstratified structure composed of beidellite/(Ca,Na)-montmorillonite (2-waters). Sample PS2 corresponds to K-illite/beidellite/(Na,Ca)-montmorillonite (R0, 85-90%S). Sample PS3 corresponds to a randomly interstratified structure of K-illite/(Na,Ca)-montmorillonite (R=0; 70%S), where no beidellitic layers did occur. The crystal chemistry of the <2  $\mu\text{m}$  clay fractions obtained by electron microprobe analysis (EMPA) is given in Table 17.

Table 17. Crystal chemistry and physico-chemical properties of clay minerals.

Sample	Structural Formula	<i>T</i> (nm)	S <sub>BET</sub> (m <sup>2</sup> /g)	CEC (meq/g)	Charge Def./Uc	Na/ Ca
BA1	Ca <sub>0.27</sub> Na <sub>0.20</sub> (Al <sub>1.30</sub> Fe <sub>0.36</sub> Mg <sub>0.33</sub> )(Si <sub>3.63</sub> Al <sub>0.37</sub> )O <sub>10</sub> (OH) <sub>2</sub>	7.4	12	0.96	- 1.38 48%O 52%T	0.74
PS2	Ca <sub>0.14</sub> Na <sub>0.38</sub> K <sub>0.08</sub> (Al <sub>1.25</sub> Fe <sub>0.34</sub> Mg <sub>0.39</sub> )(Si <sub>3.74</sub> Al <sub>0.26</sub> )O <sub>10</sub> (OH) <sub>2</sub>	4.8	26	1.04	- 1.31 62%O 38%T	2.71
PS3	Ca <sub>0.15</sub> Na <sub>0.30</sub> K <sub>0.14</sub> (Al <sub>1.17</sub> Fe <sub>0.41</sub> Mg <sub>0.42</sub> )(Si <sub>3.70</sub> Al <sub>0.30</sub> )O <sub>10</sub> (OH) <sub>2</sub>	5.1	84	0.81	- 1.45 59%O 41%T	2.00
SW1*	Ca <sub>0.12</sub> Na <sub>0.32</sub> K <sub>0.05</sub> (Al <sub>1.50</sub> Fe <sub>0.21</sub> Mg <sub>0.27</sub> Ti <sub>0.01</sub> )(Si <sub>3.99</sub> Al <sub>0.01</sub> )O <sub>10</sub> (OH) <sub>2</sub>	8.1	31.82	0.76		
SBId1**	Ca <sub>0.05</sub> Na <sub>0.12</sub> K <sub>0.16</sub> (Al <sub>1.78</sub> Fe <sub>1.04</sub> Mg <sub>0.46</sub> Ti <sub>0.49</sub> )(Si <sub>3.77</sub> Al <sub>0.23</sub> )O <sub>10</sub> (OH) <sub>2</sub>	12.3				

\* Na-Montmorillonite, Wyoming, Source: Clay Minerals Society Repository.

\*\* Beidellite Black Jack, Idaho, Source: Clay minerals Repository.

#### 4.7.2.2. Methods and analytical techniques

*Cation exchange capacity.* The  $<2 \mu\text{m}$  clay fractions were saturated with  $\text{Sr}^{2+}$  and prepared in order to determine the cation exchange capacity (CEC). The experiments were carried out by adding 0.050 grams of smectite into the polypropylene centrifuge tubes with 14.00 mL of different stock solutions at different  $\text{Sr}^{2+}$  concentrations, ranged between  $5 \times 10^{-4} \text{ M}$  and  $1.50 \times 10^{-2} \text{ M}$ . Suspensions were shaken for 34 hours, then centrifuged, separated and the solutions resulted were preserved by adding  $\text{HNO}_3$  (65%) and stored at  $4 \text{ }^\circ\text{C}$  for subsequent chemical analyses. The CEC was determined by  $\text{Sr}^{2+}$  adsorption tests at  $\text{pH}=4$ . After  $\text{Sr}^{2+}$  saturated the  $<2\mu\text{m}$  clay fractions the  $\text{Sr}^{2+}$ -aqueous solutions were analysed by atomic absorption spectrometry (AAS). The CEC value was estimated from the maximum amount of  $\text{Sr}^{2+}$  adsorbed in these conditions, taking into account the following relation:  $\text{CEC}(\text{meq/g}) = q_{\text{Sr}^{2+}}(\text{mmol/g}) \times 2$ .

*The Brunauer-Emmett-Teller specific surface area (BET).* The BET surface area of the  $<2\mu\text{m}$  clay fractions was characterized by nitrogen adsorption-desorption measurements with a Micromeritics Tristar II analyser. The samples were degassed at  $200 \text{ }^\circ\text{C}$  overnight before the measurements were taken. The surface area was calculated based on the adsorption data in the relative partial pressure range of 0.05–0.2, and the pore size distributions were determined based on the Barrett–Joyner–Halender (BJH) adsorption curve.

*X-ray diffraction.* The structural characterization of the  $<2 \mu\text{m}$  clay fractions was performed by X-ray diffraction (XRD) using a Siemens D500 machine equipped with a  $\text{CuK}\alpha$  radiation and a scanning speed of  $1^\circ 2\theta/\text{min}$  in the range  $2\text{--}50^\circ 2\theta$ . The  $<2 \mu\text{m}$  clay fractions previously analysed by X-ray diffraction (XRD) were prepared as oriented specimens on glass slide and then, were run in air-dried (AD) condition and saturated with ethylene-glycol vapour during 24 h.

*Chemical treatments for X-ray diffraction analysis.* Prior to XRD analysis, smectite heterogeneity was studied using several chemical treatments:  $\text{Mg}^{2+}$ - and  $\text{K}^+$ -saturation tests. To differentiate high- from low-charge smectite and to study the layer charge distribution, different clay fractions were saturated with 1M KCl (Barshad and Kishk, 1970) and with 1M  $\text{MgCl}_2$  (Harward et al., 1968) during 24 hours (S:L=3.57 g/L). The clay samples saturated were analysed by XRD in air-dried (AD) conditions. After X-ray run in AD, the K-saturated

clay fractions were heated at 300 °C during 2 hour, solvated with ethylene glycol (EG) and then analysed by XRD. By contrast, the Mg<sup>2+</sup>-saturated clay fractions followed a glycerol treatment before XRD analysis.

The Greene-Kelly (Hoffman-Klemen) test (Greene-Kelly, 1952a) allowed to distinguish beidellite from montmorillonite. The test started with Li<sup>+</sup> saturation of <2 µm clay fractions, adding 0.050 g of clay into 14 mL of 1M LiCl solution, during 24 hours, followed by heating at 300 °C during 6h, and glycerol treatment. The Li<sup>+</sup> irreversible migrated to the octahedral sheet converts montmorillonite to a non-expandable structure upon treatment with glycerol. The XRD analyses were carried out after heating and glycerol treatment.

Crystal thickness distribution. The XRD method is based on the observation that XRD peaks are broadened regularly as a function of decreasing crystallite size. This effect permits accurate measurement of mean crystallite sizes for periodic crystals that range from about 2 nm to about 100 nm. The Bertaut-Warren-Averbach (BWA) analysis was performed in the 3 to 6 °2θ range using the MudMaster computer program (Drits et al., 1998). The program includes corrections of the diffracted intensity ( $I(\theta)$ ) for the Lorentz-polarization (Lp) and the structural (G) factors, which are necessary for clays. A combined LpG2 factor was calculated for each sample accounting for its Fe content.

*Electron microprobe analysis (EMPA).* Polished sample surfaces were prepared from the <2 µm clay fractions, which were previously pressed in pellets with diameter of 3 mm with a PIKE Hand Press Kit 161 – 1024 (Pike technologies). The epoxy resin was prepared using the Araldite EAY 103-1 and a HY956-KG hardener (9:1 ratio) and then dispersed in a holder of 13 mm. The pellets were located in the epoxy resin, dried during 24 h and subsequently polished using the 30, 10 and 2 µm microfinishing films under dry conditions.

The major elements of minerals were determined using a Jeol Hyperprobe JXA-8500F electron microprobe operated at 15 kV accelerating voltage and 10 nA beam current. Detection limits ( $3\tau$ ) above mean background were 0.03 wt.% for most oxides with counting times of 80 s. Standards used include albite (NaK $\alpha$ ), orthoclase (AlK $\alpha$ , SiK $\alpha$ , KK $\alpha$ ), apatite (CaK $\alpha$ , PK $\alpha$ ), MgO (MgK $\alpha$ ), MnTiO<sub>3</sub> (MnK $\alpha$ ), TiO<sub>2</sub> (TiK $\alpha$ ), Fe<sub>2</sub>O<sub>3</sub> (FeK $\alpha$ ).

*Atomic absorption spectrometry.* Chemical analyses of  $\text{Sr}^{2+}$  aqueous solutions were carried out by atomic absorption spectroscopy using a flame absorption spectrometer Perkin Elmer, AAnalyst 200 model with a  $\text{Sr}^{2+}$  hollow cathode lamp, wavelength 460.73 nm, air flow 5.2 L/min and acetylene flow 2.5 L/min. The 5 mL of the acidified strontium solution was mixed with 750  $\mu\text{L}$  of lanthanum chloride ( $\text{LaCl}_3 \cdot 7\text{H}_2\text{O}$ ) solution previously prepared (176 g of  $\text{LaCl}_3 \cdot 7\text{H}_2\text{O}$  and 19.1 g of KCl diluted in 1000 mL of deionised water).

*Inductively coupled plasma-mass spectrometry.* The  $\text{UO}_2^{2-}$  aqueous solutions and the presence of  $\text{Ca}^{2+}$ ,  $\text{Mg}^{2+}$  and  $\text{Na}^+$  cations available in aqueous solutions after batch experiments were analysed by inductively coupled plasma-mass spectrometry (ICP-MS). The uranium concentrations in acidified solutions were determined by external standard calibration method using an inductively coupled plasma-mass spectrometry (ICP-MS) (THERMO X series ELEMENT2 and Amiga series, JobinYvon equipments). Calibration was done in each analytical session by the external standard method. Also, major elements of smectite and composite material were analysed by ICP-MS.

*X-ray photoelectron spectroscopy.* Uranyl-clay samples obtained after batch experiments were analysed by X-ray photoelectron spectroscopy (XPS). XPS spectra were recorded using a Physical Electronics PHI 5701 spectrometer with a non-monochromatic Al  $\text{K}\alpha$  radiation (300 W, 15 kV,  $h\nu = 1486.6$  eV) as the excitation source. Spectra were recorded at  $45^\circ$  take-off angle by a concentric hemispherical analyzer operating in the constant pass energy mode at 25.9 eV, using a 720 mm diameter analysis area. Under these conditions the Au  $4f_{7/2}$  line was recorded with 1.16 eV FWHM at a binding energy of 84.0 eV. The spectrometer energy scale was calibrated using Cu  $2p_{3/2}$ , Ag  $3d_{5/2}$  and Au  $4f_{7/2}$  photoelectron lines at 932.7, 368.3 and 84.0 eV, respectively. Charge referencing was done against adventitious carbon (C1s 284.8 eV). Powdered solids were mounted on a sample holder without adhesive tape and kept overnight in high vacuum in the preparation chamber before they were transferred to the analysis chamber of the spectrometer. Each region was scanned with several sweeps until a good signal to noise ratio was observed. The pressure in the analysis chamber was maintained lower than  $10^{-9}$  Torr. A PHI ACCESS ESCA-V6.0 F software package was used for acquisition and data analysis. A Shirley-type background was subtracted from the signals. Recorded spectra were always fitted using Gauss–Lorentz curves in order to determine more accurately the binding energy of the different element core levels. The  $\text{U}4f_{7/2}$  peak was deconvoluted using a mixed Gaussian-Lorentzian

contribution (Del Nero et al., 2004; Froideval et al., 2003). The accuracy of binding energy (BE's) values was within  $\pm 0.3$  eV.

### 4.7.3. Experimental

#### 4.7.3.1. Batch Experiments

Batch experiments were carried out to investigate the  $\text{UO}_2^{2+}$  adsorption on three different heterogeneous smectites, with a different distribution of charge deficit. The adsorption experiments were carried out at pH 4 and 6, using low ( $I=0.02\text{M}$ ) and high ionic strength ( $I=0.2\text{M}$ ), in order to promote the study of both sorption mechanisms on smectite surface: ion exchange and inner-sphere complexation on the surface edge sites. Batch experiments performed at  $\text{pH}=4$  were carried out by adding 0.025 g of the respective clay mineral with 14.00 mL ( $S:L=1.79\text{g/L}$ ) of different stock solutions at different  $\text{UO}_2^{2+}$  concentrations, ranged between  $1.00 \times 10^{-5}\text{M}$  and  $6.50 \times 10^{-4}\text{M}$ , with NaCl (0.02M). At  $\text{pH}=6$ , 0.050g ( $S:L=3.60\text{g/L}$ ) of each smectite was added, and the  $\text{UO}_2^{2+}$  concentration of stock solutions ranged between  $1.00 \times 10^{-6}\text{M}$  and  $1.00 \times 10^{-4}\text{M}$ , with NaCl (0.2M). Suspensions were shaken for 48 hours, and then centrifuged, separated and the resulted (supernatant) solutions were preserved by adding HCl and stored at  $4\text{ }^\circ\text{C}$  for subsequent chemical analysis. Uranyl stock solutions were prepared from a primary standard solution ( $1.0 \times 10^{-3}\text{M}$ ), obtained by dissolving  $\text{UO}_2(\text{CH}_3\text{COO})_2 \times 2\text{H}_2\text{O}$  in deionized water. The pH was adjusted to the required value and monitored with NaOH (0.05M) or HCl (0.05M) (Merck, Germany), using a pH meter (Corning 240) calibrated with buffer solutions (pH 4, 7 and 10, Merck).

##### 4.7.3.1.1. Isothermal models

The Langmuir model assumes that the sorption sites are identical and energetically equivalent due to its homogeneous structure (Langmuir, 1916). The equilibrium is obtained when the monolayer formation on the sorbent occurs. Langmuir isotherm is described according to the following equation:

$$q_e = \frac{q_m K_L C_e}{(1 + K_L C_e)} \quad (1)$$

where,  $q_e$  (mol/kg) and  $C_e$  (mol/L) are the equilibrium concentrations of  $UO_2^{2+}$  in the solid and the liquid phase, respectively,  $q_m$  (mol/kg) is the maximum sorption capacity, and  $K_L$  (L/kg) is the Langmuir constant related to the energy of adsorption.  $q_e$  is obtained according to Eq. 2:

$$q_e = (C_i - C_f) \frac{V}{m} \quad (2)$$

where,  $C_i$  and  $C_f$  are the concentrations of  $UO_2^{2+}$  in the beginning and the end of the adsorption process,  $V$  is the solution volume used during batch experiments (14.00 mL) and  $m$  is the mass of smectite used.

The Freundlich model was used to describe the adsorption of contaminants on heterogeneous surface consisting of sites with different exponential distribution and energies (Chen and Wang, 2007; Schwarzenbach et al., 2005). The equation of Freundlich sorption isotherm is expressed by Eq. 3:

$$q_e = K_F C_e^n \quad (3)$$

where,  $K_F$  and  $n$  are the Freundlich adsorption isotherm constants, being indicative of the adsorption extension and the degree of the surface heterogeneity.

The Sips isotherm combines both Freundlich and Langmuir isotherms where at low adsorbate concentration behaves as Freundlich isotherm, whereas at high concentration predicts a monolayer adsorption capacity characteristic to Langmuir model (Jeppu and Clement, 2012; Maurer, 2000). The mathematical representation of this model is given by Eq. 4:

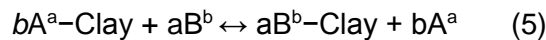
$$q_e = \frac{q_m (K_S C_e)^n}{1 + (K_S C_e)^n} \quad (4)$$

where,  $q_m$  (mol/kg) is the maximum sorption capacity, which can also be expressed as  $Nt$ , a measure of the total number of binding sites available per g of sorbent,  $K_S$  is the affinity

constant for adsorption (L/kg) and  $n$  is the Freundlich parameter that takes into account the system heterogeneity. The Sips isotherm is reduced to the Langmuir form for  $n=1$  and a homogeneous surface is considered. The greater is the difference from this value, the greater will be the clay surface heterogeneity.

#### 4.7.4. Diffuse double layer surface complexation and cation exchange modelling

The diffuse double layer surface complexation model was used to predict the  $UO_2^{2+}$  surface complexation reactions onto smectite. The PHREEQC-code (Parkhurst and Appelo, 2013) describes the surface complexation model including a combination of equilibrium protonation ( $\equiv SOH_2^+$ ), deprotonation ( $\equiv SO^-$ ) and complexation reactions based on previous  $UO_2^{2+}$  sorption experiments on montmorillonite (McKinley et al., 1995). This process was based on the geochemical code proposed by (Bachmaf and Merkel, 2011). The major surface reactions and input parameters included in our model are resumed in Table 18. The second geochemical code developed on PHREEQC was additionally used to describe the cation exchange process of  $UO_2^{2+}$  adsorption at pH 4 and pH 6 (Parkhurst and Appelo, 2013). The cation exchange on the permanently charged planar sites (Eq. 5) was modelled taking into account the adsorbent CEC ( $eq\ kg^{-1}$ ) and the selectivity coefficient for each ion exchange process occurring on the planar sites, given by Eq. 6 (Bradbury and Baeyens, 2009). The selectivity constants used to model  $UO_2^{2+}$  exchange process are resumed in Table 18. The selectivity coefficients regarding to the exchange process between  $UO_2^{2+}$  and  $Ca^{2+}$  ( $\frac{UO_2}{Ca}K_c$ ), were obtained from the ratio  $\frac{UO_2}{Na}K_c / \frac{Ca}{Na}K_c$  (Bradbury and Baeyens, 2000; Marques Fernandes et al., 2012; Tournassat et al., 2004).



$$\frac{B}{A}K_c = \frac{N_B^a}{N_A^b} \cdot \frac{A^b}{B^a} \cdot \frac{\gamma_A^b}{\gamma_B^a} \quad (6)$$

Table 18. Model parameters used to simulate the  $\text{UO}_2^{2+}$  adsorption on smectite.

Model conditions	Samples		
	BA1	PS2	PS3
Solid concentration (S:L) (g/L)		3.60 (pH 6)	1.79 (pH4)
Surface area (BET) ( $\text{m}^2/\text{g}$ )	12	26	82
Total site concentration (mol/kg)	0.084	0.092	0.071
<b>Edge site reactions</b>		<b>Log K</b>	
$\equiv\text{AlOH} + \text{H}^+ = \equiv\text{AlOH}_2^+$	12.30 <sup>a</sup>	12.30 <sup>a</sup>	12.30 <sup>a</sup>
$\equiv\text{AlOH} = \equiv\text{AlO}^- + \text{H}^+$	-13.60 <sup>a</sup>	-13.60 <sup>a</sup>	-13.60 <sup>a</sup>
$\equiv\text{AlOH} + \text{UO}_2^{2+} = \equiv\text{AlOUO}_2^+ + \text{H}^+$	7.70 <sup>b</sup>	7.94 <sup>b</sup>	7.84 <sup>b</sup>
$\equiv\text{AlOH} + 3\text{UO}_2^{2+} + 5\text{H}_2\text{O} = \equiv\text{AlO}(\text{UO}_2)_3(\text{OH})_5 + \text{H}^+$	-15.19 <sup>b</sup>	-14.95 <sup>b</sup>	-15.06 <sup>b</sup>
$\equiv\text{AlOH} + \text{Na}^+ = \equiv\text{AlONa} + \text{H}^+$	-6.60	-6.60	-6.60
$\equiv\text{SiOH} = \equiv\text{SiO}^- + \text{H}^+$	-6.95 <sup>a</sup>	-6.95 <sup>a</sup>	-6.95 <sup>a</sup>
$\equiv\text{SiOH} + \text{UO}_2^{2+} = \equiv\text{SiOUO}_2^+ + \text{H}^+$	0.75 <sup>b</sup>	0.99 <sup>b</sup>	0.89 <sup>b</sup>
$\equiv\text{SiOH} + 3\text{UO}_2^{2+} + 5\text{H}_2\text{O} = \equiv\text{SiO}(\text{UO}_2)_3(\text{OH})_5 + \text{H}^+$	-16.19 <sup>b</sup>	-15.95 <sup>b</sup>	-16.06 <sup>b</sup>
$\equiv\text{SiOH} + \text{Na}^+ = \equiv\text{SiONa} + \text{H}^+$	-10.37	-10.37	-10.37
<b>Exchange reactions</b>		<b>Selectivity coefficients (<math>K_c</math>)</b>	
$2\text{Na}^+\text{-clay} + \text{UO}_2^{2+} \leftrightarrow \text{UO}_2^{2+}\text{-clay} + 2\text{Na}^+$	2.82 ( $\text{Na}^+$ - 13%)	2.82 ( $\text{Na}^+$ -87 %)	2.82 ( $\text{Na}^+$ - 65%)
$2\text{Na}^+\text{-clay} + \text{Ca}^{2+} \leftrightarrow \text{Ca}^{2+}\text{-clay} + 2\text{Na}^+$	2.50	2.50	2.50
$\text{Ca}^{2+}\text{-clay} + \text{UO}_2^{2+} \leftrightarrow \text{UO}_2^{2+}\text{-clay} + \text{Ca}^{2+}$	1.12	1.12	1.12
$\text{Ca}^{2+}\text{-clay} + 2\text{Na}^+ \leftrightarrow \text{Na}_2\text{-clay} + \text{Ca}^{2+}$	1.70 ( $\text{Ca}^{2+}$ - 87%)	1.70 ( $\text{Ca}^{2+}$ - 13%)	1.70 ( $\text{Ca}^{2+}$ - 35%)
<b>Aqueous Speciation</b>			
$\text{UO}_2^{2+} + \text{H}_2\text{O} = \text{UO}_2(\text{OH})^+$	-5.25 <sup>d</sup>		
$2\text{UO}_2^{2+} + 2\text{H}_2\text{O} = (\text{UO}_2)_2(\text{OH})_2^{2+} + 2\text{H}^+$	-5.62 <sup>d</sup>		
$3\text{UO}_2^{2+} + 5\text{H}_2\text{O} = (\text{UO}_2)_3(\text{OH})_5^+ + 5\text{H}^+$	-15.55 <sup>d</sup>		
$\text{UO}_2^{2+} + 3(\text{H}_2\text{O}) = \text{UO}_2(\text{OH})_3^- + 3\text{H}^+$	-20.25 <sup>d</sup>		

<sup>a</sup> McKinley et al. (1995).

<sup>b</sup> Fitted binding constants.

<sup>c</sup> Calculated Selectivity coefficients.

<sup>d</sup> Guillaumont et al. (2003).

The proportion of  $\text{Ca}^{2+}$  and  $\text{Na}^+$  on smectite was taken into account in the modelling of cation exchange process. Therefore, two different exchange master species were defined according to the next geochemical code developed on pHreeqc:

```
"EXCHANGE_MASTER_SPECIES
X X- #Na-Smectite
Z Z- #Ca-Smectite
EXCHANGE_SPECIES
X- = X-; log_k 0.0
Z- = Z-; log_k 0.0
X- + Na+ = NaX; log_k 0.0
2X- + UO2+2 = UO2X2; log_k 0.45
2Z- + UO2+2 = UO2Z2; log_k 0.049
Z- + Na+ = NaZ; log_k 0.23
SOLUTION 1
pH 4.3
Na 20 # concentrations in mmol/kg H2O
U(6) 7.36e-1
Acetate 1.47
Cl 20 charge
EXCHANGE
X 1.14e-4 # 13% Na+
Z 7.43e-4 # 87% Ca2+
-equilibrate 1"
```

The permanent charged sites ( $\equiv\text{X}^-$ ) was estimated to be equal with the cation exchange capacity, whereas the reactive edge sites capacity was assumed to be 15% of the total number of crystallite edge sites available. The edge surface sites may correspond to 10-20% of the total number of sites available for sorption (Anderson and Sposito, 1991). It was also defined that the ratio between  $\equiv\text{AlOH}$  and  $\equiv\text{SiOH}$  sites is 0.83 for smectite (White and Zelazny, 1988). The aqueous speciation equilibrium constants ( $\log K$ ) considered in our model were obtained from NEA uranium thermodynamic database (Guillaumont et al., 2003; Wanner and Forest, 1992).

A combination of four surface complexes,  $\equiv\text{AlOUO}_2^+$ ,  $\equiv\text{AlO}(\text{UO}_2)_3(\text{OH})_5$ ,  $\equiv\text{SiOUO}_2^+$  and  $\equiv\text{SiO}(\text{UO}_2)_3(\text{OH})_5$ , was assumed according previous research for the best prediction of the experimental sorption data (McKinley et al., 1995). The chemical modeling program FITEQL 4.0 (Herbelin and Westall, 1999) was used to optimize the respective surface complexation constants using the DDL model by means of fitting the  $\text{UO}_2^{2+}$  sorption data from pH 4 to pH 7, using a concentration of  $\text{UO}_2^{2+}$  of  $1.0 \times 10^{-4}\text{M}$  and 0.2M of NaCl. Fig.39 shows the comparison between the U(VI) sorption data on BA1, PS2 and PS3 and the surface complexation model. The respective binding constants were then used in the PHREEQC-code in order to predict the amount of  $\text{UO}_2^{2+}$  adsorbed for different initial

concentrations of  $UO_2^{2+}$ , different pH conditions and ionic strengths. In this way, different solutions were defined in the PHREEQC-code in order to simulate the isothermal curves.

In the presence of  $CO_2$  (g) atmospheric, the  $UO_2^{2+}$  adsorption on smectite is affected at  $pH > 6.5$  with the formation of uranyl-carbonate ternary-surface complexes. These surface complexation reactions were not included in our model, restricting their efficiency to the adsorption experiments occurring from acidic to near-neutral pH conditions.

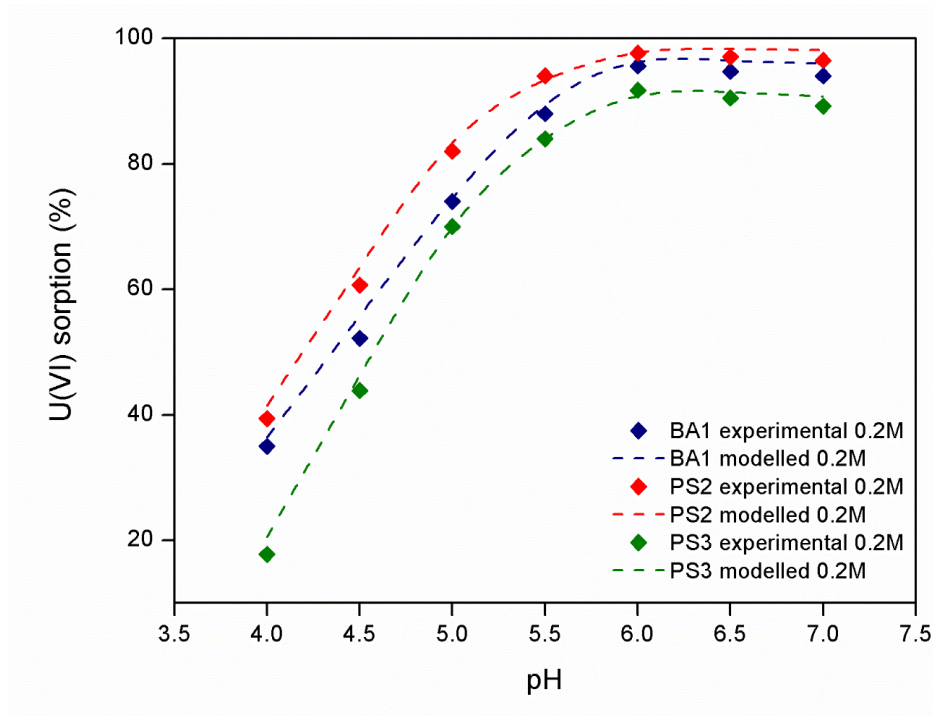


Fig.39 - Comparison of uranium adsorption data on BA1, PS2 and PS3 and the surface complexation model (FITEQL).  $[UO_2^{2+}] = 1.00 \times 10^{-4} M$ , S:L=3.60,  $P_{CO_2} = 10^{-3.5} Pa$ , 25°C, I=0.2M.

The root mean square error (RMSE) given by Eq. 7 (Powlson et al., 2013) was used to measure the difference between both models:

$$RMSE(\%) = \sqrt{\frac{\sum_{i=1}^n (x_{1,i} - x_{2,i})^2}{n}} * 100 \quad (5)$$

where  $x_{1,i}$  and  $x_{2,i}$  are the measured and calculated amounts of  $\text{UO}_2^{2+}$  adsorbed on smectite, respectively, and  $n$  is the total number of experiments carried out using different  $\text{UO}_2^{2+}$  concentrations.

## 4.7.5. Results and Discussion

### 4.7.5.1. Crystal thickness distribution

The physical and chemical properties (i.e., surface area, CEC, sorption, solubility, etc) of a clay mineral may be strongly influence by crystal thickness or particle size distribution. Mean crystal thickness ( $T$ ) of smectite crystals used in our experiments is 4.8 and 5.1 nm for samples PS2 and PS3, and 7.4 nm for sample BA1 (Table 17). The  $T$  (nm) corresponding to Na-montmorillonite SW1 and beidellite Black Jack were compared with our data (Table 17).

The  $T$  values obtained were used for calculation the total surface area (TSA) which includes the basal interfaces and edges of crystals using the following equation:  $\text{TSA} = 100/0.12T$ . The values obtained (Table 17) show that the smaller crystals have higher TSA.

### 4.7.5.2. Effect of layer charge location and heterogeneous layers distribution

The effect of layer charge distribution between tetrahedral and/or octahedral sheets of smectite was taken into account in sorption experiments. Different charge layers reveal different smectite layers compositions regarding to the degree of octahedral and tetrahedral substitutions. Also, the influence of charge distribution on selected smectite samples was evaluated taking into account the ratio between the CEC values and the respective layer charge deficits (Table 17).

Higher proportions of tetrahedral substitution ( $-0.37/(\text{Si,Al})_4\text{O}_{10}$ ) attributed to beidellite layers correspond to sample BA1, whereas the lower tetrahedral charge deficit and the higher proportion of octahedral substitution occur in samples PS2 ( $-0.26/(\text{Si,Al})_4\text{O}_{10}$ ) and

PS3 (-0.30/(Si,Al)<sub>4</sub>O<sub>10</sub>). Reduced interlayer distances induced by the increase of layer substitutions and by the proximity between the charge deficit of tetrahedral sheet and the contaminant, restrict the ion-exchanges process hampering the UO<sub>2</sub><sup>2+</sup> uptake. In this way, sample BA1 has higher charge than PS2 but lower CEC value (Table 17).

The hypothetic structures of smectite samples used in sorption experiments are shown in Fig.40, where both layer-types and charge layers are shown for each smectite sample used in sorption experiments, according to the structural and chemical data obtained by XRD and EMPA.

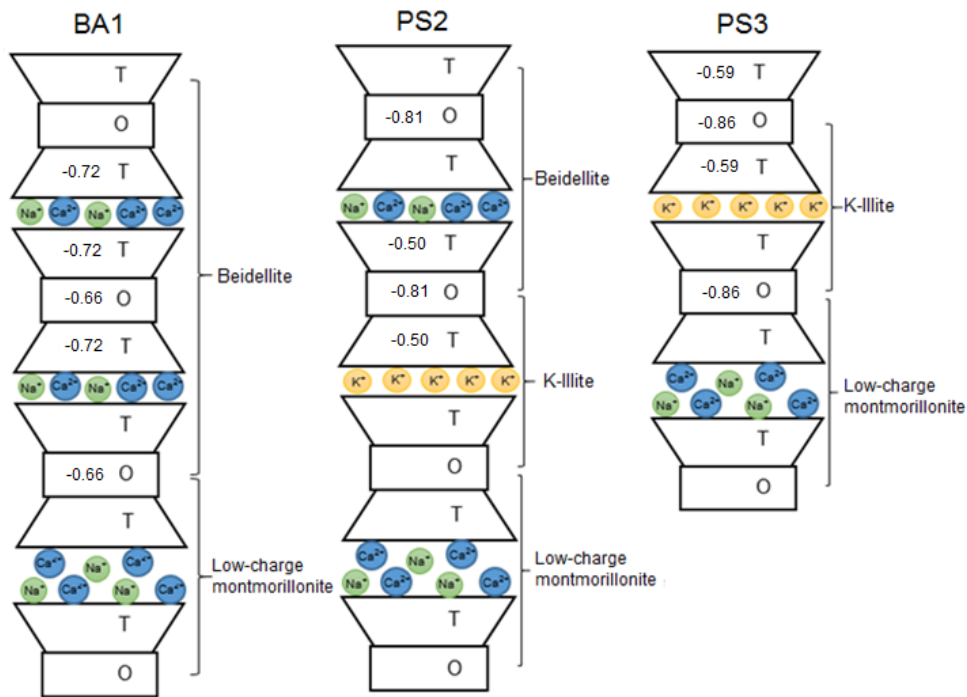


Fig.40 - Idealization of smectite structure: a) BA1 structure that results from interstratification between beidellite and low charge montmorillonite; b) PS2 interstratified structure that consists on beidellite, illite and low charge montmorillonite; c) PS3 structure composed by illite and low charge montmorillonite interstratified.

The lower proportion of tetrahedral substitutions of PS2 improved the adsorption on interlayer sites, contrary to what is observed for sample PS3 (CEC=0.81 meq/g). Usually, a decrease of CEC occurs as the percentage of illite layers increases in the randomly interstratified structure of I/S formed. Sample PS3 has the higher proportion of illite interstratified layers (≈30 %), the lower number of available sites for ion-exchange and a randomly 2W/1W smectite that favoured the decrease of contaminant adsorption.

### 4.7.5.3. $\text{UO}_2^{2+}$ aqueous speciation

The aqueous speciation of  $\text{UO}_2^{2+}$  calculated using PHREEQC 3.12-8538 (Parkhurst and Appelo, 2013) took into account the acidic conditions and lower ionic strength ( $[\text{NaCl}]=0.02\text{M}$ ), and the alkaline and higher ionic strength conditions ( $[\text{NaCl}]=0.2\text{ M}$ ). The aqueous uranyl hydrolysis and carbonate complexation constants were implemented from the Thermochemical Databases proposed by the Nuclear Energy Agency (NEA-TDB) (Guillaumont et al., 2003). The solubility constant for schoepite and  $\beta\text{-UO}_2(\text{OH})_2$  is 5.39 (Critical Stability Constants of Metal Complexes Database, NIST Standard Reference Database 46 version 7) and 5.61 (Chemical Thermodynamics Database, NIST Standard Reference Database 2, version 1.1), respectively.

The  $\text{UO}_2^{2+}$  speciation is widely dependent on the pH conditions (Chisholm-Brause et al., 1994), where different complexes formed will affect the surface complexation. The distribution of aqueous species from pH 3 to pH 6, using  $6.00 \times 10^{-4}\text{M}$  U(VI) and  $0.02\text{M}$  NaCl, and from pH 5 to pH 9, using  $1.00 \times 10^{-4}\text{M}$  U(VI) and  $0.2\text{M}$  NaCl, is shown in Fig.41. The  $\text{UO}_2^{2+}$  is the major specie up to pH 4.7, where the hydrated form will be adsorbed by smectite, whereas the formation of polynuclear species  $[(\text{UO}_2)_2\text{OH}_2^{2+}$  and  $(\text{UO}_2)_3\text{OH}_5^{2+}]$  starts from pH 3 and 3.5, respectively. The  $\text{UO}_2^{2+}$  represents 73% of the total species at pH 4, whereas  $(\text{UO}_2)_2\text{OH}_2^{2+}$  and  $(\text{UO}_2)_3\text{OH}_5^{2+}$  have both proportions of 8% (Fig.41a). The formation of  $(\text{UO}_2)_4\text{OH}_7^{2+}$  species starts from pH 5 and corresponds to 15% at pH 6, where  $(\text{UO}_2)_3\text{OH}_5^{2+}$  is a dominant species with a proportion of 60% (Fig.41b).

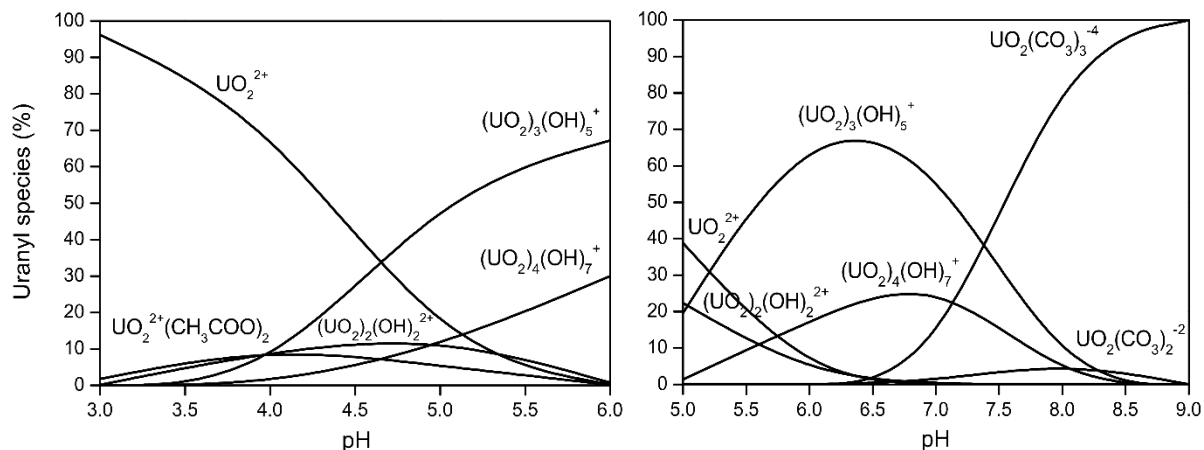


Fig.41 - Distribution of uranyl aqueous species: a) from pH 3 to pH 6, using  $6.00 \times 10^{-4}\text{M}$  ( $\text{UO}_2^{2+}$ ) and  $1.00 \times 10^{-2}\text{M}$  (NaCl) and b) from pH 5 to pH 9, using  $1.00 \times 10^{-4}\text{M}$  ( $\text{UO}_2^{2+}$ ) and  $2.00 \times 10^{-1}\text{M}$  (NaCl), considering the atmospheric  $\text{CO}_2$  effect ( $P=39\text{ Pa}$ ).

Uranyl carbonate species start to be formed from pH 6.5 in the presence of CO<sub>2</sub> (g), becoming the predominant species in alkaline conditions (Fig.41). The negative charge of uranyl carbonate complexes will compromise the adsorption on partially ionized edge sites. The UO<sub>2</sub><sup>2+</sup> is under saturated in solution and precipitation did not occur, under the imposed conditions in batch experiments.

#### 4.7.5.4. Modelling the sorption isotherms

The calculated isotherm parameters obtained from Langmuir, Freundlich and SIPS models are summarized in Table 19. The Freundlich isotherms revealed a good fit for lower amounts of UO<sub>2</sub><sup>2+</sup> adsorbed (Fig.42), confirming the heterogeneity of different energetic sites available for sorption experiments at pH 4 and pH 6. However, the experimental results are better described by Langmuir isotherm (Fig.42) when the saturation point approaches once predicts a maximum adsorption capacity ( $q_m$ ). The SIPS isotherm (Fig.42) resulted from the Freundlich and Langmuir isotherms provides the best fit of the experimental results with the higher correlation coefficients. The maximum amounts adsorbed estimated by SIPS isotherm predicts a monolayer adsorption capacity when higher UO<sub>2</sub><sup>2+</sup> concentrations are used and the saturation point is reached. Different amounts of UO<sub>2</sub><sup>2+</sup> were adsorbed by smectite at pH=4 (Table 19) such as: samples BA1 and PS3 absorbed 25% and 32% of their respective CEC, whereas sample PS2 adsorbed 44% of CEC.

Assuming that ion-exchange is the dominant adsorption mechanism under these specific conditions, three main considerations are proposed to explain the results obtained: (1) The selectivity of the exchangeable cations in the interlayer space of smectite is highly influenced by the size and valence of cation, where the preference for metal adsorption will increase as greater is the cation charge and smaller is atomic radius (Wilson, 2013). Both Na<sup>+</sup> and Ca<sup>2+</sup> are exchangeable cations segregated into interlayers of smectite and the cation selectivity is a function of layer charge. The Ca<sup>2+</sup> is preferentially kept in the interlayer site, while Na<sup>+</sup> is more easily removed by UO<sub>2</sub><sup>2+</sup> (Tsunashima et al., 1981). The interlayer composition of samples BA1 and PS3 have lower Na<sup>+</sup> compositions (43% and 50%, respectively) than sample PS2 (63%). Also, the Na<sup>+</sup>/Ca<sup>2+</sup> ratio (Table 17) reveals the major proportion of Na<sup>+</sup> in sample PS2, which may explain its higher capacity to adsorb UO<sub>2</sub><sup>2+</sup> by ion-exchange. (2) The increase of tetrahedral substitution (beidellite component) reduces the distance between the adsorbed ion and the negative charge of smectite (Ferrage et al., 2005; Ferrage et al., 2007; Teich-McGoldrick et al., 2015), producing strong interactions

between  $\text{UO}_2^{2+}$  and the internal surface of smectite. The lower proportion of tetrahedral substitutions of sample PS2 favored the release of cations from the interlayer space, enhancing the  $\text{UO}_2^{2+}$  uptake. (3) The different expansion ability of the interstratified structure (heterogeneous character) used in sorption experiments influenced the adsorption process. Ca-smectite expands slightly limiting the contaminant diffusion, whereas Na-smectite will be completely dispersed in water enhancing the exchange process (Dorfner Walter, 1991).

The heterogeneity factor ( $n$ ) obtained from the SIPS isotherm is lower at  $\text{pH}=4$ , indicating a lower heterogeneity of surface sites energy. Thus, the isotherms are concave (downward) and the contaminant (i.e.,  $\text{UO}_2^{2+}$ ) is weakly bonded to the surface if  $n < 1$  (Schwarzenbach et al., 2005; Vallero, 2010). In this case, it may be confirmed that  $\text{UO}_2^{2+}$  is adsorbed through weaker electrostatic interactions, when compared to that observed at  $\text{pH}$  6, when outer-sphere complexes in the interlayer site were formed. The lower sorption affinity is also confirmed by the lower  $K_s$  values obtained (Table 19).

Adsorption on the edge sites is strongly  $\text{pH}$ -dependent due to the presence of amphoteric surface sites. The ion exchange process is inhibited at  $\text{pH}$  6 and high ionic strength, where the adsorption occurs through the formation of  $\text{UO}_2^{2+}$  inner-sphere complexes strongly bonded onto smectite surface. The  $K_s$  also confirms this tendency (Table 19), considering the greater values obtained, indicating more favourable sorption sites. In these conditions, there is a significant decrease of the amount adsorbed (Table 19), when compared with that at  $\text{pH}$  4, since only 10-20% of the total surface charge corresponds to the edge surface sites. However, the uptake efficiency was much higher at  $\text{pH}$  6 as increasing of  $\text{UO}_2^{2+}$  concentration, once the ratio between the amounts adsorbed per mass of smectite and the amounts of  $\text{UO}_2^{2+}$  remaining in solution at equilibrium were also significantly higher.

Taking into account the contribution of the variable charge into the total net layer charge, the edge surface sites represent 15% of the total number of available sites for sorption. In this case only 32% (sample BA1), 33% (sample PS2) and 41% (sample PS3) of the external reactive sites were completely filled by  $\text{UO}_2^{2+}$  at  $\text{pH}$  6 (Table 18). The obtained proportions for samples BA1 and PS2 were expected, if we take into account the overall isoelectric point of smectite.

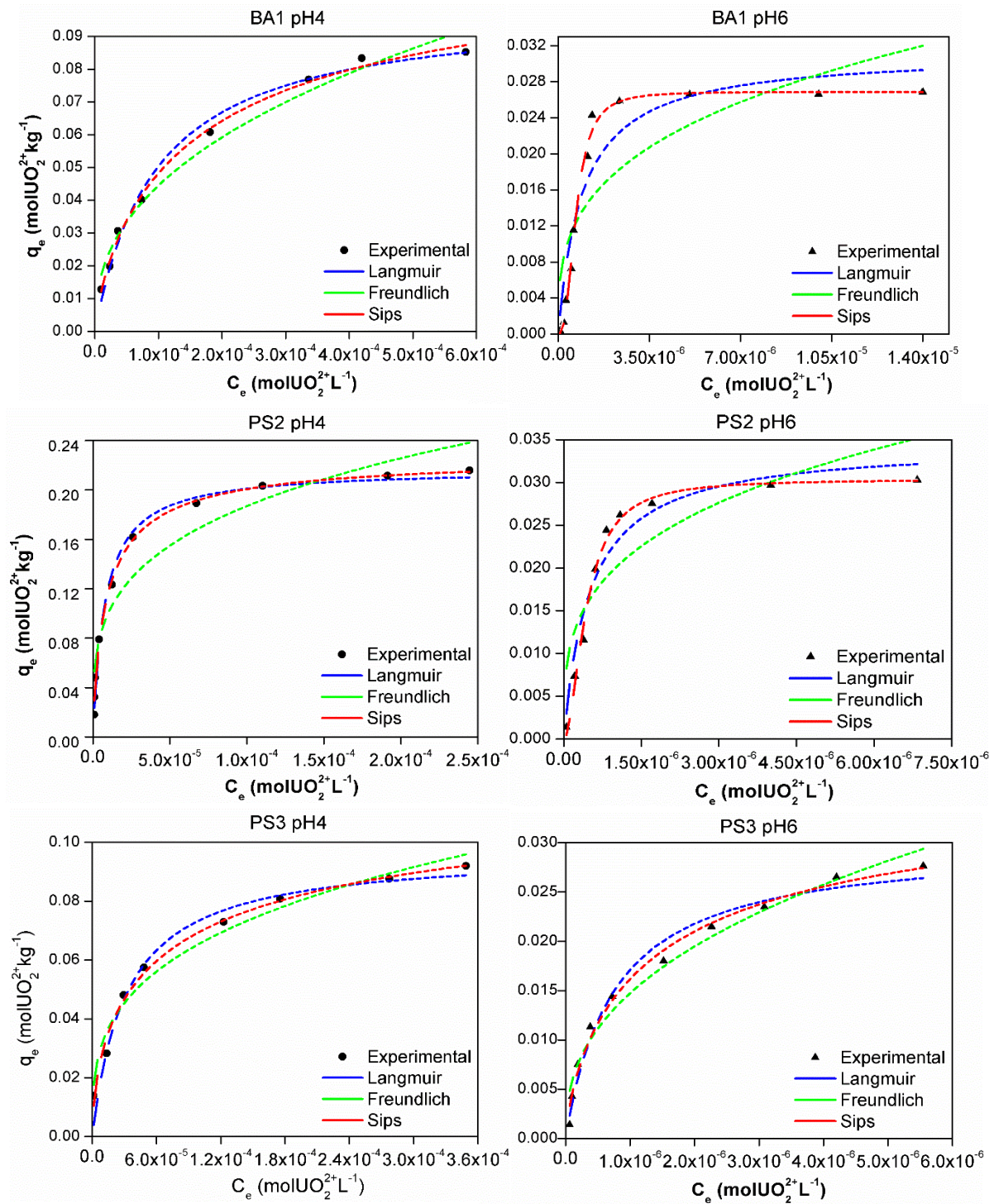


Fig.42 - Adsorption isotherms describing the  $\text{UO}_2^{2+}$  adsorption onto different smectites at pH 4 ( $I=0.02\text{M}$ ) and pH 6 ( $I=0.2\text{M}$ ).

Table 19. Isotherm parameters obtained from Langmuir, Freundlich and SIPS models fit to sorption data.

Smectite	Isothermal model	Model Parameters	Sorption experiments		
			pH 4 (I=0.02 M)	pH 6 (I=0.2M)	
BA1	Langmuir	$K_L$	$1.03 \times 10^4$	$1.07 \times 10^6$	
		$q_m$ (mol/Kg)	0.10	0.031	
		$r^2$	0.99	0.89	
	Freundlich	$K_F$	1.97	1.07	
		N	0.41	0.31	
		$r^2$	0.98	0.69	
	SIPS	$K_s$	$5.77 \times 10^3$	$1.45 \times 10^6$	
		$q_m$ (mol/Kg)	0.12	0.027	
		N	0.77	2.60	
			$r^2$	0.99	0.99
	PS2	Langmuir	$K_L$	$1.26 \times 10^5$	$1.97 \times 10^6$
			$q_m$ (mol/Kg)	0.22	0.034
$r^2$			0.99	0.94	
Freundlich		$K_F$	2.28	1.15	
		N	0.27	0.29	
		$r^2$	0.91	0.75	
SIPS		$K_s$	$1.04 \times 10^5$	$2.29 \times 10^6$	
		$q_m$ (mol/Kg)	0.23	0.030	
		N	0.83	1.87	
			$r^2$	0.99	0.99
PS3		Langmuir	$K_L$	$3.14 \times 10^4$	$1.32 \times 10^6$
			$q_m$ (mol/Kg)	0.10	0.030
	$r^2$		0.97	0.98	
	Freundlich	$K_F$	1.09	3.86	
		N	0.30	0.40	
		$r^2$	0.97	0.97	
	SIPS	$K_s$	$1.25 \times 10^4$	$6.88 \times 10^5$	
		$q_m$ (mol/Kg)	0.13	0.038	
		N	0.60	0.75	
			$r^2$	0.99	0.99

A higher proportion of illite layers ( $\approx 30\%$ ) identified in sample PS3 results in an increase of variable charge contribution in the total charge of illite/smectite, assuming a higher ratio between the edge and the basal (total) surface area (Huang et al., 2011). These structural changes affect the surface charge density of smectite, which is inversely proportional to the total number of reactive surface functional groups (Turner and Sassman, 1996). In this way, the adsorption on the edge surface sites has a greater influence in the total amount of  $\text{UO}_2^{2+}$  adsorbed on sample PS3 and their higher proportion of reactive sites may be associated with their lower charge density ( $\text{CD}=0.59 \text{ nm}^2/\text{site}$ ), when compared with samples BA1 ( $4.82 \text{ nm}^2/\text{site}$ ) and PS2 ( $2.26 \text{ nm}^2/\text{site}$ ). The higher number of reactive sites of sample PS3 justifies their higher adsorption capacity.

The increases of the energetic heterogeneity on edge surfaces, as new binding sites are formed, are suggested by the increase of the heterogeneity factors (**n**) at pH 6 (Table 19). The highly energetic sites are covered first, followed by successive occupation of sites with lower affinity. The  $\text{UO}_2^{2+}$  total concentration will define the degree of coverage of the available sites (Pabalan et al., 1996).

#### 4.7.5.5. Surface complexation and cation exchange modelling

The model applied to reproduce the  $\text{UO}_2^{2+}$  adsorption on smectite was able to provide a good fit with the experimental data obtained. The model simulation and the experimental data are represented in Fig.43 by the logarithm of sorption of  $\text{UO}_2^{2+}$  on smectite at pH 4 (0.02M) and pH 6 (0.2M) as function of logarithm of  $\text{UO}_2^{2+}$  equilibrium concentration. The RMSE values obtained at pH 4 (0.28, 0.33 and 0.40 for samples BA1, PS2 and PS3, respectively) and at pH 6, (0.06, 0.03 and 0.02) are in agreement with our experimental data obtained at both pH conditions. Accordingly, the uranyl adsorption on smectite at pH 4 could be explained by the formation of surface complexes with the permanent charged sites ( $\text{UO}_2\text{X}_2$ ) and the edge surface sites such as: aluminol ( $\equiv\text{AlOUO}_2^+$ ) and silanol ( $\equiv\text{SiOUO}_2^+$ ) sites. The contribution of the permanent charged sites is negligible ( $<1\%$ ) when compared with the surface complexation onto the aluminol and silanol sites at pH 6.

As expected, the results also reveal that the aluminol sites are more reactive than the silanol sites, and the  $\equiv\text{AlOUO}_2^+$  was the major surface species at both pH conditions. In this case, the surface complexes formed did not correspond directly to the major species detected in the U(VI) aqueous speciation, once the  $\equiv\text{AlOUO}_2^+$  and  $\equiv\text{SiOUO}_2^+$  occurred above the pH where  $\text{UO}_2^{2+}$  is dominant. The models described in literature (Korichi and Bensmaili, 2009; McKinley et al., 1995; Turner et al., 1996; Turner and

Sassman, 1996) show that the  $\text{UO}_2^{2+}$  adsorption on smectite does not form a second inner-sphere complex ( $\equiv\text{SOUO}_2(\text{OH})_5$ ) until much higher pH values and there is no evidence that this surface complex has been adsorbed through inner-sphere complexation on the edge sites of smectite (Chisholm-Brause et al., 2001). Our results revealed that the proportions of  $\equiv\text{SOUO}_2(\text{OH})_5$  species were lower than 3% for all the experiments and not represented in Fig.43.

The proportions obtained for each sorption mechanism studied at different pH are shown in Table 20. In the case of lower  $\text{UO}_2^{2+}$  concentrations, the proportions of  $\text{UO}_2^{2+}$  adsorbed either by cation exchange or surface complexation on the edge-sites are close for all smectite samples (Fig.43). However, the difference between both sorption mechanisms is very significant for sample PS2 as increasing of  $\text{UO}_2^{2+}$  concentration, which shows a proportion of  $\approx 80\%$  for cation exchange and  $\approx 20\%$  for surface complexation. This result confirms that cation exchange was favoured for sample PS2, where the proportion of  $\text{Na}^+$  ions in the interlayer composition was higher and the amount of  $\text{UO}_2^{2+}$  exchanged was more significant ( $\frac{\text{UO}_2^{2+}}{\text{Na}^+} K_c = 2.82$ ). By contrast, sample BA1 revealed the lower ratio between the amount of  $\text{UO}_2^{2+}$  adsorbed and their cation exchange capacity and show identical proportions of  $\text{UO}_2^{2+}$  adsorbed on smectite by cation exchange and surface complexation for all the concentration range (Table 20). It confirms that the results provided by this model are in concordance with our previous conclusions, which assumed the higher proportion of  $\text{Ca}^{2+}$  in the interlayer composition and the position of negative layer charge as the main factors inhibiting the cation exchange process ( $\frac{\text{UO}_2^{2+}}{\text{Ca}^{2+}} K_c = 1.12$ ).

Table 20. Proportions of  $\text{UO}_2^{2+}$  adsorbed (%) by cation exchange and by surface complexation on the edge sites.

Sorption mechanism	BA1 (%)		PS2 (%)		PS3 (%)	
	pH 4	pH 6	pH 4	pH 6	pH 4	pH 6
Cation Exchange ( $\text{UO}_2\text{X}_2$ )	48-59*	0	53-81*	0	82-72*	0
Surface complexation (total)	51-41*	100	47-19*	100	18-28*	100
$\text{AlOUO}_2^+$	98-92*	95-84*	95-86*	91-81*	48-55*	95-86*
$\text{SiOUO}_2^+$	2-8*	5-16*	5-14*	9-19*	52-45*	5-14*

\* Variation of proportions obtained from the lower to the higher  $\text{UO}_2^{2+}$  concentrations used in different sorption experiments.

Therefore, the structural changes of smectite samples, which hampers the ion-exchange process, contribute to decrease the total amount of  $UO_2^{2+}$  adsorbed but does not affect the adsorption on the edge sites of smectite, where stronger sorption complexes are formed, reducing the risk of reversibility of the  $UO_2^{2+}$  previously adsorbed.

The modelling results obtained at pH 6 indicate that the ratio between the proportion of  $\equiv AlOUO_2^+$  and  $\equiv SiOUO_2^+$  surface complexes increased as increasing of  $UO_2^{2+}$  concentrations. However, the proportion of surface complexes on the aluminol sites was higher than 75%, indicating a high reactivity of the aluminol sites at near-neutral pH conditions.

#### 4.7.5.1. X-ray photoelectron spectroscopy

The XPS spectra corresponding to  $U4f_{7/2}$  binding energy of  $UO_2^{2+}$  adsorbed at pH 4 and 6 on smectite (samples BA1, PS2 and PS3) are shown in Fig.44. The atomic concentration (%) and the Si/U and Al/U atomic ratios of the studied samples after  $UO_2^{2+}$  sorption in batch experiments are shown in Table 21.

Table 21. The element composition in atomic concentration (%) and the Si/U and Al/U atomic ratios of the studied samples after  $UO_2^{2+}$  sorption in batch experiments.

pH	Samples	Atomic Concentration (%)						Si/U	Al/U
		Si	O	Al	C	U			
4	BA1	21.06	57.66	7.18	13.69	0.13	162	55	
	PS2	20.56	56.84	7.18	15.08	0.17	121	42	
	PS3	20.53	55.74	7.33	13.50	0.13	158	56	
6	BA1	20.56	59.98	6.36	8.48	0.02	1028	318	
	PS2	19.36	59.56	7.43	8.48	0.04	484	186	
	PS3	19.13	60.97	7.57	8.31	0.05	383	151	

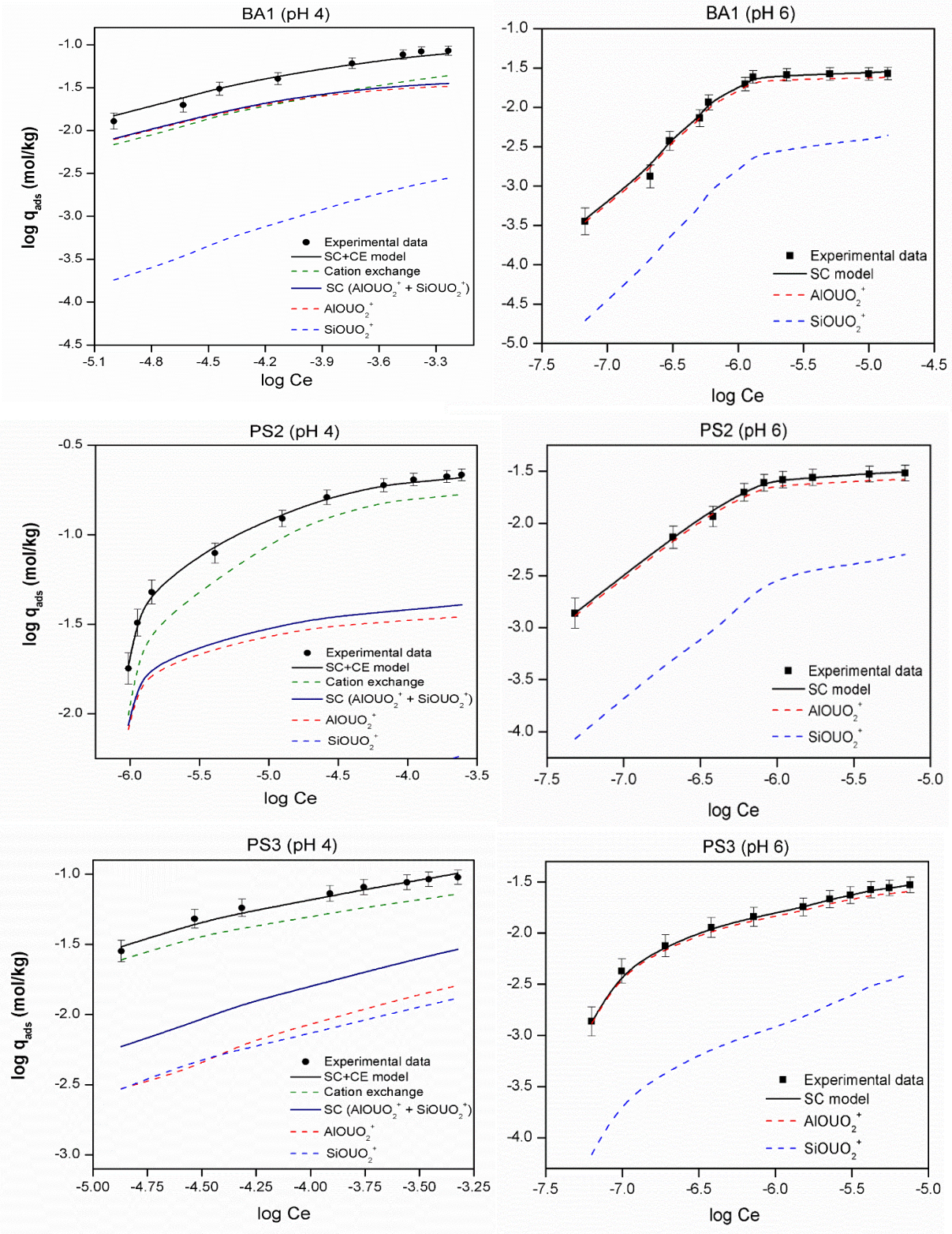


Fig.43 - Sorption of  $UO_2^{2+}$  on smectite at pH4 ( $I=0.02M$ ) and pH 6 ( $I=0.2M$ ) as function  $UO_2^{2+}$  equilibrium concentration and its model simulation.

The binding energies obtained after the deconvolution of the  $U4f_{7/2}$  peak are shown in Table 22. Two binding energy components at  $382.2 \pm 0.3$  eV and  $380.8 \pm 0.3$  eV (Fig.44) were obtained after the  $U4f_{7/2}$  peak deconvolution correspond to  $UO_2^{2+}$  adsorbed on smectite at pH 4 and low ionic strength ( $I=0.02$  M). Two different binding energy components, at 383.7 eV and 382.6 eV, assigned to the  $[UO_2(H_2O)_5]^{2+}$  adsorption via ion exchange onto montmorillonite (acidic conditions) and to free  $UO_2^{2+}$  adsorption onto aluminol edge sites, were obtained by Drot et al. (2007) and Kowal-Fouchard et al. (2004). These results are in agreement with the previous conclusions obtained by other authors, who demonstrated using molecular spectroscopic probes, the existence of both exchange-sites and edge-sites surface complexes of  $UO_2^{2+}$  on smectite (Chisholm-Brause et al., 1994; Morris et al., 1994; Sylwester et al., 2000).

The binding energy components obtained in our work reveal the effect of structural heterogeneity of smectite samples on the  $UO_2^{2+}$  sorption behaviour. This is also supported by surface complexation and cation exchange model developed in this study. A correlation between the proportion for each binding energy component (Table 22) and the proportion of  $UO_2^{2+}$  adsorbed (%) by cation exchange and by surface complexation on the edge sites (Table 20) was obtained.

Table 22. Binding energies and relative proportions of the two components fitted to  $U4f$  spectra, obtained from U(VI)-smectite samples.

Smectite	BE (eV) and relative proportions (%)			
	pH 4 ( $I=0.02M$ )		pH6 (0.2M)	
	BE (eV) I	BE (eV) II	BE (eV) I	BE (eV) II
BA1	382.2 (57%)	380.8 (43%)	381.9 (33%)	380.3 (67%)
PS2	382.2 (77%)	380.8 (23%)	381.9 (27%)	380.3 (73%)
PS3	382.2 (71%)	380.8 (29%)	381.7 (30%)	380.3 (70%)

Sample PS2 reveal a major difference between cation exchange and surface complexation expressed by the following proportions of 80% and 20%. Also, a close distribution was identified concerning the proportions between high (77%) and low (23%) binding energy components. The same behavior was also verified for samples BA1, where the cation exchange process was less pronounced and the difference between the proportions of  $UO_2^{2+}$  surface species adsorbed by cation exchange (59%) and surface

complexation (41%) was less significant according with the surface complexation model. Identical proportions were also confirmed by XPS results for sample BA1 where 57% was attributed to high binding energy component and 43% for the low binding energy component.

The sorption behavior of sample PS3 revealed higher sorption capacity by cation exchange than sample BA1 and lower sorption capacity than sample PS2. In this case, 72% and 71% of  $\text{UO}_2^{2+}$  were adsorbed by cation exchange through outer-sphere complexation according to the surface complexation model (Fig.44) and the XPS results (Fig.44), respectively, whereas 28% and 29% were adsorbed by surface complexation on the edge sites. Considering the concordance of both methods, we assumed that the two components detected at pH 4 are represented by the same species  $[\text{UO}_2(\text{H}_2\text{O})_5]^{2+}$ , but adsorbed under different binding strengths through cation exchange and inner-sphere complexation on the edge sites of smectite.

The  $\text{U}4f_{7/2}$  binding energy depends on the length of the  $\text{U-O}_{\text{eq}}$  bonds, which controls the electron density redistribution to or away from U(VI) centers (Del Nero et al., 2004; Ilton and Bagus, 2011). The lower binding energy corresponds to strong-binding complexes onto surface and short  $\text{U-O}_{\text{eq}}$  lengths that contribute with more electron density around U(VI), enhancing the electron removal (Del Nero et al., 2004; Ilton and Bagus, 2011; Sylwester et al., 2000). In such way, the stronger inner-sphere complexation on the aluminol and silanol sites was assigned to the lower binding energy ( $380.8 \pm 0.3$  eV), whereas the cation exchange process characterized by the weaker attraction between  $\text{UO}_2^{2+}$  and smectite surface was identified by the components appearing at higher binding energy ( $382.2 \pm 0.3$  eV).

The adsorption of  $\text{UO}_2^{2+}$  species at pH 6 and high ionic strength ( $I=0.2\text{M}$ ) is restricted to the edge surface complexation sites, where the  $\equiv\text{AlOUO}_2^+$  and  $\equiv\text{SiOUO}_2^+$  are the major adsorbed species (Chisholm-Brause et al., 2001; Turner et al., 1996). The two new components obtained at  $380.3 \pm 0.3$  eV and  $381.8 \pm 0.3$  eV after  $\text{U}4f_{7/2}$  peak deconvolution, correspond in fact to  $\equiv\text{AlOUO}_2^+$  and  $\equiv\text{SiOUO}_2^+$  species taking into account the surface complexation model developed (Table 20).

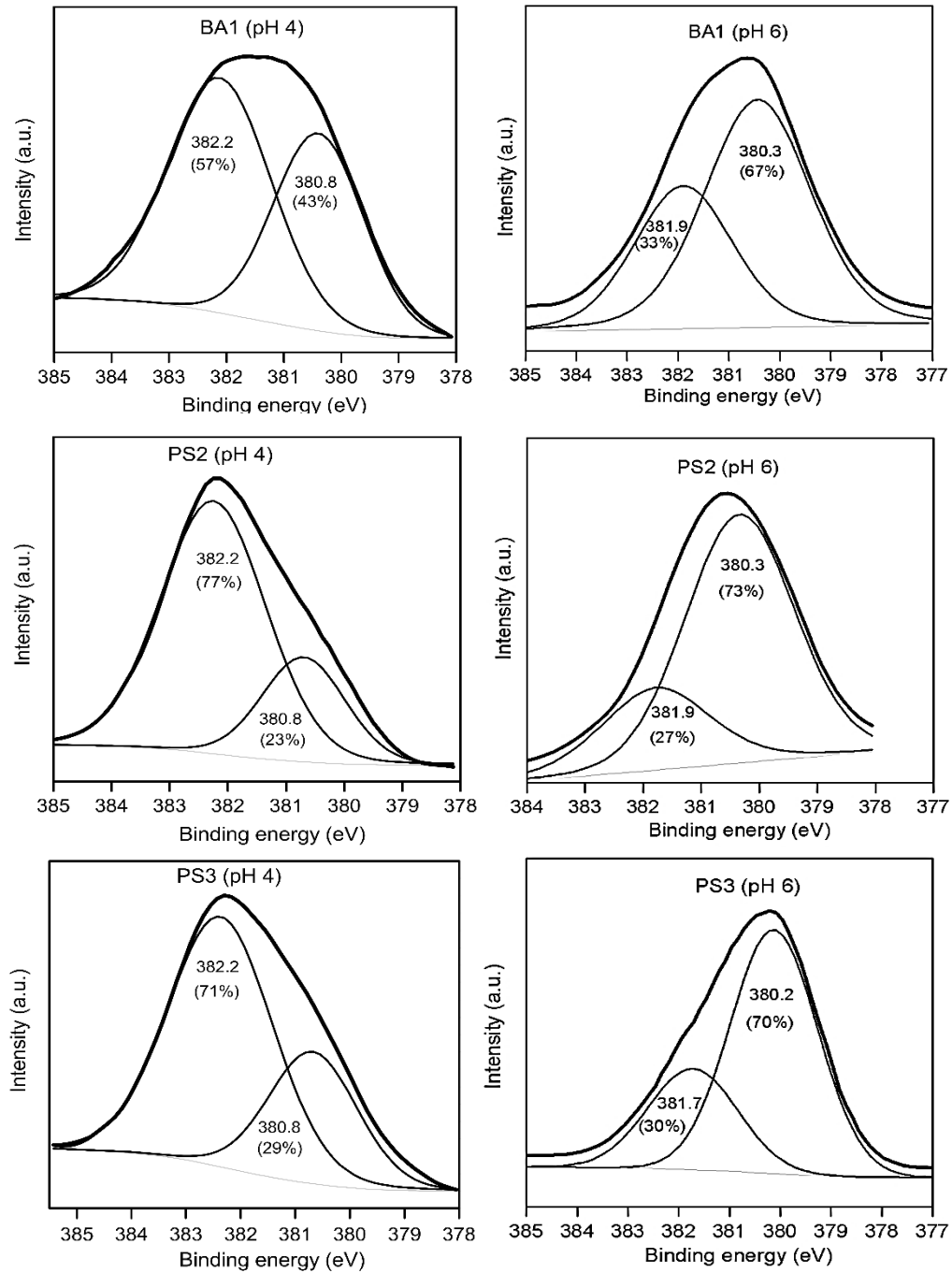


Fig.44 - U<sub>4f<sub>7/2</sub></sub> XPS spectra of the U(VI)-smectite samples (BA1, PS2 and PS3), obtained at pH 4 (I=0.02M) and pH 6 (I=0.2M), and fitting curves showing a contribution of two components for UO<sub>2</sub><sup>2+</sup> ions.

The similar proportions of each component for all the adsorbents, suggest that the structural changes did not affect significantly the adsorption behaviour when it is controlled

by the reactivity of the edge surface sites. Moreover, the higher proportion observed for the component corresponding to the lower binding energy confirms the larger affinity of the aluminol sites to adsorb  $\text{UO}_2^{2+}$ . The binding strength of different complexes formed on the surface groups will depend of the attraction of the metal lattice ( $\text{Al}^{3+}$ ,  $\text{Mg}^{2+}$ ,  $\text{Fe}^{3+}$ ,  $\text{Si}^{4+}$ ), given by valence coordination number ratio values, on surface oxygen electrons: As greater is this attraction force, weaker is the attraction of the surface oxygen on the proton proton (Froideval et al., 2003). Although the silanol group is primarily negatively charged at the same pH conditions, their lower tendency to donate its oxygen electrons and form inner-sphere complexes justifies the lower proportion of  $\equiv\text{SiOUO}_2^+$  surface species obtained (Drot et al., 2007; Kowal-Fouchard et al., 2004).

#### 4.7.6. Conclusion

Smectite samples (BA1, PS2 and PS3) with a heterogeneous structure characterized by different interlayer compositions, distinct charge deficit and distribution, and interstratified structure were used in  $\text{UO}_2^{2+}$  sorption experiments at pH 4 with low ionic strength ( $I=0.02\text{M}$ ) and pH 6 with high ionic strength ( $I=0.2\text{M}$ ). The results obtained show that the increase of layer substitutions and the proximity between the negative charge on tetrahedral sheet and the contaminant have reduced the interlayer distances, restricting the ion-exchange process. Sample BA1 has higher tetrahedral charge than PS2 but lower cation exchange capacity, whereas sample PS3 has the higher proportion of illite interstratified layers ( $\approx 30\%$ ) and the lower number of available sites for ion-exchange. Samples BA1, PS2 and PS3 have 43%, 63% and 50% of  $\text{Na}^+$  available for cation exchange, which adsorbed 25% (0.12 mol/kg), 44% (0.23 mol/kg) and 32% (0.10 mol/kg) of their respective CEC at pH 4. This reveals a strong competition between  $\text{Ca}^{2+}$  and  $\text{UO}_2^{2+}$  that restricted the sorption capacity mainly on sample BA1. The ion exchange was significantly reduced at pH 6 and higher ionic strength, where the amount of  $\text{UO}_2^{2+}$  adsorbed correspond to 32%, 33% and 41% of the total number of reactive external sites. Sorption capacity is related closely to the CEC, which is a function of total surface area and the smectite layer charge. The total surface area calculated increases as the mean crystal thickness distribution decreases and the CEC increases as total surface area increases.

A cation exchange and surface complexation model based on diffuse double layer was successfully developed, in order to predict the  $\text{UO}_2^{2+}$  sorption on smectite. The RMSE

values (%) < 0.40 for all the experiments confirm a good fit to the experimental data. The modelling results showed that  $\text{UO}_2^{2+}$  was simultaneously adsorbed in the interlayer charged sites by cation exchange reaction and through inner-sphere surface complexation into the variable charged sites at pH 4 ( $I=0.02\text{M}$ ). This reveals that samples PS2 and PS3 have higher tendency to adsorb  $\text{UO}_2^{2+}$  through ion exchange, and sample BA1 has similar proportions of  $\text{UO}_2^{2+}$  absorbed by both mechanisms. The modelling results at pH 6 ( $I=0.2\text{M}$ ) indicate that the sorption mechanism was restricted to surface complexation on the external sites of smectite where  $\equiv\text{AlOUO}_2^+$  and  $\equiv\text{SiOUO}_2^+$  were the major surface species.

The XPS results are in agreement with the modelling obtained at both pH conditions. Two different components at  $380.8\pm 0.3$  and  $382.2\pm 0.3$  eV at pH 4 after the  $\text{U}4f_{7/2}$  peak deconvolution were assigned to hydrated  $\text{UO}_2^{2+}$  adsorbed by inner-sphere complexation on the external sites of smectite and adsorbed by cation exchange, respectively. Two new binding energy components at  $380.3\pm 0.3$  and  $381.8\pm 0.3$  eV identified at pH 6 correspond to  $\equiv\text{AlOUO}_2^+$  and  $\equiv\text{SiOUO}_2^+$  surface species, respectively.

### Acknowledgements

The first author benefited a PhD scholarship (Ref. SFRH/BD/79969/2011) financed by Fundação para a Ciência e Tecnologia (FCT), Portugal. This work was funded by FEDER fund through the Operational Program Competitiveness Factors e COMPETE and by National funds through FCT. The financial support of project P12-RNM-1565 from Junta de Andalucía and FEDER funds is also acknowledged. The first author thanks to Dr. Maria Marques Fernandes and Dr. Bart Baeyens for very fruitful, constructive discussions and friendly accompany during the work visit in the Paul Scherrer Institute - Villigen, CH. The authors thank to Dr. Gianluca Li Puma for editorial handling and to the three anonymous reviewers for excellent critical review, helpful suggestions and for thorough reading of the initial manuscript.

### 4.7.7. References

- Anderson, S.J., Sposito, G., 1991. Cesium-Adsorption Method for Measuring Accessible Structural Surface Charge. *Soil Science Society of America Journal* 55, 1569-1576.
- Barshad, I., 1960. X-ray analysis of soil colloids by a modified salted paste method. *Proceedings 7th nat. Conf. Clays* 5, 350-364.
- Barshad, I., Kishk, F.M., 1970. Factors affecting potassium fixation and cation exchange capacities of soil vermiculite clays. *Clay and clay minerals* 18, 122-137.

- Bauer, A., Schafer, T., Dohrmann, R., Hoffmann, H., Kim, J.I., 2001. Smectite stability in acid salt solutions and the fate of Eu, Th and U in solution. *Clay Minerals* 36, 93–103.
- Bouchet, A., Proust, D., Meunier, A., Beaufort, D., 1988. High-charge to low-charge smectite reaction in hydrothermal alteration processes. *Clay Minerals* 23, 133-146.
- Bradbury, M.H., Baeyens, B., 2000. A generalised sorption model for the concentration dependent uptake of caesium by argillaceous rocks. *Journal of Contaminant Hydrology* 42, 141-163.
- Campos, B., Aguilar-Carrillo, J., Algarra, M., Gonçalves, M.A., Rodríguez-Castellón, E., Esteves da Silva, J.C.G., Bobos, I., 2013. Adsorption of uranyl ions on kaolinite, montmorillonite, humic acid and composite clay material. *Applied Clay Science* 85, 53-63.
- Catalano, J.G., Brown Jr, G.E., 2005. Uranyl adsorption onto montmorillonite: Evaluation of binding sites and carbonate complexation. *Geochimica et Cosmochimica Acta* 69, 2995-3005.
- Chen, H., Wang, A., 2007. Kinetic and isothermal studies of lead ion adsorption onto palygorskite clay. *Journal of Colloid and Interface Science* 307, 309-316.
- Chisholm-Brause, C., Conradson, S.D., Buscher, C.T., Eller, P.G., Morris, D.E., 1994. Speciation of uranyl sorbed at multiple binding sites on montmorillonite. *Geochimica et Cosmochimica Acta* 58, 3625-3631.
- Chisholm-Brause, C.J., Berg, J.M., Matzner, R.A., Morris, D.E., 2001. Uranium(VI) Sorption Complexes on Montmorillonite as a Function of Solution Chemistry. *Journal of Colloid and Interface Science* 233, 38-49.
- Christidis, G.E., Blum, A.E., Eberl, D.D., 2006. Influence of layer charge and charge distribution of smectites on the flow behaviour and swelling of bentonites. *Applied Clay Science* 34, 125-138.
- Dazas, B., Lanson, B., Delville, A., Robert, J.-L., Komarneni, S., Michot, L.J., Ferrage, E., 2015. Influence of Tetrahedral Layer Charge on the Organization of Interlayer Water and Ions in Synthetic Na-Saturated Smectites. *The Journal of Physical Chemistry C* 119, 4158-4172.
- Del Nero, M., Froideval, A., Gaillard, C., Mignot, G., Barillon, R., Munier, I., Özgümüş, A., 2004. Mechanisms of uranyl sorption. Geological Society, London, Special Publications 236, 545-560.
- Dorfner Walter, K., 1991. Ion Exchangers. Gruyter & Co., Berlin & New York.
- Drits, V., Eberl, D.D., Środoń, J., 1998. XRD measurement of mean thickness, thickness distribution and strain for illite and illite-smectite crystallites by the Bertaut-Warren-Averbach technique. *Clays and Clay Minerals* 46, 38-50.
- Drot, R., Roques, J., Simoni, É., 2007. Molecular approach of the uranyl/mineral interfacial phenomena. *Comptes Rendus Chimie* 10, 1078-1091.
- Eberl, D.D., 1978. The reaction of montmorillonite to mixed layer clay: The effect of interlayer alkali and alkaline earth cations. *Geochimica et Cosmochimica Acta* 42, 1-7.
- El Khames Saad, M., Khiari, R., Elaloui, E., Moussaoui, Y., 2014. Adsorption of anthracene using activated carbon and *Posidonia oceanica*. *Arabian Journal of Chemistry* 7, 109-113.
- Ferrage, E., Lanson, B., Sakharov, B.A., Drits, V.A., 2005. Investigation of smectite hydration properties by modeling experimental X-ray diffraction patterns: Part I: Montmorillonite hydration properties. *American Mineralogist* 90, 1358-1374.
- Ferrage, E., Lanson, B., Sakharov, B.A., Geoffroy, N., Jacquot, E., Drits, V.A., 2007. Investigation of dioctahedral smectite hydration properties by modeling of X-ray diffraction profiles: Influence of layer charge and charge location. *American Mineralogist* 92, 1731-1743.

- Froideval, A., Del Nero, M., Barillon, R., Hommet, J., Mignot, G., 2003. pH dependence of uranyl retention in a quartz/solution system: an XPS study. *Journal of Colloid and Interface Science* 266, 221-235.
- Giaquinta, D.M., Soderhom, L., Yuchs, S.E., Wasserman, S.R., 1997. The speciation of uranium in smectite clay: Evidence for catalyzed uranyl reduction. *Radiochimica Acta* 76, 113–121.
- Greathouse, J.A., Cygan, R.T., 2006. Water structure and aqueous uranyl (VI) adsorption equilibria onto external surfaces of beidellite, montmorillonite, and pyrophyllite: results from molecular simulations. *Environmental Science and Technology* 40, 3865–3871.
- Greene-Kelly, R., 1952a. Irreversible dehydration in montmorillonite. *Clay Minerals Bull.* 1, 221
- Greene-Kelly, R., 1952b. Irreversible dehydration in montmorillonite. *Clay Minerals Bulletin* 1, 221-225.
- Grenthe, I., Fuger, J., Konings, R., Lemire, R.J., Nguyen-Trung, C., Muller, A.B., Wanner, J., 1992. *The chemical thermodynamics of uranium*. Elsevier, New York.
- Guillaumont, R., Fanghänel, T., Fuger, J., Grenthe, I., Neck, V., Palmer, D.A., Rand, M.H., 2003. *Update on the Chemical Thermodynamics of Uranium, Neptunium, Plutonium, Americium and Technetium*. Elsevier Science, Amsterdam.
- Guimarães, V., Rocha, F., Bobos, I., 2015a. Reactivity of heterogeneous smectites from Portugal. *Clay minerals* (submitted).
- Guimarães, V., Rodríguez-Castellón, E., Algarra, M., Rocha, F., Bobos, I., 2015b. Kinetics of uranyl ions sorption on heterogeneous smectite structure at pH 4 and 6 using a continuous stirred flow-through reactor. *Applied Clay Science* (accepted).
- Harward, M.E., 1967. Properties of Vermiculites and Smectites: Expansion and Collapse. *Clays and Clay Minerals* 15, 179.
- Harward, M.E., Carstea, D., Sayegh, A., 1968. Properties of vermiculite and smectites: Expansion and Collapse. *Clays and clay minerals* 15, 179.
- Hennig, C., Reich, T., Dahn, R., Scheidegger, A.M., 2002. Structure of uranium sorption complexes at montmorillonite edge sites. *Radiochimica Acta* 90, 653-657.
- Herbelin, A.L., Westall, J.C., 1999. FITEQL 4.0: a Computer program for determination of chemical equilibrium constants from experimental data; Report 99-01. Department of Chemistry, Oregon State University, Corvallis.
- Huang, P.M., Li, Y., Sumner, M.E., 2011. *Handbook of Soil Sciences: Properties and Processes*, Second Edition. Taylor & Francis, p. 1442.
- Hudson, E.A., Terminello, L.J., Viani, B.E., Denecke, M.A., Reich, T., Allen, P.G., Bucher, J.J., Shuh, D.K., Edelman, N.M., 1999. The structure of U<sup>6+</sup> sorption complexes on vermiculite and hydrobiotite. *Clays and Clay Minerals*, 439–457.
- Hyun, S.P., Cho, Y.H., Hahn, P.S., Kim, S.J., 2001. Sorption mechanism of U(VI) on a reference montmorillonite: Binding of the internal and external surfaces. *Journal of Radioanalytical and Nuclear Chemistry* 250, 55-62.
- Ilton, E.S., Bagus, P.S., 2011. XPS determination of uranium oxidation states. *Surface and Interface Analysis* 43, 1549-1560.
- Inoue, A., Utada, M., Wakita, K., 1992. Smectite-to-illite conversion in natural hydrothermal systems. *Applied Clay Science* 7, 131-145.
- Jackson, M.L.R., Barak, P., 2005. *Soil Chemical Analysis: Advanced Course*. Parallel Press, University of Wisconsin-Madison Libraries, USA.
- Jeppu, G.P., Clement, T.P., 2012. A modified Langmuir-Freundlich isotherm model for simulating pH-dependent adsorption effects. *Journal of Contaminant Hydrology* 129–130, 46-53.

- Kim, S.J., 2001. Sorption mechanism of U(VI) on a reference montmorillonite: Binding to the internal and external surfaces. *Journal of Radioanalytical and Nuclear Chemistry* 250, 55-62.
- Korichi, S., Bensmaili, A., 2009. Sorption of uranium (VI) on homoionic sodium smectite experimental study and surface complexation modeling. *Journal of Hazardous Materials* 169, 780-793.
- Kowal-Fouchard, A., Drot, R., Simoni, E., Ehrhardt, J.J., 2004. Use of Spectroscopic Techniques for Uranium(VI)/Montmorillonite Interaction Modeling. *Environmental Science & Technology* 38, 1399-1407.
- Laird, D.A., 2006. Influence of layer charge on swelling of smectites. *Applied Clay Science* 34, 74-87.
- Langmuir, I., 1916. The constitution and fundamental properties of solids and liquids. Part I. Solids. *Journal of the American Chemical Society* 38, 2221-2295.
- Lee, J.O., Kang, I.M., Cho, W.J., 2010. Smectite alteration and its influence on the barrier properties of smectite clay for a repository. *Applied Clay Science* 47, 99-104.
- Marques Fernandes, M., Baeyens, B., Dähn, R., Scheinost, A.C., Bradbury, M.H., 2012. U(VI) sorption on montmorillonite in the absence and presence of carbonate: A macroscopic and microscopic study. *Geochimica et Cosmochimica Acta* 93, 262-277.
- Maurer, S., 2000. Prediction of Single Component Adsorption Equilibria. Utz, Wiss.
- McKinley, J.P., Zachara, M., Smith, S.C., Turner, G.D., 1995. The influence of hydrolysis and multiple site-binding reactions on adsorption of U(VI) to montmorillonite. *Clays and Clay Minerals* 43, 586-598.
- Meunier, A., Proust, D., Beaufort, D., Lajudie, A., Petit, J.C., 1992. Heterogeneous reactions of dioctahedral smectites in illite-smectite and kaolinite-smectite mixed-layers: applications to clay materials for engineered barriers. *Applied Geochemistry* 1, 143-150.
- Morris, D.E., Chisholm-Brause, C.J., Barr, M.E., Conradson, S.D., G., E.P., 1994. Optical spectroscopic studies of the sorption of UO<sub>2</sub><sup>2+</sup> species on a reference smectite. *Geochimica et Cosmochimica Acta* 58, 3613-3623.
- Musso, T.B., Parolo, M.E., Pettinari, G., Francisca, F.M., 2014. Cu(II) and Zn(II) adsorption capacity of three different clay liner materials. *Journal of Environmental Management* 146, 50-58.
- Olguin, M.T., Solache-Rios, M., Acosta, D., Bosch, P., Bulbulian, S., 1997. UO<sub>2</sub><sup>2+</sup> sorption on bentonite. *Journal of Radioanalytical and Nuclear Chemistry* 218, 65-69. 218, 65-69.
- Pabalan, R.T., Bertetti, F.P., Prikryl, J.D., Turner, D.R., 1996. Uranium (VI) sorption onto selected mineral surfaces: Key geochemical parameters. *Abstracts of Papers of the American Chemical Society* 211:55-Geoc.
- Pabalan, R.T., Turner, D.R., 1997. Uranium(VI) sorption on montmorillonite: Experimental and surface complexation modeling study. *Aquatic Geochem.* 2, 203-226.
- Papirer, E., 2000. *Adsorption on Silica Surfaces*. Taylor & Francis, New York.
- Parkhurst, D.L., Appelo, C.A.J., 2013. Description of input and examples for PHREEQC version 3--A computer program for speciation, batch- reaction, one-dimensional transport, and inverse geochemical calculations, Description of input and examples for PHREEQC version 3. U.S. Geological Survey Techniques and Methods, p. 497.
- Powlson, D.S., Smith, P., Smith, J.U., 2013. *Evaluation of Soil Organic Matter Models: Using Existing Long-Term Datasets*. Springer-Verlag, Heidelberg.
- Proust, D., Lechelle, J., Meunier, A., Lajudie, A., 1990. Hydrothermal reactivity of mixed-layer kaolinite/smectite and implications for radioactive waste disposal. *European Journal of Mineralogy* 2, 313-325.

- Pusch, R., Kasbohm, J., Knutsson, S., Yang, T., Nguyen-Thanh, L., 2015. The Role of Smectite Clay Barriers for Isolating High-Level Radioactive Waste (HLW) In Shallow and Deep Repositories. *Procedia Earth and Planetary Science* 15, 680-687.
- Schindler, M., Legrand, C.A., Hochella Jr, M.F., 2015. Alteration, adsorption and nucleation processes on clay–water interfaces: Mechanisms for the retention of uranium by altered clay surfaces on the nanometer scale. *Geochimica et Cosmochimica Acta* 153, 15-36.
- Schlegel, M.L., Descontes, M., 2009. Uranium uptake by hectorite and montmorillonite: a solution chemistry and polarized EXAFS study. *Environmental Science and Technology* 43, 8593–8598.
- Schwarzenbach, R.P., Gschwend, P.M., Imboden, D.M., 2005. *Environmental Organic Chemistry*. Wiley, New York.
- Sylwester, E.R., Hudson, E.A., Allen, P.G., 2000. The structure of uranium (VI) sorption complexes on silica, alumina, and montmorillonite. *Geochimica et Cosmochimica Acta* 64, 2431-2438.
- Teich-McGoldrick, S.L., Greathouse, J.A., Jové-Colón, C.F., Cygan, R.T., 2015. Swelling Properties of Montmorillonite and Beidellite Clay Minerals from Molecular Simulation: Comparison of Temperature, Interlayer Cation, and Charge Location Effects. *The Journal of Physical Chemistry C* 119, 20880-20891.
- Tsunashima, A., Brindley, G.W., Bastovanov, M., 1981. Adsorption of uranium from solutions by montmorillonite; compositions and properties of uranyl montmorillonites. *Clays and Clay Minerals* 29, 10-16.
- Turner, D.R., Sassman, S.A., 1996. Approaches to sorption modeling for high-level waste performance assessment. *Journal of Contaminant Hydrology* 21, 311-332.
- Turner, G.D., Zachara, J.M., McKinley, J.P., Smith, S.C., 1996. Surface-charge properties and UO<sub>2</sub><sup>2+</sup> adsorption of a subsurface smectite. *Geochimica et Cosmochimica Acta* 60, 3399-3414.
- Vallero, D., 2010. *Environmental Contaminants: Assessment and Control*. Elsevier Science.
- Wanner, H., Forest, I., 1992. Chemical Thermodynamics of Uranium, in: Agency, O.N.E. (Ed.), *Data Bank Issy-les-Moulineaux France*.
- White, G.N., Zelazny, L.W., 1988. Analysis and Implications of the Edge Structure of Dioctahedral Phyllosilicates. *Clays and Clay Minerals* 36, 141-146.
- Wilson, J., 2013. *Rock-forming Minerals: Sheet silicates: clay minerals*. Volume 3C. Geological Society of London.
- Zachara, J.M., McKinley, J.P., 1993. Influence of hydrolysis on the sorption of metal cations by smectites: Importance of edge coordination reactions. *Aquatic Sciences* 55, 250-261.



## 5. Conclusions

The main purpose of this project was to study the behavior and reactivity of Portuguese smectite submitted to  $\text{Sr}^{2+}$  and  $\text{UO}_2^{2+}$  adsorption under variable pH, ionic strength and contaminant concentration.

The detailed physicochemical characterization of selected Portuguese smectite samples allow us to conclude that they consist on interstratified structures distinguished by different compositions and distinct layer charges and charge distribution. Smectite BA1 was identified as 100% smectite, including beidellite and montmorillonite layers interstratified, whereas samples PS2 and PS3 consist of I-S mixed-layer minerals, containing a proportion of 10% and 30% of illite, respectively. The XRD results revealed that both samples, PS2 and PS3, are characterized by random interstratification and disorderly stack sequence, and were identified with the grade of ordering R0. The XRD results also showed that the basal spacing of samples BA1 and PS2 have only partially expanded after  $\text{Li}^+$  saturation and Glycerol solvation, confirming that part of layer charge resides in the tetrahedral sheets. Considering it, the interstratified structure of smectite BA1 was characterized by the presence of tetrahedral sheets with charges between 0.23 and 0.38/ $\text{O}_{20}(\text{OH})_4$ , with higher proportion of expanded layers, whereas smectite PS2 was characterized by tetrahedral charges  $>0.38/\text{O}_{20}(\text{OH})_4$  and by lower proportion of expanded layers to 16.5 Å. The behaviour of smectite PS3 was different after Glycerol solvation, once all the layers remained collapsed, indicating that the tetrahedral charges are lower than 0.23/ $\text{O}_{20}(\text{OH})_4$ .

The use of distinct adsorbates,  $\text{Sr}^{2+}$  and  $\text{UO}_2^{2+}$ , in our experiments provided different sorption results at similar conditions, which confirmed that the mechanism of adsorption is highly dependent on the size of the ion. The  $\text{Sr}^{2+}$  sorption experiments have carried out using distinct pH, 4 and 8, and different ionic strength ( $1 \times 10^{-2}\text{M}$  and  $1 \times 10^{-3}\text{M}$ ). The results revealed that the amount of  $\text{Sr}^{2+}$  adsorbed increases as increasing of  $\text{Sr}^{2+}$  concentration during the flow-through experiments. In this case, the gradient of concentration acted as an increasing driving force resulting into the increase of equilibrium sorption until the saturation point was reached. The amount of  $\text{Sr}^{2+}$  desorbed at pH 4 was about half of the amount desorbed at pH 8, revealing that at pH 4 the retention of  $\text{Sr}^{2+}$  onto montmorillonite was enhanced. It suggest that  $\text{Sr}^{2+}$ , due to their size and ion charge, has significantly higher tendency to be adsorbed on the interlayer of smectite than  $\text{K}^+$ . The kinetic experimental data indicated that

pseudo-first order model had the best fit to the experimental data obtained for both pH conditions.

The effect of pH and ionic strength was evaluated by means of batch experiments. The adsorption was higher at pH 8 and lower ionic strength ( $[KNO_3]=1.0 \times 10^{-3}M$ ) with a maximum adsorption capacity of 41.49  $mgSr^{2+}/g$ . However, the effect of pH in adsorption becomes less significant as ionic strength increases (from 33.22  $mgSr^{2+}/g$  – pH=8 to 32.89  $mgSr^{2+}/g$  – pH=4, at higher ionic strength ( $[KNO_3]=1.0 \times 10^{-2}M$ ) and different pH (4 and 8)). It suggests that  $Sr^{2+}$  is mainly adsorbed by ion-exchange at both pH conditions, and although there are more sites available for sorption at pH 8,  $K^+$  has greater tendency to be adsorbed on the edge sites of smectite than  $Sr^{2+}$ . The correlation coefficients indicated that the Langmuir model fits better the experimental data than the Freundlich model, indicating that sorbent structure seems to be homogeneous, with similar and energetically equivalent sorption sites.

Contrary to  $Sr^{2+}$ , the  $UO_2^{2+}$  sorption capacity was highly dependent on the pH conditions and the type of surface complexation of smectite. In this case, three different smectite samples (BA1, PS2 and PS3) were used in the  $UO_2^{2+}$  adsorption at pH4 (0.1mM) and lower ionic strength and at pH 6 and higher ionic strength (0.2M). The results indicated that ion-exchange (outer-sphere complexation) was the dominant mechanism at pH 4, where sample PS2 revealed the higher adsorption capacity, adsorbing more 34% and 138% of  $UO_2^{2+}$  than samples BA1 and PS3, respectively. The amount of  $UO_2^{2+}$  adsorbed decreased as increasing of pH and ionic strength (pH=6 ; I=0.2M), for all smectite samples, suggesting that the dominant mechanism of adsorption is the inner-sphere complexation in external hydroxyl groups of smectite, and the ion-exchange process is suppressed by the significant increase of  $Na^+$  concentration on solution. These conclusion are in agreement with previous results published by other authors.

The reversibility of the  $UO_2^{2+}$  sorption process was studied by means of flow through experiments. The desorption experiments occurred at pH 4 were not completed for samples BA1 and PS2 after 10 hours. However, the results obtained show higher reversibility in acidic conditions for both samples, suggesting that the  $UO_2^{2+}$  previously adsorbed may be completely desorbed. A different behavior was observed for sample PS3, which retained about 82% of the amount of  $UO_2^{2+}$  previously adsorbed. The results obtained demonstrated a great influence of the structural changes in the adsorption and reversibility of  $UO_2^{2+}$  on smectite. The experiments conducted at pH 6 demonstrated a significant decrease of the amount of  $UO_2^{2+}$  desorbed from the three smectite samples, indicating that the surface

complexation process was changed. This confirmed that inner-sphere complexation on the edge sites of smectite is the dominant mechanism at near neutral pH and high ionic strength.

The interpretation of kinetic data demonstrated that the type of surface complexation involved and the structural properties of smectite affected significantly the reversibility of  $\text{UO}_2^{2+}$  previously adsorbed and the kinetics of sorption processes. Therefore, pseudo-first order model provided the best fit to the experimental data obtained for  $\text{UO}_2^{2+}$  adsorption on samples BA1 and PS2 at pH 4, whereas pseudo-second order model fitted better the experimental results obtain during the adsorption at pH 6 and higher ionic strength, and the experimental data obtained for sample PS3 at pH 4.

Batch experiments of  $\text{UO}_2^{2+}$  adsorbed on heterogeneous smectite structures (BA1, PS2 and PS3), using pH 4 and lower ionic strength ( $I=0.02$ ) and pH 6 and higher ionic strength ( $I=0.2$  M) were conducted. The results obtained show that the increase of layer substitutions and the proximity between the negative charge on tetrahedral sheet and the contaminant have reduced the interlayer distances, restricting the ion-exchange process. Sample BA1 has higher tetrahedral charge than PS2 but lower cation exchange capacity, whereas sample PS3 has the higher proportion of illite interstratified layers ( $\approx 30\%$ ) and the lower number of available sites for ion-exchange. Samples BA1, PS2 and PS3 have 43%, 63% and 50% of  $\text{Na}^+$  available for cation exchange, which adsorbed 25% (0.12 mol/kg), 44% (0.23 mol/kg) and 32% (0.10 mol/kg) of their respective CEC at pH 4. This reveals a strong competition between  $\text{Ca}^{2+}$  and  $\text{UO}_2^{2+}$  that restricted the sorption capacity mainly on sample BA1. The ion exchange was significantly reduced at pH 6 and higher ionic strength, where the amount of  $\text{UO}_2^{2+}$  adsorbed correspond to 32%, 33% and 41% of the total number of reactive external sites. Sorption capacity is related closely to the CEC, which is a function of total surface area and the smectite layer charge. The total surface area calculated increases as the mean crystal thickness distribution decreases and the CEC increases as total surface area increases.

A cation exchange and surface complexation model based on diffuse double layer was successfully developed, in order to predict the  $\text{UO}_2^{2+}$  sorption on smectite. The RMSE values ( $\% < 0.40$ ) for all the experiments confirm a good fit to the experimental data. The modelling results showed that  $\text{UO}_2^{2+}$  was simultaneously adsorbed in the interlayer charged sites by cation exchange reaction and through inner-sphere surface complexation into the variable charged sites at pH4 ( $I=0.02\text{M}$ ). This reveals that samples PS2 and PS3 have higher tendency to adsorb  $\text{UO}_2^{2+}$  through ion exchange, and sample BA1 has similar proportions of  $\text{UO}_2^{2+}$  absorbed by both mechanisms. The modelling results at pH 6 ( $I=0.2\text{M}$ )

indicate that the sorption mechanism was restricted to surface complexation on the external sites of smectite where  $\equiv\text{AlOUO}_2^+$  and  $\equiv\text{SiOUO}_2^+$  were the major surface species.

The XPS results were in agreement with the modelling results obtained at both pH conditions. Two different components at  $380.8\pm 0.3$  and  $382.2\pm 0.3$  eV at pH 4 after the  $\text{U4f}_{7/2}$  peak deconvolution were assigned to hydrated  $\text{UO}_2^{2+}$  adsorbed by inner-sphere complexation on the external sites of smectite and adsorbed by cation exchange, respectively. Two new binding energy components at  $380.3\pm 0.3$  and  $381.8\pm 0.3$  eV identified at pH 6 correspond to  $\equiv\text{AlOUO}_2^+$  and  $\equiv\text{SiOUO}_2^+$  surface species, respectively. After desorption process, the proportion of the higher binding energy component obtained at pH 4 decreased, suggesting that the  $\text{UO}_2^{2+}$  weakly adsorbed was previously desorbed. The proportions of both binding energy components remained unchanged before and after desorption process, indicating the higher retention of  $\text{UO}_2^{2+}$  on smectite surface.

The sorption experiments developed in this study constituted a breakthrough in the knowledge of Portuguese smectite. It was focus in the application of these materials as possible adsorbents (clay liners) in order to retain radionuclides and avoid the environment contamination. Generally the results revealed that, depending on the pH conditions and ionic strength, Portuguese smectite may have great capacity to adsorb and retain  $\text{Sr}^{2+}$  and  $\text{UO}_2^{2+}$ . The results also demonstrated that the structural heterogeneity of smectite, characterized by different layer charge and charge distribution, affects the adsorption capacity, and draws attention to the need for additional studies in order to better understand the possible risk of this situation to the existing radioactive waste repositories, where the smectite structural changes result from the increase of temperature due to waste packaging.

For future work it is also intended to study in more detail the surface complexation process by means of EXAFS, taking into the account that our results revealed that the amount of layer charge, as well as, the charge location, affects the attraction/bond strength between smectite and radionuclide.